

PROPERTIES OF LIGHTNING DERIVED FROM
TIME SERIES ANALYSIS OF VHF RADIATION DATA

By

PEDRO L. RUSTAN, JR.

A DISSERTATION PRESENTED TO THE GRADUATE COUNCIL OF
THE UNIVERSITY OF FLORIDA
IN PARTIAL FULFILLMENT OF THE REQUIREMENTS FOR THE
DEGREE OF DOCTOR OF PHILOSOPHY

UNIVERSITY OF FLORIDA

1979

UNIVERSITY OF FLORIDA



3 1262 08676 742 2

ACKNOWLEDGEMENTS

I gratefully express my appreciation to the members of my supervisory committee for their support and cooperation. In particular, I thank Dr. M. A. Uman for his guidance, enthusiasm, and professional expertise, and Dr. D. G. Childers for his probing questions and constant support of this research. Special thanks are due to Dr. J. McClave (Statistics) for providing programs for data modeling. I am also thankful to Mr. Paul Krehbiel at the New Mexico Institute of Mines and Technology, and Mr. Carl L. Lennon and Mr. William E. Jafferis at the Kennedy Space Center for their generous help in providing data, the main ingredients of this work. I acknowledge the work of Mr. Ronald Jacobs from Eglin AFB in digitizing the analog tapes. A special note of appreciation for the continuing help of Dr. W. H. Beasley and Mr. W. G. Baker and many other colleagues working in the University of Florida Lightning Research Laboratory. The author especially thanks his wife, Alexandra, without whose love, patience, and understanding this work could not have been completed.

This investigation was made possible by the Air Force Institute of Technology. The research reported here was jointly supported by NASA KSC Contract NAS10-9378; NSF Grant ATM-76-01454; and ONR Contract N0001475C0153.

TABLE OF CONTENTS

	<u>Page</u>
ACKNOWLEDGEMENTS	ii
ABSTRACT	vi
CHAPTER	
I INTRODUCTION	1
II GENERAL REVIEW OF LIGHTNING AND PREVIOUS LIGHTNING VHF TOA RESEARCH	6
2.1 Description of Cloud-to-Ground and Intracloud Lightning	6
2.2 Description of Electromagnetic Radiation Emitted by Intracloud and Cloud-to-Ground Flashes	10
2.3 Lightning Direction Finders	14
2.4 Review of Proctor's Work	16
2.5 Review of Lennon's Work	25
III DATA ACQUISITION AND PROCESSING	29
3.1 Data Recording	29
3.2 Telemetry System	33
3.3 Data Pre-Processing and A/D Conversion	40
3.4 Electric Field Meters	43
3.5 Charge Locations Derived from Electric Field Stations	44
3.6 Charge Locations Derived from VHF Noise Sources	47
IV COMPUTER ALGORITHM FOR LOCATION OF LIGHTNING CHANNELS	49
4.1 General	49

	<u>Page</u>
4.2 Data Characteristics	50
4.3 Technique for Determining Delays Based on the Data Characteristics	55
4.4 Algorithm Flow Chart	62
4.5 Display of Three-Dimensional Locations and Their Time of Occurrence	68
V ANALYSIS OF RESULTS	72
5.1 The 165959 Flash	73
5.2 The 180710 Flash	123
5.3 The 181806 Flash	166
5.4 The 182356 Flash	220
5.5 The 180644 Flash	264
5.6 The 181416 Flash	273
VI DATA MODEL	281
6.1 Noise Level	284
6.2 Stepped Leader	284
6.3 J-Change	285
6.4 Characteristics of VHF Radiation	286
VII CHARACTERISTICS OF THE VHF RADIATION DURING THE DIFFERENT PHASES OF LIGHTNING	287
7.1 Cloud-to-Ground Lightning	290
7.2 Intracloud Lightning	305
VIII CONCLUDING COMMENTS AND SUGGESTIONS FOR FUTURE RESEARCH	309
APPENDIX	
A DERIVATION OF SOURCE LOCATION FROM DIFFERENCE OF TIME OF ARRIVAL MEASUREMENTS	311
B ACCURACY OF THE LOCATION OF LIGHTNING SOURCES USING THE HYPERBOLIC EQUATIONS	315

	<u>Page</u>
B.1 Error Analysis for the Locations of the 165959 Flash on 19th July 1976	324
B.2 Error Analysis for the Locations of the 181806 Flash on 8th August 1977	324
B.3 Error Analysis for the 180710 and 182357 Flashes on 8th August 1977	324
C COMPUTER ALGORITHM TO DETERMINE VHF SOURCE LOCATIONS FROM THE DIFFERENCE IN THE TIME OF ARRIVAL OF VHF RADIATION DATA	330
D COMPUTER ALGORITHM TO DISPLAY A THREE-DIMENSIONAL DRAWING OF VHF NOISE SOURCES	356
E FREQUENCY DOMAIN APPROACH TO DETERMINE DIFFERENCE IN THE TIME OF ARRIVAL	364
E.1 Measurement of Time Delay by Determining the Peak of the Impulse Function	366
E.2 Measurement of Time Delay by Measuring the Phase of the Frequency Response Function	367
REFERENCES	369
BIOGRAPHICAL SKETCH	376

Abstract of Dissertation Presented to the Graduate Council
of the University of Florida in Partial Fulfillment of the Requirements
for the Degree of Doctor of Philosophy

PROPERTIES OF LIGHTNING DERIVED FROM
TIME SERIES ANALYSIS OF VHF RADIATION DATA

By

Pedro L. Rustan, Jr.

December 1979

Chairman: Martin A. Uman
Co-Chairman: Donald G. Childers
Major Department: Electrical Engineering

The purpose of this research is to derive lightning properties by correlating three-dimensional VHF source locations, characteristics of the VHF (30 to 50 MHz) radiation, and electric field intensity (0.1 Hz to 1.5 MHz). We study the discharge initiation, propagation, overall geometry, and charge magnitude and location for the various phases of both cloud-to-ground and intracloud lightning. We analyze in detail four cloud-to-ground and three intracloud flashes, all selected randomly. The experimental data were recorded during the summers of 1976 and 1977 at the Kennedy Space Center (KSC). The VHF radiation was recorded using the multiple VHF stations of the KSC Lightning Detection and Ranging (LDAR) system. We located the VHF noise sources from the difference in the time of arrival (DTOA) between the pulses received at the multiple VHF stations using a hyperbolic geometry. The electric field data were recorded by the New Mexico Institute of Mines and Technology (NMIMT) and the University of Florida. Leader-return strokes

charge magnitude and locations, calculated for us by NMIMT, were correlated with our VHF source locations.

Previous work on three-dimensional "channel structure" during lightning flashes was performed by Proctor in South Africa, who pioneered the technique of VHF source locations. Proctor's determination of DTOA was done manually by pulse shape identification on 253 MHz signals. The three-dimensional source locations presented in this thesis for the different phases of lightning discharges were obtained using a computerized technique which allows a large amount of data to be analyzed quickly.

The data were recorded with a wideband VHF receiver having a band-pass filter of 30-50 MHz and a logarithm envelope detector. The detected signals from three of the stations were transmitted to the fourth station where all were recorded on four tape channels having a bandwidth of 400 Hz to 1.5 MHz. The analog tapes were digitized at 4.35 MHz, a sample every 229 nanoseconds. Between 20×10^3 and 25×10^4 pulses per flash were recorded during active VHF radiation. A newly developed computer algorithm employing cross-correlation and pattern recognition was written to determine the DTOA between the individual pulses. Once the DTOA's were calculated, we used a three-dimensional hyperbolic position measuring system to determine the source locations.

The significance of this research is the following: (1) We develop an important new tool for lightning research: a computer program which, using digital tape data from four VHF stations, can determine source locations every 7 to 10 microseconds. An average of about 20,000 locations was found for each one of the studied flashes. (2) We derive properties of the lightning flashes studied. Some of these results

are: a) From observing the initial lightning VHF noise we can determine whether a flash will become a cloud-to-ground or an intracloud discharge. b) Cloud-to-ground flashes were initiated by a process we name preliminary breakdown. The VHF sources during the preliminary breakdown formed an inclined cylinder 5 to 12 km long and about 500 meter radius between a height of 4 and 10 km. c) The VHF radiation of stepped leaders and return strokes during cloud-to-ground flashes have unique characteristics which can be used to identify these events by studying the VHF noise alone. The stepped leader has the lowest level of radiation of any process in the flash, but it radiates along the whole path from the charge center to ground. d) Dart leaders do not emit VHF radiation along their paths to ground, but rather in the neighborhood of the previous J-changes. e) The paths of the VHF sources during J-changes were inclined 25° , 35° , 45° , and 55° off vertical. The path of the VHF sources during J-changes was well defined after the first few strokes of a cloud-to-ground flash, but the path became less organized as the stroke order increased. The first J-change of all the ground flashes propagated downward toward the previous charge center lowering negative charge.

CHAPTER I

INTRODUCTION

The main purpose of this research is to determine VHF lightning source locations in three dimensions and to relate these results to other simultaneously recorded data, notably the dc to 1.5 MHz wideband electric field, in order to obtain a better understanding of the physics of the lightning discharge. The VHF radiation data were recorded during the summers of 1976 and 1977 at the Kennedy Space Center (KSC) using the KSC Lightning Detection and Ranging (LDAR) system. The VHF locations were determined from the difference in the time of arrival of the VHF radiation pulses at four LDAR ground stations. This study was part of the Thunderstorm Research International Project (TRIP). TRIP brought together a group of outstanding scientists in atmospheric electricity from the USA and foreign countries with the purpose of performing coordinated measurements during thunderstorms. The work reported in this thesis represents an important new dimension in lightning research. For the first time the use of a fully computerized algorithm has made it possible to understand in more detail the different phases of a lightning flash. We now have a much fuller understanding of the electrical activity inside a thundercloud and we are better able to describe the generation and propagation of the different phases of both cloud and ground lightning flashes. It is to be hoped that the new techniques developed as a part of this study will facilitate future research in the field of atmospheric electricity.

In this introductory chapter we shall briefly survey the organizational aspects of this thesis as well as some of the information presented. Chapter II presents a general review of lightning and previous lightning VHF time of arrival (TOA) research. Systematic lightning research started in the middle of the eighteenth century with the work of Benjamin Franklin. Modern lightning, however, did not start until the early part of the twentieth century with the electric field measurements of C. T. R. Wilson published in 1916. Within ten years, cathode-ray-oscillography and high speed photography were introduced to the study of thunderstorm electricity. The first published suggestion that VHF radiation might be used to determine source locations in three dimensions appears to be due to Oetzel and Pierce (1969). The pioneering work in the determination of source locations by calculating the difference in the time of arrival was published by Proctor (1971). Proctor's original work was performed manually and provided new information about the different phases of a lightning discharge.

Chapter III presents a description of the system used to perform the VHF measurements. In addition, this chapter presents a brief discussion of the measuring system used for the electric field measurements and of the point charge models which are used to interpret the results. The original VHF data are analog (400 Hz to 1.5 MHz) tape recordings of the output of envelope detectors of four ground-based VHF (30 to 50 MHz) receivers located at the Kennedy Space Center. The amplitude scale of the VHF radiation was made logarithmic to provide 80 dB dynamic range for the input signal. The VHF analog data for the four stations were subsequently digitized at a sampling rate of 4.35 MHz.

Chapter IV describes the computer algorithm used for the location of lightning VHF sources. Digital tapes containing VHF time-series data from four stations were processed with the purpose of determining the differences in the time of arrival (DTOA) between pulses in one reference station and the remaining three stations. The computer algorithm to determine DTOA was based on cross-correlation and pattern recognition techniques. The cross-correlation function was optimized to determine DTOA between the central and each one of the remote stations every 94 μ sec. For long processes when there was little variation from one DTOA to the next by using 94 μ sec intervals, a longer sampling interval of 376 μ sec was used. Even though the cross-correlation provides the DTOA for the 94 μ sec intervals, it does not determine the DTOA for individual pulses with a width much less than 94 μ sec. Therefore, we used pattern recognition to determine DTOA between individual pulses which were within ± 3.7 μ sec of the cross-correlated DTOA result. Using this technique we obtained a source location every 7 to 10 microseconds.

Chapter V gives the lightning source locations and other derived physical properties for the selected flashes. We randomly selected four cloud-to-ground and two intracloud flashes from a group of about 1,000 which had correlated electric fields. The six flashes are referred to in this thesis by the Universal Time of occurrence of the flash. Except for the first flash at 165959 on 19th July 1976, all of the remaining flashes were recorded on 8th August 1977. The cloud-to-ground flashes are presented in sections 5.1 through 5.4, followed by the two intracloud flashes in sections 5.5 and 5.6. We correlated the different phases of each lightning flash with the electric field record at a

University of Florida station and at a network of eight electric field stations designed and operated by the New Mexico Institute of Mines and Technology (NMIMT). In addition, for two of the ground flashes, we correlated our results with photographs of the lightning channels to ground obtained from the KSC TV network.

Chapter VI presents a statistical model for the VHF radiation data. This model was derived with the purpose of classifying the properties of the time-series data. The Box and Jenkins (1976) technique was used to identify a time-series model and to estimate the parameters of the model.

Chapter VII summarizes the properties of the different phases of cloud-to-ground and intracloud lightning derived from the flashes studied in Chapters V and VI. The main properties of the different phases studied were the characteristics of the VHF radiation, the length, direction and velocity of propagation of the various lightning paths associated with different discharge phases, the charge transfer associated with each of the lightning phases, and the total volume occupied by the flashes.

Finally, Chapter VIII provides some concluding remarks and suggests some of the areas for future research.

Appendices A through E are provided to present mathematical derivations or computer listings which were not appropriate for the text. Appendix A gives the derivation of three-dimensional locations obtained from the difference in the time of arrival. Appendix B provides the error analysis in the determination of the three-dimensional locations. Appendix B also shows four tables with tabulated RMS errors associated with channel locations as a function of position. Appendix C gives a Fortran computer listing used to determine DTOA in accordance with the

techniques described in Chapter IV. Appendix D provides a listing of the computer algorithm to display the channel locations in three dimensions. Lastly, Appendix E presents two frequency domain techniques which could be used to obtain DTOA. These techniques were not used because they do not adapt to the experimental data as well as the selected time domain technique described in Chapter IV.

CHAPTER II

GENERAL REVIEW OF LIGHTNING AND PREVIOUS LIGHTNING VHF TOA RESEARCH

2.1 Description of Cloud-to-Ground and Intracloud Lightning

This section contains an introduction to the basic terminology of the physics of lightning. Lightning is a transient, high current electric discharge whose path length is measured in kilometers. A lightning discharge starts when the electric field in some region of the cloud exceeds the breakdown strength of air, that is, equal to or less than 3×10^6 V/m, depending on pressure, temperature, and the presence of precipitation. The most common source of lightning and the only one considered in this thesis is the thundercloud. A typical Florida thundercloud has a top between 9 and 15 km above sea level (Jacobson and Krider, 1976).

The lightning produced by the thundercloud can take place within a cloud (intracloud), between cloud and earth, between clouds, or between the cloud and the surrounding air. Our study includes the intracloud and the cloud-to-earth lightning usually called cloud-to-ground or ground discharge. A complete discharge is called a flash. Either discharge, the intracloud or the cloud-to-ground flash, typically lasts 0.5 seconds.

Regardless of the type of flash being studied, one of the most important factors in thunderclouds is the location and size of the charge regions. The simplest and most accepted model of a thundercloud was given by Wilson (1916). He assumed that the center of electric charges

within a thundercloud might be considered as point charges if the dimension of the charge region was small compared to the ground distance to the ground observation point. Under these assumptions the thundercloud charge was treated as an electric dipole with an upper part that carried a positive charge and a lower part that carried a negative charge. Electric field measurements performed by Malan (1963), and balloon tests made by Simpson and Robinson (1941), and Gish and Wait (1950) yielded an average value of 40 coulombs for each of the charge regions. However, measurements of charge neutralization of the order of 40 coulombs or larger in single ground flashes made by Brook et al. (1962), Uman et al. (1978), and Krehbiel et al. (1979) make us suspect that 40 coulombs is too low an estimate for cloud charge. In addition, Malan (1952) estimated that about half of the cloud negative charge was neutralized during the lightning flash. Since the external electric field often used to compute the cloud's static charge is due to the net of the thundercloud charge and the surrounding space charge, the actual value of the thundercloud charge is larger than reported values. In our study we used the difference in the electric field during the different phases of a lightning flash to determine the charge being transferred or destroyed in a thundercloud, so the actual value of static charge is not important to our work.

A ground flash is composed of one or more separate strokes in the same or separate channels. Each stroke lasts for milliseconds and the time interval between strokes is roughly 50 msec. A stroke is composed of a downward propagating leader, which lowers cloud charge and cloud potential toward ground level, followed by a return stroke, an earth-potential wave, which propagates back up the leader channel, discharging

the leader to ground. Stepped leaders precede first strokes and some subsequent strokes and move downward in about 50 meter steps with about 50 microseconds interval between steps. The velocity of the individual steps is too fast to be determined from available streak photographs. The stepped leader moves toward earth with a typical average velocity of 2.0×10^5 m/s. Dart leaders precede most subsequent strokes. Dart leaders occur if additional charge is moved from another region of the cloud to the top of the leader channel in a time less than about 100 msec. A dart leader serves the same purpose as the stepped leader in that it deposits charge along the channel and lowers cloud potential to ground. The dart leader is less branched and has higher velocity than the stepped leader. The elucidation of these processes is mostly credited to Schonland and his co-workers in South Africa (1934 to 1938) who used photographic techniques and electric field measurements. Discharges also take place in the cloud in the time between strokes. Interstroke electric field changes observed on the ground are termed J-changes; interstroke impulsive electric field changes are termed K-changes (Kitagawa and Kobayashi, 1958; Uman, 1969; Pierce, 1977).

Ground flashes can be classified as hybrid or discrete flashes (Malan, 1954; Kitagawa et al., 1962). A lightning flash which involves one or more continuing currents between strokes is called a hybrid flash. A flash which involves only discrete strokes and no continuing current is called a discrete flash. Between 29 and 46 percent of all ground flashes have strokes followed by a continuing current (Livingston and Krider, 1978; Kitagawa et al., 1962), that is, hybrid characteristics. The J-change is differentiated from the continuing current stroke because the J-change has no channel luminosity and at close range the J-change electric field

has different polarity. The work on cloud-to-ground discharges presented in this thesis will provide the VHF noise source locations for each phase of hybrid and discrete flashes. Whenever wideband electric field measurements were available, we attempted to calculate the charge involved along the radiating paths. These findings provide additional insights into the mechanisms of ground flashes.

The intracloud discharge is not as thoroughly investigated as the ground discharge. On the basis of electric field waveforms, Kitagawa and Brook (1960) studied the nature of electrical discharges inside thunderclouds. They included the cloud to cloud, cloud to the surrounding air, and the intracloud discharge, treated them as identical, and referred to them as cloud flashes. Three phases of the cloud flash were classified: initial, very active, and junction phase. The initial phase was characterized by a large number of small impulses. The active phase had larger and more regular impulses. The final phase had a number of rapid regular impulses. Ogawa and Brook (1964) studied the variations of the electric field with time and distance during the initial and junction phases of intracloud discharges. They claimed that positive charge was lowered during the initial phase by downward positive streamers, and that negative recoil streamers occurred during the junction phase. This viewpoint is partially shared by Takagi (1961) who proposed a mid-gap streamer where positive streamers propagate downwards into the negative charges and negative streamers propagate upwards into the positive charges. However, earlier work by Pierce (1955) and Smith (1957) suggested that the intracloud discharge raised negative charges. Khastgir and Saha (1972), using questionable models attempted to prove analytically that the experimental electric field curves of Ogawa and Brook (1964) could be interpreted as

either positive descending streamers, negative ascending streamers, or a combination of both of these processes. The work in intracloud discharges presented in this thesis will provide the VHF noise source locations in three-dimensional space and in time. These findings should provide additional information to help understand the mechanisms of the intracloud discharge.

2.2 Description of Electromagnetic Radiation Emitted by Intracloud and Cloud-to-Ground Flashes

The most recent comprehensive study of the electromagnetic radiation produced by lightning discharges is given by Pierce (1977). Briefly, this section presents a review of the radiation fields due to the intracloud and cloud-to-ground flashes over the frequency range from 1 KHz to 1 GHz.

One means of learning about discharge processes associated with cloud-to-ground and intracloud lightning discharges is by measuring the resultant electromagnetic radiation. Numerous investigators (e.g., Malan, 1958; Brook and Kitagawa, 1964; Takagi and Takeuti, 1963; Pierce, 1960; Kimpara, 1965; Uman, 1969; Proctor, 1971; Takagi, 1975; Krider et al., 1977, 1979; Taylor, 1978; LeVine and Krider, 1977; Serhan et al., 1979) have studied the electromagnetic radiation of lightning in various frequency ranges with the purpose of deriving some conclusions about the lightning discharge.

The electric field due to a small straight vertical conducting element above a conducting plane can be calculated exactly at any distance. These results are found in Uman and McLain (1970), and McLain and Uman (1971).

$$\begin{aligned}
\vec{E}(D,t) = & \frac{1}{2\pi\epsilon_0} \left[\int_{z_1}^{z_2} \frac{2-3\sin^2\theta_j}{R_j^3} \int_0^t i\left(z, t - \frac{R_j}{c}\right) d\tau dz \right. \\
& + \int_{z_1}^{z_2} \frac{2-3\sin^2\theta_j}{cR_j^2} i\left(z, t - \frac{R_j}{c}\right) dz \\
& \left. - \int_{z_1}^{z_2} \frac{\sin^2\theta_j}{cR_j} \frac{\partial i}{\partial t} \left(z, t - \frac{R_j}{c}\right) dz \right] \vec{a}_z
\end{aligned} \quad (2.1)$$

where the subindex j represents the contribution due to one of the current elements. The pertinent geometry, distance, and angles are defined in Figure 2.1.

A spark channel carrying a transient current, usually referred to as current element, acts as a radio antenna and emits electromagnetic radiation. The radiation field from a current element is the term that contains the time derivative of the current in equation (2.1). That is

$$\vec{E}_{\text{Rad}}(D,t) = \frac{1}{2\pi\epsilon_0 c^2} \int_{z_1}^{z_2} \frac{\sin^2\theta_j}{R_j} \frac{\partial i}{\partial t} \left(z, t - \frac{R_j}{c}\right) dz \vec{a}_z \quad (2.2)$$

Malan (1958, 1963) first obtained correlation between the low frequency electric fields and the radiation fields produced by intracloud and cloud-to-ground lightning flashes in the 1 KHz to 10 MHz range. Brook and Kitagawa (1964) measured radiation fields at frequencies of 420 and 850 MHz from lightning flashes 10 to 30 km away. Horner (1964), Kimpara (1965), Pierce (1967), Oetzel and Pierce (1969), and Pierce (1974) provided good reviews of correlated electric and radiation fields extending from 1 KHz to 100 MHz. These reports showed that at frequencies less than 300 KHz few current elements are active during the flash. Isolated radiation pulses were obtained primarily during return strokes

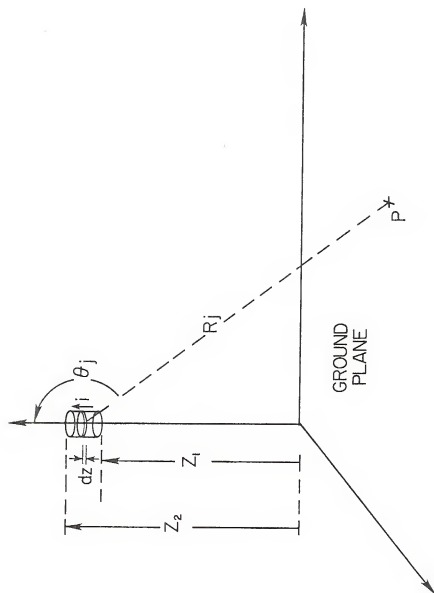


Figure 2.1. Radiation field of a small current element.

and K-changes. The maximum energy of the radiation spectrum is at VLF. The average source spectrum has a maximum at about 5 KHz and decreases inversely proportional to frequency above 10 KHz. In the frequency range from 300 KHz to 30 MHz the number of current elements increases but the magnitude of the return stroke radiation pulse decreases. As the frequency increases above 30 MHz the number of current elements increases with a peak at 50 MHz, and then decreases (Oetzel and Pierce, 1969). Above 30 MHz the magnitude of the pulses decreases with increasing frequency. At LF and VLF the length of the return stroke channel and the K-change channel are of the order of magnitude of these wavelengths, since the radiation half cycle time is the channel length divided by the propagating velocity and this is the only radiation that exists. As frequency increases into the HF and MF range, there are more current elements with length comparable to the wavelength. We expect that most current elements active during lightning discharges have lengths of the order of tens of meters which will be detected with a center frequency of tens of MHz.

Another important variable to consider in the study of atmospherics is the effect of the propagation medium between the current elements and the group receiving stations. Excellent reviews of the propagation conditions of atmospherics can be found in Horner and Bradley (1964), Oetzel and Pierce (1969), Harth (1974), and Pierce (1977). The characteristics are a function of the frequency of the emitting source, the propagating distance, and the reflective properties of the earth and the ionosphere. The ionosphere has complex reflection properties as a function of frequency. According to Pierce (1977), the propagating conditions of atmospherics can be separated into three groups. Below

300 KHz the earth and the lower ionosphere create a quasi-waveguide; between 300 KHz and 30 MHz reflections occur from the ionosphere; above 30 MHz atmospherics penetrate the ionosphere. In the research reported in this thesis, the atmospherics were recorded in the VHF range (30 to 50 MHz) where at the close ranges considered there is no appreciable ionospheric reflection.

2.3 Lightning Direction Finders

The distant electromagnetic radiation associated with lightning is usually called spherics. Spherics have been used as lightning direction finders in the VLF and VHF range. The standard method of location of distant ground flashes in the VLF range uses cathode-ray direction finders (CRDF). This method was originally developed by Watson-Watt and Herd (1926). It consists of two or more direction finding stations, each with two vertical loop antennas usually tuned to a VLF frequency. The azimuth angle of the flash is usually determined by displaying the two perpendicular antenna magnetic field outputs on the perpendicular scope axes. Two or more stations can be used to determine the location of the discharge from the intersection of the azimuth vectors. For discharge distances less than 100 or 200 km from the stations, the accuracy of this standard technique has been found to be poor. This is caused by the fact that if return strokes are not vertical, the antennas will be sensing not only the vertical magnetic field but also the horizontal component. As much as 20 degrees error has been found by Nishino et al. (1973) at a distance of 200 km from the discharge. Uman et al. (1975) observed that even at 10 km the initial peak magnetic fields occurs in the first 5 μ sec and hence is due to the vertical channel position near ground. VLF direction finders have been improved

considerably by Krider et al. (1976) using the properties of the magnetic field previously observed by Uman et al. (1975). The improved VLF direction finder has been successfully tested to detect the location of ground flashes within 200 km of the stations (Krider et al. (1976)).

Oetzel and Pierce (1969) suggested that time-of-arrival techniques could be used for line-of-sight direction finding in the VHF (30-100 MHz) range. VHF direction finders were developed along these lines by Cianos et al. (1972); Murty and MacClement (1973); MacClement and Murty (1978); and Taylor (1976, 1978). These VHF direction finders made it possible to locate lightning discharges within a range of 100 or 200 km from the stations. Cianos et al. (1972) used two VHF stations (25 to 35 MHz) separated by 122 meters. Using this system the difference in the time of arrival (DTOA) was measured with an accuracy of 10 nsec, and the azimuth angle of about 2000 impulses per flash was located. The Cianos VHF direction finder operated in real-time for distances up to about 150 km. The VHF direction finder described by Murty and MacClement (1973) operated in the 82-88 MHz range and used difference in the time of arrival (DTOA) to determine the azimuth angle of atmospherics up to 160 km apart. DTOA within 25 nsec were measured from the scope traces. The latter system was improved by MacClement and Murty (1978) to include a third station. The third station permitted measurement of elevation in addition to the azimuth angle. The system operated in the 66-72 MHz range and DTOA were measured with an accuracy of 10 nsec. This system operated in real-time and located the azimuth and elevation angles of about 300 impulses per flash. A two station VHF (20-80 MHz) direction finder was also reported by Taylor (1975). This system was later improved by Taylor (1978) to include a third station

to determine elevation angles. His 1978 system used a vertical and a horizontal antenna, 13.7 meters apart, at each of two stations separated by 17.8 km. The horizontally and vertically spaced antennas were used to measure azimuth and elevation, respectively. Time measurements were performed to 0.4 nsec with angle accuracy of ± 0.5 degree.

In addition to the VLF magnetic field ratio techniques and the VHF time of arrival direction finders previously described, Lewis (1960) used a VLF direction finder with DTOA techniques. Lewis used four stations in a Y configuration with the central station at the intersection of the Y. The distance between the central and the remote stations (at the three ends of the Y) ranged between 100 and 120 km. This system was used in relation to a system implemented in England to detect spherics over the Atlantic Ocean and Western Europe. The waveforms from the four stations were photographed on continuously moving 35-mm film. Only three stations were needed for direction finders. The remaining two stations were used for redundancy. The reported accuracy for this system was about 0.5 degree of latitude and of longitude.

2.4 Review of Proctor's Work

In addition to the previously described direction finders, channel locations have been reported by other means, such as, thunder measurements (e.g., Holmes et al., 1971; Nakano, 1973; and Teer and Few, 1974), and radar studies based on the appearance and decay of ionized channels (Hewitt, 1953, 1957). However the most relevant work to date is a DTOA hyperbolic system that uses a minimum of four stations to determine the three-dimensional channel locations (Proctor, 1976; Lennon, 1975).

By the time Oetzel and Pierce (1969) had suggested in print that spherics locations could be determined by measurements of DTOA in the VHF

range, Proctor, working in South Africa, had built and tested a five station system to measure noise impulses in the VHF range. Proctor has written only a Ph.D. thesis and a limited number of papers and reports about his work in South Africa. Next we will present a summary of Proctor's work (Proctor, 1971, 1974a, 1974b, 1974c, 1974d, and 1976) and its relationship to the work presented in this thesis.

Proctor (1971) describes his telemetry system and gives some preliminary results. The system consists of four 253 MHz crystal-controlled receivers located at the ends of a cross (the remote stations), and a fifth station (the central station) at the center of the cross. The distance from the central to the remote stations ranged between 10.7 and 26.7 km. All stations consisted of a 10 MHz bandwidth VHF receiver centered at 253 MHz and progression detection i.f. amplifiers to give the receiver a logarithm response near 80 dB. This detection technique is very similar to the band-pass filter and logarithm envelope detector used in the telemetry of the work reported in this thesis. The remote station spherics were retransmitted to the central station by frequency modulated 10 GHz links with 5 MHz bandwidth. Therefore the overall bandwidth was 5 MHz for the remote stations and 10 MHz for the central station. All five signals together with 5- μ sec timing markers were displayed on cathode ray tubes (CRT's) and they were photographed by 35-mm rotating drum cameras. The film moved with a velocity of 8 m/sec. CRT's were also used to display electric field change and time markers. When the operator had decided that the storm was sufficiently close for channel reconstruction (usually less than 20 km), a trigger signal selected a threshold level to start the film. The maximum continuous film time is 250 msec. Since most flashes last more than 250 msec

and the triggering signal might not detect the beginning of the flash, only limited information is recorded. The records are read by operators who first identify the same pulse in all the stations and then measure the DTOA between the four remotes and the central station. The records are enlarged to .36 cm/ μ sec for reading purposes. Using a transparent graticule, DTOA can be measured to .1 μ sec. Redundant sets of readings are obtained by using the additional station. The by-hand DTOA for every pulse are fed into a computer which is programmed to solve the hyperbolic equations and print the three dimensional locations. This tedious technique required 8 man-months to determine the locations of one 250 msec sample. The reported accuracy of the locations for a 20 km range is 25 meters for X and Y, and 140 meters for Z. Proctor (1971) states that a limited number of 250 msec intervals had been processed. Actually, from studying the article, we reasonably infer that only one 250 msec interval was completely processed.

The results reported by Proctor (1971) for the different phases of the discharge are as follows. One stepped leader was processed with 225 locations. The radiation started at a height of 5 to 6.5 km above sea level (ground level 1.5 km). The noise sources extended upward and downward but the median height moved downward at 3×10^5 m/sec for 7 msec. The active region became greater by the end of the leader and extended from near ground to a height of 6.5 km above mean sea level (MSL). Poor height resolution at low heights does not permit the determination of accurate channels. The noise emitted by dart leaders was reported to be similar to stepped leaders. This information is in conflict with the work presented in this thesis. We claim that stepped leaders have unique, identifiable pulses not seen anywhere else in a cloud-to-ground

or intracloud discharge. It was reported by Proctor that the noise from dart leaders emanated from the upper part (heights of 5 or 6.5 km above sea level) of the channel. During the return strokes the noise was continuous for 100 or 200 μ sec. Many sources were active and few fixes were determined along the channel. Proctor (1971) reported activity within 250 μ sec following the return stroke. This activity was located in the previous return stroke branches. The interstroke process reported was confined to one flash. The interstroke emitted a large fraction of the VLF noise during the ground discharge. It was reported to start 10 or 12 msec after the first return stroke and involved regions between 3 and 4 km of altitude. Interstroke noise after subsequent strokes was reported to extend the previous channel in an upward direction. Proctor (1971) reported no information about fixes in an intracloud discharge.

Proctor presented his next report in the 5th International Conference in Atmospheric Electricity (Proctor, 1974a). By this time 18 flashes (250 msec intervals) had been analyzed. This paper is the first publication to discuss the location of noise sources during a cloud flash. It is claimed that cloud flashes emit pulsed radiation during their initial and very active (VA) phases, but only pulsed trains, less than one millisecond width, in the final stage. These trains were also reported in the VA phase. According to Proctor, these trains are emitted by two kinds of events. One produces a long propagation from the previous noise sources while the other one produces a shorter path which moves toward the starting volume of the flash going throughout non-previously located channels. Proctor associates these trains with K-changes. The speed of the train of pulses ranged between 3×10^6 and

3×10^7 m/sec. The manner in which the sources form appeared erratic. During the initial stage they seem to be confined to a volume less than 1 km^3 ; then the channel emerged. The emerging channel is accompanied with a sharp change of electric field during the beginning of the discharge. The propagating streamer during a cloud flash, according to Proctor, emits radiation from near the tip of the advancing leader, in contrast to the stepped leader which radiates from both extremities as well as in the intervening channels. Four isolated regions were presented in the horizontal projections of the source locations. It is reasonable to assume that these sources would in some way be connected if all the VHF noises were identified.

Proctor classifies two types of cloud flashes in accordance with the pulse rate of the emitting cloud. The low pulse repetition frequency (prf) flash emits about 2000 pulses/sec while the high prf flash emits about 30,000 pulses/sec.

Proctor (1974a) correlates VHF noise source locations with the weather radar precipitation echoes. Some flashes were contained almost entirely in the regions of heavy precipitation. Some of the streamers terminated at the end of the precipitation echoes. Some other flashes followed the path of highest reflectivity gradients. The radar correlation reported was performed using a constant altitude plan position indicator (CARPI).

Proctor (1974b, 1974c, and 1974d) consist of three special reports published by the Council for Scientific and Industrial Research (CSIR) in Johannesburg, South Africa. These reports deal with the sources of cloud-flash spherics, instantaneous spectra of spherics, and VHF radio pictures of lightning. Next we give our views of the significant findings in these reports which have not been discussed previously.

Simultaneous recordings of the radiation field of lightning flashes were performed at one site. The selected frequencies were 30, 250, 600, and 1430 MHz. This experiment shows that pulses were emitted at all these frequencies for the low prf cloud flashes but were not the same, in general, for the high prf cloud flashes. This is an important result which has also been studied in recent years by Krider et al. (1979). Krider et al. compared the wideband electric field (1 KHz to 2 MHz) and the 300 KHz bandwidth RF receivers at 3, 69, 139, and 295 MHz for a distant storm (50 km away). These results illustrate that pulses were simultaneous in all these frequencies and a wideband (dc to 1.5 MHz) electric field pulse (radiation term) also occurred at the same time. Proctor determined the DTOA between the leading and trailing edges within single pulses and consecutive pulses. He could find no definite relationship between the direction of the vectors and the direction of the channel. But most vectors, either between the leading and trailing edge of the same pulse or between the trailing edge of one pulse and the leading edge of the next pulse, had a component in the direction of the channel tip.

From the study of the pulse width during cloud flashes, Proctor concluded that the average extent of the active source was about 240 meters. He claimed that channels are formed in a stepped information. This viewpoint was first proposed by Schonland et al. (1938) and later reported by Pierce (1955), Ishikawa (1960), Takagi (1961), and Krider et al. (1979).

Proctor noted that the return stroke had differences in the pulse width (in the tens of microseconds) between the different stations. He related the difference in the pulse width to the velocity of the propagating potential wave via a Doppler-type effect. Pulse width differences in the order of a few μsec were found in all wide pulses (over 50 μsec).

Proctor has estimated the amount of charge, the charge density, and the current flow during the initial phase of a cloud flash. VHF source locations during this phase propagated upwards in a path about 25 degrees off vertical. The technique used consists of determining the centroid of VHF locations every millisecond, and finding the amount of charge for the given field change. The charge density and the current are determined at each millisecond interval taking into consideration the field generated by the two point charges and the leader. Using this technique, the following parameters were determined: a) 10 Coulombs for the initial phase of the IC (fast field change), b) 1 Coul/km charge density, and c) a current of .2 kA every 3 msec. Since only one field meter was used to determine the electric field and a number of assumptions had to be used about the charge structure, these results are questionable.

The most recent work published by Proctor is his Ph.D. thesis (Proctor, 1976). Next we will present a summary of our view of the new ideas presented in his thesis.

Proctor classifies the VHF noise (253 MHz, 5 MHz bandwidth) pulses in three groups: P pulses, Q noise trains, and S pulses. The P pulses are nearly rectangular in shape with an average pulse width of 1 μ sec. By comparing the same pulses with wider bandwidth (10 MHz), Proctor claimed that P pulses were a rapid succession of very short spikes which had been smeared into one pulse by the limited receiver bandwidth. During a cloud flash these pulses appear at a rate of about 4.7 for groups of 310 μ sec intervals. The time between groups was about 1.8 msec. The Q noise trains consist of rapid successions of spikes. They are common to all flashes and are more frequent in the junction phase of a cloud flash. They appear to be related to very rapid movement of charges and

often accompany a K-change. S pulses are those that do not fit the two categories previously described. In addition, Proctor often refers to R noise as the abrupt (starting noise) pulse which is characteristic of most return strokes.

The P-type of pulse has been the subject of additional analysis. In general, it was reported that the rate of electric field change was directly related to the frequency of P pulses. That is, a sequence of P pulses indicated fast E field change while their absence indicated a reduction in the slope of the field change. P pulses seem to be emitted from regions near the advancing tip. By determining a fix at the leading and trailing edge of the pulse, propagation vectors have been found. The sources appeared to form at very high velocities near the speed of light. The directions of the vectors grouped in cones whose axes appeared to lie in similar directions for any one storm. Proctor speculated that the geomagnetic field might have some influence in the direction of the sources.

The Q noise trains and K-changes were also studied further by Proctor (1976). Of 26 Q noise trains reported in one flash, only eight had detectable K-changes and six of these were associated with positive streamers. Proctor attributed this difference to the low gain of the field meters. Contrary to Proctor, the work reported in the present finds that more than 50 percent of the Q noise trains did not show any field meter change. Our equipment was sufficiently sensitive to detect a 2 volt/meter change. The Q noise that Proctor reported was weak and only 5 out of 26 channel locations were studied. These Q noises were emitted from regions below the lower extremity of the flash. K-changes

do not always involve the main channel. Some K-changes propagated in channels which were not connected with the previous channels.

The velocity of the main channel in a cloud flash reported by Proctor was 1.7×10^5 m/sec. This value was obtained by finding the velocity between centroids 1 msec apart and located along the channel. The velocity determined in this manner during the propagation of the main channel in a cloud flash seems to be associated with the P pulses. A high velocity between 2.7×10^6 and 3.0×10^7 m/sec is associated with Q noise trains.

From the five cloud flashes reported by Proctor (1976), four extended near-horizontal while one was near-vertical. The vertical flash extended between -11°C and -52°C (6.3 to 13.0 km MSL) while the horizontal flashes developed at temperatures of 0, -7, -10 and -21°C . It is worth noting that the mainly horizontal flashes extended over a height of 5 km while the vertical flash extended over a height of 7 km. The vertical flash was associated with upward propagation of negative charge. The diameters of the concentrated VHF sources were between 100 and 600 meters. Even though some noise sources were located in a much wider diameter, Proctor attributed the wide channel to multiple branching.

Additional information in ground flashes provided by Proctor (1976) follows: (1) Dart leaders were characterized by one or more successions of wide pulses (tens of microseconds) separated by low amplitude Q noise trains. The VHF noise sources during the dart leader connected separate regions that had been previously ionized, and were not located near the dart leader path to ground. (2) There was no apparent time difference (greater than 10 μsec) between the occurrence of the electric field and VHF for the first return stroke. However, in most cases the VHF waveform

during consecutive return strokes either preceded or followed the electric field waveforms by as much as a few hundred microseconds. In two reported cases the VHF was absent during consecutive return strokes. The locations of the beginning of the return stroke were usually found near the top of the previous leader channel. The locations at the end of the return stroke were usually found 1 or 2 km above the previous return stroke sources. Very few locations were found near the previous leader channel to ground. (3) Proctor reported that the largest amount of VHF noise sources occurred during J-changes, but very little effort was spent analyzing the process. He reported near-horizontal and near-vertical J-changes and that some VHF noise sources active during J-changes occurred in sequence.

2.5 Review of Lennon's Work

Lennon (1976) described a VHF (30-50 MHz) DTOA Lightning Detection and Ranging (LDAR) "real-time" system operated at the Kennedy Space Center during the 1974-1975 period. Originally the system consisted of four remote and one central stations. During 1977 the system was extended to include six remote and one central station. Even though only three remote and one central station are needed for DTOA measurements, the additional stations provided redundancy. The remote stations were located an average of 10 km from the central station forming two Y configurations which share the central station. The system was designed to sense the log of the envelope detected VHF radiation from atmospherics in all the stations and retransmit the information from the remotes to the central station. The signals from three of the remote stations were retransmitted to the central station using 10 MHz bandwidth microwave

links (around 7.4 GHz). The signals from the other three remote stations used 5 MHz bandwidth cables. At the central station a Biomation 1010 was assigned to each of the VHF signals. Biomation 1010's were used to digitize 2048 consecutive samples with a sample every 50 nanoseconds. The output from the Biomation is transferred to the preprocessor. The preprocessor has several functions. First, it performs a reasonableness check by determining the largest signal in all the stations and by checking if the DTOA of the largest signal is within the limitations of the physical geometry. In addition, for this test to succeed, the central station largest peak has to occur first. If these conditions are met, the preprocessor is used to measure the DTOA between the largest signal in the central and each one of the remote stations. Using the hyperbolic system equations described by Holmes et al. (1951), Appendix A, two sets of three-dimensional locations are calculated. If the values of the two sets of stations do not agree within a few hundred meters, the data are rejected. Otherwise the data are stored in digital tape and displayed in a Plan Position Indicator (PPI) and a Range Height Indicator (RHI) CRT screen. Since this process takes less than 100 msec, the output locations are represented in near "real-time." Two milliseconds after the first sample, the Biomation 1010's are ready to receive a new set of data and repeat the same process.

This technique can provide very accurate fixes whenever only one large VHF pulse is detected in all the stations. Since the data bandwidth is 5 MHz and the sampling frequency is 20 MHz, this is a highly accurate system. The system accuracy is within tens of meters for X and Y, and 150 meters for Z. For a study of lightning channels, however, this processing is not adequate because a maximum of one location is determined

every 2 msec. In practical applications reasonable locations are only obtained every 5 or 10 msec. In addition, using only amplitude thresholds the LDAR system can match the wrong pulses and pass the redundancy test. Let us illustrate this problem with an example. Assume that there are two active VHF regions emitting radiation of the same magnitude, and these regions are located at any height and are a few kilometers on the opposite side of the central station. Pulses, received from the A and B regions in an interval of a few tens of microseconds, will be tested simultaneously in the Biomation. The pulse from A will be larger in the station closer to A, whereas the pulse from B will be larger in the station closer to B. Regardless of redundancy, there will be a consistent matching of pulses from A and B and meaningless results will be obtained.

The work described in this dissertation used some of the components of the LDAR system. These components were the sensors and the telemetry for the four stations. Instead of the Biomations, we recorded the 4-station (3 remotes and 1 central) VHF data on analog tape. The VHF noise from the analog tape was later digitized and processed to reconstruct the lightning VHF sources. By using a computer implemented algorithm to process the data and display the output, our technique can provide source locations every 5 or 10 μ sec. For any given flash we determine about 500 locations for every location of the original LDAR system. This abundant information permits us to study the lightning channels inside a thundercloud, not visible to any type of photography. Our computerized data processing provides tens of thousands of locations per flash after two hours of computer processing, thus far surpassing the by-hand technique used by Proctor (1976), which can determine about 1000 locations

per flash after 10 man-months of processing. However, since our data are recorded on analog tape with a frequency response between 400 Hz and 1.5 MHz, our source locations are not as accurate as those reported from the LDAR or Proctor (1976) systems. In the next two chapters we described the telemetry and data processing techniques used in this research.

CHAPTER III

DATA ACQUISITION AND PROCESSING

Figure 3.1 shows a general block diagram of the data acquisition and processing used in this research. The VHF radiation generated by lightning flashes during thunderclouds was detected at four selected ground receivers (RX), and recorded simultaneously at one station (recorder). Four VHF radiation channels were simultaneously slowed down (data pre-processing) and then digitized (A/D converter) at a rate greater than twice the bandwidth of the recorded signal. A computer algorithm, to be described in Chapter IV, was developed to determine the VHF source locations from the difference in the time of arrival (DTOA) of the four time series VHF data. The results were interpreted and related to other correlated data. In this chapter we describe the technique used for data recording, the properties of the telemetry system, the data pre-processing and A/D conversion, and other correlated measurements used to supplement this research.

3.1. Data Recording

The LDAR system used to obtain the original data consisted of a central and six remote stations forming two Y configurations, with the central station at the center of the Y. Figure 3.2 shows the station geometry. The detected VHF radiation at the remote stations was retransmitted to the central station and recorded. There were two methods of retransmission: microwave and wideband cables. Signals from

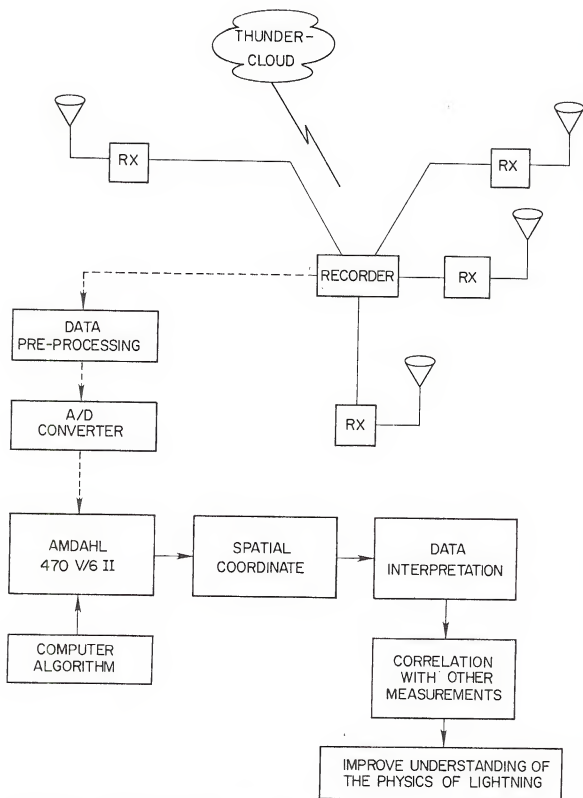


Figure 3.1. General block diagram.

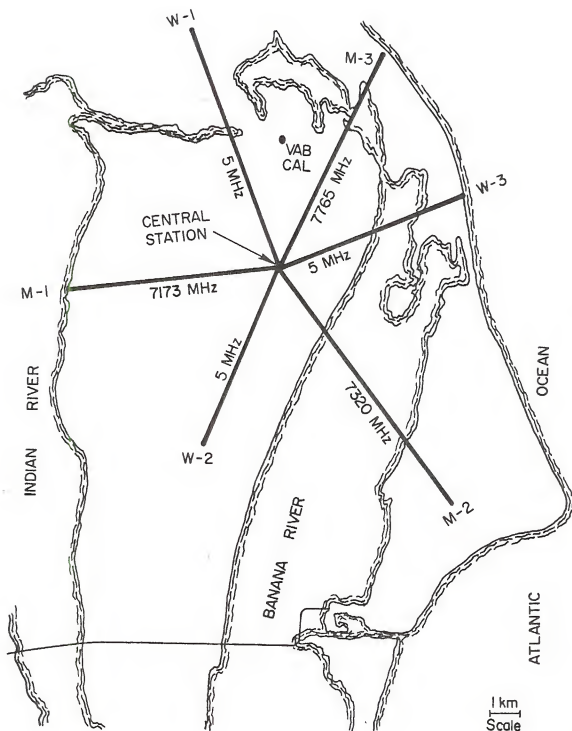


Figure 3.2. Lightning Detection and Ranging (LDAR) system geometry.

the three remote stations in one of the Y configurations (M1, M2, and M3, Figure 3.2) were retransmitted to the central station using 10 MHz bandwidth microwave links. Signals from the other three stations (W1, W2, and W3, Figure 3.2) forming the second Y were retransmitted to the central station using 5 MHz bandwidth A-2A cables. All seven VHF radiation signals were recorded at 120 ips on a 14 channel analog recorder operating in a direct mode with a frequency response from 400 Hz to 1.5 MHz. Timing information in IRIG B format (accuracy to fractions of milliseconds) was recorded on one of the remaining tape recorder channels. A minimum of four receiving stations is needed to obtain the VHF radiation used for the determination of three-dimensional locations (Holmes and Reedy, 1951). Appendix A contains a derivation of the three-dimensional locations obtained from the measurement of the difference of the time of arrival between the remotes and the central station. The baseline between the remotes and the central station in Figure 3.2 is approximately 10 km. The 10 km choice was made by KSC personnel to obtain accuracy in the order of 100 meters using a real time system for source locations within the KSC geographical area. Figure 3.2 also shows the location of the Vertical Assembly Building calibration signal (VAB CAL) used to obtain the calibration error in the measurement of source locations. An error analysis for the three-dimensional locations is shown in Appendix B. During this research there were some variations in the selection of the three remote stations for different flashes. Appendix B also shows the selected remote stations for the different flashes analyzed in this thesis.

3.2 Telemetry System

Figure 3.3 shows the telemetry system used at each receiving station. The signal $w_1(t)$ is received by a 5 meter-high linear antenna array that detects the electric field. The signal is passed through a 30-50 MHz bandpass filter (30-50 MHz for 1976 data, 40-50 MHz for 1977 data), included in the VHF receiver. Then the logarithm of the magnitude of the envelope signal is obtained using an envelope detector.

Figure 3.3 is redrawn in Figure 3.4 to show the operation of the receiving system. Here, $f_o = 40$ MHz, and the bandwidth, $2B$, is equal to 20 MHz. Figure 3.5(a) shows an approximation to the squared bandpass filter. The $g_1(f)$ filter has gain N_1 . Figure 3.5(b) shows the corresponding time domain function, $g_1(t)$, of the wideband VHF receiver.

$$g_1(t) = 2 N_1 B \frac{\sin(2\pi Bt)}{2\pi Bt} \cos(2\pi f_o t) \quad (3.1)$$

Equation (3.1) can be obtained from Figure 3.5(a) by doing the inverse Fourier Transform of $g_1(t)$. The $g_1(t)$ term consists of a slow varying waveform of the form sint/t which constitutes the envelope of the waveform $\cos(2\pi f_o t)$ which has been modulated. The output $u_1(t)$ can be written as

$$u_1(t) = w_1(t) * 2N_1 B \frac{\sin(2\pi Bt)}{2\pi Bt} \cos(2\pi f_o t) \quad (3.2)$$

where $*$ is the convolution operator.

The spectra of atmospherics from nearby lightning discharges has been studied by various investigators (e.g., Takagi and Takeuti, 1963).

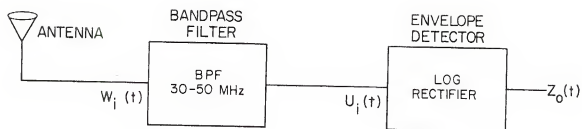


Figure 3.3. VHF receiver and envelope detector.

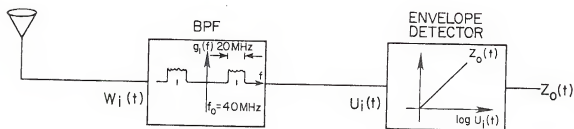


Figure 3.4. Description of VHF receiver and envelope detector.

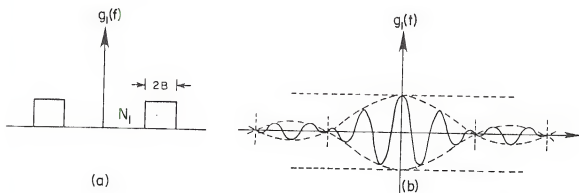


Figure 3.5. Approximation for band-pass filter: (a) frequency domain, and (b) time domain.

The general characteristics are shown in Figure 3.6(a). Figure 3.6(b) shows an approximation of the frequency domain of the signal after the VHF receiver.

The rectifier part of the envelope detector from $u_i(t)$ to $z_o(t)$ is a log IF device designed by RHG Lab with center frequency at 40 MHz for the 1976 data and 45 MHz for the 1977 data. The IF device has a 3 dB bandwidth which corresponds to the bandwidth of the VHF receiver. The device risetime is better than .05 microseconds and its dynamic range is about 80 dB. The input-output characteristic of the log IF is given in Figure 3.7. The actual values are tabulated in Table 3.1. It should be noted that the use of the log IF device is quite convenient in this application because it permits an input range from 30 microvolts (-80 dBm) to 300 millivolts (0 dBm), a factor of 10^4 , for an output range from .255 to 2.5 volts, a factor of 10.

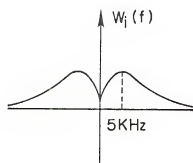
Assuming that $W_i(f)$ is constant over the frequency range of interest (30 to 50 MHz), the $u_i(t)$ can be represented as a time dependent modulation $P(t)$ multiplied by a phase displacement, i.e.,

$$u_i(t) = P(t)\cos(\omega_o t + \theta) \quad (3.3)$$

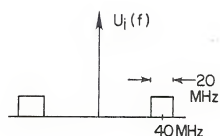
Therefore

$$\begin{aligned} z(t) &= \log|P(t)\cos(\omega_o t + \theta)| = \log|P(t)| \\ &+ \log|\cos(\omega_o t + \theta)| \end{aligned} \quad (3.4)$$

The second term will be filtered out by the envelope detector because it is at a frequency higher than 50 MHz. The $\log|P(t)|$ will be recovered at the output.



(a)



(b)

Figure 3.6(a). Input spectra.

Figure 3.6(b). Spectra after the VHF receiver.

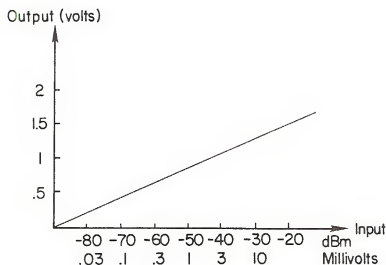


Figure 3.7 Log IF input-output characteristics.

Table 3.1. Log IF Test Values

Input (dBm)	Output (volts)
-80	.255
-70	.542
-60	.798
-50	1.090
-40	1.394
-30	1.675

$$z(t) = \log|P(t)| \quad (3.5)$$

The $z(t)$ signal represents the time dependent logarithmic envelope of the VHF radiation.

From standard envelope detection treatment (e.g., Thomas, 1969; Davenport and Root, 1958), we know that the frequency spectrum of $z(f)$ is concentrated in several regions as shown in Figure 3.8. The $z(t)$ output data is recorded on analog tape with a frequency response from 400 Hz to 1.5 MHz. Figure 3.9 shows the frequency content of the signal that is recorded in the tape recording channels. The $z_o(t)$ signal is composed of unipolar pulses. Since the recorder had a 400 Hz lower cutoff frequency, the VHF radiation out of the recorder has no frequency component below about 400 Hz and is roughly symmetrical about the center-line through the radiation.

3.2.1 Description of Center Frequency, Bandwidth, and Magnitude Level in the Telemetry System

3.2.1.1 Center Frequency. The choice of the 30 to 50 MHz range for the band-pass filter was made for various reasons. First of all, the lower limit was selected above the HF range where multiple reflection of the ionosphere will occur disturbing the signal (Horner, 1964; Pierce, 1976). Furthermore, the upper frequency limit was chosen below the VHF band for television channels, FM radio, and other sources of interferences. Thus the use of the 30-50 MHz range reduces the noise level. In addition, previous work (Oetzel and Pierce, 1969; Cianos et al., 1972) on measuring the radio emissions from lightning have proved that the largest number of detectable radiation pulses are present between 20 and 100 MHz. As the frequency increases above the HF range,

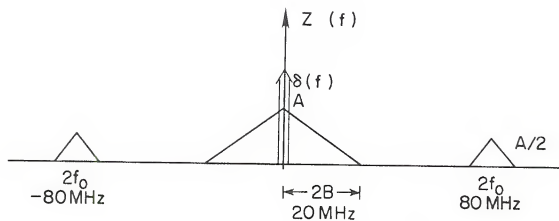


Figure 3.8. Frequency spectrum at the output of the envelope detector.

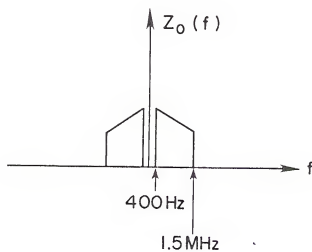


Figure 3.9. Frequency spectrum at the recorder.

the number of pulses and their magnitude decreases. Oetzel and Pierce (1969) claimed that the maximum signal-to-noise ratio is obtained between 20 and 100 MHz. Probably the lower part of the VHF range, around 30 MHz, is the ideal center frequency to study lightning radiation channels.

3.2.1.2 Bandwidth. The receiver bandwidth is an important factor in determining the pulse characteristics. It is desirable to use wideband receivers, since if narrow bandwidths are used, the detected radiation pulses will appear almost identical making cross-correlation difficult. The minimum pulse width detected in a telemetry system is inversely proportional to the receiver bandwidth and the minimum rise-time is the reciprocal of the bandwidth. Therefore, a VHF receiver with a narrow bandwidth of 1 KHz will only detect pulses equal or greater than 1 msec. Studies performed by Oetzel and Pierce (1969), Pierce (1977), and Proctor (1976) have shown that the maximum number of VHF lightning radiation pulses ranged between 10,000 and 500,000 pulses per second. That is a maximum pulse repetition rate of a pulse every 20 μ sec. In order to measure time difference between the individual pulses, resolution of about one microsecond is needed, which requires a bandwidth of 1 MHz. However to determine lightning source locations to an accuracy of hundreds of meters, time differences must be measured to a fraction of a microsecond (Appendix B). With the exception of Lewis (1960), who used a bandwidth of 41 KHz with center frequency in the VLF range, all the recent researchers who have measured the difference in the time of arrival on radiation from lightning have used a wideband system and a center frequency in the VHF range (e.g., Proctor (1971), bandwidth 5 MHz with center frequency at 253 MHz; Taylor (1973), bandwidth 60 MHz

with center frequency at 50 MHz; Cianos et al. (1972), bandwidth of 10 MHz with center frequency at 30 MHz). In the work reported herein a 20 MHz bandwidth centered at 40 MHz is used for 1976 and a 10 MHz bandwidth centered at 45 MHz is used for 1977 data.

3.2.1.3 Amplitude. Oetzel and Pierce (1969) summarized previous work on amplitude spectra of the radiation from lightning between 100 KHz and 10 GHz. The receiver bandwidths were normalized to 1 KHz and to 10 km range. The various data after normalization agreed within an order of magnitude. On the basis of those results, we have determined that the signal amplitude at 40 MHz with 20 MHz bandwidth is about 30 mV/m at a range of 10 km. The relative magnitude of the VHF radiation signals reported herein vary between a noise level of -70 dBm (.1 mv) and a maximum detected amplitude about -20 dBm (30 mv), a factor of 300.

3.3. Data Pre-Processing and A/D Conversion

Analog tapes containing six randomly selected lightning flashes recorded in the Kennedy Space Center, Florida, were sent to Eglin AFB for digitization. Figure 3.10 shows the digitization process used at Eglin AFB. The data pre-processing and A/D conversion consisted of four different steps, three of which were the slow-down process, the final step was the digitization process. The selected time intervals were first slowed down by a factor of 4 in a direct-recording-reproduce mode. The purpose of this step was to reduce the upper frequency content of the data from 1.5 MHz to 375 KHz. Using the direct mode the recorded lowest frequency range will be multiplied by the slow-down factor, that is, from 400 Hz to 1.6 KHz. Since the wider pulses observed in the final processed data were in the neighborhood of 200 μ sec, limiting the

EGLIN AFB
ADTCADUA (MATH LAB)

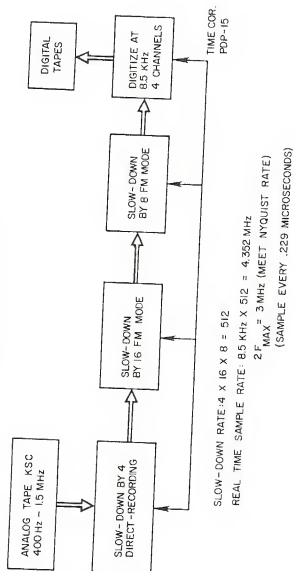


Figure 3.10. Slow-down and digitization technique used at Eglin AFB.

pulse risetime to $1/1.6 \text{ KHz} = 625 \text{ } \mu\text{sec}$ did not reduce the information content. The significant aspect of this step was to reduce the bandwidth of the analog data to within 500 KHz, the maximum available bandwidth for FM modules. The remaining two slow down processes used FM modules, first a factor of 16, then by a factor of 8. The FM modules were used because they maintain the low frequency content of the data. As part of the latter slow-down process, the four channels containing the desired information were digitized simultaneously at a rate of 8.5 KHz. Since the total slow-down rate was $4 \times 16 \times 8 = 512$, the real time sample rate became $8.5 \text{ KHz} \times 512 = 4.352 \text{ MHz}$. This sample frequency is well beyond the Nyquist rate of two times the maximum tape frequency. Using this high sampling rate, digitized points can be linearly interpolated with straight lines without significant loss of characteristics (Jerri, 1977).

Time correlation is an important factor of the slowing down and digitization process. The original IRIG B recorded in the tape is still readable during the first factor of 4 slow-down. At this stage a different IRIG A (ten times faster than IRIG B) is recorded on a different channel and the initial desired processing time is converted to the new IRIG A code. In the next slow-down (a factor of 16), the previous IRIG A is still readable and a new IRIG A is introduced. The desired starting time is converted from the previous IRIG A to the new IRIG A. During the final slow-down process (a factor of 8), a time code generator automatically reads the initial converted starting time, which is typed in as part of the program, and starts digitizing when this time is reached. Although the initial absolute time can only be read in millisecond or a fraction thereof, from the original IRIG B timing

signal, the time difference between different events in the same flash is only limited to a maximum of two or three microseconds due to tape stretching. This procedure of time conversion allows us to read accurately the original time-of-the-day with an absolute resolution of about 100 μ sec.

The twelve seconds for the six selected lightning flashes were expanded to $12 \times 512 = 6144$ seconds prior to digitization. The 6144 second data were digitized at 4.352 MHz for a total of 52.244×10^6 sample points per channel or 208.9×10^6 total samples for the four channels. The digitized data were recorded using 2400 feet, 7 track, 800 bpi, digital tapes. Approximately 1.638×10^6 samples per channel can be stored on a 7 track tape. Therefore about $52.244/1.638 = 32$ tapes were needed for processing.

The tapes containing the calibration pulses were processed in a manner similar to the one previously described for the lightning data. Two differences were noted: 1) there was no need to convert timing information, and 2) the digitization rate was increased to 8 MHz, a sample every 115 nanoseconds. Appendix B shows the uncertainties in the three-dimensional locations due to the calibration error.

3.4 Electric Field Meters

The waveforms recorded by the electric field measuring systems of the University of Florida (U of F) and New Mexico Institute of Mines and Technology (NMINT) were used for correlation with the radiation field. The electric field measuring systems used by U of F were similar to that described by Fisher and Uman (1972) and later by Krider and his co-workers (Krider et al., 1975, 1977). The correlated waveforms from the U of F electric field system for 1976 consisted of an FM channel with a frequency

response from DC to 20 KHz and a direct recording channel with frequency response from 300 Hz to 300 KHz. The electric field input to the recorder had a response from 0.2 Hz to 1.5 MHz. In 1977 the recording system was improved such that the analog data was recorded with a FM frequency response from DC to 500 KHz, and a direct recording with a frequency response from 400 Hz to 1.5 MHz.

The correlated waveforms from the NMIMT electric field stations consisted of a network of nine stations spread out over the KSC area (Krehbiel et al., 1974). The electric field sensed at eight remote sites was retransmitted as amplitude modulation over a microwave telemetry link to the central station (station nine). At the central station the electric field from all the stations was recorded on analog tape. The NIMIT electric field meter had a system decay of 10 sec and a frequency response from 0.1 Hz to 5 KHz.

KSC IRIG B time code information was stored in all the analog tapes containing electric field information. Time correlation between any of the electric field stations and the four LDAR VHF radiation data was accurate to one hundred microseconds.

3.5. Charge Locations Derived from Electric Field Stations

The electric field (E) detected at a horizontal distance d from a charge Q at a height z from a perfectly conducting ground plane is given by Uman, 1969, pp. 48-49.

$$E = \frac{2 Q z}{4\pi\epsilon_0 (z^2 + d^2)^{3/2}} \quad (3.6)$$

where ϵ_0 is the permittivity of free space. The term d^2 can be expressed

as

$$d^2 = (x-x_i)^2 + (y-y_i)^2 \quad (3.7)$$

where (x_i, y_i) is the ground coordinate at the electric field station.

Therefore the electric field at any station can be expressed as

$$E_i = \frac{2 Q z}{4\pi\epsilon_0 ((x-x_i)^2 + (y-y_i)^2 + z^2)^{3/2}} \quad (3.8)$$

Assuming a one point charge model where the charge Q at (x, y, z) is removed producing a field change E_i , four electric field measurements are needed to determine the four unknowns Q , x , y , and z . Fitzgerald (1957) obtained an analytical solution for this equation when the ground-based electric field stations were located at the vertices of a parallelepiped. Krehbiel et al. (1974) derived an analytical solution to equation (3.8) without limiting conditions, assuming that a solution does exist. The solutions obtained from a set of four stations using this technique were 1 to 3 km away from each other because the electric fields at each station were slightly in error. However when several solutions of a group of four stations were used, about 75% of the solutions fell in a volume of 1 or 2 km³. This is a reasonable technique for finding the charge center neutralized by return strokes whenever $d \gg z$. When d is comparable to z , the point charge model is not a reasonable approximation to finding the value of Q and its location, and a solution using this model usually does not exist.

Jacobson and Krider (1976) improved the analytical solution derived by Krehbiel et al. (1974) using a nonlinear least square iteration technique where all the electric field stations are considered. Iterations are

performed to determine Q , x , y , and z which minimizes C^2 in

$$C^2 = \sum_{i=1}^N \frac{E_{mi} - E_{ci}}{\sigma_i}^2 \quad (3.9)$$

where E_{mi} and E_{ci} are the measured and calculated field, N is the number of measurements, and σ_i is the measurement error. The values of the charge centers presented in this thesis, unless specified otherwise, have been obtained using the least square technique as described by Krehbiel et al. (1979).

A reasonable model for the charge neutralized during some lightning phases, especially J-changes and the intracloud discharge, consists of a point charge which we move from height h_2 and horizontal distance d_2 to a height h_1 and horizontal distance d_1 . The change of electric field is (Uman, 1969, p. 70),

$$E = \frac{2Q}{4\pi\epsilon_0} \left(\frac{h_2}{(h_2^2 + d_2^2)^{3/2}} - \frac{h_1}{(h_1^2 + d_1^2)^{3/2}} \right) \quad (3.10)$$

where Q is the charge moved and ϵ_0 is the permittivity of free air. The values of d_2 and d_1 are expressed as

$$\begin{aligned} d_2 &= ((x_2 - x_1)^2 + (y_2 - y_1)^2)^{1/2} \\ d_1 &= ((x_1 - x_1)^2 + (y_1 - y_1)^2)^{1/2} \end{aligned} \quad (3.11)$$

Seven parameters are needed to solve equation (3.13), namely, the coordinates of each of the ends and the charge involved. Jacobson and Krider (1976) extended their application of the nonlinear least square fit to solve equation (3.10).

3.6 Charge Locations Derived from VHF Noise Sources

The VHF radiation during initial and subsequent stepped leaders has unique properties. The stepped leader VHF radiation has lower amplitude and higher frequency than any other event during a lightning flash. Initial stepped leaders are preceded by lower frequency pulses with higher magnitude that we have called the preliminary breakdown (PB). Similarly, stepped leaders before subsequent strokes are preceded by higher magnitude pulses which characterize the J-process. In addition, the beginning of subsequent stepped leader VHF radiation is often accompanied by correlated change of slope in the electric field record. During the entire first stepped leader VHF radiation, significant correlated electric field change is detected. However, stepped leader electric field change has been detected as much as 1.2 msec prior to the first stepped leader VHF radiation which corresponds to about 2 km change in the VHF sources. These properties are discussed in detail in Chapters V and VI. In this section we discuss the use of VHF noise sources to determine the charge value and its location.

On the basis of the above statements, we have chosen the noise source location where the VHF radiation changes characteristics from PB or J-change to stepped leader. The location of this point charge which will be lowered to ground by the stepped leader-return stroke process. This is a reasonable assumption since stepped leader VHF sources are detected from this point on and throughout most of its path to ground. We have proceeded to solve equation (3.8) for the value of the point charge (Q). The value of (x,y,z) in (3.8) corresponds to the VHF source for the beginning of the stepped leader in the VHF record; the value of (x_1,y_1) and E_1 are the ground coordinates and electric field change

during the correlated electric field change. Since the electric field records from at least eight ground stations in the KSC area were provided by Krehbiel (private comm.), we could verify our results by using different electric field stations. We found that as long as the horizontal distance from the electric field station to the point charge source was further than the height of the source, our charge calculation was within 20% for the E-field at each station. Throughout this work, we selected an electric field station which gave results in the middle of the 20% deviation. The fact that we obtained inconsistent results for a horizontal distance less than the height is an indication that a point charge is not a good approximation within this range. For all the stepped leader-return stroke studied in this thesis, we have calculated the value of its charge source using this technique and whenever available we have compared this result with the values obtained by Krehbiel (private comm.) using the technique described by Krehbiel et al., (1979). As we shall see, our results compare well with those of Krehbiel for charge magnitude and location.

CHAPTER IV

COMPUTER ALGORITHM FOR LOCATION OF LIGHTNING CHANNELS

One important task of this research is the development of an algorithm to measure time delays between every "identifiable" pulse detected at the central and at the three remote stations. From the measured time delays, the three-dimensional locations of the VHF radiation sources are determined by using hyperbolic equations (Holmes and Reedy, 1951). In this chapter, we review the available techniques for determining time delays, and then we describe the technique chosen for the present study.

4.1 General

Two types of computer processing are performed as part of this thesis: First, we determine and display locations as calculated from the measured time delays. Second, we determine a data model for the VHF radiation time series data. The first task is described in this chapter whereas the second task is studied in Chapter VI.

Since the Second World War the measurement of time delays has been an important aspect of engineering work. Some important applications of time delay measurements over the last 30 years include:

- a) Radar technology based on the measurement of time delay between a transmitted and a received pulse (Skolnik, 1962). Some of the applications required estimating the distance to other planets.

- b) Navigation (Aircraft, Missile, Vessel). Time delays are widely used in the field of aircraft and missile navigation to determine a location update (Holmes and Reedy, 1951). The LORAN worldwide system presently used for civilian and military aircraft navigation update is based on the measurement of time delay between signals at known positions to determine the aircraft position (Pitman, 1962).
- c) Seismic signal processing for oil and gas (Wood and Treitel, 1975). Time differences between reflected seismic signals map structural deformation and provide the locations of oil and natural gas layers.
- d) Ground response to earthquake conditions (Enochson, 1973). The time difference at two separate ground locations is used to determine the transit time of particle velocity waves through soil when activated with earthquake loading conditions.
- e) Digital signal processing. Measurement of time delays between a stimulus and a response to a system or between two time series has wide applications in the field of communication (Roth, 1971).
- f) Determination of lightning channels. Oetzel and Pierce (1969) proposed the determination of lightning channels by measuring the time delays between four stations. A similar technique was independently implemented in South Africa in 1968 and described by Proctor (1971). In the USA a real-time system was developed by Lennon (1975).

4.2 Data Characteristics

In order to find a systematic technique for measuring the difference in the time of arrival between four data channels, it is necessary to study

the properties of the multiple channel VHF radiation and the properties of the time-series data.

4.2.1 Properties of the Multiple Channel VHF Radiation

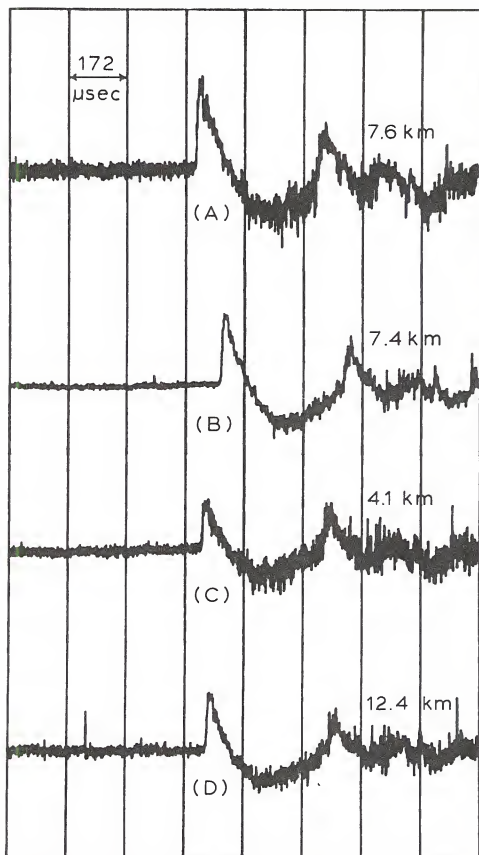
Some of the important properties of multiple channel VHF radiation are as follows:

1. The VHF radiation received at the three remote stations was retransmitted to the fourth station (central). Since VHF radiation was also recorded at the central station, any radiation pulse, from anywhere in space, identified at the central station will arrive before the arrival of the same pulse retransmitted from the remote stations. Figure 4.1 shows an example of the four channel VHF radiation. The signal from the central station (A) arrives before the signal from the three remote stations (B, C, and D).

2. Since the radiation field is inversely proportional to the distance from the space source location to the ground receiving stations, there are differences in the magnitude of the radiation at each of the stations. For ease of comparison the four channels are normalized with respect to the central station. The amplitude normalization has no effect in the shape of the pulses and provides a more effective comparison between the four stations' data.

3. From equation (2.1) we know that the radiation field is proportional to the sine square of the angle between the center line of the radiating element and the line to the ground station. Therefore, some high amplitude pulses in a ground station with an angle near 90° might fall within the noise level in another station 20 km away with an angle near 180° . This will be the case for a near-vertical radiating source located immediately above a ground based station. In this case $\theta = 180^\circ$

Figure 4.1. Four channel VHF radiation directly from the recorder for the beginning of the intracloud flash occurring at 181416 UT on 8th August 1977. (A) is the VHF radiation at the central station 7.6 km from the discharge. (B), (C) and (D) are the VHF noise for the remote stations, 7.4, 4.1, and 12.4 km from the discharge, respectively.



for that station and no VHF radiation is detected whereas significant radiation is located at the other stations.

4. Since the analog tape direct recording follows a Butterworth response with a 3 dB drop-off at 400 Hz and 1.5 MHz, only pulses with an original period between 2.5 msec and 0.66 μ sec could be properly measured with this recorder bandwidth. The largest pulse width measured was about 500 μ sec; therefore, the lowest recorder frequency did not limit the characteristic of the data pulses. In addition, we studied the characteristics of the VHF pulses obtained with a 5 MHz bandwidth using the Biomation 1010 in the LDAR real-time system. We determined that about 5% of the VHF pulses had a width between 0.2 and 0.6 μ sec. These pulses and any shorter ones were lost in our analysis.

4.2.2 Properties of the Multiple Time-Series Data

We displayed some selected data with a 10 dB signal-to-noise ratio, from the four channels, with a resolution of 1 μ sec per cm for the purpose of studying the characteristics of the pulses in the series. From this display we manually determined the DTOA between identifiable pulses. Some of the important characteristics that we identified are listed below:

1. With the exception of the stepped leader radiation discussed in Chapters V and VI, the time-series data contained an envelope with pulse widths between 5 and 500 μ sec. In addition, there were higher frequency pulses of a pulse width usually less than 3 μ sec superimposed on the envelope.

2. To identify uniquely the same pulse on any two of the time-series, two selection criteria were used. First, we matched the lower frequency envelope on which the pulses were superimposed. Second, we

identified the corresponding pulses within the envelope. When we performed our manual matching of pulses, we attempted to determine a minimum time interval needed for a unique identification of the envelope. After studying different sections of the data, we determined that the minimum sample interval to uniquely characterize the envelope was about 100 μ sec. In addition, we attempted to determine a time interval required to uniquely identify the duration of the individual pulses which are superimposed in a selected time interval of 100 μ sec. Our results indicated that a maximum interval of about 3 μ sec was required.

3. An additional test that we performed was to pass the time-series data through a low pass filter that eliminated all pulses wider than 10 μ sec. When we attempted to match the individual pulses manually, we were only 20% successful. On the other hand, when we smoothed the data, getting rid of the high frequency pulses, we were 100% successful on matching the envelope for a sample interval of about 100 μ sec. In the latter test, we have lost information on the individual high frequency pulses.

4. To determine some additional characteristics of the time-series, we measured the time delays of 185 consecutive individual pulses between the central and each one of the remote stations in one flash and 50 pulses in another flash. We learned that time delays for over 95% of the consecutive pulses are within a ± 2.5 μ sec interval.

4.3 Technique for Determining Delays Based on the Data Characteristics

Our next step was to develop a computer algorithm to determine time delays based on the data characteristics of our time-series. To meet the data properties in Section 4.2.2, we chose to use cross-correlation

and pattern recognition techniques. On the basis of Sections 4.2.2(1) and (2), we decided to use cross-correlation functions with sample intervals of 94 or 376 μsec , which correspond to either one or four blocks of digital data, to determine the time delay of the envelope signal. To comply with property 4.2.2(3), we smoothed the data before the calculation of the time delays. The smoothing was performed by using moving averages of 16 data samples across the cross-correlated interval. The peaks of the cross-correlation functions were used to determine the cross-correlated time delays and the corresponding locations. The cross-correlation functions are weighted toward the locations of the envelope pulses in the sample interval. Once the cross-correlation DTOA's are known, the computer uses a pattern recognition scheme to identify the DTOA between individual events in the envelope-detected signal. A search over a $\pm 3.7 \mu\text{sec}$ interval around the cross-correlated DTOA's is used. This time interval was chosen to comply with the properties of the time-series described in Section 4.2.2(2). Next we present a description of the cross-correlation and pattern recognition techniques.

4.3.1 The Cross-Correlation Function

The cross-correlation technique we use has been applied in a variety of fields, e.g., statistical theory of communication (Lee, 1960), geophysics (Enochson, 1973), biomedical engineering (French and Holden, 1977), radar detection (Skolnik, 1962).

Let x_n and y_n be two time-series. In our application y_n can be the central station data while the x_n can represent any of the remote stations. The discrete cross-correlation function between x_n and y_n can be defined as

$$R_{xy}(j) = \sum_{n=0}^{N-1} x_n y_{n+j} \quad (4.1)$$

where N is the number of data samples. Since the signal at the central station (y_n) always arrives first (property 4.2.1(1)), we have to delay the y_n signal by a certain amount τ . In addition, a noise term r_n is used to account for properties 4.2.1(2), (3), and (4), and different background noise. Therefore

$$x_n = y_{n+\tau} + r_n \quad (4.2)$$

Substituting equation (4.2) into (4.1), we get

$$R_{xy}(j) = \sum_{n=0}^{N-1} (y_{n+\tau} + r_n) y_{n+j} = \sum_{n=0}^{N-1} y_{n+\tau} y_{n+j} + \sum_{n=0}^{N-1} r_n y_{n+j} \quad (4.3)$$

or

$$R_{xy}(j) = R_{yy}(j - \tau) + R_{ny}(j) \quad (4.4)$$

Depending on the cross-correlated value of the noise $R_{ny}(j)$, the peak value of $R_{xy}(j)$ will occur in the neighborhood of $j = \tau$. Our task is to find the maximum value of R_{xy} and see what the lag τ is for a maximum. If data from ensemble averages of x_n and y_n are processed, the cross-correlated noise term can be averaged out and a more accurate value of R_{xy} can be determined. However each selected interval of the multiple series has different time delays and additional data for averaging is not available. In addition, the VHF radiation properties 4.2.1(2) to (4) indicated that there might be substantial differences between the data recorded in the different stations.

The cross-correlation function $R_{xy}(j)$ was normalized as

$$r_{xy}(j) = R_{xy}(j) / \left(\sum_{n=0}^{N-1} x_n^2 \sum_{n=0}^{N-1} y_n^2 \right)^{\frac{1}{2}}, \quad -1 \leq r_{xy}(j) \leq 1 \quad (4.5)$$

To prevent any error due to ambiguous selection of $r_{xy}(j)$ when the function flattens out near maximum, four decimal digits are used for comparison. For S/N greater or equal to 10 dB the optimum value of $r_{xy}(j)$ ranged between 0.9300 and 0.9850. Once the four station time-series data are cross-correlated for a selected time interval of either 94 or 376 μsec , the procedure is continued for the next interval. For the cross-correlation function to be applied the signal level must be greater than the noise level. Before the beginning of the flash, the noise threshold level is calculated and the data is not processed if the S/N is equal to or less than 0 dB.

Once we have determined the cross-correlated time delays, we need to calculate the time delays of the higher frequency pulses superimposed on the envelope (see properties 4.2.2(1) and (2)). To achieve this task we used pattern recognition techniques.

4.3.2 The Pattern Recognition Technique

Widrow (1974) has divided the field of pattern recognition into two broad schools: the first group classifies the data by comparing individual features with a pattern recognition list, the other group attempts to fit the data to some type of template matching. Gottman and Gloor (1976) working in electroencephalogram and Weinberg and Cooper (1972) working in neurophysiology applied the first and second pattern recognition techniques, respectively, obtaining successful results. Additional pattern recognition applications include

chromatograms (Widrow, 1974), speech (Boudry and Dupeyrat, 1974), and picture rasters (Erich and Foith, 1976). We classified our data with a pattern recognition list similar to those described by Gottman and Gloor (1976). Before we could apply the pattern recognition list to match the individual pulses around the cross-correlation time delay, we had to define a pulse model. Next we provide our pulse model definition.

4.3.2.1 Pulse Model. We divided the four time-series in subsets of 3.7 μ sec (16 samples), roughly the maximum pulse rate for which the data could have the identifiable characteristics needed for pattern recognition. Then, the sample value which corresponds to the peak of the data subset is determined. This sample value is needed to perform peak recognition of the time-series. The peak recognition is performed as follows: 1) We determine the time delay for the cross-correlated interval of either 94 or 376 μ sec between the central and each of the remote stations. 2) We determine the time at which peak values occurred for each data subset within the 94 or 376 μ sec interval for all the time-series. 3) We add the time value of (1) and (2) above to obtain the corresponding cross-correlated value in the remote stations for the peak of the pulses. 4) Finally, we determine how many peaks in the remote station are within the $\pm 3.7 \mu$ sec search interval. This procedure limits the number of peaks to be considered to a maximum of 3. At this time in the algorithm the peak recognition is completed; now we have to determine which pulse at the remote stations that produced the peaks which met (4) above, is similar to the pulse at the central station. One of these peaks within the search interval will be selected

only if the pulse that produced the peak has similar characteristics in the central and on each of the remote stations.

The pulse model used to determine whether any of the pulses from the considered peaks in the remote stations correspond to the same pulse in the central station is a) values of ascending and descending slopes, b) number of reversals in the ascending and descending slopes, and c) the total area under the pulse. Figure 4.2 illustrates a typical pulse and how we selected the additional pulse properties to complete the pattern recognition technique.

Using the guidelines of identifiable characteristics, we selected 15 sample points for pulse recognition, centering the individual peak in the middle of the pulse. The description of the individual pattern recognition features mentioned in a, b, and c were as follows: a) the ascending and descending slopes (AS and DS) were calculated by making straight line approximations between the peak and the value of the extreme of the pulse. However if the pulse increases in magnitude in three consecutive samples before arriving to the pulse boundary (7th sample), the slope was arbitrarily determined between the peak and the 5th data sample. b) The number of reversals is determined by counting the number of times that there is a change of slope and dividing this number by 2. In Figure 4.2 there are two changes of slopes to the right of the peak (reversal to the right, RR), corresponding to one reversal and there are four changes of slopes to the left (reversal to the left, RL), which correspond to two reversals. c) Since all the remote stations' data were normalized with respect to the central station, we also calculated the area under the curve as a measurement of the narrowness of the pulse (NAR). The tolerances allowed

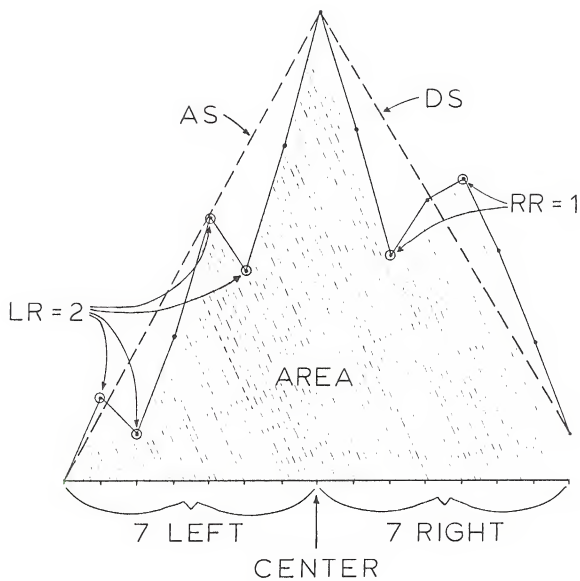


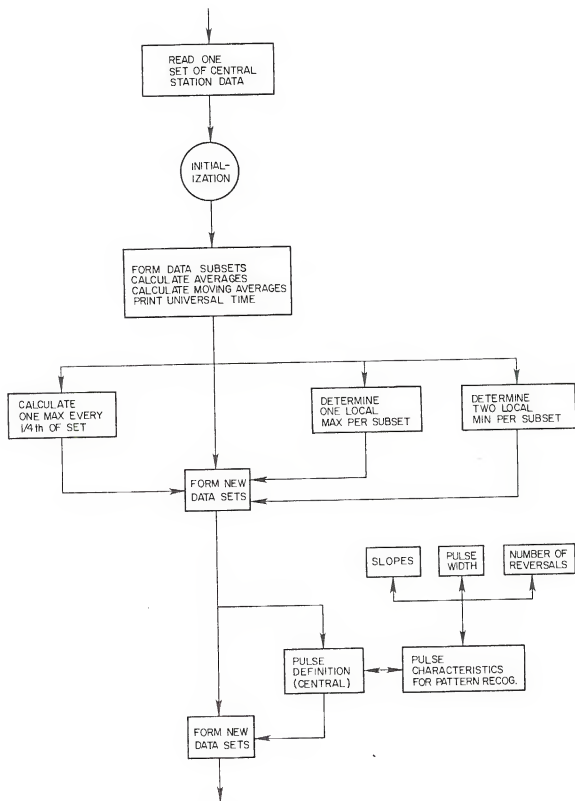
Figure 4.2. Pulse model.

in matching pulses were: a 20° difference of slope was allowed for AS and DS, one difference in reversals was allowed for RR and LR, and a 25% variation was allowed for the area under the pulse (NAR). We refer to the five additional requirements needed for selecting the individual pulses as AS, DS, RR, LR, and NAR. We weighted these factors to match the individual peaks as a function of the time interval away from the cross-correlation time delay. If peaks were selected within $0.92 \mu\text{sec}$ (4 data samples) from the cross-correlation time delay, the pulse that generated the peak was required to meet at least two of the five requirements. Stricter requirements of 3 out of 5, 4 out of 5, and 5 out of 5 were needed to match peaks between ± 0.92 and $\pm 1.84 \mu\text{sec}$ (4 to 8 data samples), ± 1.84 to $\pm 2.76 \mu\text{sec}$ (8 to 12 data samples), and ± 2.76 to $3.7 \mu\text{sec}$ (12 to 16 data samples), respectively, from the cross-correlation time delay. It is worth noting that an identifiable pulse in the central station has to pass a separate test at each of the three remote stations before a location is calculated. A failure of the pattern recognition at any of the stations will prevent the determination of a source location.

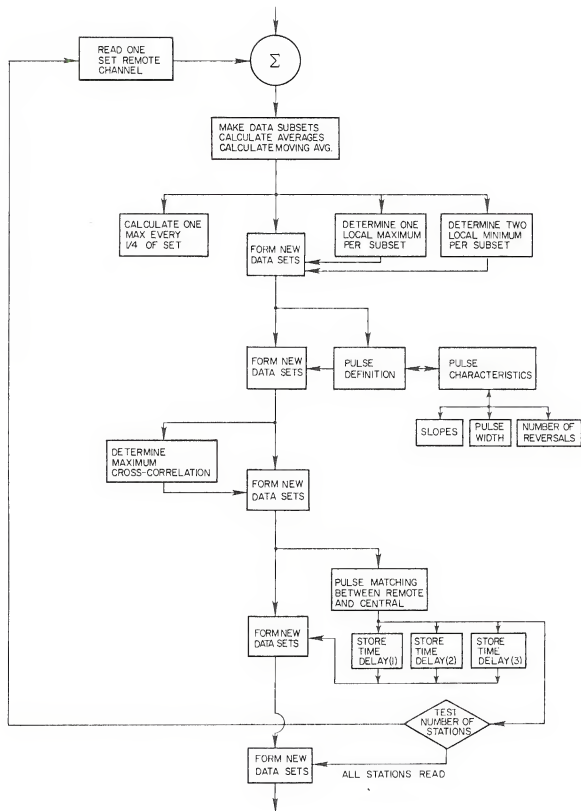
4.4 Algorithm Flow Chart

A simplified algorithm flow chart is shown in this section. This algorithm has been developed using the techniques discussed in Section 4.3. Only those most general steps are included in the flow chart. This algorithm was written in FORTRAN language using a structured programming sequence (Rogers, 1975) for execution in the AMDAHL 470-VI. For a detailed description of the procedure used, reference is made to the LITMAT program in Appendix C. In the next flow chart (Figure 4.3) a set of data is defined as the time interval for which the

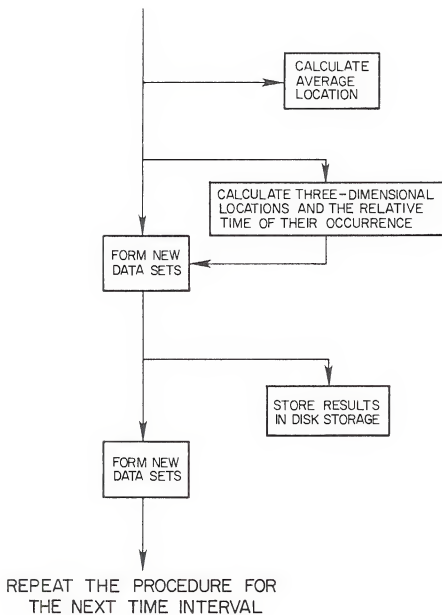
Figure 4.3. Block diagram of the LITMAT algorithm to obtain the cross-correlated and all the noise sources based on the calculation of time delays.



(a)



(b)



cross-correlation is calculated, either 94 or 376 μsec . The graph is expanded in Figures 4.3(a), 4.3(b), and 4.3(c). Figure 4.3(a) shows the algorithm initialization and the characterization of the central station. Figure 4.3(b) shows a similar technique for the remote station and its relationship with the central station to determine the time delays. Finally, Figure 4.3(c) concludes the algorithm with a determination of the three-dimensional locations. If additional data are desired, the algorithm is repeated.

4.4.1 The Algorithm Limitations

The principal limitations in the development of this algorithm are the time interval selected for the cross-correlation function and the selected features for pattern recognition. Next we provide some arguments about these limiting factors.

The longest time delay between the central and a remote station is determined for source locations near the ground and on the opposite side of the line joining the central and the remote stations. For a 10 km baseline between central and remote stations, the search for appropriate time delays should include $\pm 33 \mu\text{sec}$ from the central station data. From the test described in Section 4.2.2(3), we could have several pulses which met any given tolerances for AS, DS, RR, RL, and NAR within the $\pm 33 \mu\text{sec}$ interval. This argument implies that pattern recognition alone is not a sufficient factor for the determination of time delays. Also from Section 4.2.2(3) we learned that we were 100% successful matching the envelope of the time-series data. Therefore, the use of the cross-correlation function is an essential part of the algorithm. The cross-correlation time interval of 94 or 376 μsec was chosen on the basis of the data properties and this is one of the

limiting factors of the algorithm development. If the individual pulses within the cross-correlated interval originate from the same source or from closely scattered sources, the cross-correlation locations represent a true representation of the source locations. For example, a spark channel which propagates at a velocity of 5×10^5 m/sec will cover 47 meters during a 94 μ sec cross-correlated interval. Therefore, consecutive cross-correlation locations represent a true representation of the locations of the spark channel. We successfully determined the location of the noise sources because 95% of the DTOA's measured in consecutive pulses were about ± 2.5 μ sec from the cross-correlated value, which represents 2 or 3 km apart. However, if there were several channels located several kilometers apart or if there was at least one channel propagating at a velocity in the order of 10^8 m/sec, our locations may not represent the true location of the originating source.

4.5 Display of Three-Dimensional Locations and Their Time of Occurrence

All the VHF source locations and their time of occurrence were stored in digital tapes. The time was needed to differentiate between the different phases of a lightning flash. We developed three computer programs to display the source locations. 1) An algorithm was written to display the data in a three-dimensional isometric view. The computer code for this program is included in Appendix D. 2) The source locations were displayed in two-dimensional projections. These projections were: (a) EW-NS, (b) EW-height, and (c) NS-height. 3) Fixed histograms are generated to show the relative radius, azimuth, and elevation of the noise sources with respect to a reference point. All these visual aids are used to display the results derived in Chapter V.

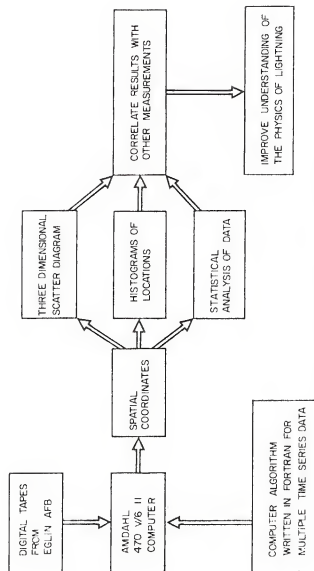
The value of computer graphics should not be underestimated. Any attempt to represent the locations by hand was tedious and resulted in large errors. All the graphics for the VHF noise and its source locations were displayed on the Gould Electrostatic Plotter of the University of Florida Computer System.

Figure 4.4 shows a computer processing block diagram. This diagram shows the procedure that we followed to process and interpret the digital input data.

4.6 Velocity of Propagation of Noise Sources

We determined the velocity of propagation of the noise sources by using the three-dimensional locations and their time of occurrence. We chose only those lightning events on which the location of the noise sources formed a channel following a regular progressing sequence. To determine whether the events followed a progressing sequence we calculated the value of the velocity of propagation using all the cross-correlated locations.

Let $P_1(x_1, y_1, z_1)$, $P_2(x_2, y_2, z_2)$, ..., $P_n(x_n, y_n, z_n)$ be the locations of cross-correlated sources at time t_1 , t_2 , ..., t_n , respectively. Then velocities of propagation can be calculated by determining the distance P_{mn} and dividing it by the time interval t_{mn} where m and n are any two sources ($m < n$). A total of $\frac{n(n-1)}{2}$ velocities can be calculated from n locations. Only about 50 or 60% of all the velocities that we obtained during the specific lightning events that we studied using the above techniques showed a velocity of propagation the same as would be found by taking the starting and ending point. Therefore, we decided to use the following procedure to determine channel velocities. 1) Determine whether the VHF sources followed a progressing sequence. A velocity of



EXECUTE IN FORTRAN II OVER 800 LINES OF CODE WITH
12 SUBROUTINES ABOUT \$1 CPU TIME PER 1 MSEC OF STORM ACTIVITY

Figure 4.4. Computer processing block diagram.

propagation is calculated only for those events on which consecutive cross-correlated locations were in the neighborhood of the previous ones, and a path was formed by displaying the noise sources in the desired process (stepped leader and some PB, K- and J-changes).

2) Determine the $\frac{n(n-1)}{2}$ velocities using all the cross-correlated source locations. 3) Test if these velocities were grouped at any specific value. A velocity value is used only if a certain value or range of value repeats for at least 50% of the test data ($n(n-1)/4$). For an additional check we determined velocities using all the individual source locations for three stepped leaders, but the procedure was quite a bit longer and resulted in the same velocity value.

The results showed that we could determine the velocities of about 50 or 60% of the events that met conditions 1), 2), and 3) simply by their starting and ending points. In addition, about 15% of the events failed condition 3) and no velocity of propagation could be determined consistently. Throughout this thesis the only velocity values found are those that met the three conditions above.

CHAPTER V

ANALYSIS OF RESULTS

This chapter presents a detailed description of six lightning flashes that occurred during the summers of 1976 and 1977 at the Kennedy Space Center. We have correlated the three-dimensional locations with other storm and lightning parameters measured (see Chapter III), primarily the electric field. We have studied four cloud-to-ground (CG) flashes and two intracloud (IC) flashes. The six lightning flashes are identified by their time of occurrence and type below:

- (5.1) 165959, a three stroke CG flash to the 150 meter weather tower on 19th July 1976 followed by an IC discharge.
- (5.2) 180710, a three stroke CG flash on 8th August 1977.
- (5.3) 181806, a six stroke CG flash on 8th August 1977 followed by continuing current.
- (5.4) 182356, an eight stroke CG flash on 8th August 1977.
- (5.5) 180644, an IC discharge at the beginning of the storm on 8th August 1977.
- (5.6) 181416, a small IC discharge on 8th August 1977.

All of the above flashes were at relatively close range, 3 to 17 km from the central station. The coordinates given throughout this thesis are referenced to the central station whose absolute coordinate in the Florida grid system is (187023,466021) meters. The three coordinate parameters given always correspond to the East-West location, North-South location, and altitude, respectively.

5.1 The 165959 Flash

This flash is the most comprehensively studied single lightning flash in the history of lightning research (Uman et al., 1978 and Rustan et al., 1979).

The flash consisted of a three strokes to ground followed by an IC discharge. The duration of the flash VHF radiation was 939 msec of which the last 600 msec were part of the IC discharge. The locations of the three charge regions for the three return strokes obtained from measuring the return stroke electric field change at multiple ground-based locations (Uman et al., 1978) correlate well with the VHF source locations. Figure 5.1 shows the relationship between the VHF radiation and the electric field for the entire discharge. Table 5.1 shows a complete summary of the identified phases of the flash. For each phase we have provided the duration of the VHF radiation, the average velocity of propagation of the noise sources (if applicable), and the upper and lower location of the VHF noise sources. An error analysis for the VHF noise source locations is given in Appendix B. Table B.1 shows a summary of the uncertainty in the determination of the locations of the sources in this flash as a function of position. In the next subsections we consider in detail what we learned from the study of different phases of the flash, given in Table 5.1.

5.1.1 Preliminary Breakdown

Observation of the VHF records for one second prior to the first stroke shows that the VHF radiation above the system noise level began 4.9 msec before the return stroke and continued until the return stroke. The first 2.2 msec of the VHF pulses we identify with the "preliminary breakdown," the final 2.7 msec with the stepped leader. The wideband

Figure 5.1. Simultaneous records of the logarithm amplitude VHF radiation observed at 10 km, and the electric field 13 km away, during the 165959 flash. The following events in the flash are shown: R1, R2, and R3 represent the three return strokes; SL is the stepped leader before R1; DL is the dart leader before R2; SDL is the stepped dart leader before R3; J1 and J2 are the interstroke processes; FR is the activity following the first return stroke, SP's are the solitary pulses; and IC is the intracloud discharge, of which the final 99 msec is not shown.

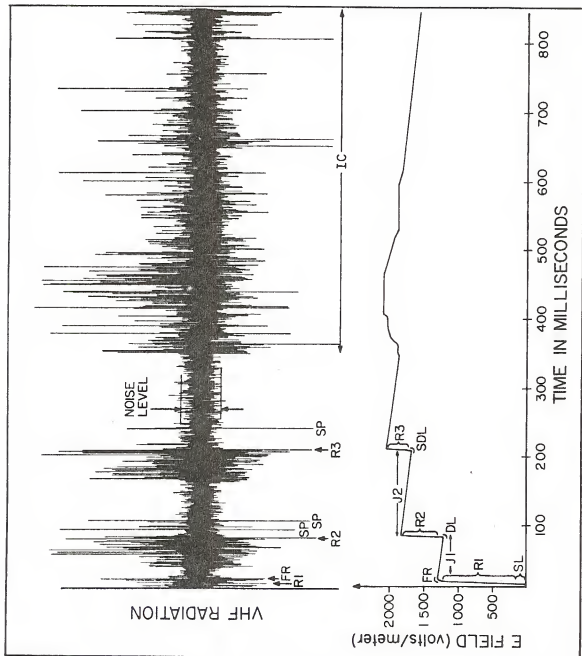


Table 5.1. Time-Table for the VHF Activity in the 165959 Flash.

Start Time (msec)	Event	Duration (msec)	Average Velocity m/sec	Coordinates (km)					
				UPPER			LOWER		
				x	y	z	x	y	z
0.0	Preliminary Breakdown (PB)	2.2	1.0×10^6	0.3	11.6	7.1	.2	10.8	5.1
2.2	Stopped Leader (SL)	2.7	$1.3 \text{ to } 7.0 \times 10^6$	0.2	10.8	5.1	-1.3	9.7	2.2
4.9	First Return Stroke (R1)	0.25							
5.15	Quiet Period	2.4							
7.55	Follow Return Stroke (FR)	4.27							
11.82	Quiet Period	15.5		0.5	12.2	7.0	1.1	10.2	1.3
27.37	VHF Portion of J1	43.27	1.5×10^5	0.0	16.0	13.7	-0.2	12.3	7.9
70.59	Dart Leader (DL)	.35	$1.8 \text{ to } 2.6 \times 10^6$	-0.1	12.0	7.8	0.3	11.2	6.6
70.94	Second Return Stroke (R2)	.26							
71.20	1st Quiet Period of J2	11.52							
82.72	SP No. 1 (SP1)	.775	$1 \text{ to } 4 \times 10^7$						
83.50	2nd Quiet Period of J2	3.2							
86.7	SP No. 2 (SP2)	.95	$1 \text{ to } 4 \times 10^7$						
87.65	3rd Quiet Period of J2	7.78							
95.43	SP No. 3 (SP3)	.57	$1 \text{ to } 4 \times 10^7$						

electric field records indicate that there is a small electric field pulse of 2 μsec width at about the time of the initial VHF radiation, but a clear correlation between VHF and electric field does not exist until the final .8 msec of the preliminary breakdown which corresponds to a steady electric field change.

Figure 5.2 shows simultaneous records of VHF radiation during 117 μsec of the preliminary breakdown that preceded the initial stepped leader. During the preliminary breakdown the log amplitude of the envelope-detected VHF noise is characterized by large pulses having a duration of 40 to 150 μsec . Superimposed on these slow pulses are pulses of 1 to 5 μsec width. Pulses 1, 2, 3, and 4 of Figure 5.2 illustrate the difference in the time of arrival of typical pulses at the four stations. The "r" value shown in the figure represents an approximate distance between the VHF source and the individual ground-based stations. The computer algorithm when applied to the data in Figure 5.2, generated source locations for pulses 1 through 4 and for 10 additional pulses.

Figure 5.3(a) shows all the 150 source locations identified during the preliminary breakdown which occurred between locations A and B. It is worth noting that most of the sources are concentrated within a cylinder of 500 meter radius and many are inside the Q_1 volume, source of the first return stroke charge (Figure 5.3(b)). Figure 5.3(b) shows the cross-correlated noise sources, 94 μsec intervals, associated with the preliminary breakdown. The cross-correlated locations are weighted toward the location of the larger pulses in the 94 μsec interval because it is these that play the dominant role in maximizing the cross-correlation function. The cross-correlated noise sources started near

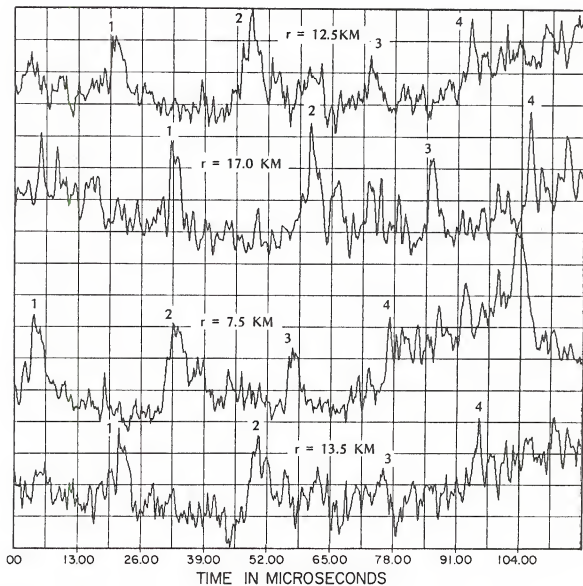
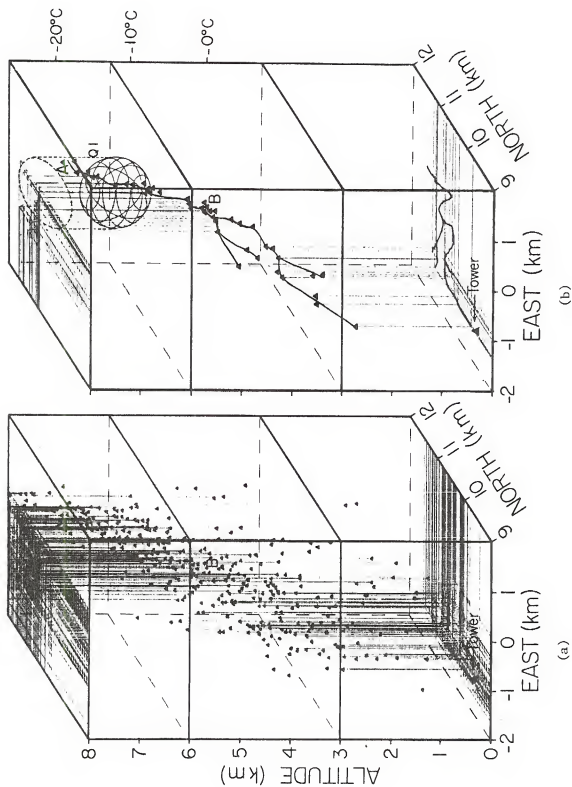


Figure 5.2. Simultaneous records of the logarithm VHF radiation at four different ground-based stations. Pulses 1, 2, 3, and 4 are identified as examples of pulses arriving at different times at different stations. The parameter "r" represents the actual distance from the stations to the cloud source.

Figure 5.3(a). All of the 422 VHF noise sources detected for both the preliminary breakdown (A to B) and the stepped leader (below B) during the first 4.5 msec of the 4.9 msec before the first return stroke.

Figure 5.3(b). Cross-correlated VHF noise sources, 94 μ sec intervals during the preliminary breakdown (A to B) and during the stepped leader (below B). The sphere Q1 represents an estimate of the volume enclosing the charge source for the first return stroke as derived from electric field records (Uman et al., 1978).



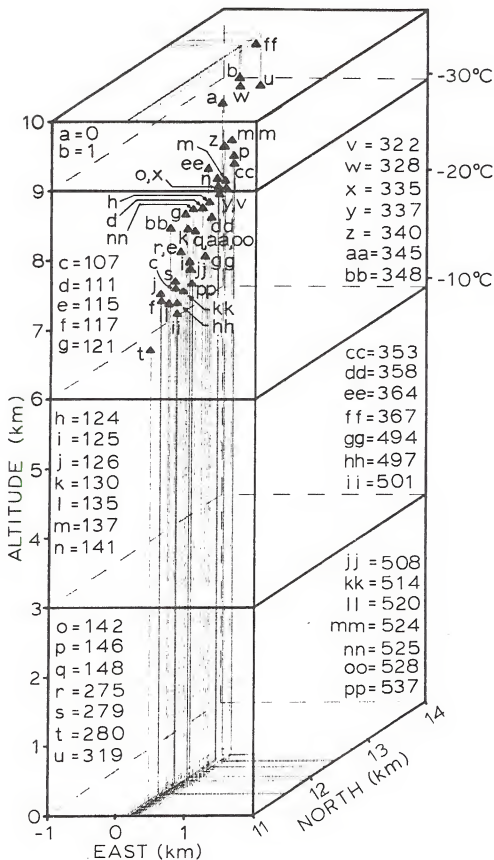
the top and the back edge of the Q1 volume and generally propagated in a downward direction. The preliminary breakdown started at a height of 7.1 km (point A at about -18°C free air temperature) and propagated a distance of 2.3 km to a height of 5.1 km (point B at about -6°C) before the first detectable slow change of the electric field associated with the stepped leader occurred. The cross-correlated source locations during the preliminary breakdown interval are very much in a straight line and exhibit an average velocity of propagation of about 1.0×10^6 m/sec.

In addition to determining the cross-correlated and all the individual source locations (Figure 5.4(b)) using the computer algorithm described in Chapter IV, we determined the individual source locations manually during the first 537 μsec of the preliminary breakdown. This task was performed to identify any propagation of the sources on a time scale of every 2 or 3 μsec instead of every 7 or 10 μsec , the limit using the computer algorithm. These results are shown in the three-dimensional graph in Figure 5.4. The sources A through RR are time tagged and shown in alphabetical order A \rightarrow Z, AA \rightarrow RR. This initial stage of the PB extends 1.5 km horizontally and 3.6 km vertically. The sequence of the VHF sources shows that the activity started at about 9 km and there was propagation initially upwards and downwards.

5.1.2 First Stepped Leader

The VHF radiation during the stepped leader consists of a low amplitude high frequency pulse train, a characteristic radiation observed during the first leader and again prior to the third stroke, but not in any other part of the flash. The stepped leader VHF is

Figure 5.4. Three-dimensional view of the VHF noise sources during the first 537 μ sec of the preliminary breakdown. The sources A through RR are time tagged (in microseconds) and shown in alphabetical order A \rightarrow Z, AA \rightarrow RR.



markedly different from the preliminary breakdown VHF which precedes it. Figure 5.5 shows the VHF noise during the stepped leader. By comparing the VHF noise during the preliminary breakdown shown in Figure 5.2 with Figure 5.5 we can see the remarkable difference between the two processes. The stepped leader pulses in Figure 5.5 have a pulse width less than one microsecond and an interpulse interval which decreases with increasing time, starting at about 11 μ sec and decreasing to about 1 μ sec. The characteristic leader pulses start about 0.8 msec after initial electric field change of the flash. The leader pulses are probably related to the electrical breakdown associated with leader steps. As the leader progresses downward it generates more branches and hence more steps and pulses per unit time. If a normal interstep time is assumed to be 50 μ sec (Uman, 1969), then at least four steps are simultaneously active during the beginning of the leader, increasing to about 50 simultaneous steps. Figure 5.3(a) shows all the 272 identified stepped leader radiation sources while Figure 5.3(b) shows the cross-correlated, 94 μ sec intervals, locations. Even though the VHF noise changed characteristics between the preliminary breakdown and the stepped leader, the source locations of the stepped leader appear continuous with that of the preliminary breakdown channel. In addition, the stepped leader sources spread horizontally as the leader moves downward, most likely due to the stepped leader branches. The individual and the cross-correlated stepped leader source locations of Figure 5.3 did not occur in a regularly progressing sequence. The channel shape shown in Figure 5.3(b) is our best estimate from an overall view of the individual locations, the cross-correlated locations, and the sequences of occurrence of the locations.

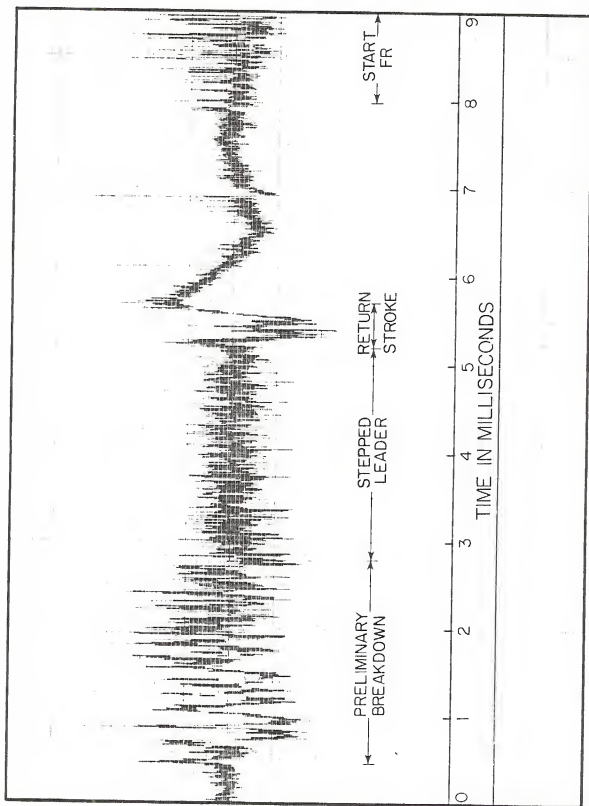


Figure 5.5. Logarithmic-amplitude VHF radiation at the beginning of the 165959 cloud-to-ground flash.

A two-dimensional view with all the detected preliminary breakdown and stepped leader sources is shown in Figure 5.6. Figure 5.6(a) shows the plan view while Figures 5.6(b) and 5.6(c) show the elevation views of all the located stepped leader sources. In both graphs, Figures 5.3 and 5.6, the 150-meter weather tower struck by the flash is shown. The weather tower is located at $(-1.1, 9.5)$. Figure 5.6 also shows the cross-correlated locations represented with circles. It is worth noting that these cross-correlated locations form a narrow channel during the preliminary breakdown, but this channel is widened at a later stage during the stepped leader process.

The velocity during the first 700 microseconds of the stepped leader ranged between 1.3 and 3.8×10^6 m/sec and during the next 1.8 msec showed a nearly linear increase from about 1.5×10^6 m/sec at about 5 km altitude to about 7.0×10^6 m/sec at 2.2 km. Although there was strong VHF radiation during the last 0.4 msec of the stepped leader, no sources were located during this time. It is probable that the pulses on the four channels could not be correlated because too many VHF sources, leader steps, were simultaneously active over a large volume.

Figure 5.7 shows three sequences of histograms of all the source locations from the beginning of the preliminary breakdown to the last detectable source in the stepped leader. The time sequences t_1 , t_2 , and t_3 in Figure 5.7 correspond to 1.5 msec intervals from the beginning of the preliminary breakdown to the end of the detected VHF sources from the stepped leader. Figure 5.7(a) is a distance histogram referenced to the weather tower, as the time progresses the radiation sources approach the 150 meter weather tower. Figure 5.7(b) and Figure 5.7(c) show polar histograms of all the radiation sources with reference

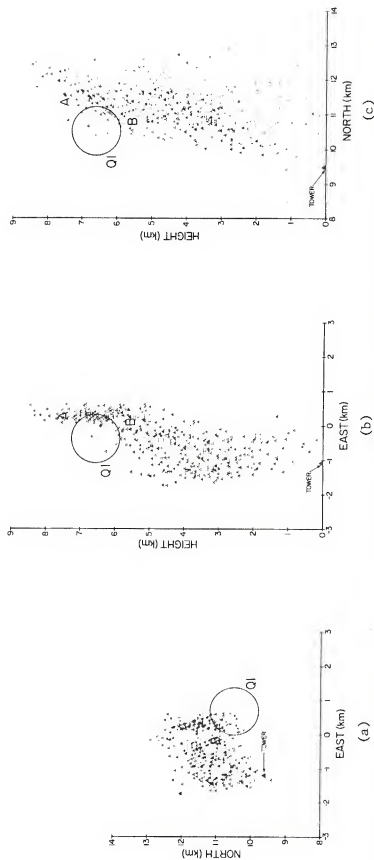
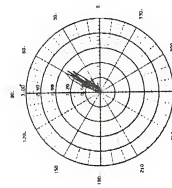
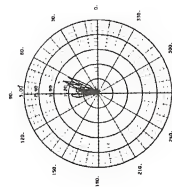
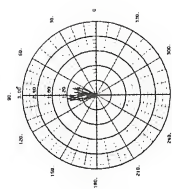
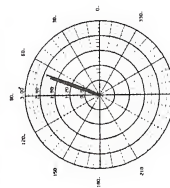
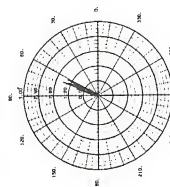
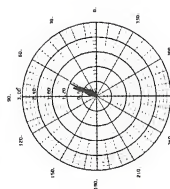
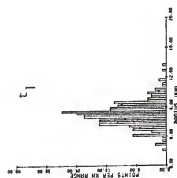
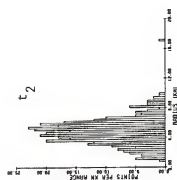
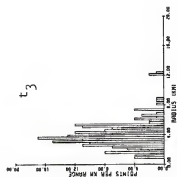


Figure 5.6. Two-dimensional views: (a) top view, EL-NS, (b) elevation view, EM-height, and (c) elevation view, ES-height of all the sources (triangles) and the cross-correlated source locations (squares), 376 μsec intervals, during the PB and first stepped leader. The circle Q1 is the two-dimensional projection of Q1 in Figure 5.3.

Figure 5.7. Three sequences of histograms, t_1 , t_2 , and t_3 (1.5 msec intervals) of all the detected sources in the PB and stepped leader. Sequences (a), (b), and (c) correspond to t_1 , t_2 , and t_3 , respectively. There are three histograms in each sequence. The top row shows distance histograms referenced to the weather tower. The middle row shows histograms of the elevation angle of the sources referenced to the weather tower. The bottom row shows histograms of the azimuth angle of the sources referenced to the weather tower.



(c)

(b)

(a)

to the spherical azimuth angle (ϕ), and the elevation angle (θ), respectively.

5.1.3 First Return Stroke

Figure 5.8 shows the VHF noise during the first return stroke. The first return stroke was characterized by small high frequency pulses riding on the envelope of a high amplitude pulse of about 250 μ sec. Only five VHF pulses could be correlated during the stroke, probably because there were too many sources active and these sources were spread over too large a volume of space. Three of the correlated sources were located along the stepped leader channel, a fourth source was located at the top of the highest average location of the preliminary breakdown, and the fifth source was located 1 km above the fourth source. The estimated total length of the return stroke channel from the tower through the five sources was 8.8 km. Since the VHF return stroke noise lasted about 250 μ sec, we estimated that the return stroke propagated at about 3.5×10^7 m/sec. Since the cross-correlated location might not be a true representation of the actual source location when a potential wave propagates in a channel at a velocity of 10^7 or 10^8 msec, return stroke velocities obtained from VHF source locations might be off by an order of magnitude.

Krehbiel (Uman et al., 1978) determined that a charge of -24 Coul was lowered by the first return stroke using the technique described in Section 3.5. We used the technique described in Section 3.6 and determined that a charge of -19 Coul was lowered by the first leader-return stroke process. Our point charge source for the transition region between PB and stepped leader in the VHF record was within 1.5 km of the location determined using multiple electric field records.

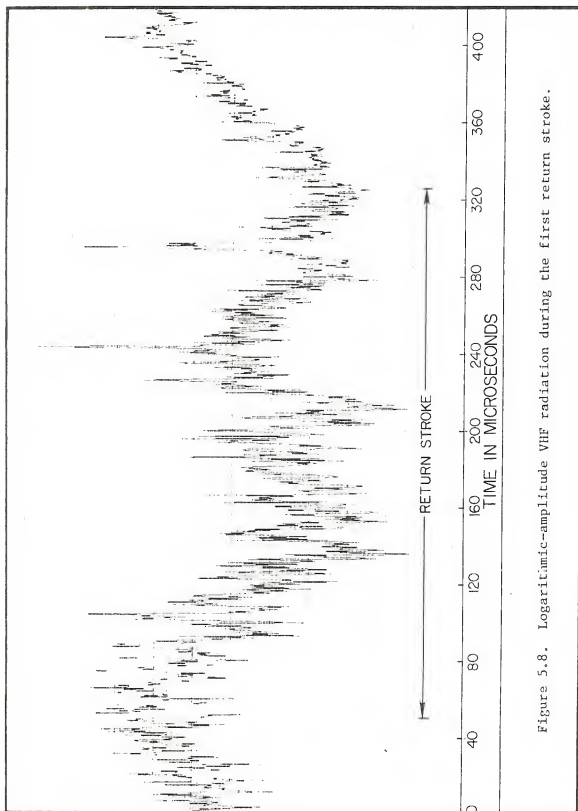


Figure 5.8. Logarithmic-amplitude VHF radiation during the first return stroke.

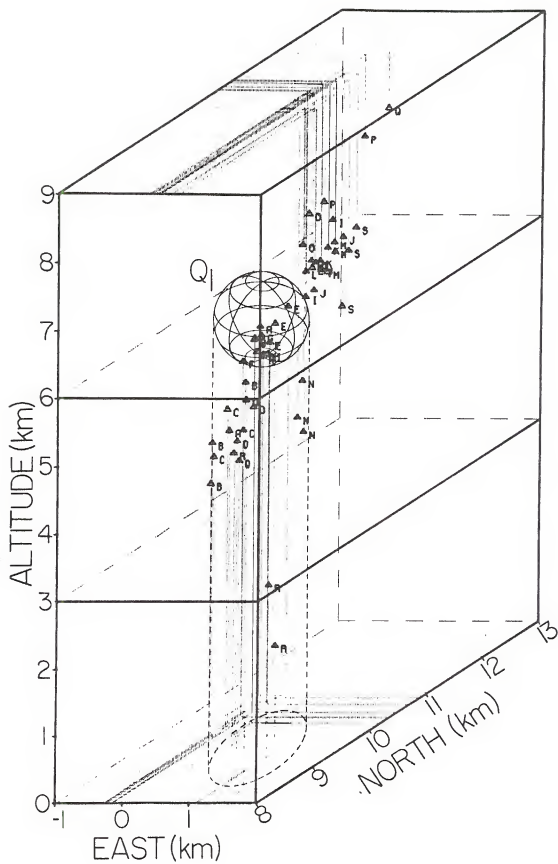
5.1.4 Activity Following the First Return Stroke (FR)

For 2.4 msec after the first return stroke there was a quiet period. No VHF sources were identified during this period. The VHF radiation after the quiet period was significant, lasting 4.3 msec with a pulse about every 4 μ sec. This activity is shown by FR (following return stroke) in Figure 5.1. The source locations of the FR period propagated upward between 2 and 7 km in height. The lower sources were located in the neighborhood of the eastern locations of the stepped leader sources in Figure 5.3(a). However, most of the radiation originated at a height between 4.5 and 5.8 km, that is, in the lower portion of the preliminary breakdown and upper portion of the stepped leader. Figure 5.9 shows the location of the cross-correlated VHF noise sources, 94 μ sec intervals, during the FR interval. We have labeled A through Q the progressing sequence of the sources. Figure 5.8 also shows the location of the previous return stroke charge source. The FR activity terminated with a large low frequency pulse similar to the characteristic return stroke pulses. The electric field records indicate that either negative charge was lowered or positive charge was raised or both during the 4.3 msec of VHF activity. Taking into account the locations of the VHF noise it appears that the FR activity raised positive charges.

5.1.5 First J-Change (J1)

Even though the FR activity is in the interstroke process, its properties seemed to be related to the previous return stroke. The J1

Figure 5.9. Cross-correlated VHF noise sources, 94 μ sec intervals, during the FR period. The sources are labeled A through S to indicate the progressing sequence of their occurrence. Each label is repeated three times. No time sequence is given for each repeated letter. The sphere Q1 is described in Figure 5.3.

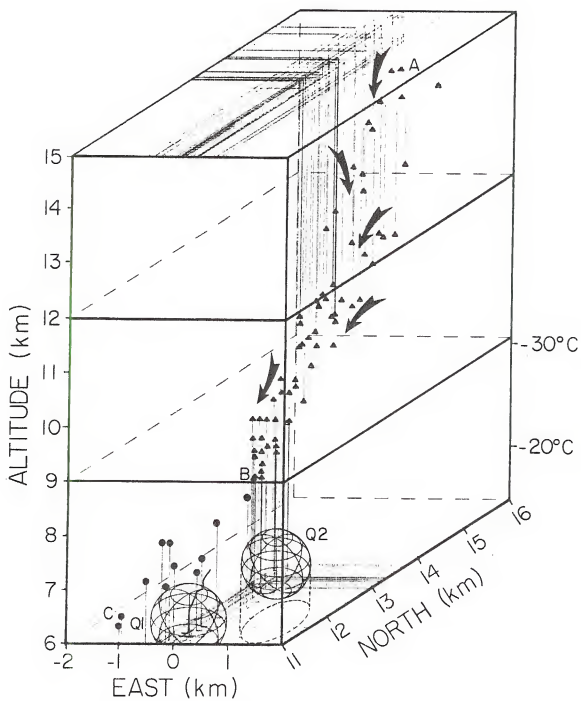


change reported in this section started with the 15.5 msec quiet period in the VHF noise record following the FR activity. Quiet periods after return strokes have been the subject of considerable study. Malan (1958) first reported quiet periods of 5 to 20 msec after the return stroke. A summary of quiet period studies has recently been published by Clegg and Thomson (1979). It is not possible to determine the location of noise sources, if they exist, during this quiet period because the VHF radiation is comparable with the system noise level. However, during the quiet period there is a steady electric field change and hence charge motion is taking place. For the final 43.3 msec of the inter-stroke interval there is significant VHF radiation with the initial pulse repetition rate nearly doubling in the 21 msec prior to the dart leader.

Figure 5.10 shows a three-dimensional view of the lightning channels active during the J-change between the first and second return stroke (J1, Figure 5.1). The sources start near the top of the cloud and propagate downward in a path 35° off vertical into the region associated with the stroke charge. The motion (in km) is approximately from A (0.0, 16.0, 13.7) to B (-0.2, 12.3, 7.9). Eighty-two cross-correlated source locations, 376 μ sec intervals, are displayed in Figure 5.10. The arrows indicate the direction of burst of sources occurring during the overall propagation from A to B which took place at an average velocity of about 1.5×10^5 m/sec.

The change in electric field during J1 was measured at eight separate ground stations at distances from 2 to 20 km from the noise source locations. The experimental J-change fields during the VHF radiation can be remarkably well modeled by equation (3.10) if we assume

Figure 5.10. Cross-correlated VHF noise sources, 376 μ sec intervals, during the first J-change. Parts A and B represent the beginning and the end of the J-change region, respectively. The arrows indicate the direction of propagation of groups of sources which occurred in bursts. During the dart leader following the J-change, a 4 km near-horizontal channel joint B with C (shown as circles), a region near the previous leader channel. Also shown as a continuous line in the neighborhood of Q1 is the upper part of the preliminary breakdown which preceded the first return stroke. Both first and second stroke charge volumes are shown.



a negative point charge moves downward from A to B (Figure 5.10). Deriving a charge value from the E-field at each station yields 2.4 Coulombs with a standard deviation of 0.7 Coulombs, representing a charge moment of 13.4 ± 4.0 Coul-km. This value of charge moment is an order of magnitude larger than previous estimates of the maximum charge moment during the J-process (Brook et al., 1962). The experimental data do not fit nearly as well if points other than A and B along the VHF radiation path are chosen as the starting and ending points of the negative charge motion.

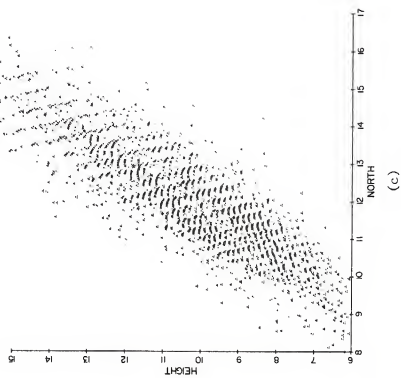
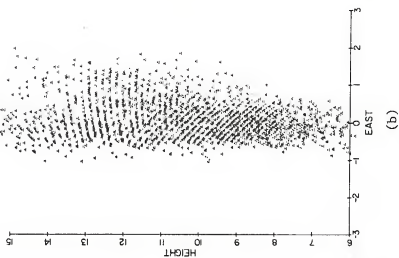
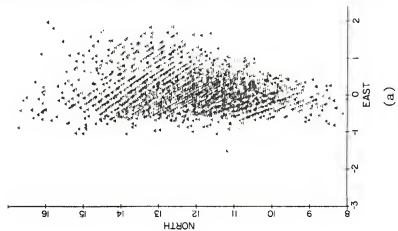
Figure 5.11 shows two-dimensional graphs of all the 3377 noise sources detected during the VHF portion of the J1 change. Figure 5.11(a) shows the plan view while Figure 5.11(b) and Figure 5.11(c) show the two corresponding elevated views. The VHF sources are spread out at the beginning of J1 (near the 14 km height) occupying a radius of 1.5 km or 2 km, but as the VHF sources propagated downward to near the O2 source region, the channel narrows down in the east direction to about 1 km radius. It appears that negative charge flow is detected from a region about 2 km below the cloud tops.

5.1.6 Dart Leader Before the Second Return Stroke

The VHF dart leader radiation started about 350 μ sec before the second return stroke. The beginning of the dart leader was characterized by a high amplitude, 110 μ sec wide pulse. The remaining 240 μ sec width with about 7 μ sec between pulses. Figure 5.12 shows the VHF noise during the dart leader and subsequent return stroke.

The VHF dart leader sources are located in a 4 km near-horizontal channel connecting B to C in Figure 5.10. The velocity of propagation of the BC channel is between 1.8 and 2.6×10^6 m/sec. The radiation

Figure 5.11. Two dimensional views: (a) top view, EW-NS, (b) elevation view, EW-height, and (c) elevation view, NS-height of all the 3777 noise sources detected during the J1 process.



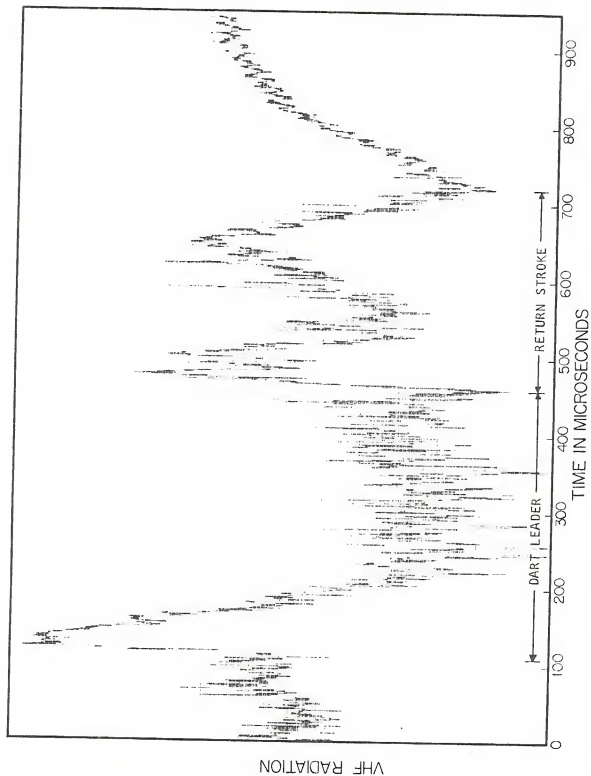


Figure 5.12. Logarithmic-amplitude VHF radiation during the dart leader and the second return stroke.

from the dart leader joins the bottom of the J1 change with the beginning of the preliminary breakdown as shown in Figure 5.10. Our calculations of the locations of the VHF noise sources during the dart leader are in agreement with the work of Brook and Kitagawa (1964) and Proctor (1971), which suggested that most of the radiation during the dart leader's trip to ground is from within the cloud rather than from the dart leader channel. Comparing the location of the noise sources with the correlated electric field and VHF radiation is not possible to determine where the charge in motion during J1 entered the previous ionized return stroke channel and descended to ground. In addition to the BC channel, Figure 5.10 shows a continuous line from the preliminary breakdown channel. The noise sources of the dart leader (shown as dots in Figure 5.10) not only connected the two previous channels but also extended horizontally over 1 km beyond the top of the preliminary breakdown.

5.1.7 Second Return Stroke

The second return stroke lasted approximately 259 μ sec in the VHF record as shown in Figure 5.12. The four source locations identified during the second return stroke were located within 1 km radius of the highest cross-correlated source location of the preliminary breakdown. These findings suggest that the preliminary breakdown has become part of the active leader channel used by the consecutive strokes which propagate in the defunct return stroke path to ground. No sources were identified in the return stroke channel to ground.

5.1.8 Solitary Pulses During the Quiet Period of J2

Three solitary VHF pulses (SP's) occurred during the 84 msec quiet period after the second return stroke (Figure 5.1). The duration of the SP's in the timing sequence they appear was 0.78, 0.95, and 0.57 msec. The SP's VHF amplitude and frequency content are similar to the return stroke. Figures 5.13(a), 5.13(b), and 5.13(c) show the VHF noise for the three SP's during the quiet portion of J2.

The SP's propagated upwards for 2 to 5 km in a near-vertical path from the previous ionized region of the negative charge center on the bottom of J1 and the top of the preliminary breakdown. The velocity of propagation of the J2 SP's is between 1 and 4×10^7 m/sec. All three SP's started within 2 km from each other but consecutive SP's extended over a larger volume of space. Figures 5.14(a), 5.14(b), and 5.14(c) show cross-correlated source locations, 94 μ sec intervals, for the three SP's. Even though the first source location always coincides with the lowest source of the SP's, sources within a few hundred microseconds of the beginning of the SP's were located at the top of the channel. In the last two SP's there were detected noise sources occurring near the end of the SP's which locations occurred in the path between the lowest and highest sources. These three SP's did not have detectable correlated electric field changes and therefore the charge transferred by this type of pulses must be relatively small. It is tempting to associate the SP's with K-changes (Uman, 1969), thought to be in-cloud upward-moving mini-return strokes initiated when charge of one sign moving downward encounters charge of opposite sign. The absence of VHF radiation preceding the upward moving SP's and absence of appreciable rapid electric field change associated with the SP's is puzzling.

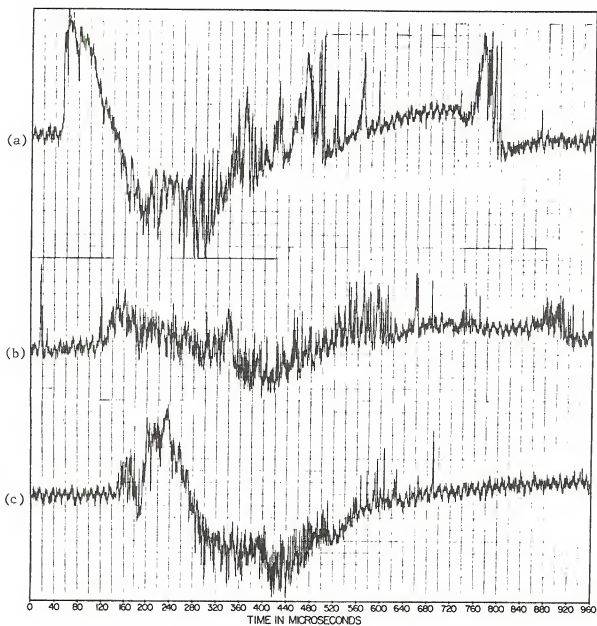
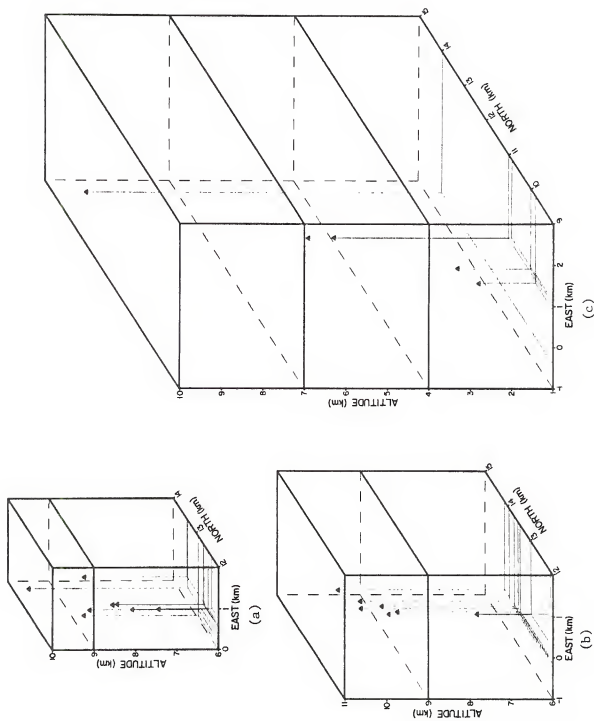


Figure 5.13. Logarithmic-amplitude VHF radiation during the three solitary pulses (SP's) in the J2 process.

Figure 5.14. Cross-correlated VHF noise sources, 94 μ sec intervals, during the three SP's shown in Figure 5.13.



5.1.9 Second J-Change

Significant VHF radiation was measured during the last 47 msec of the second J-change (J2, Figure 5.1). The VHF noise sources started at (1.2, 12.5, 11.2), that is, about 2.1 km below and 4 km southeast of the starting point of J1. During the first 19 msec there was activity taking place one or two kilometers upwards and downwards, but in the last 25 msec the noise sources propagated primarily downwards, ending at (0.1, 11.8, 8.5). Figure 5.14 shows a three-dimensional view of the cross-correlated VHF noise sources, 376 μ sec intervals, active during J2. Figure 5.15 also shows the charge center for the last two return strokes (Q2 and Q3) and the location (A) of the end of J2.

We modeled the field change during the VHF portion of J2 with equation (3.10) and derived a charge for the E-field at each of the stations. For the J2 process, starting and ending points chosen were (1.2, 12.5, 11.2) and (0.1, 11.8, 8.5), a path 32° off vertical. We found a negative charge lowered of 3.4 Coul, with a standard deviation of 1.8 Coul, representing a charge moment of 16.2 ± 8.5 Coul-km. The velocity of propagation during the final 25 msec was 2.0×10^5 m/sec. The model fit is not as good as for the first J-change as might be expected in view of the fact that the second J-change originally propagated both upwards and downwards.

5.1.10 Stepped-Dart Leader (SDL) Before Third Return Stroke

For 2.2 msec after the second J-change, the VHF radiation waveforms showed a high frequency pulse train without any low frequency envelope, very similar to the radiation observed during the first stepped leader. The electric field records verify a stepped leader was occurring. Figure 5.16 shows the VHF radiation during the stepped leader.

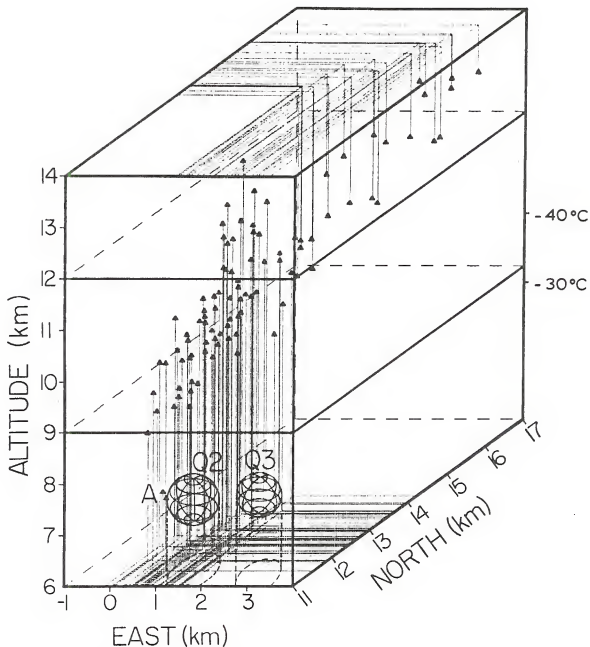


Figure 5.15. Cross-correlated VHF noise sources, 376 μ sec intervals, during the continuous VHF radiation of the J2 process. A represents the end sources of the J2 process. Spheres Q2 and Q3 represent the charge center for the second and third return stroke (Uman et al., 1978).

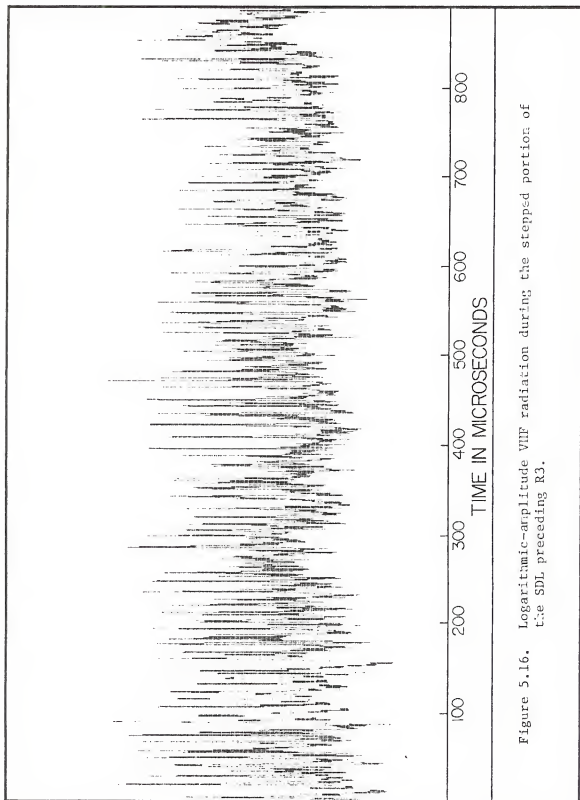


Figure 5.17 shows a histogram of the interval between VHF pulses. If we associate the high frequency VHF pulses with leader steps, the average time interval between leader steps was 8.2 μsec (Figure 5.17) with a standard deviation of 3.5 μsec . If there was a typical value of 50 μsec between leader steps, about 5 branches were simultaneously active.

The location of the VHF noise sources during the stepped leader extended the path of the previous J-change as shown in Figure 5.18. The VHF sources propagated from an altitude of about 8 km, the end of J2, to a height of 3.3 km below which no radiation sources were located. The bottom of the stepped leader nearly coincides with the previous channel. The stepped leader velocity determined from the cross-correlated source locations was about 4.5×10^6 m/sec. After the last stepped leader location and for 1.1 msec, the electric field showed a more rapid variation of slope than previously and the VHF radiation indicated the long-duration pulse characteristic of dart leader, return strokes, and SP's. The noise sources were located around an altitude of 3.5 km, that is, near the bottom of the stepped leader channel. In view of the above it is reasonable to assume that the stepped leader contacted the previous stroke channel and at that point became a dart leader, making the whole leader process a stepped-dart leader.

5.1.11 Third Return Stroke

The third return stroke lasted about 130 μsec in the VHF record. The beginning of the return stroke VHF record shows a wide 80 μsec pulse which seems to be an indication of the propagation of a potential wave. All the four cross-correlated noise sources detected during the third return stroke were located near the top of the stepped-dart leader channel, which coincided with the end of J2.

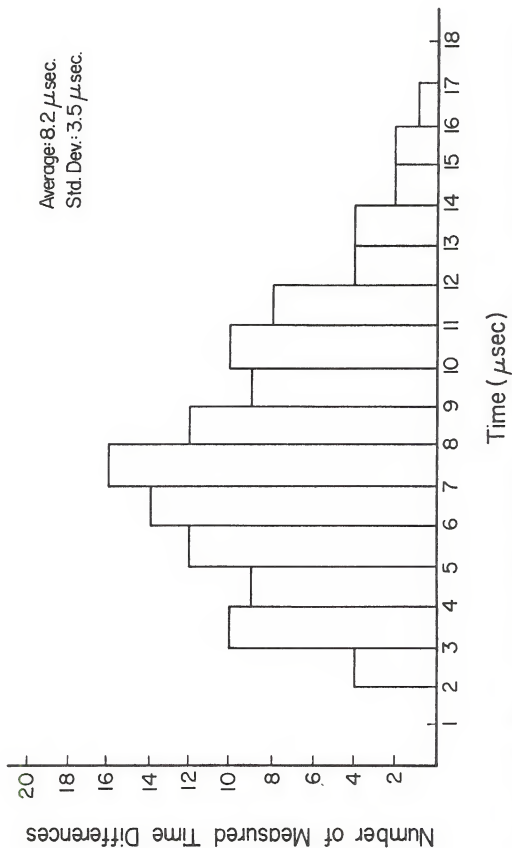
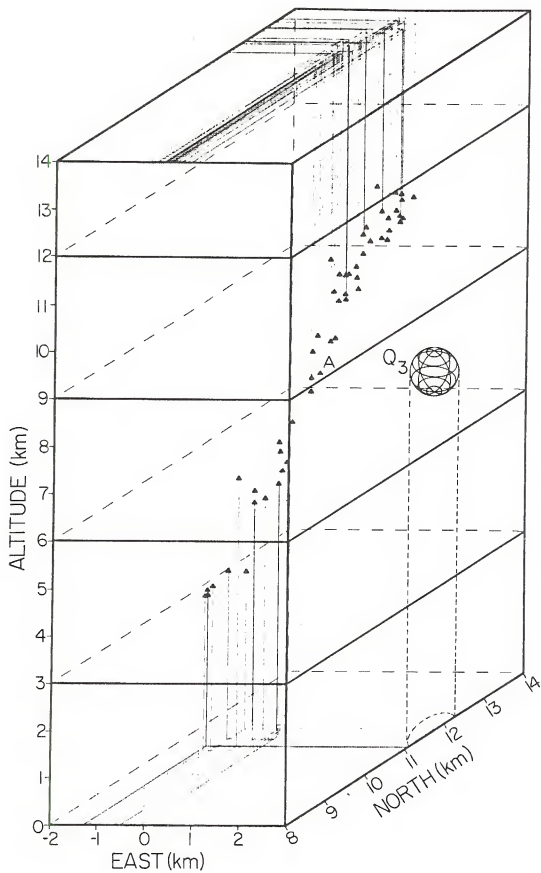


Figure 5.17. Histogram of the interval between VHF pulses during the stepped-dart leader preceding the third return stroke.

Figure 5.18. Cross-correlated VHF noise sources, 94 μ sec intervals, during the 2.2 msec of the stepped portion of the stepped-dart leader that preceded the third return stroke. A corresponds to the location at the end of the J2 process as shown in Figure 5.15. Q3 is the charge center for the third return stroke from Uman et al., (1978).



We used the technique described in Section 3.6 choosing (A) in Figure 5.15 as the point charge source and determined that -6 Coul were lowered by the third leader-return stroke process. This result is comparable to the -9 Coul determined by Uman et al. (1978).

5.1.12 Solitary Pulse Between the Cloud-to-Ground and the Intracloud Discharge

Thirty milliseconds after the last and final return stroke of the CG discharge, a large SP was observed. The SP lasted about 625 μ sec and started with an 80 μ sec wide pulse very similar to the first SP between the second and third return stroke.

The sources of the SP propagated upwards to the NE in a path 35° off vertical starting about an altitude of 4 km. This SP VHF amplitude and the propagation of its source locations were larger than the SP's between R2 and R3. The vertical inclination of this SP and the source of its upper region coincided with the intracloud discharge that followed.

5.1.13 The Intracloud Discharge

The continuous VHF radiation from the intracloud discharge following the cloud-to-ground discharge began 12.8 msec before the first sharp increase in the IC electric field (Figure 5.1). Figure 5.19 shows the VHF radiation during the beginning of the IC discharge. There is a remarkable difference between the beginning of the IC and the beginning of the CG in Figure 5.4, which suggests that we can distinguish these flashes after only 3 msec of VHF radiation. The first three sources during the IC were located near (3.1, 12.1, 11.2), in the middle of the path to be eventually covered by the intracloud discharge. The entire discharge extended about 10 km in a path 35° off vertical between A (6.0, 13.6, 14.0) and B (1.7, 9.5, 5.9) of Figure 5.20 which shows the

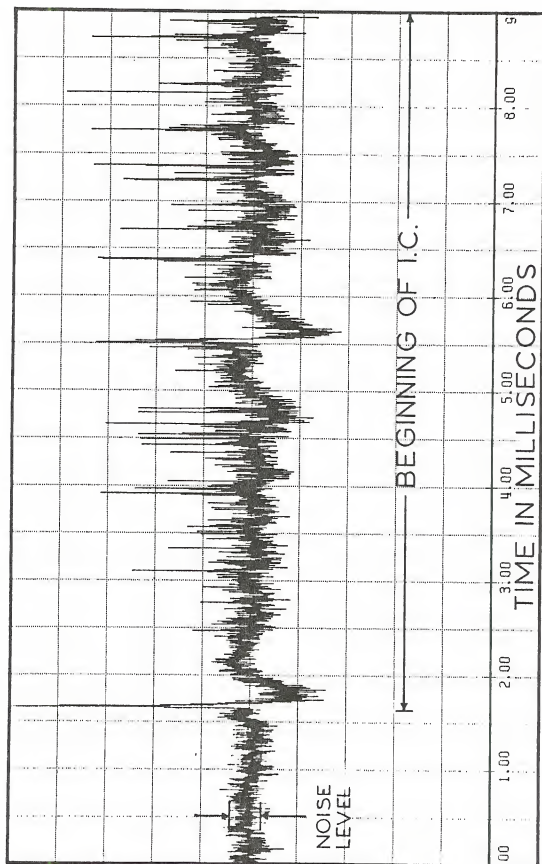


Figure 5.19. Logarithmic-amplitude VHF radiation during the beginning of the intracardiac discharge.

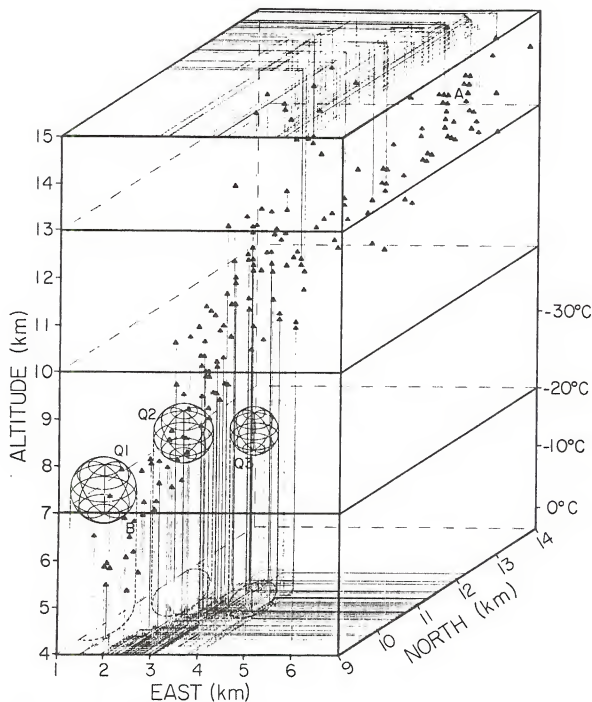
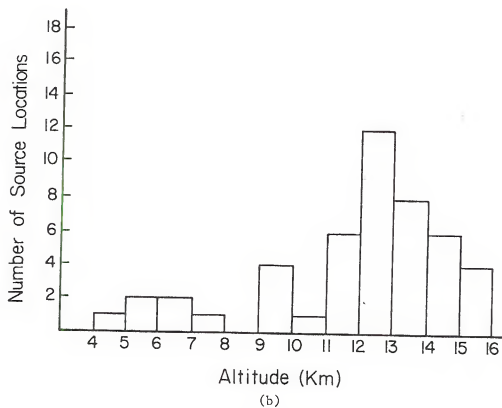
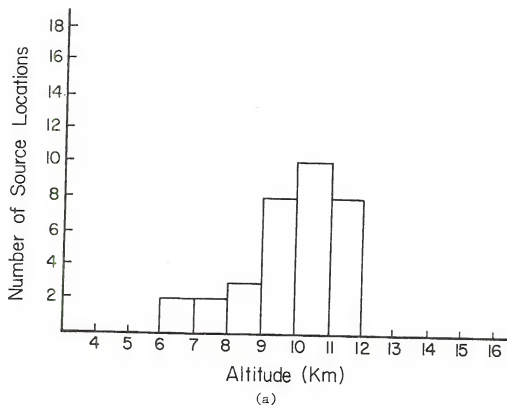


Figure 5.20. Cross-correlated VHF noise sources, 376 μ sec intervals, during the initial and active phase of the intracloud discharge. Points A and B represent the termination regions of the main 10 km intracloud discharge channel. Charge volumes for all three return strokes are shown (Q1, Q2, and Q3).

cross-correlated source locations, 376 μ sec intervals, for the entire discharge. During the first 4.6 msec of the VHF radiation, the average noise sources were located within half a kilometer perpendicular distance of the bottom-half of the line joining A and B. During the next 11.2 msec the noise sources moved to the upper half of the path between A and B. Figures 5.21(a) and 5.21(b) show histograms of the average source locations, every 94 μ sec, for the first 5.6 and 11.2 msec, respectively. For the first 16.8 msec, 85% of all the average sources were located within half a kilometer perpendicular distance of a line joining A and B. During the remainder 484 msec of the IC discharge, VHF sources traversed from the path between A and B many times, widening the VHF source volume to over 1 km radius. VHF sources also extended an additional 2 km at the ends, near A and B.

The intracloud discharge can be divided into three phases: initial, very active, and junction, as done by previous investigators (Kitagawa and Brook, 1960). The initial phase started with a large 10 μ sec wide VHF pulse. This phase lasted about 64 msec and consisted of a low rate of VHF radiation, approximately one pulse every 25 μ sec. In the electric field waveform of Figure 5.1, the initial phase includes the rising part of the IC record. The active portion of the VHF radiation lasted about 437 msec and was characterized by a faster pulse rate, about a pulse every 10 μ sec. The total of the initial and the active phase, 501 μ sec, corresponded to the portion of the IC discharge for which the VHF noise was more or less continuous. For the next 99 msec, not shown in Figure 5.1, five solitary pulses were observed. The SP's occurred 49.3, 58.7, 70.5, 75.7, and 97.1 msec after the continuous radiation. We associate the quiet period where the five SP's occurred with the junction phase

Figure 5.21. Histograms of the altitude of the source locations during (a) the first 5.6 msec, and (b) the next 11.2 msec of the intracloud discharge.



of the intracloud discharge. The VHF noise for these SP's closely resembles the SP's during the J-changes of the cloud-to-ground discharge. The VHF locations for these SP's propagated upwards for about 6 to 8 km starting in a region one to three km east of B. None of the SP's propagated along the primary AB path of the intracloud discharge. Their starting location was as noted and their path was either vertical or northwest, instead of the 35° northeast path of the IC discharge. We attempted to fit a point charge model, equation (3.10), to the multiple stations electric field records, for the location of the continuous radiation of the IC discharge but could obtain no reasonable results. On the other hand, because of the polarity of the IC field and its reversal with distance (Uman, 1978), it is clear that the bulk of the charge motion was either negative upwards or positive downwards.

5.1.14 Concluding Remarks About This Flash

Some of the new information about the flash derived from the VHF noise, its source locations, and the correlated wideband electric field records follows: (1) The first stepped leader was preceded by a 2.2 msec preliminary breakdown located near and inside the charge source of the stepped leader. The stepped leader had an average velocity which increased from 1.3×10^6 m/sec at 5.1 km height to 7.0×10^6 m/sec at 2.2 km, the lowest height for which average source locations were obtained. (2) Continuous VHF radiation was detected in the final 65% of the time between the first two return strokes. During this portion of the first J-change, radiation sources and negative charge propagated downward 5.7 km in a path 35° off vertical at an average velocity of 1.5×10^5 m/sec. The negative charge lowered during this portion of the J-change was 2.4 ± 0.7 Coulombs. A 4 km near-horizontal channel which

propagated at an average velocity of 1.4×10^6 m/sec connected the bottom end of the first J-change sources with the charge region of the previous stepped leader. (3) Continuous VHF radiation was detected in the final 35% of the time between the second and third return strokes. During this part of the second J-change, radiation sources propagated both upwards and downwards for the first 15 msec, then propagated downward 4.7 km for 25 msec at an average velocity of 2.0×10^5 m/sec. The negative charge lowered during this portion of the J-change was 3.4 ± 1.8 Coulombs. (4) Following the second J-change, a new stepped leader propagated from 7 km, the bottom of the J-change VHF source locations, downward to a height of 3.2 km, where it joined the previous stepped leader channel, and, presumably, return stroke channel. The stepped leader average velocity was 4.5×10^6 m/sec. (5) During the intracloud discharge following the third return stroke, sources of VHF radiation covered a path from near the source charges of the return strokes to about 14.0 km, near the cloud top. The VHF noise sources traversed the same path many times, widening the main channel and extending the ends. The VHF radiation during the IC discharge displayed the three phases described in the literature for IC discharges which were not associated with a ground discharge.

5.2 The 180710 Flash

On 8th August 1977 a thunderstorm moved west from the Atlantic coast side of the Cape Canaveral AFS, Florida, and at 1810 UT the cloud tops were reported at a height of 12.9 km. At 180710 UT the first cloud-to-ground flash of the newly developed thunderstorm was recorded. Details of that flash are reported in this section. Two other cloud-to-ground flashes in this storm occurring at 181806 and 182357 UT are also studied in this thesis (see Sections 5.3 and 5.4).

The VHF portion of the 180710 flash lasted 282 msec and consisted of three separate strokes to ground. Figure 5.22 shows the relationship between the VHF radiation recorded 10 km from the flash and the electric field recorded 3 km away. It is evident from either the VHF or the electric field records that there were stepped leaders associated with all three of the return strokes in this flash. At 3 km from the flash the three stepped leaders were within the electric field reversal distance (Uman, 1969, Chapter 3) and hence had initially negative-going electric fields, while an electric field station at 19 km showed positive stepped leaders field changes. Table 5.2 contains a complete summary of the various phases of the flash. All the cross-correlated noise source locations reported in this flash were determined by using 94 μ sec intervals. The location of the charge region for the first return stroke was provided by Krehbiel (private com) using the technique described by Krehbiel et al., (1979). An error analysis for the VHF noise source locations is given in Appendix B. Table B.3 shows a summary of the uncertainty in determination of the locations of the sources in this flash as a function of position. In the next subsection we consider in detail what we learned from the VHF radiation about the different events that took place in the 180710 flash.

Figure 5.22.

Simultaneous records of the logarithm of the amplitude of the VHF radiation observed at 9 km, and the electric field 3 km away, during the 180710 flash. The following events in the flash are shown: R1, R2, and R3 correspond to the three return strokes; SL1, SL2, and SL3 are the three stepped leaders; J1 and J2 are the J-change processes; PB is the preliminary breakdown; PR is the activity after the first return stroke; K is the K-change pulse that initiated the J1 process; CAFS and DAFS are the continuous and discrete activity after the return stroke; last SP corresponds to the last solitary pulse during the DAFS process.

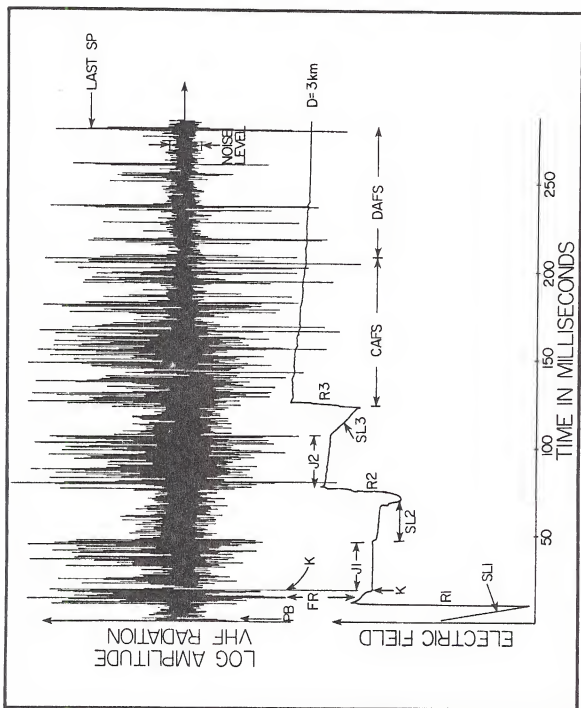


Table 5.2. Events in the 180710 Flash.

Universal Time at the Start of the VHF Radiation: 18 hr 07m10s 743.5 msec, 8th August 1977										
Start Time (msec)	Event	Duration (msec)	Coordinates (km)						Velocity m/sec	
			UPPER			LOWER				
			x	y	z	x	y	z		
0	Preliminary Breakdown (PB)	2.1	4.6	10.8	7.1	5.1	11.7	6.1	Between 0.8×10^6 and 1.7×10^6 m/sec	
2.1	First Stepped Leader (SL1)	7.9	5.1	11.7	6.1	6.8	16.7	1.9		
10.0	First Return Stroke (R1)	.4	4.8	10.9	4.5	5.7	12.8	0.8		
10.4	Following First Return Stroke (FR)	8.4	4.7	10.9	6.5	4.0	9.9	3.7	9.5 x 10 ⁶ m/sec during initial K-change Between 2.4 and 5.3 x 10 ⁶ m/sec	
18.7	First J-Change (J1)	28.4	7.6	13.4	10.6	3.9	10.00	5.7		
47.1	Second Stepped Leader (SL2)	29.0	4.5	10.6	6.6	5.6	8.3	0.7		
76.1	Second Return Stroke (R2)	0.5	4.8	8.9	7.1	4.7	8.8	6.3	Between 7.6×10^5 and 1.1×10^6 m/sec	
76.6	Second J-Change (J2)	31.2	6.5	10.3	9.3	4.0	8.7	4.9		
107.8	Third Stepped Leader (SL3)	15.5	4.9	11.2	6.8	7.7	15.7	.7		
123.3	Third Return Stroke (R3)	.6	5.1	11.2	6.8	4.8	11.2	6.4		
123.9	Continuous VHF Activity after R3	87.1	7.9	14.2	10.0	4.1	8.0	3.4		
211.0	Discrete VHF Activity after R3	71.0	5.3	14.6	9.4	4.1	9.8	5.6		

5.2.1 Preliminary Breakdown (PB)

The VHF radiation started 10.0 msec prior to the first return stroke. The first 2.1 msec of the 10.0 msec was associated with the preliminary breakdown. The VHF noise characteristics of the PB are shown in Figure 5.23 along with the VHF noise during the stepped leader, first return stroke, and some of the activity after the return stroke. Correlation with the electric field record was only possible to within 750 μ sec. At a distance of 3 km there was detectable field change 9.0 ± 0.75 msec prior to the first return stroke, that is, about half-way through the preliminary breakdown. Thus the electric field change started about 1.0 msec after the initial preliminary breakdown pulse shown at 2.0 msec in Figure 5.23.

The first cross-correlated noise source was located at A (4.6, 10.8, 7.1) in Figure 5.24(a) and corresponded to the highest detectable cross-correlated source of the preliminary breakdown-stepped leader process. The noise sources during the preliminary breakdown as found by the computer did not occur in a regularly progressing sequence. Attempts to determine a preliminary breakdown velocity did not produce consistent results. At the end of the preliminary breakdown the noise sources were at B (5.1, 11.7, 6.1). The cross-correlated noise sources during the PB extended between 4.2 and 5.3 km EW, 9.8 and 13.0 km NS, and between 4.9 and 7.1 in altitude.

In addition to determining the cross-correlated and all the individual source locations (Figure 5.24(b)) using the computer algorithm described in Chapter IV, we determined the individual source locations manually during the first 600 μ sec of the preliminary breakdown. This task was performed to show the progressing sequence of the initial

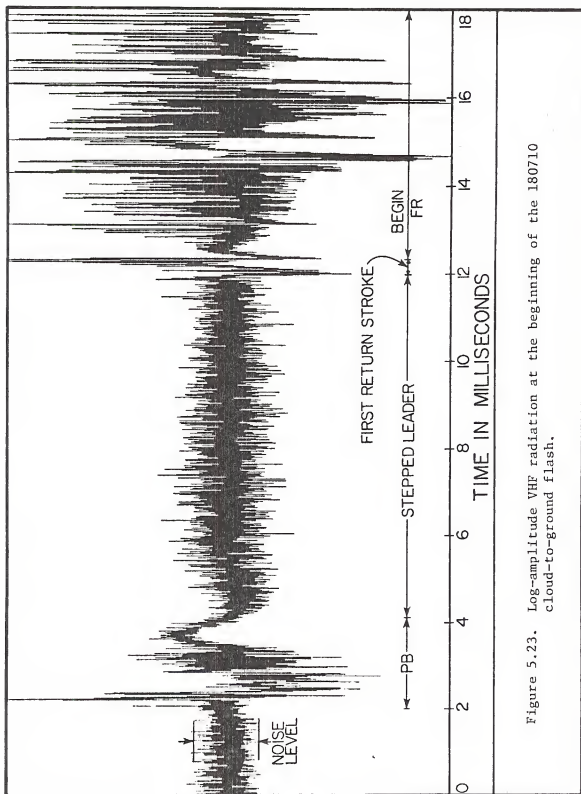
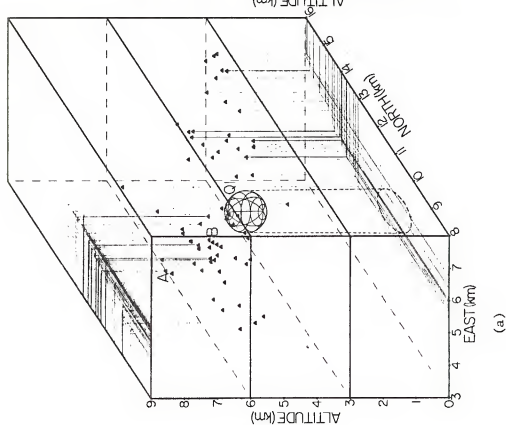
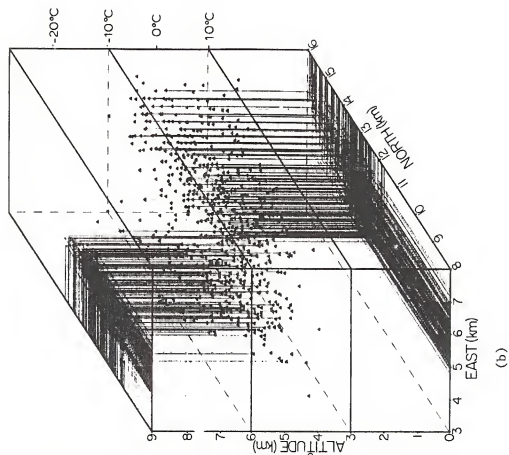


Figure 5.24(a). Three-dimensional view of the cross-correlated noise sources during the first PB-stepped leader process. Point A is the location of the first cross-correlated source during the PB. Point B is a similar source at the beginning of the stepped leader. The sphere Q1 represents the source charge for the first return stroke provided by Krehbiel (private com) using the techniques of Krehbiel et al., (1979).

Figure 5.24(b). Similar three-dimensional view for all the individual detected sources.



sources every 2 or 3 μsec (if active VHF radiation was recorded), instead of every 7 to 10 μsec , the limiting using the computer algorithm. These results are shown in the three-dimensional graph in Figure 5.25. The sources A through EE are time tagged and shown in alphabetical order A \rightarrow Z, AA \rightarrow DD. This initial stage of the PB extends 8 km horizontally and 7 km vertically. The sequence of the VHF sources shows that the activity started at 7.4 km and there was propagation initially horizontally and then vertically.

5.2.2 First Stepped Leader

The last 7.9 msec prior to the first return stroke are associated with the stepped leader in the VHF noise record. Figure 5.24(a) and Figure 5.24(b) show the cross-correlated, and all the individual detected noise sources respectively, during the PB-stepped leader process. Figures 5.26(a), 5.26(b), and 5.26(c) show two-dimensional projections of all the sources in Figure 5.24. The noise sources extended north-northeast 10 km in the horizontal direction from a height of 6.1 km at the beginning of the stepped leader to a height of 1.9 km. It is worth noting that the leader extended 5 km over water and away from the most eastern end of the KSC which is located at (5.3, 8.3). This large horizontal propagation of the stepped leader may be related to the fact that the leader propagated over water. The velocity of the stepped leader ranged between .8 and 10^5 and 1.7×10^6 m/sec.

5.2.3 First Return Stroke

The first return stroke VHF radiation lasted 400 μsec . The noise was characterized by high frequency pulses riding on the envelope of a low frequency pulse as shown in Figure 5.23.

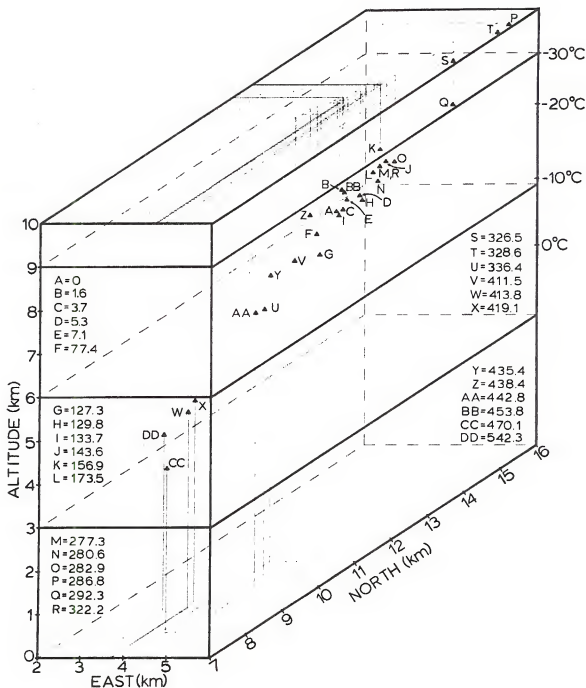
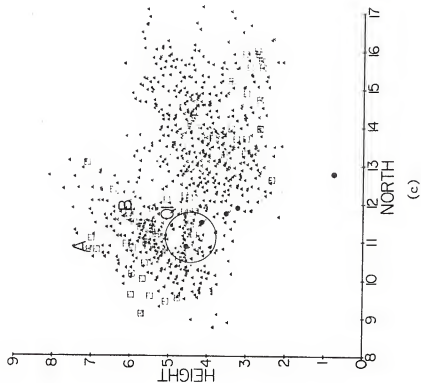
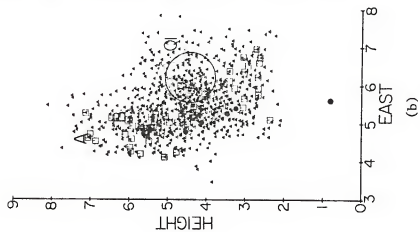
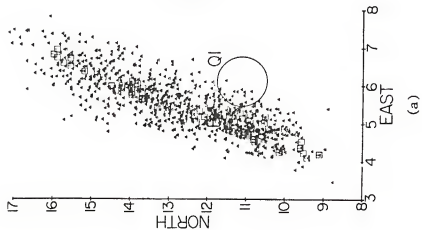


Figure 5.25. Three-dimensional view of the VHF noise sources during the first 600 μsec of the preliminary breakdown.

Figure 5.26.

Two-dimensional views: (a) EW-NS, (b) EW-height, and (c) NS-height of all the sources (triangles) and the cross-correlated source location (squares) during the PB and the first stepped leader. The five circles represent the location of the cross-correlated noise sources during the first return stroke. The circle Q1 is the two-dimensional projection of Q1 in Figure 5.25.



The five return stroke cross-correlated noise sources, 94 μ sec intervals, are shown as circles in Figure 5.26. The noise sources during the return stroke occurred in ascending order between a height of 0.8 and 4.5 km at a velocity of 1.2×10^7 m/sec. This return stroke velocity, calculated by determining the cross-correlated VHF noise source locations at the beginning and at the end of the return stroke and dividing by the duration of the VHF record, can have large errors. These errors are caused by two main factors: (1) In a 94 μ sec interval the return stroke upward propagating wave will extend several kilometers and a cross-correlation location might not be a true representation of the source. (2) It appears that the return stroke VHF radiation is only obtained by extensions of the previously ionized stepped leader channels, and therefore return stroke source locations may not be a true representation of the actual extent of the return stroke channel.

Krehbiel (private com), using the method of Krehbiel et al. (1979), calculated that -21.1 Coul were lowered by the first return stroke from a charge center located at Q1 (6.2, 11.1, 4.4). Figures 5.24 and 5.26 show the location of the return stroke charge source. Assuming a source location at point B (this is the source location for the transition between PB and stepped leader in the VHF noise) and using the technique described in Section 3.6, we calculated that -13.4 Coul were lowered by the leader-return stroke process. The difference between our assumed charge calculation source location at B (5.1, 11.7, 6.1) and Krehbiel's calculated first return stroke charge is significant. However, Krehbiel (private com) has indicated large uncertainty in the determination of the locations of Q1.

5.2.4 Following First Return Stroke (FR)

We have divided the interval between the first two return strokes in three sections: (a) activity following return stroke (FR), (b) the J1 process, and (c) the stepped leader.

The FR is the first interval after the first return stroke. The FR interval is characterized by having large high frequency pulses riding on the envelope of pulses of 3 to 30 μ sec width. The VHF noise sources during the FR interval were located in the neighborhood of the previous stepped leader-return stroke channel between the heights of 3.7 and 6.5 km as shown in Figure 5.27. During the FR interval the electric field decreased sharply at a station located 3 km away from the charge center, while a station 19 km away showed a slight increase in field magnitude. This field reversal indicates that during the FR interval either negative charge was lowered from a region in the neighborhood of the first return stroke charge center (as in the stepped leader), or that positive charge (most likely from the previous return stroke) was raised to a region above the previous charge source. We attempted to determine which one of these situations was occurring by studying the progressing sequence of the VHF noise sources. However, the VHF sources were unorganized and we could not determine a direction of propagation.

5.2.5 The J1 Process

The J1 process started with a K-change and followed immediately after the FR interval. The K-change was characterized by a change of slope in the electric field record and a correlated large VHF pulse. The VHF noise during the J1 process appears similar to that in the FR interval, and is identified by the following two factors: (1) There was

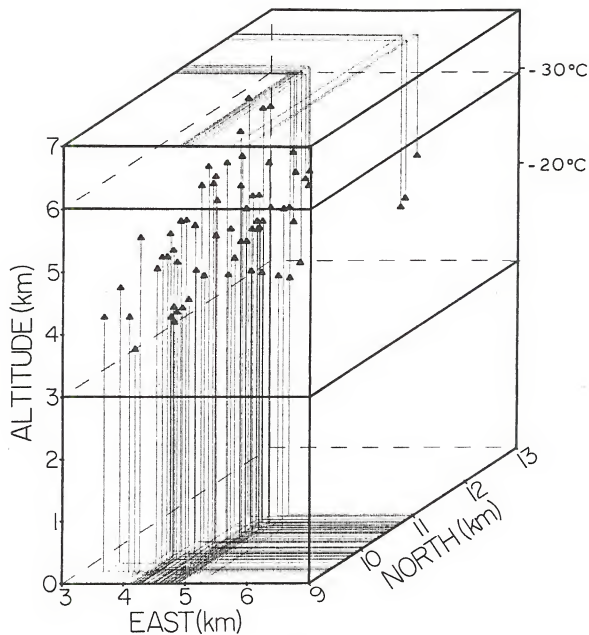


Figure 5.27. Three-dimensional view of the cross-correlated noise sources during the 8.4 msec FR interval.

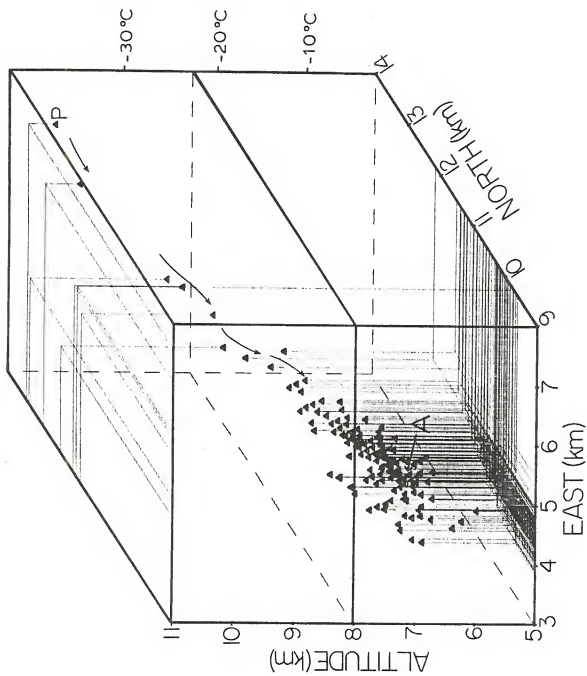
a change of slope in the electric field record at the beginning of the J1 process (K-change, Figure 5.22), and (2) The VHF noise sources were located in a different region from the FR.

Figure 5.28 shows the cross-correlated VHF noise sources during the J1 process. The K-change starting the J-process propagated from point P in Figure 5.28, at a height of 10.6 km and descended into a lower region between the heights of 5.7 and 7.5 km. The arrows in Figure 5.28 show the initial sequence of the progressing of the K-change. The K-change lasted 1.1 msec for an average velocity of 9.5×10^6 m/sec and showed a descending path of the VHF noise sources from P to near the center of the lower crowded region in Figure 5.28. By measuring the electric field change and applying equation (3.10) between the end points of the propagation path, we determined the K-change lowered .9 Coulombs. During the remaining 27.3 msec of the J1 process the VHF noise sources did not show any regular progressing sequence. The bulk of the VHF sources during the J1 process are located about 2 km above the FR sources as can be seen by comparing Figures 5.28 and 5.27.

5.2.6 Second Stepped Leader

The second stepped leader had a VHF duration of 29 msec and started immediately after the end of the VHF associated with the first J-change process. From an analysis of only the electric field record shown in Figure 5.22 it is not clear whether the second stepped leader started at the end of J1 or at the time of the faster changing slope prior to the second return stroke. However, since stepped leaders have been shown in this thesis to exhibit low amplitude and high frequency VHF radiation, the comparison of the electric field with the VHF record in Figure 5.22 shows clearly the point of the beginning of the stepped leader process.

Figure 5.28. Three-dimensional view of the cross-correlated VHF noise sources during the first J-change process. Point P represents the location of the beginning of the K-change that initiated the J-change. The arrows show the regular progressing sequence of propagation of the VHF noise sources during the K-change. Point A is the start of the following stepped leader shown in Figure 5.29.



This is another example of the utility of VHF records for a clear identification of the different events in a lightning discharge.

Figures 5.29(a) and 5.29(b) show a three-dimensional view of the 188 cross-correlated sources, 94 μ sec intervals, and the 2991 individual source locations, respectively, during the second stepped leader. Figure 5.30 shows the two-dimensional projections of all the individual noise sources (triangles), and cross-correlated sources (rectangles). The stepped leader VHF noise sources started from the lower concentrated J1 noise source volume in Figure 5.29 and descended in a near-vertical path. The VHF noise sources were detected between a height of 6.6 and .7 km. From the VHF source locations in Figure 5.29(a), we estimated the ground contact point as $(5.3 \pm .5, 8.5 \pm .5)$. This point is located about 1.5 km east of the UC-7 field mill station.

From a study of the location and the sequence of the noise sources in Figure 5.29, we estimated that the second stepped leader had at least two detected branches labeled M and N in Figure 5.29. During the first 18.2 msec the second stepped leader propagated vertically from a height of 6.7 to about 4.0 km, with about 3.5 km horizontal propagation. During the remaining 10.8 msec the VHF noise sources are grouped in a more nearly vertical channel. The stepped leader average velocity ranged between 2.4 and 5.3×10^5 m/sec.

5.2.7 Second Return Stroke

Figure 5.31 shows the VHF noise during the period including the second stepped leader, the return stroke, and the beginning of the J2 process. The return stroke had a duration of 316 μ sec in the VHF record. The VHF cross-correlated source locations, 94 μ sec intervals, during the second return stroke, were located in the neighborhood of the upper part

Figure 5.29(a). Three-dimensional view of the cross-correlated noise sources during the second stepped leader. Point A is the location of the first stepped leader cross-correlated source.

Figure 5.29(b). Similar three-dimensional view for all the individual detected sources.

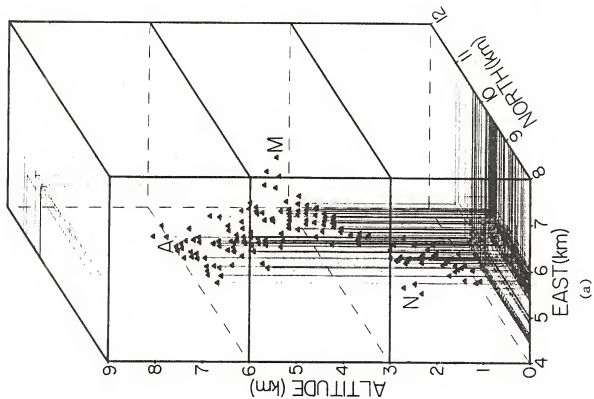
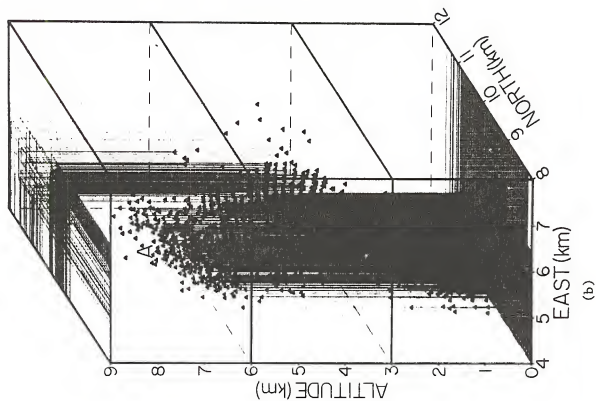
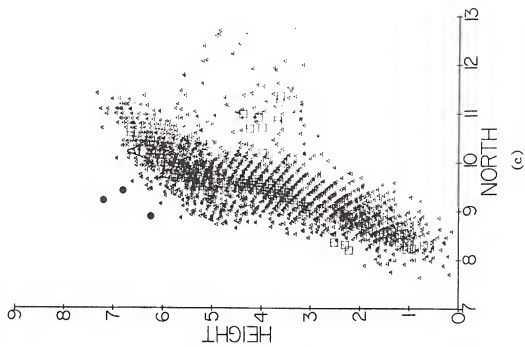
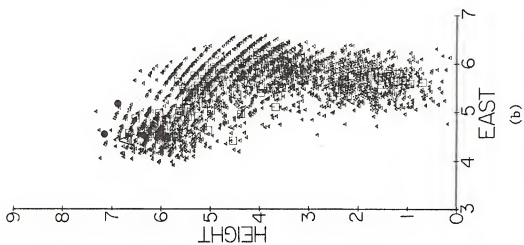
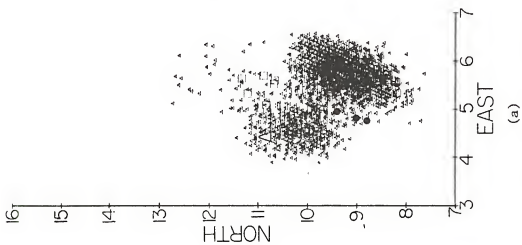


Figure 5.30. Two-dimensional views: (a) EW-NS, (b) EW-Height, and (c) NS-Height of all the sources (triangles) and the cross-correlated source location (squares) during the second stepped leader. The three circles represent the location of the cross-correlated noise sources during the second return stroke.



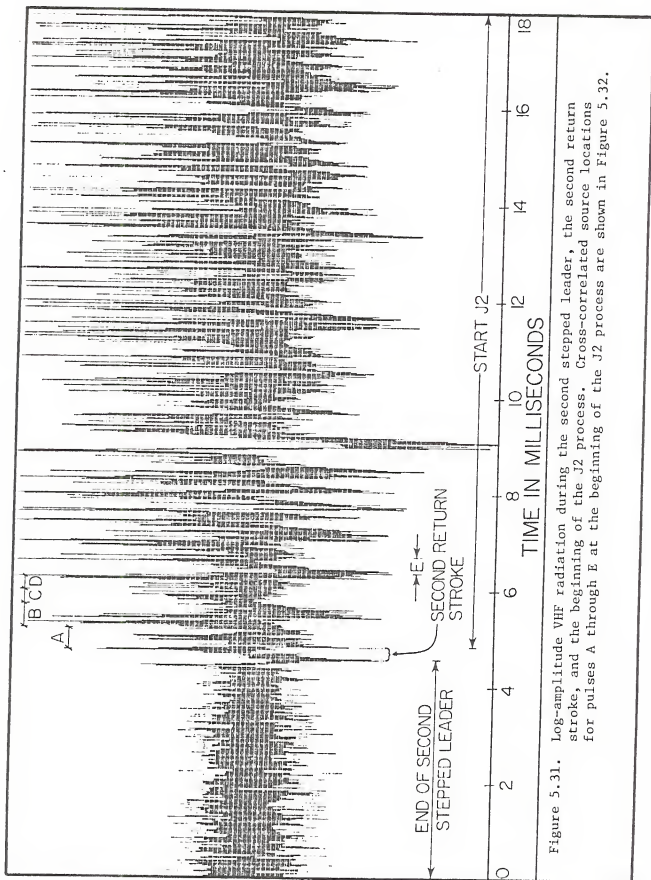


Figure 5.31. Log-amplitude VHF radiation during the second stepped leader, the second return stroke, and the beginning of the J2 process. Cross-correlated source locations for pulses A through E at the beginning of the J2 process are shown in Figure 5.32.

of the previous stepped leader channel. Figure 5.30 shows the three return stroke sources (circles).

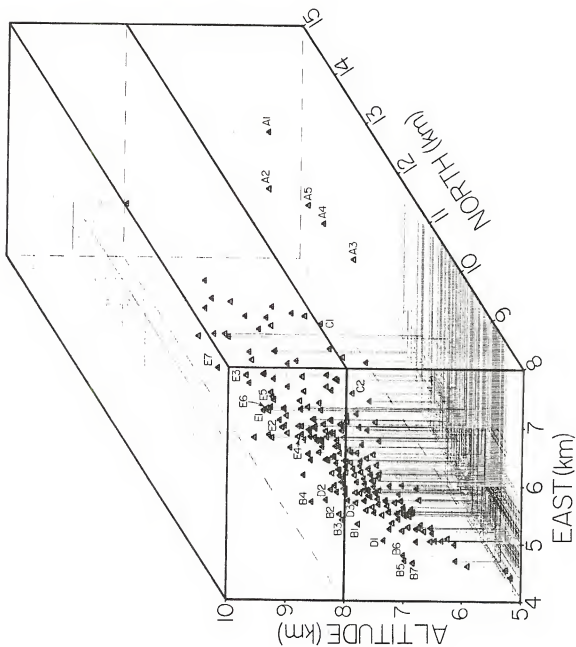
Assuming point A in Figure 5.29 and Figure 5.30 as the point charge for the second leader-return stroke and using the technique described in Section 3.6, we determined that -11.5 Coul were lowered by the leader-return stroke process. A charge value and location for the second or the third return stroke using the technique of Krehbiel et al. (1979) was not available for comparison of our results because the electric field records at some of the stations were saturated.

5.2.8 Second J-Change (J2)

Figure 5.32 shows the VHF noise sources, 94 μ sec intervals, during the second J-change. The J2 VHF noise lasted 31.2 msec of which the first 12.4 msec are shown in Figure 5.31 along with the VHF of the previous stepped leader and return stroke. The J2 noise sources extended about 5.3 km in a path 45° off-vertical. The location of the J2 process was nearly coincident with the previous J1 process, but the J2 process extended an additional 2 km in a northerly direction and was located about .6 km higher than J1. In addition, the J2 noise sources were more spread out than J1.

We studied the progressing sequence of the VHF noise pulses and their source locations during the J2 interval with the purpose of improving our understanding of the properties of this process. The first six VHF pulses are labeled alphabetically A to F in Figure 5.31. The source locations, 94 μ sec intervals, for each of these pulses are also labeled in a regular progressing sequence. The process started with pulse A which generated locations A1 to A5, followed by pulse B that generated locations B1 to B7. The first two pulses, A and B, were located furthest

Figure 5.32. Cross-correlated source locations during the J2 process. The regular progressing sequence of occurrence of the source locations at the beginning of J2 is as follows: A1 to A5, B1 to B7, C1 and C2, D1 to D3, and E1 to E7.



away to the NE and SW sides, respectively, in Figure 5.32. The next three VHF pulses (C, D, and E) were also located in the outer region. We continued this analysis throughout the entire J2 process to determine whether the VHF noise sources were grouped along any specific pattern when the third stepped leader developed. The main result of this analysis was that as the J2 process progressed the VHF sources formed along the outside of a cylinder, but near the end of the process the J2 sources filled most of the internal regions of this cylinder. The third stepped leader developed from Q (4.9, 11.2, 6.8) in Figure 5.32, which is located inside the cylinder.

5.2.9 Third stepped leader

Figure 5.33(a) and Figure 5.33(b) show the cross-correlated and all the individual noise sources, respectively, during the third stepped leader. Figure 5.34 shows two-dimensional projections of the cross-correlated (squares), and all the detectable sources (triangles). Both first and third stepped leaders propagated downwards about 4 km and horizontally about 3.5 km in the first 5.5 msec. The channel of the respective VHF sources remained at least 1 km apart. The third stepped leader lasted 15.5 msec and propagated from a region inside the J2 process source volume. The VHF source for the stepped leader propagated off the Atlantic coast in the north-northeast direction about 10 km, descending from 6.8 km to a height of 0.7 km. The stepped leader velocity ranged between 7.6×10^5 m/sec and 1.1×10^6 m/sec.

It is significant to note that the three stepped leaders propagated from a common volume that can be approximated as a sphere with a 1 km radius. It appears that the location of the charge volume is not the principal factor determining whether subsequent return strokes will be

Figure 5.33(a). Three-dimensional view of the cross-correlated noise sources during the third stepped leader. Point A is the location of the first stepped leader cross-correlated source.

Figure 5.33(b). Similar three-dimensional view for all the individual detected sources.

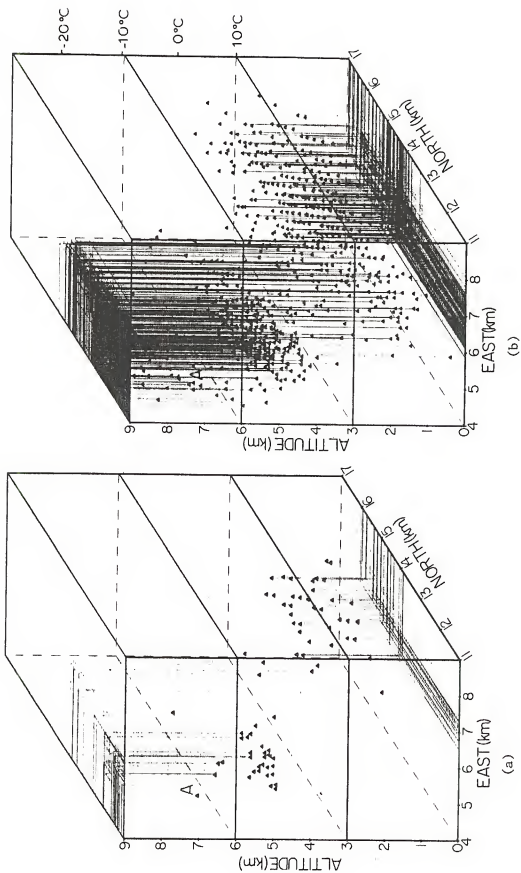
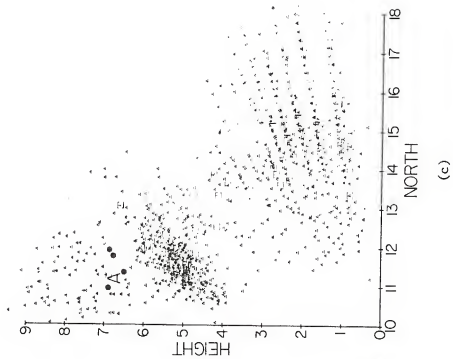
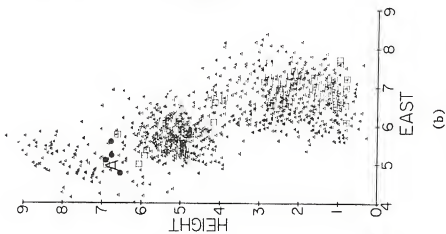
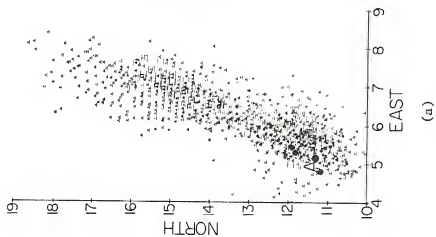


Figure 5.34. Two-dimensional views: (a) EW-NS, (b) EW-Height, and (c) NS-Height of all the sources (triangles) and the cross-correlated source locations (squares) during the third stepped leader. The four circles represent the location of the cross-correlated noise sources during the third return stroke.



preceded by stepped or by dart leaders. In addition, the amount of charge lowered by the subsequent stepped leaders was larger than the charge lowered by dart leaders. It is apparent in this flash that there are other factors such as the wind which might destroy the old return stroke channel and necessitate the formation of a new stepped leader.

5.2.10 Third Return Stroke

The VHF noise for the third stroke lasted 540 μ sec. The five return stroke VHF cross-correlated sources, 94 μ sec intervals, were located in the neighborhood of the previous stepped leader as shown in Figure 5.34. Assuming A (4.9, 11.2, 6.8), the highest detectable noise source at the beginning of the leader to be the point charge of the stepped leader and using the technique described in Section 3.6, we estimated that -9.3 Coul were lowered by the third stepped leader-return stroke process.

5.2.11 VHF Activity After Third Return Stroke

We have divided the VHF radiation that followed the final return stroke in two intervals. The first interval is described in this section as the continuous VHF radiation activity following the final return stroke (CAFS). The second interval is designated as the discrete VHF activity following the final return stroke (DAFS).

5.2.11.1 Continuous VHF Activity After Third Return Stroke. The CAFS followed immediately after the third return stroke and lasted 87.1 msec. Figure 5.35 shows the cross-correlated noise sources, 94 μ sec intervals, during this interval. The noise sources were located in the neighborhood of the previous J-changes but their path extended 2 km further toward the north. In addition the source locations were spread

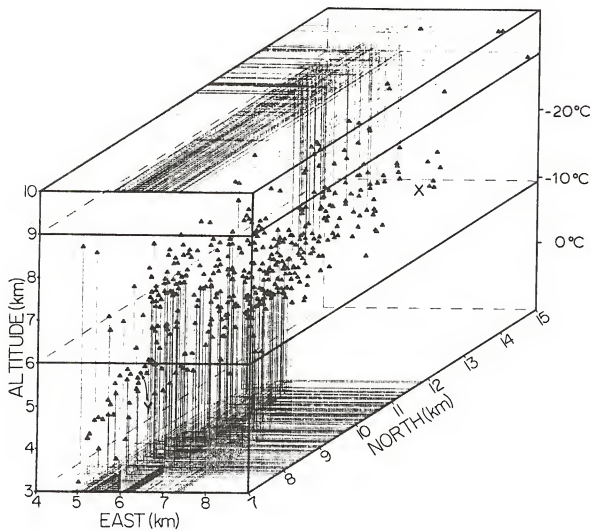


Figure 5.35. Three-dimensional view of the cross-correlated VHF noise sources during the 87.1 msec continuous VHF radiation activity following the return stroke.

out over a larger volume between the heights of 3.4 and 10 km. We studied the progressing sequence of the VHF sources and searched for any pattern in the development of the source locations. We determined that some of the large VHF pulses during this interval had correlated electric field changes. Every time a group of large pulses appeared, they were at a new location. The largest variation in the VHF source locations for consecutive pulses was about 5.4 km in the horizontal direction and 1 km in height. During the CAFS interval the electric field stations 3 and 19 km away showed the same sign in the slopes of the electric field change. This is probably due to the large horizontal component of the VHF sources in Figure 5.35 (Malan and Schonland, 1951; Uman, 1969; Krehbiel, 1979). Using a two-point charge model (equation (3.10)) for the X and Y locations in Figure 5.35, we found that -13.5 Coul were lowered or raised within the cloud during this interval.

The characteristics of the VHF noise during CAFS and its source locations are very similar to the J1 and J2 processes. From the characteristic of the VHF noise it is not evident that a new stepped leader will not occur until the VHF pulse rate decreases and quiet periods start developing at the beginning of DAFS. The VHF radiation of all the subsequent stepped and dart leaders studied in this thesis were preceded by a J-change VHF pulse rate of at least a pulse every 10 μ sec for at least 10 msec. The CAFS has this pulse rate but did not produce a leader. It appears that the VHF pulse rate and duration of VHF activity is a necessary condition for leader development but it is not a sufficient condition.

5.2.11.2 Discrete VHF Activity After Third Return Stroke. The discrete VHF activity after return stroke (DAFS) followed the CAFS phase and lasted 71 msec in the VHF record. Six solitary pulses (Figure 5.1) could be observed in this final stage of the flash. Three of these SP's showed correlated electric field changes. The last SP lasted 1.9 msec, had a correlated rapid electric field change, and possessed the largest amplitude of the VHF radiation of any pulse in the flash. The VHF radiation and the location of its cross-correlated noise sources are shown in Figures 5.36 and 5.37, respectively. The first five noise sources (A to E in Figure 5.36) corresponded to the first two wide pulses at the beginning of the SP. These sources were located in a regular progressing sequence and propagated 2 km south and 1 km downward at a velocity of 8.8×10^6 m/sec. The source locations of the remaining 1.4 msec were located in the different regions shown in Figure 5.37. The most concentrated VHF source region, J to S, corresponded to the lowest crowded VHF source region of J1, J2, and CAFS, most likely a negative charge region because that is where the stepped leaders originated. At the end of the SP some of the noise sources, T to W, were located in the same returning path to A. The location of these noise sources showed some evidence that this 1.9 msec SP was a K-change as described by Kitagawa and Kobayashi (1958) except that Kitagawa estimated downwards velocity in the order of 10^4 m/sec. By measuring the electric field changes as a function of distances, Kitagawa and Kobayashi (1958) concluded that K-changes resulted when charges moving downward encounter charges of the opposite sign and upward moving return strokes occur. The noise sources indicate this type of effect. Positive charges located near A were lowered to the main active negative charge region (J to S) and an upward moving

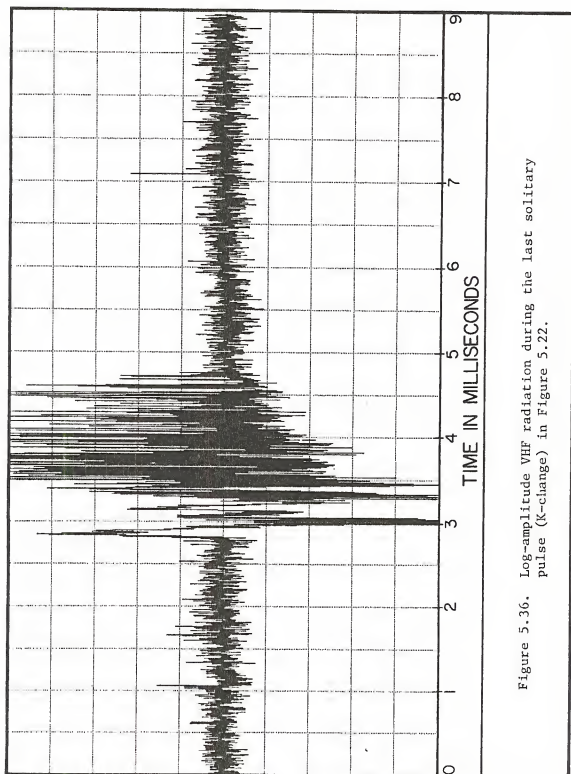
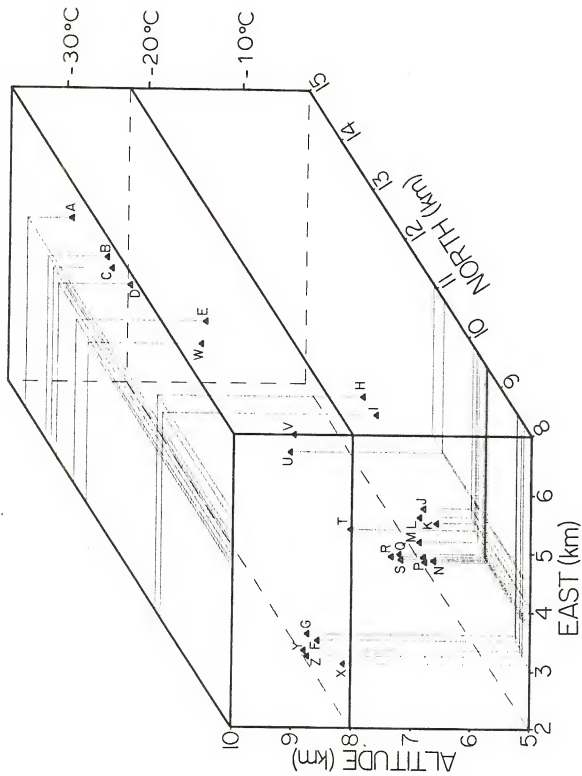


Figure 5.36. Log-amplitude VHF radiation during the last solitary pulse (K-change) in Figure 5.22.

Figure 5.37. Three-dimensional view of the cross-correlated VHF noise sources during the last SP (K-change). The letters A through Z show the location of the progressing sequence of the VHF noise sources.



propagation ended the process. The regions F, G, X, Y, Z and H, I correspond to the outer region of the previous J1, J2, and CAFS volume. Finally it is worth noting that the initial horizontal and downward propagation velocity of 8.8×10^6 m/sec (A to E) is comparable to the upward propagation of 9.1×10^6 m/sec (S to W).

5.2.12 Volume of the Flash

Figures 5.38(a), 5.38(b), and 5.38(c) show two-dimensional projections of the 34,478 noise sources located during the flash. The average rate of pulses is about one every 8 μ sec. The pattern evident in Figure 5.37 is explained in Appendix B. The flash occurred near the coast of the Atlantic Ocean in the central part of the Cape Canaveral AFS, from 3 to 8 km EW, 7 to 17 km NS, and up to 12 km in height. With the exception of the three stepped leaders most of the flash concentrated between 4 and 7 km EW, 9 to 12 km NS, and 4 to 8 km in height. The flash extended throughout a volume of about 500 km^3 during a time of 282 msec.

5.2.13 Concluding Remarks About the Flash

We now provide a summary of what we have learned about this flash.

(1) The flash lasted 282 msec and consisted of three return strokes each preceded by a separate stepped leader to ground. (2) The flash started with a PB that lasted 2.1 msec. During the first 600 msec of the PB the VHF sources propagated upwards and horizontally and there was no detectable correlated electric field change. During the last msec of the PB the noise sources filled a path in an unorganized way of 1 km in both the horizontal and vertical direction. (3) The three stepped leaders lasted 7.9, 29.0, and 15.5 msec, respectively. All three stepped leader paths to ground started within 2 km of each other and

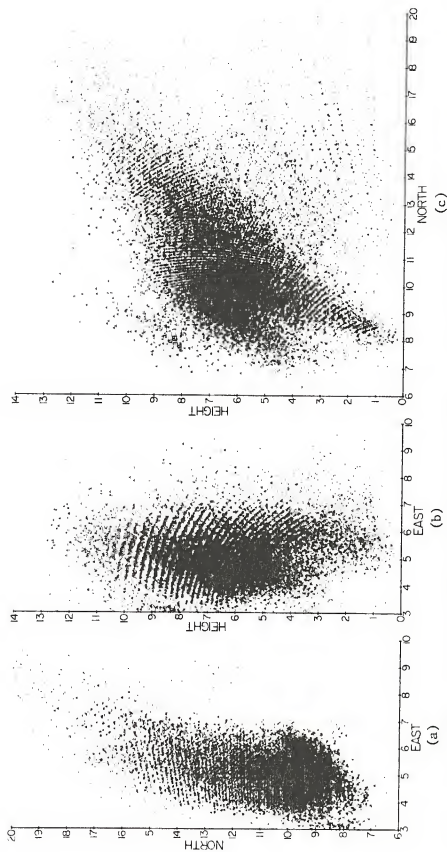


Figure 5.38. Two-dimensional views: (a) EW-NS, (b) EW-Height, and (c) NS-Height of all the 34,478 noise sources (triangles) during the 282 msec flash. The cross-correlated VHF sources are also shown (squares).

between a height of 6 and 7 km. The first and third stepped leaders propagated over water and had large horizontal components. The second stepped leader had a large horizontal component during the first 18.2 msec, then was propagated vertically making a ground contact near the coast. The three stepped leader velocities were: 0.8×10^5 to 1.7×10^6 m/sec, 2.4 to 5.3×10^5 m/sec, and 7.6×10^5 to 1.1×10^6 m/sec, respectively. The charge lowered by each one of the three leader-return stroke processes was calculated by using a point charge model: -13.4, -11.5, and -9.3 Coulombs, respectively, were lowered by these processes. (4) The VHF sources corresponding to the VHF radiation in the first 8.8 msec after the first return stroke were located in the upper part of the previous stepped leader-return stroke process. By correlating with the electric field we determined that either positive charges were raised or negative charges were lowered from higher regions in the cloud. (5) The second and third stepped leaders were preceded by J-change processes that lasted 28.4 and 31.2 msec, respectively. During these processes the bulk of the VHF noise sources were located in overlapping cloud regions between the heights of 6 and 9 km. The first J-change started with a K-change that propagated for about 6 km lowering 0.85 Coulombs. The progressing sequence of the VHF locations during the second J-change formed along the surface of a cylinder and as the process continued the sources filled the inside of the cylinder. (6) Two types of VHF radiation, continuous and discrete, occurred on sequence after the third return stroke. The VHF sources during the 87.1 msec of continuous VHF activity were located in the neighborhood of the previous J-change. The discrete activity consisted of 5 solitary pulses. The second, third, and last pulse had identifiable rapid

electric field change. Therefore we associated these pulses with K-changes. At the beginning of the last K-change the VHF sources propagated downward about 4 km into the main negative charge region. At the end of the K-change there was some upward propagation. Except by the velocity of the downward propagation, this behavior is in agreement with a model proposed by Kitagawa et al. (1958). That is, the lowering of positive charges within the cloud is followed by mini-return strokes.

(7) A total of 34,478 noise sources, an average of one every 8 μ sec, were detected during the flash. The flash extended a volume of about 500 km³.

5.3 The 181806 Flash

On 8th August 1977 at 181806 a cloud-to-ground flash was photographed via a television camera (Figure 5.39) and videotape recorder striking the 150-meter weather tower struck previously by the July, 1976 165959 flash. The VHF portion of the 181806 flash lasted 418 msec and consisted of a six strokes to ground followed by a 216 msec continuing current. Figure 5.40 shows the relationship between the VHF radiation and the electric field for the entire discharge. Table 5.3 contains a complete summary of the various phases of the flash. The upper and lower locations, the duration of the phases, and the average velocity if defined, of the VHF noise sources in each phase are given. Even though the upper and lower coordinates are given for each event in Table 5.3, only the events with velocities listed showed continuous upwards or downwards propagation between these upper and lower coordinates, source locations as a function of time for the other events being less organized. These charge regions are correlated with the VHF source locations for each of the return strokes. The accuracy in the determination of source locations for the entire flash is given in Appendix B. In the next sections we consider in detail what we learned from the VHF radiation about the phases of the 181806 flash listed in Table 5.3.

5.3.1 Preliminary Breakdown (PB)

The VHF radiation started 7.8 msec prior to the first return stroke. The first 1.9 msec of the 7.8 msec were associated with the preliminary breakdown. The VHF noise during this 1.9 msec is characterized by high frequency pulses riding on the envelope of pulses having between 20 and 40 μ sec width. Figure 5.41 shows the VHF noise during the PB, the stepped leader, and the first return stroke. The electric field change

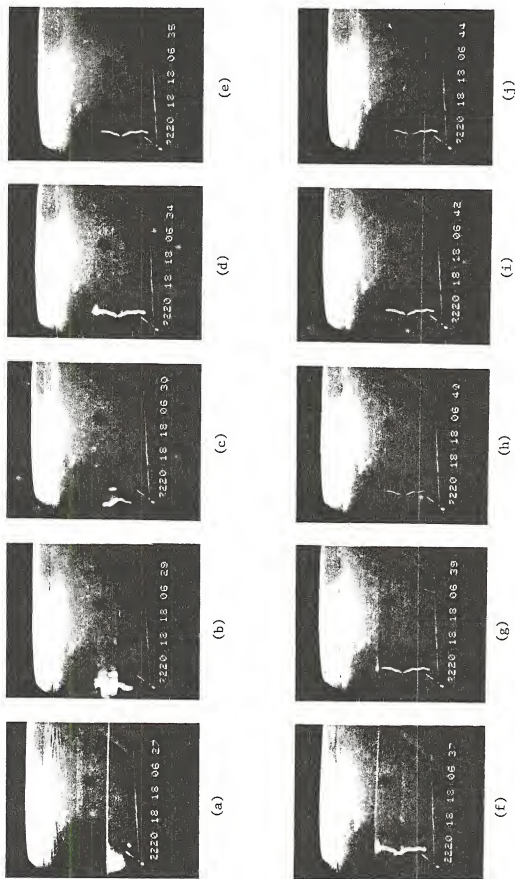


Figure 5.39. Sequence of photographs during the 101306 flash. The Julian day is 220 and the time is shown in each photo. Sequence (a) through (h) shows the two stepped leader return stroke channels. Sequences (a), (b), and (c) correspond to the first stroke that hit the tower while sequences (d) through (j) show the remaining strokes in a separate channel. This photo is a courtesy of Douglas Jordan of the University of Florida.

Figure 5.40. Simultaneous record of the logarithmic-amplitude VHF radiation observed at 10 km, and the electric field 14 km away, during the 181806 flash. The following events in the flash are shown: R1 to R6 represents the six return strokes; SL1 and SL2 are the two stepped leaders; J1 to J5 are the interstroke processes; FR is the activity following the first return stroke; and CC is the continuous current interval.

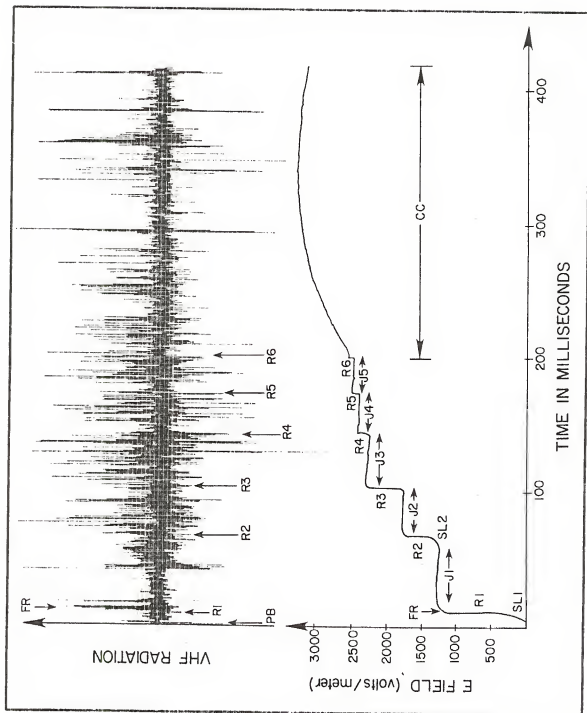


Table 5.3. Events in the 181806 Flash.

Universal Time at the Start of the VHF Radiation: 18 18 06 266.13, 8th August 1977										
Start Time (msec)	Event	Duration (msec)	Coordinates (km)						Velocity m/sec	
			UPPER			LOWER				
			x	y	z	x	y	z		
0	Preliminary Breakdown	1.9	-0.08	9.2	9.5	-0.86	9.1	6.7	(*) 9.2×10^5	
1.9	First Stepped Leader	5.9	-0.86	9.1	6.7	-0.82	8.7	2.7	1.0×10^6	
7.8	Return Stroke (R1)	0.475	0.1	9.6	10.2	-1.5	9.7	2.9		
8.2	Following 1st Return Stroke	8.86	-0.4	9.0	8.4	-1.5	8.8	5.1	1.2×10^7	
17.0	Semi-Quiet Period	7.5	-0.3	9.1	9.5	-0.8	9.0	6.5		
24.5	Quiet Period	16.5								
41.0	First J-Change	8.1	1.8	11.4	14.2	0.7	9.2	10.5	5.0×10^5	
49.1	New Stepped Leader	17.5	0.7	9.2	10.5	-2.4	8.9	2.8	6.7×10^5	
66.6	Return Stroke (R2)	.859	1.8	11.1	14.5	-1.0	8.3	6.5		
67.5	Quiet Period	.5								
68.2	J-Change (J2)	36.2	1.9	10.08	12.7	-0.4	8.9	5.8		
104.4	Dart Leader	.495	0.3	9.8	8.5	-0.6	9.7	7.5		
104.9	Return Stroke (R3)	.092	0.8	11.8	12.6	-1.4	11.8	12.2		
105.0	Quiet Period	1.1								

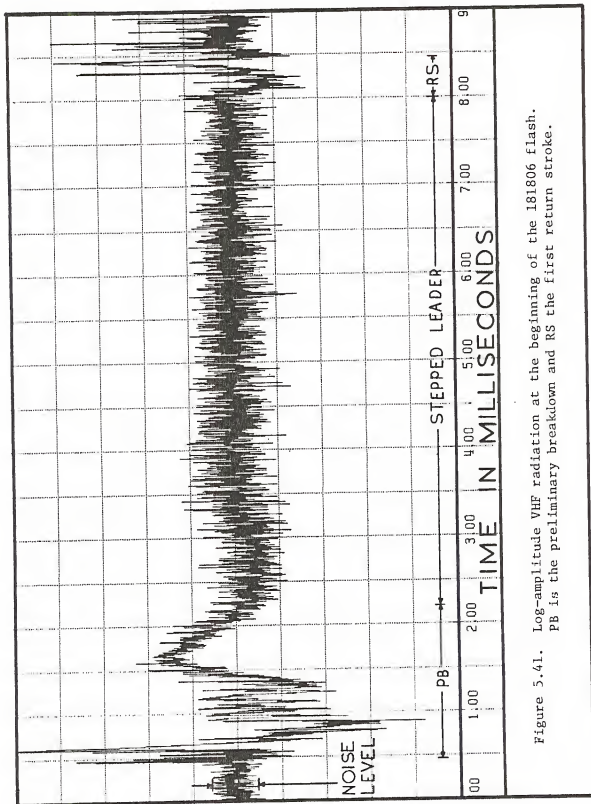


Figure 5.41. Log-amplitude VHF radiation at the beginning of the 181806 flash.
PB is the preliminary breakdown and RS the first return stroke.

starts about the middle of the PB interval and correlated VHF and electric field pulse occur. After this point and continuing throughout the rest of the PB and the stepped leader, large electric field pulses are correlated with VHF pulses.

In addition to determining the cross-correlated, 94 μ sec intervals, and all the source locations using the computer algorithm described in Chapter IV, we matched the pulses manually during the first 120 μ sec of the flash. We determined 36 locations during this interval, a location every 3.3 μ sec, about twice as many sources as determined by the computer algorithm. Figure 5.42 shows a three-dimensional view of all the VHF sources during the 120 μ sec interval. The labels A to Z, and AA to JJ show the regular progressing sequence of the noise sources. The VHF sources formed a path 20° off vertical between the heights of 5 and 11 km.

During the PB the cross-correlated noise sources were located between 9.5 and 6.7 km of altitude. However, all the PB noise sources extended between the heights of 10.3 and 6.5 km. The upper and lower cross-correlated source locations are shown as A and B in Figures 5.43 and 5.44. Even though the cross-correlated noise sources showed a predominant downward propagation, the first few individual sources did not correspond with the highest source locations. The first cross-correlated source detected was at 7.9 km. The cross-correlated source locations, 94 μ sec intervals, propagated upwards during the first 4.9 msec. However, during the final 1.0 msec of the preliminary breakdown, that was coincident with appreciable electric field change, the propagation of the cross-correlated VHF sources is only downwards. All the VHF noise sources during the entire PB interval were located with a cylinder of 500 meter radius in the path from A to B as shown in Figures 5.43 and

Figure 5.42. Three-dimensional view of all the VHF noise sources during the first 120 μ sec interval at the beginning of the 181806 cloud-to-ground flash.

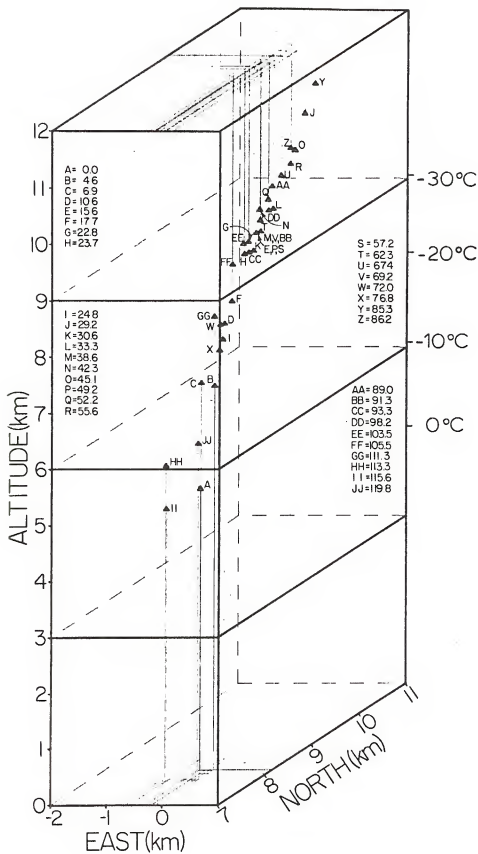
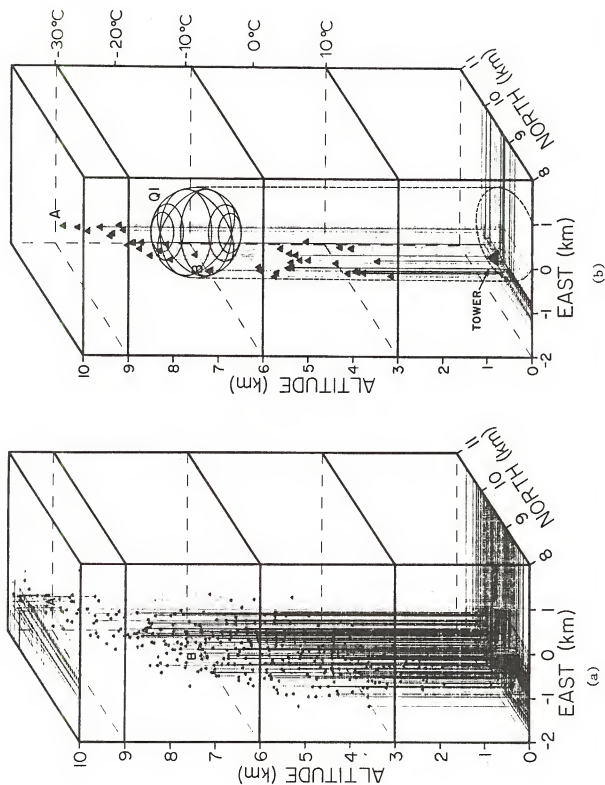


Figure 5.43(a). Three-dimensional view of the cross-correlated noise sources during the first PB-stepped leader process. Point A corresponds to the height cross-correlated source during the PB. Point B is a similar source at the beginning of the stepped leader. The sphere Q1 represents the source charge for the first return stroke by Krehbiel (private com) using the techniques of Krehbiel et al., (1979).

Figure 5.43(b). Similar three-dimensional view for all the individual detected sources.



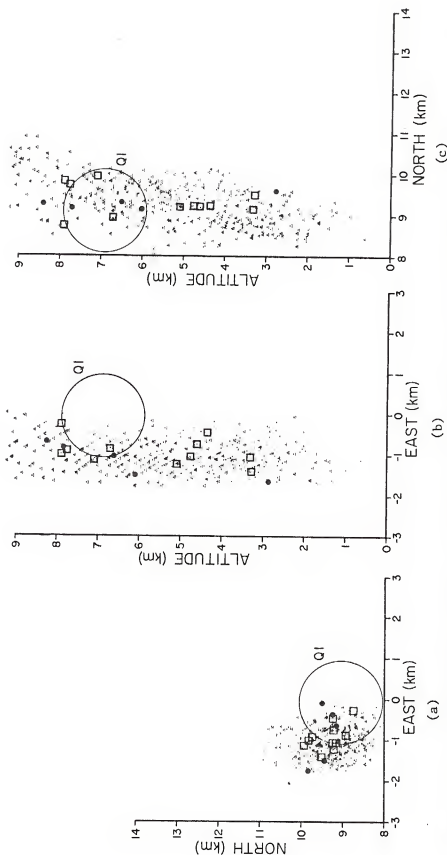


Figure 5.44. Two-dimensional views: (a) NS-EW, (b) EW-height, and (c) NS-height of all the sources (triangles) and the cross-correlated source locations (squares) during the P8 and the first stepped leader. The five circles represent the location of the cross-correlated noise sources during the first return stroke. The circle Q1 is the two-dimensional projection of Q1 in Figure 5.43.

5.44. The average velocity of propagation during the final msec of the PB was 9.2×10^5 m/sec.

5.3.2 First Stepped Leader

The first stepped leader immediately followed the preliminary breakdown and lasted 5.9 msec. The VHF noise during the stepped leader was characterized by high-frequency low-amplitude radiation. As we shall show from an examination of all the flashes in this thesis, these high frequency pulses are typical of stepped leaders and hence we can with confidence associated them with the stepped leader process. The VHF noise sources could be correlated during the first 3.5 msec of the leader. During the last 2.4 msec the pulse rate becomes faster than a pulse every 2 μ sec and the pulses could not be correlated because too many VHF sources were simultaneously active over a large volume. In addition, the magnitude of the VHF stepped leader pulses decreased.

The stepped leader followed a near-vertical path from the PB to the tower. Figure 5.43 shows the VHF noise sources during the PB and the stepped leader. Figure 5.43(a) shows the 416 detected individual sources. Figure 5.43(b) shows the cross-correlated sources (94 μ sec intervals) and the location of the tower struck by the flash. The stepped leader cross-correlated sources were detected between a height of 6.7 and 2.7 km. Point B shows the source location around the transition point between the two different characteristics of the VHF noise representing the PB and the SL. Figure 5.44 shows the two-dimensional projections of all the PB and stepped leader sources. The cross-correlated values, 376 μ sec intervals, are shown as a square of larger size than the actual source locations which are shown as triangles. The circles in Figure 5.44 correspond to the return stroke

charge sources to be discussed in the next section. The near-vertical path of the PB and the stepped leader is evident from this picture. The stepped leader velocity was 1.0×10^6 m/sec. Photographs taken of this flash (Figure 5.39) showed that the first channel struck the 150-meter weather tower. Figure 5.45 shows three sequences of histograms of all the source locations during the PB and the first 3.2 msec of the stepped leader. These graphs are similar to those provided in Figure 5.7 and they illustrate the propagation of noise sources for three time sequences, every 1.5 msec.

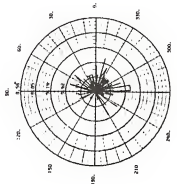
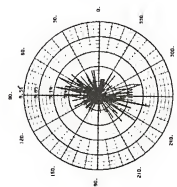
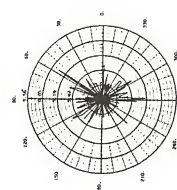
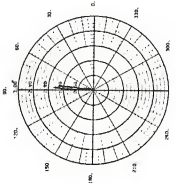
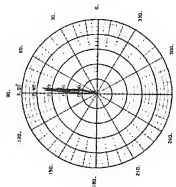
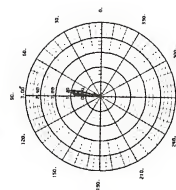
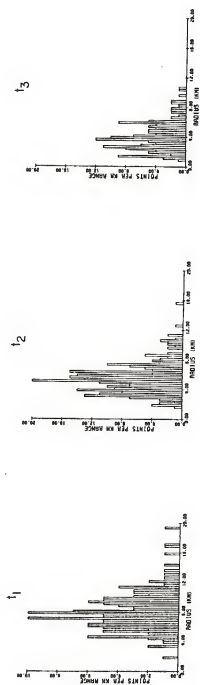
5.3.3 First Return Stroke

The first return stroke VHF radiation lasted 475 μ sec. The noise was characterized by a low frequency envelope with a succession of pulses between 10 and 50 μ sec width. Noise sources were located during and immediately following the return stroke. The return stroke cross-correlated noise sources, 94 μ sec intervals, are shown as circles in Figure 5.44. The return stroke noise sources are located in the preliminary breakdown and stepped leader channel regions.

The charge and locations of the six return stroke charge regions (Q1 through Q6) were provided by Krehbiel (private com) and were found using the technique of Krehbiel et al. (1979). Krehbiel's results are summarized in Table 5.4. The Q1 charge center in Table 5.4 is within random error in source location from B (-0.9, 9.1, 6.7) which is the point charge location of the transition in the VHF record between the PB and the stepped leader. At a station 10.9 km from the tower, the electric field change from the first leader-return stroke sequence was 990 volts/meter. Using location B as the charge center and the technique

Figure 5.45.

Three sequences of histograms, t_1 , t_2 , and t_3 (1.5 msec intervals) of all the detected sources in the PB and the stepped leader. Sequences (a), (b), and (c) correspond to t_1 , t_2 , and t_3 , respectively. There are three histograms in each sequence. The top row shows distance histograms referenced to the weather tower. The middle row shows histograms of the elevation angle of the sources referenced to the weather tower. The bottom row shows histograms of the azimuth angle of the sources referenced to the weather tower.



(c)

(b)

(a)

Table 5.4. Charge and Locations of the Six Return Strokes as provided by Krehbiel (private com) using the technique described by Krehbiel et al. (1979).

Return Stroke	Charge (Coulombs)	Location (km)
Q1	-25.7	(-0.1, 9.1, 6.9)
Q2	- 9.6	(0.2, 11.2, 8.1)
Q3	-10.0	(-0.4, 9.2, 7.4)
Q4	- 4.9	(1.4, 11.9, 7.4)
Q5	- 2.9	(1.6, 11.1, 7.0)
Q6	- 3.4	(1.6, 11.3, 6.9)

described in Section 3.6, we found that -17.2 Coulombs were lowered by the first return stroke.

5.3.4 Following First Return Stroke (FR)

Figure 5.46 shows the VHF noise during the FR period. Strong VHF radiation with a pulse every 3 μ sec was detected during the first 8.9 msec after the first return stroke. Two large pulses were detected 4.4 and 8.7 msec after the beginning of the FR. These pulses were 250 and 100 μ sec wide, respectively, and had the largest amplitude of any VHF pulses in the entire flash. These wide pulses contained superimposed pulses that propagated upwards at a velocity of 1.2×10^7 m/sec.

About 90% of the VHF noise sources during the FR were located in the previous stepped leader-return stroke channel between the heights of 5 and 8 km. The remaining 10% of the sources were located between the heights of 3 and 5 km and above 8 km. Figure 5.47 shows the cross-correlated locations, 376 μ sec intervals, for the FR period. The locations are labeled to indicate the sequence on which the events occurred. The noise sources propagated upwards between the heights of 5 and 8 km. By correlating the VHF radiation sources with the electric field record during this time period, we conclude that either positive charges were raised by the FR interval or that negative charges were lowered from higher altitudes as the VHF sources move upward.

5.3.5 Semi-Quiet Period (SQP) Following the FR

The VHF activity continued for 7.5 msec after the first FR at an average rate of a pulse every 25 μ sec. This time interval appears to be a transition between the high pulse rate from the FR and the quiet period with almost absent VHF radiation that followed the SQP. About

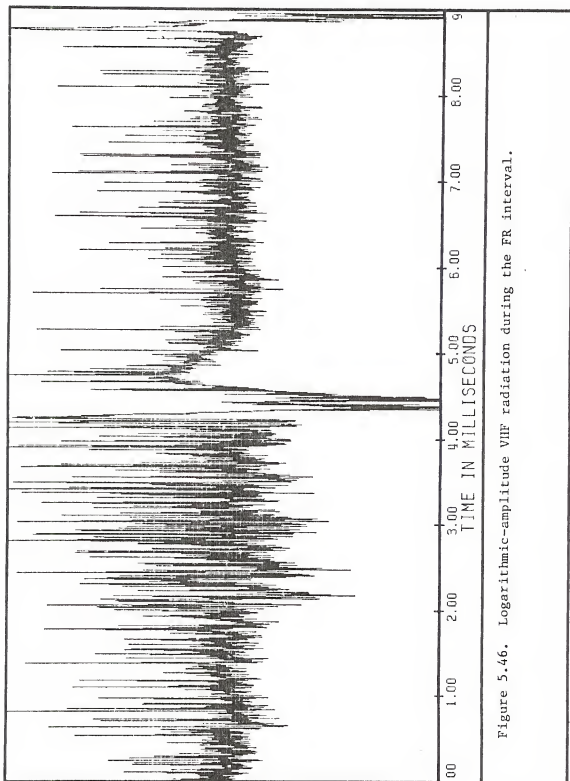
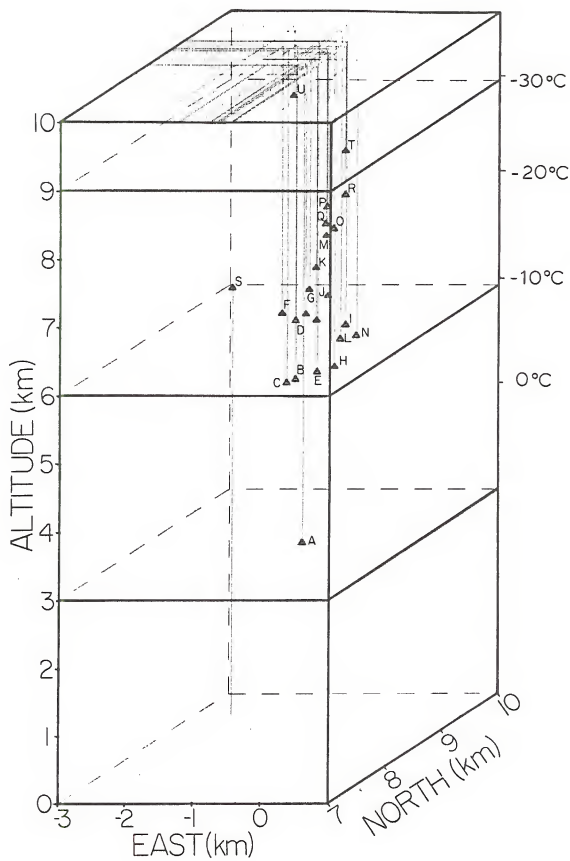


Figure 5.46. Logarithmic-amplitude VHF radiation during the FR interval.

Figure 5.47. Three-dimensional view of the cross-correlated noise sources, 94 μ sec intervals, during the FR interval. The labels A to U show the progressing sequence of occurrence of the sources.



85% of all the VHF sources during this period were located between the altitudes of 6.5 and 9.5 km. The remaining 15% of the sources were located near the altitude of 2 km in the neighborhood of the previous channel. The SQP interval extended the upward propagation of the sources during the previous FR interval. The end of the SQP interval coincides with the highest detectable sources during the previous PB.

5.3.6 First J-Change Process and Second Stepped Leader

For 16.5 msec after the SQP interval there was a quiet period in which no VHF noise sources were detected. After this period the VHF portion of the interstroke interval started. The VHF noise during the interstroke interval would normally be called a J-change. However, this J-change is identical to the VHF noise during the PB that preceded the first stepped leader as if an entirely new flash were beginning. The only difference is that the PB's that precede first stepped leaders studied in this thesis range between 1 and 3 msec and the J-change or PB VHF noise that preceded the second stepped leader lasted 8.1 msec. After the first 8.1 msec we detected the high-frequency low-amplitude waveform which is typical of stepped leader.

Figure 5.48 shows a three-dimensional view of the cross-correlated sources, 376 μ sec intervals, detected during the J-change (J1) or PB2 and subsequent stepped leader. Figure 5.49 shows two-dimensional projections of the 1897 noise sources detected during these processes. The fact that the source locations at the high altitudes are oriented in patterns, either near-vertical for the east-height plot or near-horizontal for the north-height plot, is attributed to the quantization error in the determination of the coordinates. Appendix B shows a

Figure 5.48. Three-dimensional view of the cross-correlated VHF sources, 94 μ sec intervals, during the J1 or PB2 and the second stepped leader. The labels A, B, C, and E, F, G show different regions of propagation of the VHF noise sources. Q2 is the source charge for the second return stroke obtained from electric field records.

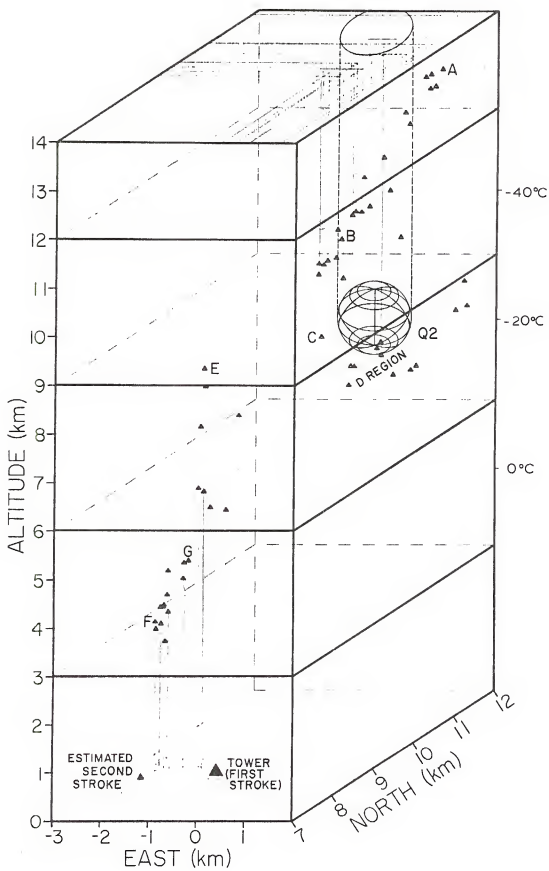
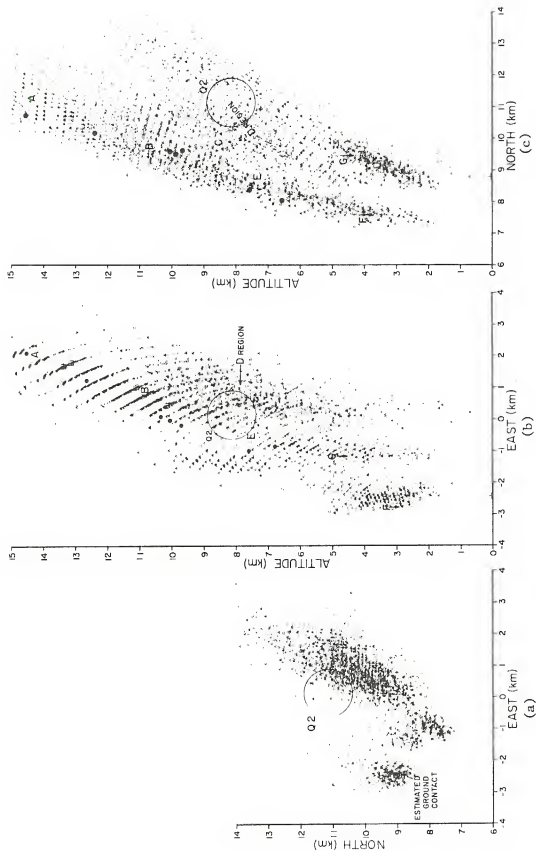


Figure 5.49. Two-dimensional views: (a) top view, EW-NS, (b) elevation view, EW-height, and (c) elevation view, NS-height of all the sources (triangles) and the cross-correlated source locations (squares), 376 μ sec intervals, during the J1 or PR2 and the second stepped leader. The labels A, B, C and E, F, G show different regions of propagation. The circles are the cross-correlated sources, 94 μ sec intervals, of the second return stroke. The circle Q2 is the projection of Q2 in Figure 5.48.



derivation of the quantization and calibration RMS error in the determination of the three dimensional coordinates.

The noise sources during the J-change or PB2 started at a height of about 14.2 km (point A, Figures 5.48 and 5.49) and propagated downward in a path 25° off-vertical to a height of 10.5 km (point B, Figures 5.48 and 5.49). The velocity of propagation was 5.0×10^5 m/sec. Even though the VHF noise changed characteristics at point B, the noise sources continued their downward propagation. Applying the dipole model of equation (3.10) to the 8.1 msec J1 or PB2 for an electric field station located 12 km from the tower, we find that 1.8 Coul were transferred between A (1.8, 11.4, 14.2) and B (0.7, 9.2, 10.5). The J1 or PB2 process apparently made available some of the negative charge lowered by the new stepped leader. The stepped leader duration was 17.5 msec. The stepped leader propagated from point B to C in about 2.6 msec. At this time and for the next 8.7 msec two active regions D and E (Figures 5.48 and 5.49) started emitting VHF radiation. The D region is in the neighborhood of the Q2 charge center while the E region appears to extend the leader path toward the lower altitudes. The VHF radiation was only detected during the first 3.4 msec of the remaining 6.2 msec of the 17.5 msec stepped leader. In this time interval all the VHF noise sources were located below a height of 6.5 km. From a study of all the noise sources during the 3.4 msec (Figures 5.49(b) and 5.49(c)), it appears that the VHF radiation between the height of 5 and 1.5 km was emitted by two separate channels. We labeled these channels as F and G in Figures 5.49(b) and 5.49(c). From the location of the first return striking the 150-meter weather tower and from the locations of other objects on the ground in Figure 5.39, we estimated the ground

contact about (-2.5, 8.4). This is 1.4 km west and .9 km south of the 150-meter weather tower struck by the first return stroke channel. Channel F corresponds to a vertical extension of the location of the stepped leader-second return stroke luminosity while the G channel locations are in the neighborhood of the first stepped leader channel. The average velocity for the stepped leader was 6.7×10^5 m/sec.

From the VHF source locations and the sequence of photographs it is clear that the second stepped leader developed in a separate channel to ground as shown in the sequence of pictures in Figure 5.39. The four succeeding strokes to ground traversed the second stepped leader-return stroke channel. It is possible that the J1 or PB2 process is not directly related to the first leader return stroke sequence. In that case we have two separate flashes: a single stroke flash and a five stroke flash with continuing current. However, the longer duration of the preliminary breakdown of the second flash compared to the duration of the PB's for the other flashes described in this thesis, and the fact that the VHF noise sources at the beginning of the second flash were located at much higher altitudes than other PB's sources in this thesis tend to indicate that the second stepped leader had different characteristics from usual first stroke PB's. Further, the time between the first two strokes was 58 msec, a typical interstroke time, indicating that there probably was a connection between the two strokes.

5.3.7 Second Return Stroke

The second return stroke had a duration of 859 μ sec in the VHF record as shown in Figure 5.50. The return stroke radiation was characterized by a succession of low frequency pulses between 10 and 100 μ sec wide with superimposed high frequency pulses. Seven average

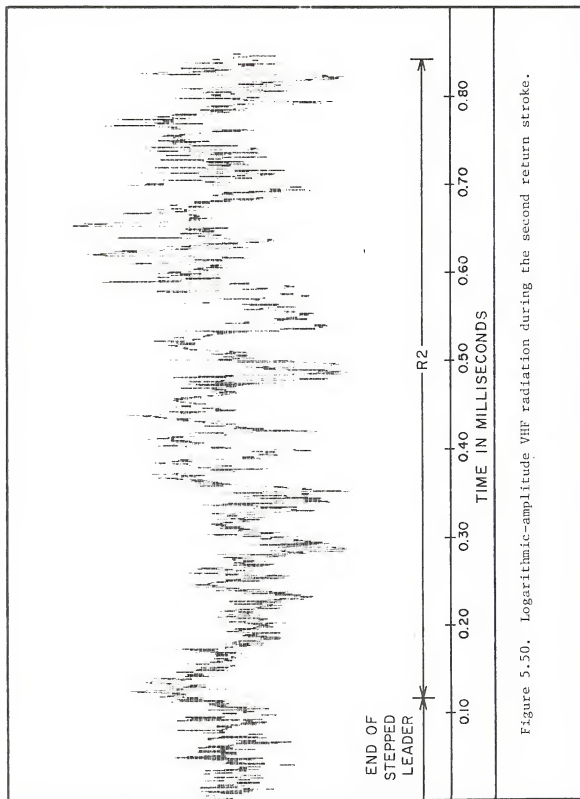


Figure 5.50. Logarithmic-amplitude VHF radiation during the second return stroke.

return stroke locations, 94 μsec intervals, are shown as circles in Figure 5.49. The return stroke channel locations extended from 6.5 to 14.5 km of altitude. The return stroke channel propagated not only throughout the previous leader but also in the previous J-change (J1) or preliminary breakdown (PB2). This is a reasonable result since the entire channel was apparently negative charged and the return stroke neutralized part of this charge. Three of the seven return stroke source locations were between 9 and 10 km. It was at about this location (point B, Figures 5.48 and 5.49) that the VHF noise changed characteristics from J1 or PB2 to stepped leader. Taking point B (0.7, 9.2, 10.5) as the point source of the second return stroke and using the techniques described in Section 3.6, we calculated that -8.2 Coulombs were lowered by the second leader-return stroke sequence. This number compares reasonably well with the -9.6 Coul shown in Table 5.6.

5.3.8 Second J-Change Process

Figure 5.51 shows the cross-correlated VHF noise sources, 376 μsec intervals, during the second J-change (J2). The J2 process started after a quiet period of .5 msec, lasted 36.2 msec, and extended in a path 32° off vertical between the heights of 5.8 and 12.7 km. Figure 5.51 also shows the Q3 location given in Table 5.6. The VHF noise sources during the first millisecond were located at the bottom, the middle, and the top of the J2 channel. These sources do not appear to propagate upward in the channel, rather the noise sources are located along isolated volumes along the path that joins these locations. During the remaining 35 msec, 78% of the VHF noise sources are located between the heights of 7.5 and 11.5 km. It is worth noting that even

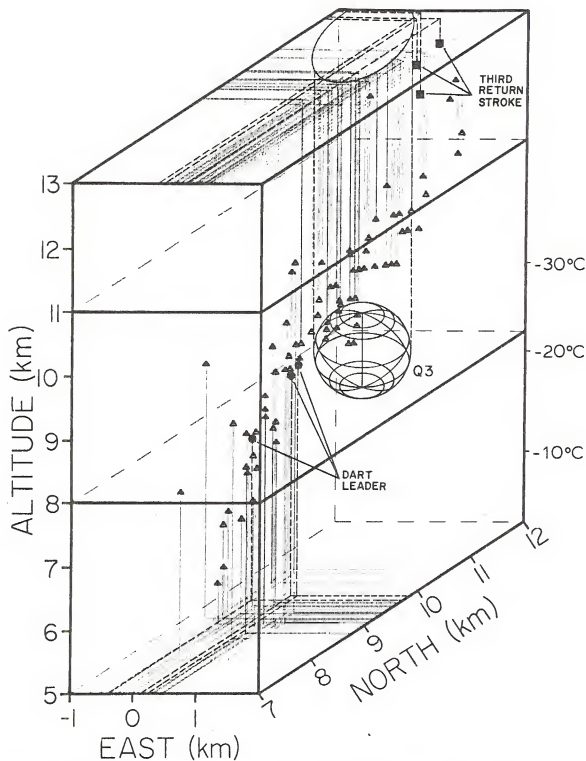


Figure 5.51. Three-dimensional view of the cross-correlated noise sources during J2, the dart leader, and the third return stroke. The location of the third stroke spherical charge center is shown as Q3.

though the VHF noise sources do not appear in a regular progressing sequence throughout the channel, about 80% of all the source locations are located within 1 km perpendicular distance of a line 32° off vertical leading toward the northeast. It appears that the VHF radiation during the latter part of the J-change joins previous regions from an earlier part of the J-change. In addition, during the last 7.2 msec of the J-change all the VHF noise sources were located in the lower half of the channel between the heights of 5.7 and 9 km.

5.3.9 Dart Leader and the Third Return Stroke

Figure 5.52 shows the VHF radiation during the dart leader and the third return stroke. The dart leader lasted 495 μ sec and was followed by a 92 μ sec return stroke.

The VHF sources of the dart leader were located between the heights of 7.5 and 8.5 km, in the neighborhood of the previous J-change. Three dart leader's cross-correlated locations, 94 μ sec intervals, are shown as circles in Figure 5.51. The third return stroke VHF noise sources were located near the top of the J2 channel. Three return stroke sources, 94 μ sec intervals, are shown as squares in Figure 5.51. It is worth noting that while the VHF noise of the dart leader was located in the bottom half of the previous J-change, the return stroke sources were located near the top of the previous channel.

5.3.10 Third J-Change (J3)

Figure 5.53 shows the cross-correlated VHF noise sources, 376 μ sec intervals, during the third J-change process. Figure 5.53 also shows the location of the fourth return stroke spherical change center (Q4). There was a 1.1 msec quiet period between the previous return stroke

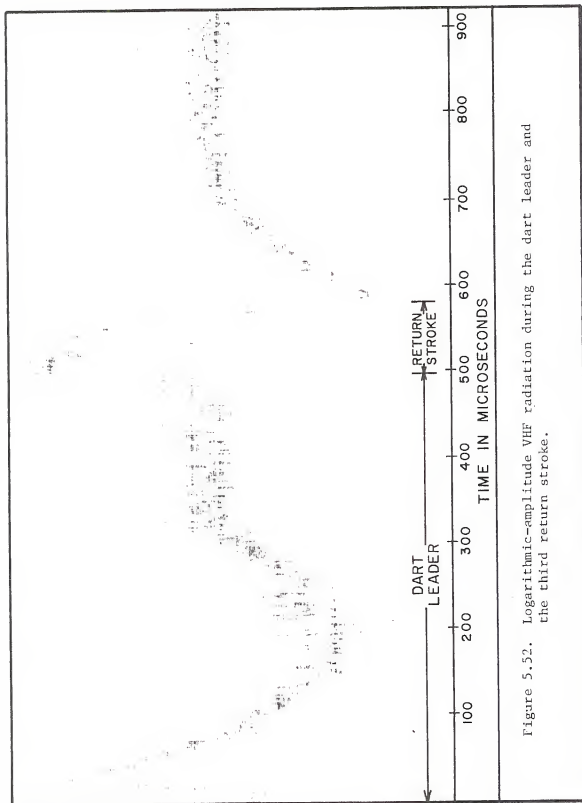


Figure 5.52. Logarithmic-amplitude VHF radiation during the dart leader and the third return stroke.

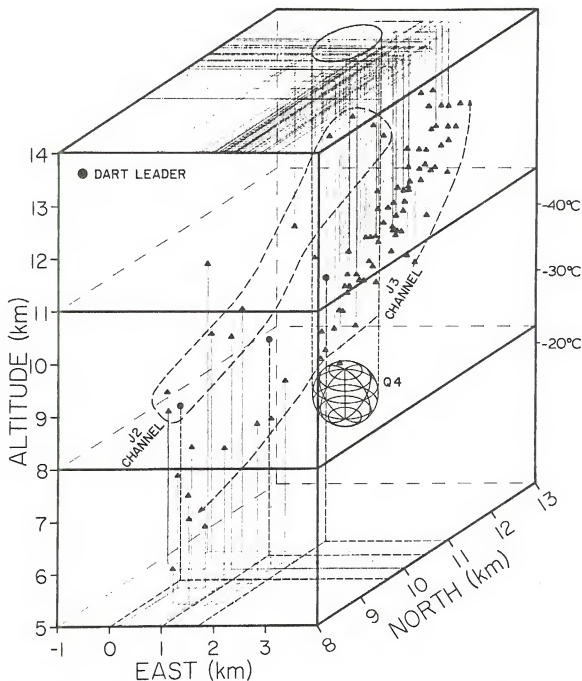


Figure 5.53. Three-dimensional view of the cross-correlated noise sources during J3, and the dart leaders. Source locations of the previous J2 channel which continue to radiate during J3 are also shown. The location of the fourth stroke spherical charge center is shown as Q4.

and J3. The third J-change lasted 37.7 msec and extended in a path 35° off vertical between the heights of 5.7 and 13.0 km. The channel was located 1.5 km east and .5 km north of the previous J-change channel. As with J2, the locations of the VHF sources did not follow any regular sequence along the channel. About 70% of all the sources were located between the heights of 9 and 12 km in a path 35° off vertical. Some of the VHF sources from J2 were still active during J3. These sources are located west and north of the J3 channel as can be seen in Figure 5.53. The VHF sources during the J3 process spread out over similar and parallel paths, but at higher altitude than J2. The overall radiation region during J3 becomes wider because active sources from the previous J-change radiate again or continue to radiate.

5.3.11 Dart Leader and the Fourth Return Stroke

Figure 5.54 shows the VHF noise at the end of the J3 process and during the dart leader preceding the fourth return stroke. Correlation with the electric field records indicate that the dart leader started at 20 ± 30 μ sec from the beginning of Figure 5.54. We studied the VHF records for 2 msec following the two 80 μ sec pulses that marked the beginning of the dart leader but we did not detect any large pulses. Since return strokes are characterized by wide pulses of large amplitude and the multiple electric field stations showed an abrupt field change characteristic of return stroke, we concluded that the fourth stroke did not produce any VHF radiation. It appears that the VHF radiation from consecutive return strokes is due to the extension of the previous channel in a non-previously ionized region. Probably the fourth return stroke propagated only throughout a previously ionized channel, consequently produced no VHF radiation.

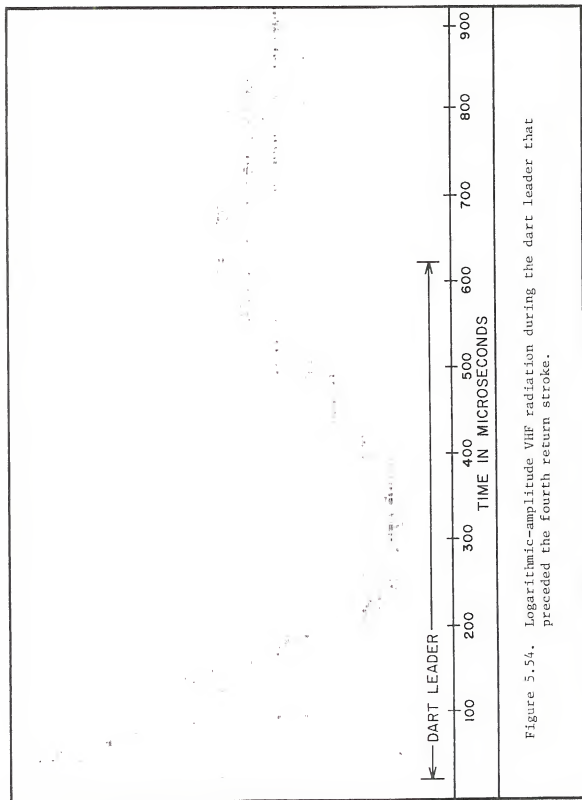


Figure 5.54. Logarithmic-amplitude VHF radiation during the dart leader that preceded the fourth return stroke.

Three dart leader sources, 94 μ sec intervals, are shown in Figure 5.53. As previously discussed in Section 5.3.10, the J3 process was located east and north of the J2 process. The VHF noise from the dart leader was emitted from a non-previously ionized region that joined the old J2 and the new J3. Both the new J3 and the old J2 are shown in Figure 5.53. This type of behavior was also observed in the dart leader in the 165959 flash previously studied.

5.3.12 Fourth J-Change (J4)

The fourth return stroke was followed by a 3.8 msec quiet period in which no VHF sources were detected. Figure 5.55 shows the cross-correlated noise sources, 376 μ sec intervals, during the J4 process. Figure 5.55 also shows the location of the fifth return stroke spherical charge center (Q5). The J4 process lasted 24.7 msec and was located 1.7 km east of the previous J-change. About 50% of all the noise sources were located in a path 35° off vertical leaning toward the northeast between the heights of 12 and 14 km. In general, the VHF noise sources are much more dispersed than in the previous J-changes and did not propagate in any ordered way.

Some of the noise sources in the neighborhood of J3 were still active during J4. About 90% of all the J4 sources occurred between the heights of 11 and 14 km. This J4 process extends higher than J3 which extends higher than J2.

5.3.13 Dart Leader and Fifth Return Stroke

Figure 5.56 shows the VHF noise during the dart leader and the fifth return stroke. Correlation with the electric field records indicates that the dart leader started about 80 ± 30 μ sec from the

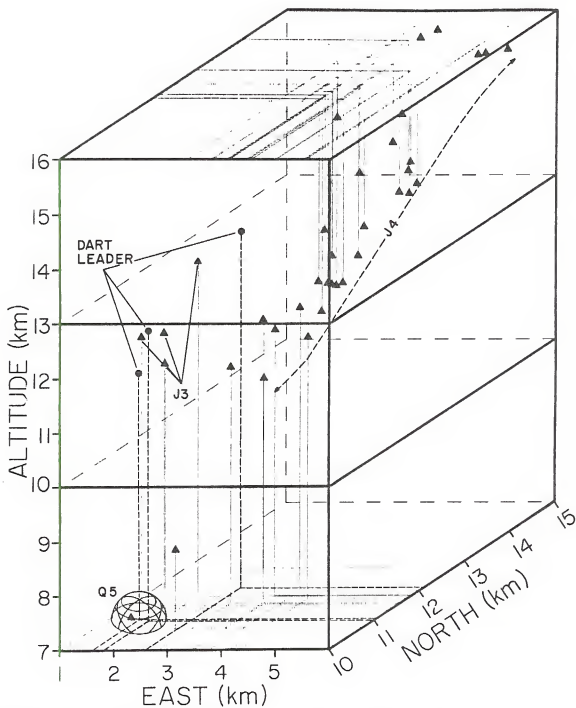


Figure 5.55. Three-dimensional view of the cross-correlated noise sources during J4, and the dart leader. Source locations of the previous J3 channel which continues to radiate during J4 are also shown. The location of the fifth stroke spherical charge center is also shown.

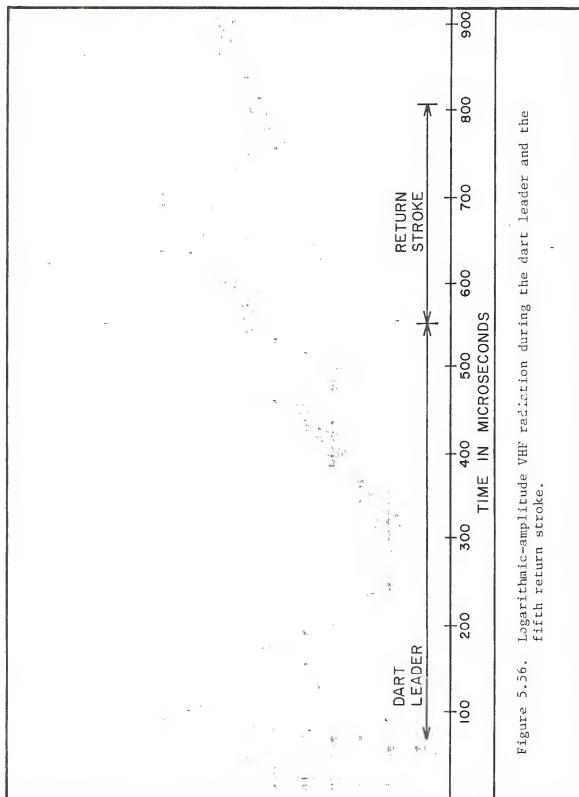


Figure 5.56. Logarithmic-amplitude VHF radiation during the dart leader and the fifth return stroke.

beginning of Figure 5.56. The beginning of the dart leader record prior to the fifth return stroke in Figure 5.56 is almost identical to the beginning of the dart leader record prior to the fourth return stroke in Figure 5.54. However, the fifth return stroke was characterized by a sequence of large pulses with a width between 3 and 15 μ sec. The pulse 40 to 100 μ sec wide that usually characterizes the return stroke can be barely observed in the envelope of the VHF radiation.

The cross-correlated locations of three dart leader sources, 94 μ sec intervals, are shown as circles in Figure 5.55. The dart leader sources are located near the defunct J3 channel. From a plot of the cross-correlated locations in Figure 5.55, we cannot see if the dart leader joins the J3 and J4 regions. However, a plot of all the dart leader sources shows that VHF radiation was emitted from 1 km west to 1.7 km east of J3, which is the location of the J4 channel. We conclude that radiation from the dart leader joined J3 and J4. No source locations were identified with the fifth return stroke. The few isolated VHF return stroke pulses in Figure 5.56 showed varied characteristics in the different stations making impossible the identification of its source locations.

5.3.14 Fifth J-Change (J5)

The VHF radiation of the fifth J-change started after a quiet period of 7 msec in which no VHF sources were detected. As shown in Table 5.3 this is the longest of all the quiet periods that followed the return strokes. Figure 5.57 shows the active VHF noise sources, 376 μ sec intervals, during the 19.3 msec of the fifth J-change. Figure 5.57 also shows the location of the spherical charge center of the sixth return stroke (Q6). The sources were located over a volume

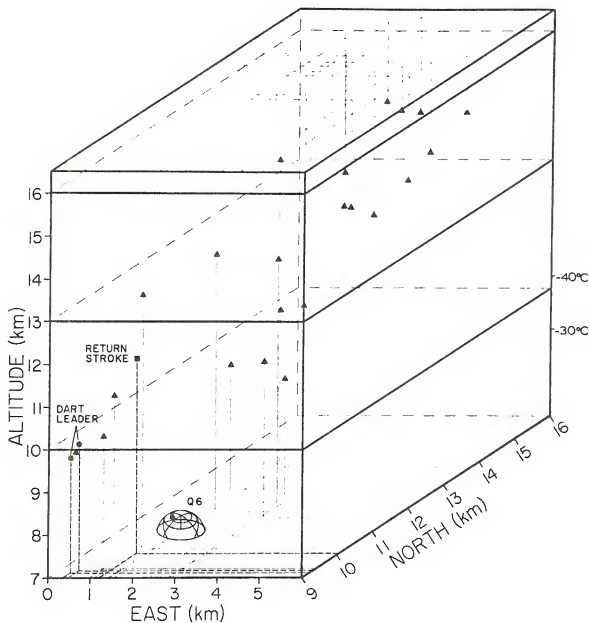


Figure 5.57. Three-dimensional view of the cross-correlated noise sources during J5, the dart leader and the sixth return stroke. The location of the sixth return stroke charge center is also shown.

of 4 km in the east and north direction and 8 km in height starting less than 1 km east of J4. The noise sources extended between a height of 7.5 and 15.0 km. These locations did not form an organized channel, rather they occurred over the entire volume. It appears that the lack of organization in the location of the VHF noise sources might be an indicative factor of the termination of the flash. That is, as long as the noise sources appear along some organized formation, sufficient charge is available for a consecutive return stroke. It is also worth noting that only the VHF noise sources from J1 showed a well-organized propagation pattern. This was the case for the two J-changes in the 165959 flash previously described.

5.3.15 Dart Leader and Sixth Return Stroke

Figure 5.58 shows the VHF noise during the dart leader and the sixth return stroke. The return stroke lasted about 180 μ sec and was preceded by a 470 μ sec dart leader. The VHF noise in Figure 5.58 are similar to the dart leader and third return stroke in Figure 5.52.

Two noise sources for the dart leader and one for the sixth return stroke, 94 μ sec intervals, are shown as circles and squares, respectively, in Figure 5.57. There was no identifiable pattern detected when relating all the locations of the dart leader, the return stroke, and the previous J-change. The non-existence of a J-change channel across which charges could propagate coupled with the continuing decrease in the field change for consecutive return strokes (Figure 5.40) have indicated the termination of additional strokes to ground during this flash.

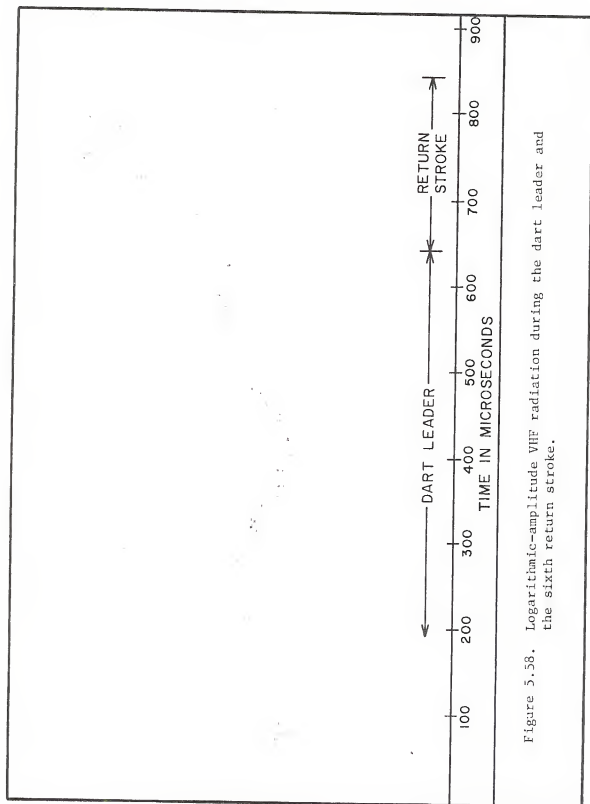


Figure 5.58. Logarithmic-amplitude VHF radiation during the dart leader and the sixth return stroke.

5.3.16 Continuing Current

The six-stroke cloud-to-ground flash was followed by a 1.5 quiet period and then a 216 msec continuing current. The reason we determined that this period of time was a continuing current is as follows: (1) The electric field variation in stations located 2 to 21 km away from the discharge rose steadily during this time interval. Distant intracloud discharges with significant vertical components should exhibit a falling electric field as in the 165959 flash. (2) The luminosity following the last return stroke was observed on TV and compared to that following a stroke with no steady field change. We determined that the last return stroke channel had some luminosity for 195 msec, a time about 100 msec longer than the luminosity observed in a similar flash without a following field change indicative of continuing current.

The VHF noise sources during the continuing current (CC) interval developed in a 14 km channel 40° off vertical between height of 2.8 and 15 km. The western tip of the channel was located in the neighborhood of the western part of J3, but the channel extended 4 km further toward the northeast at the higher altitudes. Similar to the first few J-changes, the noise sources were organized into a relatively well defined channel. Figure 5.59 shows the cross-correlated noise sources, 94 μ sec intervals, during the first 23 msec of the CC interval. It appears that negative charges propagated throughout the CC channel to the return stroke channel. Since VHF radiation is not emitted by channels carrying relatively steady currents, most of the VHF source locations were detected above a height of 4 km. The noise sources in Figure 5.59 did not occur sequentially in a downward path but were located randomly

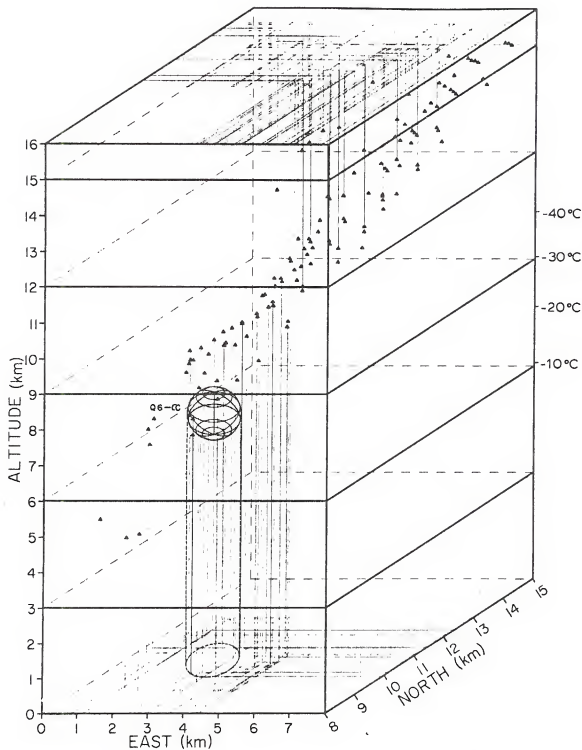


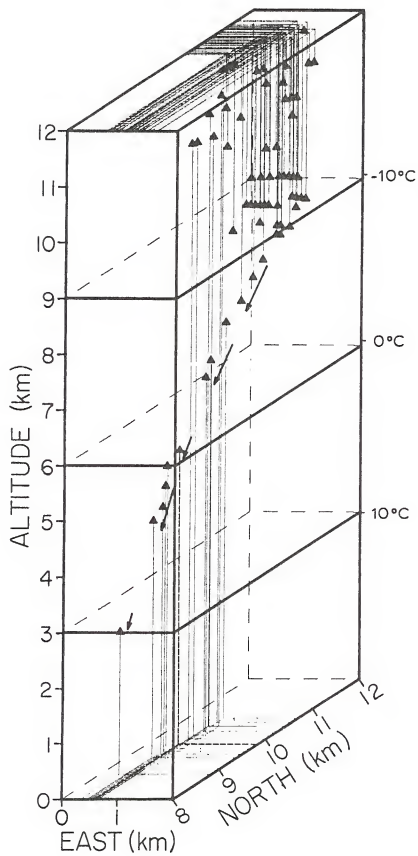
Figure 5.59. Three-dimensional view of the cross-correlated noise sources during the first 23 msec of the CC interval. The location of a spherical charge center for the sixth return stroke and the first 23 msec of the CC interval is shown as Q6-CC.

along the path during these 23 msec. For the remaining 193 msec of the CC interval, VHF sources were located along the previous path for the first 62 msec, and in a newly developed channel during the last 138 msec. After the first 85 msec of the CC interval most of the VHF radiation was concentrated in solitary pulses (SP's), similar to those previously described in this thesis during the study of the 165959 flash. The source locations during the SP's developed in a downward propagating path which merged with the CC channel between the heights of 4 and 10 km. The longest of these SP's lasted 11.5 msec and propagated downward between the heights of 11.8 and 2.8 km in a path 20° off vertical at a velocity of 6.2×10^5 m/sec. Figure 5.60 shows the cross-correlated noise sources, 94 μ sec intervals, during this SP. The arrows indicate the regular progressing sequence during the SP. The VHF noise sources during the 11.5 msec SP were located further west than the other SP's and furthest away from the main CC channel. The VHF noise for this SP is shown in Figure 5.40 and corresponds to the third SP from the end of the CC interval. The SP's during the CC interval have opposite direction and lower velocities than the SP's of the IC discharge in the 165959 flash. It appears that negative charges propagated in the SP's during the CC interval. Probably SP's during the CC interval developed new paths for negative charges to propagate down the channel.

5.3.17 Volume of the Flash

Figures 5.61(a), 5.61(b), and 5.61(c) show the two-dimensional projections of the 18,887 noise sources located during the flash. The average rate of a pulse location is one every 22 μ sec. The pattern evident in Figure 5.61 results from the quantization error for finding locations with a discrete time interval of 229 nanoseconds as explained

Figure 5.60. Three-dimensional view of the cross-correlated noise sources during a SP in the CC interval. The arrows indicate the regular progressing sequence of the noise sources during the SP.



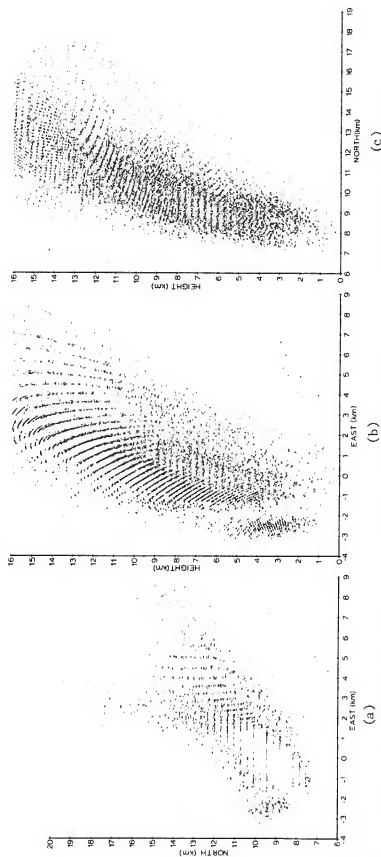


Figure 5.61. Two-dimensional views: (a) NS-EM, (b) EW-height, and (c) NS-height of all the sources (triangles) and the cross-correlated sources (squares) during the entire flash.

in Appendix B. The flash extended east and north from the -3 to 7 km EW, and from 7 to 17 km NS. It appears that every event in the flash developed further toward the north and the east. The flash extended throughout a volume of 450 km^3 during a 416 msec interval.

5.3.18 Concluding Remarks About This Flash

Some of the new information about the flash derived from the VHF noise source, its source locations, and the correlated electric field records follows: (1) The flash lasted 418 msec and consisted of six strokes to ground followed by a continuing current. The flash had two stepped leaders which followed different channels to ground. (2) The flash started with a 1.9 msec preliminary breakdown which was located near and inside the charge source of the stepped leader. All of the VHF noise sources for the PB were located within a cylinder of 2.8 km vertical length and a .5 km horizontal radius. From the electric field records we find that detectable charge motion was only associated with the final 1.0 msec of the 1.9 msec preliminary breakdown. The average velocity of propagation of the final millisecond of the PB was 9.2×10^5 m/sec. (3) A 5.9 msec stepped leader followed the preliminary breakdown. The stepped leader path to ground extended 1 km horizontally, was near-vertical, and started within .6 km horizontal distance of the 150-meter weather tower. The stepped leader started at a height of 6.7 km and propagated downwards at an average velocity of 9.2×10^5 m/sec. From the path of the first stepped leader VHF noise sources and the leader-return stroke field changes we estimated that -17 Coulombs were lowered by the first return stroke. This result is comparable to the -24 Coulombs estimated by Krehbiel (private com) using the technique by Krehbiel et al. (1979). (4) Strong VHF radiation was detected for

8.9 msec after the first return stroke. During this interval the VHF noise sources propagated upwards in the neighborhood of the previous stepped leader-return stroke channel between the heights of 5.1 and 8 km at a velocity of 1.2×10^7 m/sec. It appears that during this interval either positive charges were raised or negative charges were lowered from higher altitudes as the VHF sources moved upwards.

(5) The VHF radiation associated with the source of the second return stroke started with an 8.1 msec J-change (J1) or a new preliminary breakdown (PB2). During this interval VHF noise sources propagated downwards from a height of 14.2 to 10.5 km in a path 25° off vertical at a velocity of 5.0×10^5 m/sec. Using a point charge model we determined that -1.8 Coulombs were lowered during this interval.

(6) Following J1 or PB2 a new stepped leader developed at about a height of 10.5 km and propagated downwards at a velocity of 6.7×10^5 m/sec striking the ground at a point about 1.4 km west and 0.9 km south of the first stroke. From the path of the stepped leader and the leader-return stroke field changes we estimated that -8.2 Coul were lowered by the second return stroke. This result compares well with the -9.6 Coul calculated by Krehbiel (private com). (7) The VHF radiation from the dart leaders was detected prior to the last four return strokes. The dart leader VHF radiation started with a pulse between 80 and 150 μ sec wide. The noise sources during dart leaders were located in the neighborhood of the previous J-change channel and in the region between the last two J-change channels. (8) The VHF radiation during return strokes was characterized by one or a succession of pulses between 10 and 100 μ sec wide with the exception of the fourth return stroke which had no detectable VHF radiation. The first return stroke had detectable VHF

radiation in the location of the previous stepped leader and preliminary breakdown. However, VHF noise sources for subsequent return strokes were located near the top of the previous J-change channel.

(9) The VHF radiation associated with the J-change (J2 to J5) processes was detected during the last 90% of the time between the last four return strokes. The VHF noise sources during the J2 process formed a 1 km radius cylinder between the heights of 12.7 and 5.8 km in a path 32° off vertical. Each subsequent J-change process (J3 to J5) was located 1 to 2 km further eastward, was 1 to 2 km longer, and was parallel to the previous J-change channel. In addition, subsequent J-changes had a less organized channel formation. Since the VHF noise sources during the last J-change did not form an organized channel, this might be an indication that no sufficient charge can be made available for subsequent return strokes. (10) Continuous VHF radiation was detected during the first 85 msec of the continuing current interval. During this initial 23 msec the VHF noise sources formed a 14 km channel eastward and parallel to the previous J-changes. The channel extended to a height of 15 km. In the following 55 msec of the continuous VHF radiation of the first 85 msec, the VHF noise sources widened the 14 km channel. During the last 138 msec of the continuing current interval isolated SP's channels propagated downward merging into the main CC channel. The longest SP during the CC lasted 11.5 msec and propagated downward between the heights of 11.8 and 2.8 km in a path 20° off vertical at a velocity of 6.2×10^5 m/sec. The remaining SP's also propagated downwards from the 10 to 14 km of altitude until they joined the main 14 km channel. Since the lowest part of the CC channel was located in the neighborhood of the previous leader path to ground, it appears that the CC interval lowered negative charge to ground. This

charge was located eastward to the previous J-changes and extended from a height of 15 to 2.8 km. (11) We located 18,877 noise sources during this flash, an average of a VHF source location every 22.1 μ sec. However, there were some quiet periods with no detectable VHF radiation, and periods in which the pulse rate was less than a pulse every 22 μ sec. During active VHF radiation we detected a pulse every 9 μ sec. The flash extended from 7 to 17 km in the north direction, -3 to 7 km in the east direction, and up to a height of 16 km. The space volume covered by this flash exceeded 450 km³.

5.4 The 182356 Flash

On 8th August 1977 at 182356 UT a multiple channel cloud-to-ground flash was photographed (Figure 5.62) via a television camera and video-tape recorder. The VHF portion of the flash lasted 506 msec and consisted of eight return strokes, six of which were preceded by stepped leaders. Figure 5.62 a, b, c, d, f, and h shows all six different return stroke channels to ground. Figure 5.63 show the relationship between the VHF radiation and the electric field for the entire discharge. Return strokes R1, R2, R3, R4, R5, and R7 in Figure 5.63 were preceded by stepped leaders. The stepped leaders preceding R3 and R4 developed simultaneously about 4 km apart. The fourth stepped leader began first in the cloud, but the third stepped leader made ground contact first, 5.4 msec prior to the fourth stepped leader. We have correlated the VHF record and its source locations with the New Mexico Institute of Mines and Technology (NMIMT) measured multiple electric field records and calculated charge locations. Table 5.5 contains a complete summary of the various phases of the flash: the upper and lower locations, the duration of the phases, and the average velocity if defined, of the VHF noise sources. The accuracy in the determination of source locations as a function of position is considered in Appendix B, Table B.4. All the cross-correlated noise sources presented for this flash are calculated using 94 μ sec sample intervals. In the next sections we consider in detail what we learned from the VHF radiation about the various phases of the 182356 flash listed in Table 5.4.

5.4.1 Preliminary Breakdown

The VHF radiation started 7.7 msec prior to the first return stroke. The first 1.8 msec of the 7.7 msec was associated with the preliminary

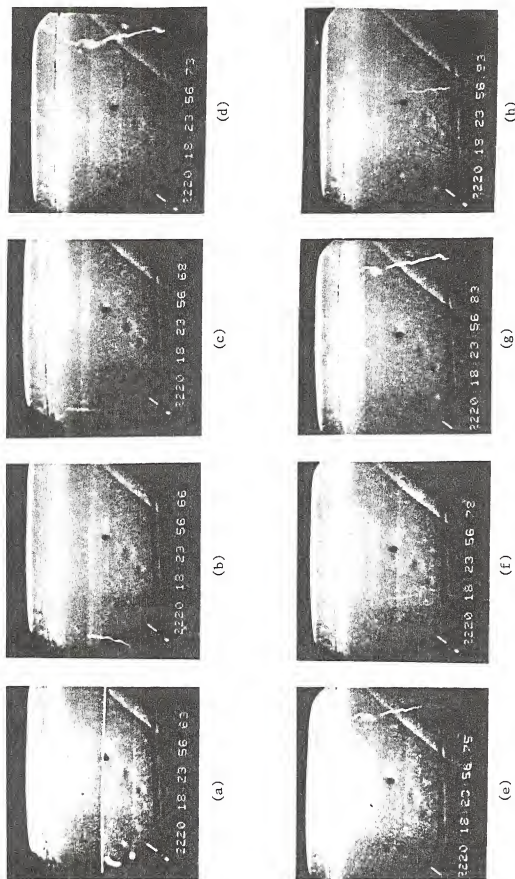


Figure 5.62. Sequence of photographs during the 182356 flash. The Julian date (220) and the time is shown in each photo. Sequences a, b, c, d, f, and h show the six different stopped leader-return stroke channels to ground. This photo is a courtesy of Douglas Jordan of the University of Florida.

Figure 5.63. Simultaneous records of the logarithmic-amplitude VHF radiation detected at 9 km, and the electric field 12 km away, during the 192356 flash. The following events in flash are shown: R1 to R8 are the eight return strokes; J1 to J6 are the six J-changes; FR is the activity following the first return stroke; SP is a solitary pulse during the activity after the return strokes; and SL is the first stepped leader.

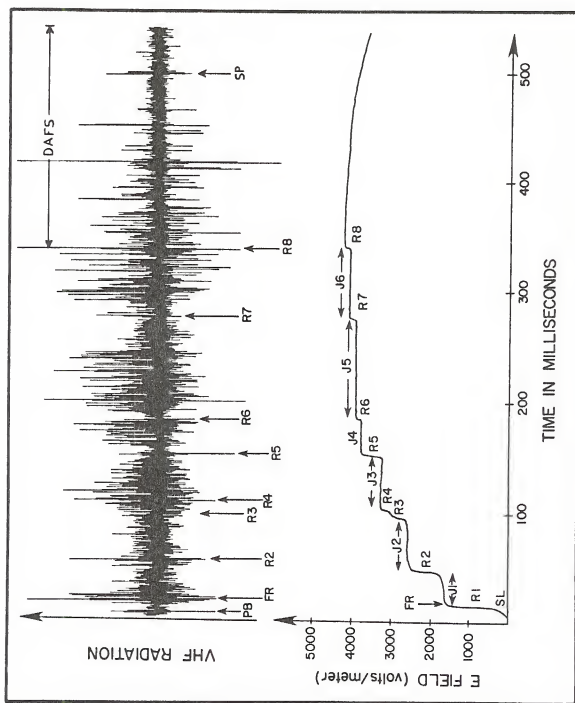


Table 5.5. Events in the 182356 Flash.

Universal Time at the Start of the VHF Radiation: 18 23 56.267, 8th August 1977									
Start Time (msec)	Event	Duration (msec)	Coordinates (km)						Velocity m/sec
			UPPER			LOWER			
			x	y	z	x	y	z	
0	Preliminary Breakdown	1.8	-5.2	8.3	9.8	-4.2	7.9	4.6	
1.8	First Stepped Leader	5.9	-4.0	11.1	5.9	-4.1	10.6	3.4	1.9×10^6 to 4.3×10^6 m/sec
7.7	First Return Stroke	.500	-4.2	10.7	6.0	-4.1	10.5	4.5	
8.2	Following First Return Stroke	7.1	-5.5	11.7	9.5	-4.7	8.2	4.9	
15.3	J1 Change	13.2	-3.1	12.2	7.5	-4.1	8.9	6.0	
28.5	2nd Stepped Leader	14.2	-4.5	12.6	6.7	3.8	9.7	4.0	2.6×10^5 m/sec
42.7	2nd Return Stroke	.81	-3.6	12.1	6.5	-4.3	12.7	5.1	
43.5	Quiet Period of J2	5.7							
49.2	J2 Change	7.2	-5.2	9.1	9.0	-4.0	8.0	5.2	
56.4	3rd Stepped Leader	35.0	-4.2	11.2	7.9	-3.5	12.6	1.8	2.3×10^5 m/sec
91.4	3rd Return Stroke	.2							
91.6	4th Stepped Leader	5.2	-5.2	9.1	8.9	-6.0	7.8	3.7	2.9×10^5 m/sec
96.8	4th Return Stroke	.25							

Table 5.5 - cont.

Time Start (msec)	Event	Duration (msec)	Coordinates (km)						Velocity m/sec
			UPPER			LOWER			
			x	y	z	x	y	z	
97.0	J3 Change	21.1	-5.6	9.4	9.6	-4.7	8.2	5.8	5.1×10^5 m/sec
118.1	5th Stepped Leader	30.1	-4.8	8.8	9.6	-3.3	11.6	3.1	
148.2	5th Return Stroke	.45							
148.6	Quiet Period of J4	3.7							
152.3	J4 Change	26.8	0.9	11.2	12.8	0.6	10.2	5.2	
179.1	Dart Leader	1.5	-5.3	7.8	8.8	-4.9	7.1	7.7	1.6×10^5 m/sec 2.9×10^5 m/sec
180.6	6th Return Stroke	.4	-5.0	8.2	7.8	-4.9	8.3	7.1	
181.0	Quiet Period of J5	8.5							
189.5	J5 Change	55.0	0.7	12.5	12.8	-4.0	7.6	5.3	
244.5	Stepped Leader	30.6	-5.2	8.3	7.7	-4.3	9.2	3.0	
275.1	7th Return Stroke	.38							1.6×10^5 m/sec 2.9×10^5 m/sec
275.5	J6 Change	60.3	-1.2	11.1	13.7	0.7	12.1	5.2	
335.8	Dart Leader	1.7							
337.5	8th Return Stroke	.27							
337.7	Discrete Activity after 8th Return Stroke	168.7	0.2	15.1	13.2	-3.8	7.9	5.1	

breakdown (PB). The VHF PB radiation consisted of a succession of six pulses with widths between 80 and 150 μ sec superimposed on a more slowly varying envelope. Figure 5.64 shows the VHF radiation during the PB, the stepped leader, first return stroke, and the activity following the first return stroke. We can divide the 1.8 msec PB in three sections of .6 msec each. Detectable electric field change started following the first .6 msec period. During this first .6 msec interval the cross-correlated source locations showed an ascending motion between the heights of 5.5 and 9.8 km. During the second .6 msec interval, the VHF noise sources propagated downward in a path that lies within 500 meters of the previous ascending path. During the last .6 msec the noise sources propagated for the most part horizontally in a northerly direction.

Figures 5.65(a) and 5.65(b) show a three-dimensional graph of all the sources and the cross-correlated sources, respectively, during the PB and the stepped leader. The PB sources are located in the southern part of the NS axis, and at an altitude between 5.5 and 9.8 km. We have progressively lettered the first 23 cross-correlated noise sources in Figure 5.65(b). Sources A through T correspond to the PB, and sources U to W mark the initial portion of the stepped leader VHF noise. The unlettered points occurred after W and are associated with the stepped leader.

5.4.2 First Stepped Leader

The first stepped leader electric field change was detected at the time the VHF sources were located in the D through J region in Figure 5.65, about 0.6 msec into the discharge. The stepped leader shown in the VHF noise record propagated downward from a region in the neighborhood

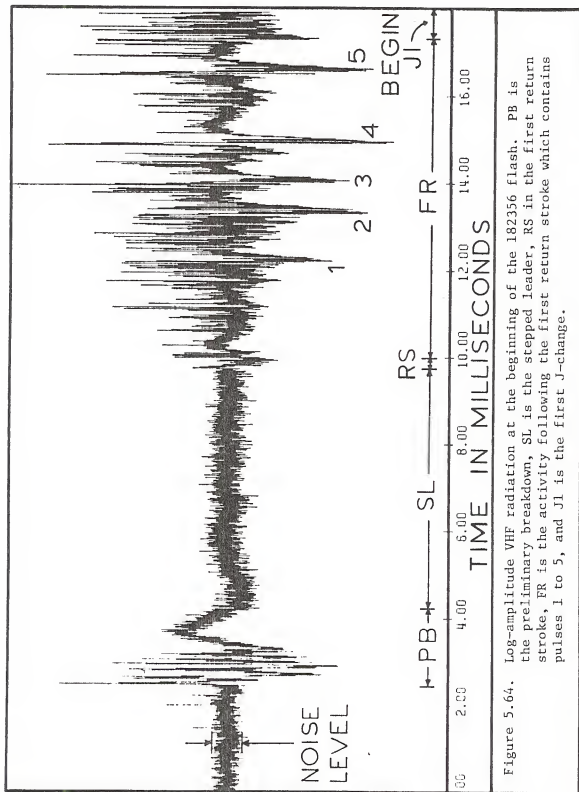
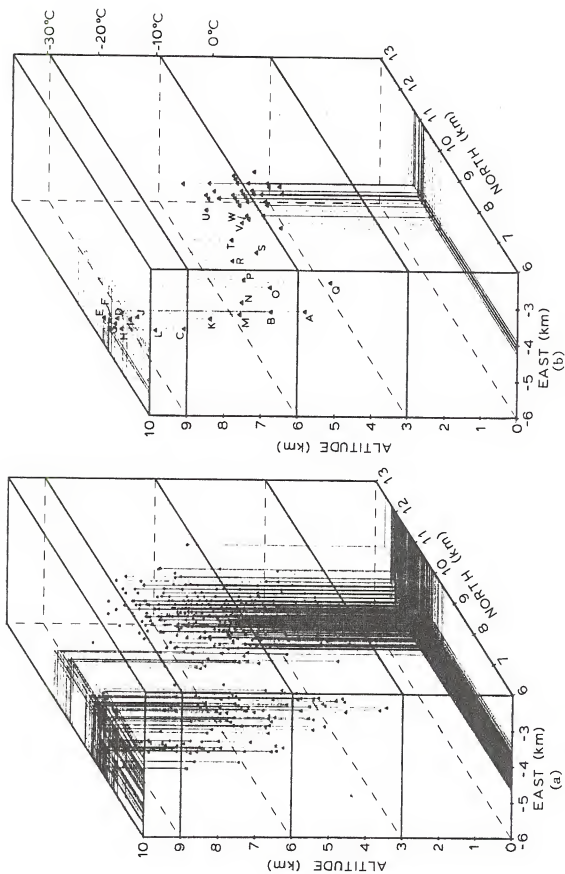


Figure 5.65. Three-dimensional view of the noise sources during the first preliminary breakdown and stepped leader. Figure 5.65(a) shows all the individual noise sources. Figure 5.65(b) shows the cross-correlated noise sources. The letters in Figure 5.65(b) show the progressing sequence of the noise sources. Letters A to T correspond to the PB, letters U to W to the beginning of the stepped leader, and all the unlabeled sources that occurred after W.



of the T to W source locations. The lowest detectable stepped leader source was at a height of 3.4 km. It can be observed from the log-amplitude VHF scale in Figure 5.64 that the radiation of the PB is several orders of magnitude larger than that of the stepped leader. In addition, the stepped leader VHF radiation decreases as it propagates near ground. Therefore, it appears difficult to detect stepped leader sources near ground with lower amplitude radiation and too many leader sources active over a large volume. The stepped leader average velocity ranged between 1.9×10^6 and 4.3×10^6 m/sec for heights between 5.9 and 3.4 km.

5.4.3 First Return Stroke

The first return stroke VHF radiation (Figure 5.64) lasted 500 μ sec. The return stroke noise sources were located in the neighborhood of the T, U, V, and W region in Figure 5.65(b). Using T (-3.9, 11.7, 5.8) in Figure 5.65(b) as the point where the VHF noise changed characteristics from the PB to stepped leader, and the technique described in Section 3.6, we estimated that -20.5 Coul were lowered during the first stepped leader return stroke process. We have correlated the VHF record and its source locations with the New Mexico Institute of Mines and Technology (NMINT) measured multiple electric field records and calculated charge locations. Table 5.6(a) shows the value of the source charge and its location for the first, second, fourth, and fifth return stroke as provided by Krehbiel (private com) using the technique of Krehbiel et al. (1979). Table 5.6(b) shows the value of the source charge and its location for each of the stepped leader-return stroke processes obtained by using the techniques in Section 3.6. The first stepped leader-return

Table 5.6(a). Return Stroke Charge Value and Location as determined by Krehbiel (private com) using the technique of Krehbiel et al. (1976). R3 is missing because the beginning of the field change was not easily distinguishable. R7 and R8 are missing because most electric field stations were saturated.

Return Stroke	Charge (Coulombs)	Location (km)
R1	-21.4	Q1 (-4.0, 7.4, 7.5)
R2	- 9.5	Q2 (-3.5, 8.0, 7.6)
R4	- 2.9	Q4 (-4.6, 6.7, 7.6)
R5	-10.2	Q5 (-3.5, 8.1, 6.8)
R6	- 6.2	Q6 (-2.6, 7.5, 6.8)

Table 5.6(b). Stepped Leader-Return Stroke Charge Value and Location for Each of the Return Strokes Preceded by Stepped Leaders as determined from the VHF source locations and one electric field record using the technique described in Section 3.6. R6 and R8 are missing because the return stroke was preceded by dart leaders.

Return Stroke	Charge (Coulombs)	Location (km)
R1	-20.5	(-3.9, 11.7, 5.8)
R2	- 8.2	(-3.7, 11.7, 5.9)
R3	-14.4	(-4.4, 12.8, 6.2)
R4	- 3.6	(-4.1, 7.8, 6.1)
R5	-16.2	(-4.2, 11.2, 6.9)
R7	-24.1	(-5.3, 8.3, 6.9)

stroke charge using our technique in Table 5.6(b) compares reasonably well with the value obtained in Table 5.6(a).

5.4.4 Activity Following the First Return Stroke (FR)

The FR activity followed immediately after the first return stroke (Figure 5.64), lasted 7.1 msec and contained five large pulses (1 to 5 in Figure 5.64) about 200 μ sec wide with an interval between the pulses ranging from .4 to 1.7 msec. The VHF noise sources during each of these pulses propagated downward in a southerly direction at a velocity between 1.5 and 3.5×10^7 m/sec. The longest of these paths extended 4.3 km vertically and 3.2 km horizontally. Figure 5.66 shows the cross-correlated VHF sources during the FR interval. We fitted a point charge model to the FR interval assuming a charge transfer from A to B in Figure 5.66. A charge transfer of 4.5 ± 2.1 Coul was determined by using the six more distant electric field stations between 9 and 21 km from the source. We used points other than A and B in Figure 5.66 and obtained a charge transfer between 1.8 and 5.1 Coul. For all our charge models the stations located closer to the source (3 to 7 km) gave inconsistent results. It appears that the charges are not concentrated and the point charge model is not a good approximation for close stations.

From the characteristics of the VHF radiation, the source locations, and the point charge model, we conclude that either negative charge at higher altitudes was lowered toward the top of the previous return stroke channel or that positive charge from the previous return stroke continued its upward propagation. A total charge of 4.5 Coul distributed in 5 large pulses is about .9 Coul transfer per event. This number is comparable with the .85 Coul calculated for the K-change that initiated the J1 process in the 180710 flash.

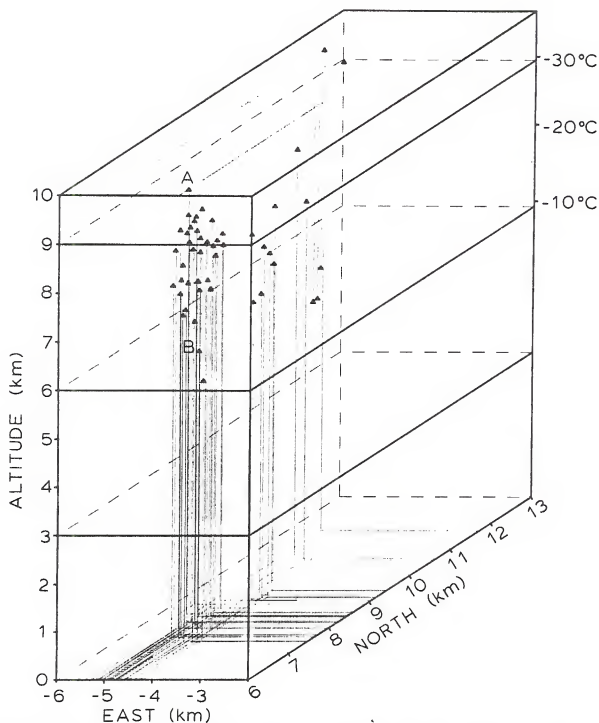


Figure 5.66. Three-dimensional view of the noise sources during the FR interval. The sources A and B represent arbitrary locations which were chosen to perform a point charge model.

5.4.5 The J1 Change

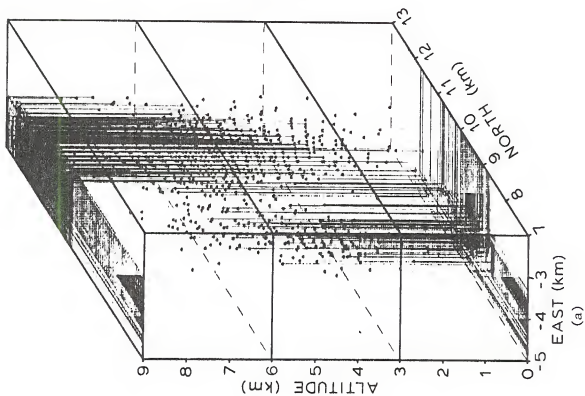
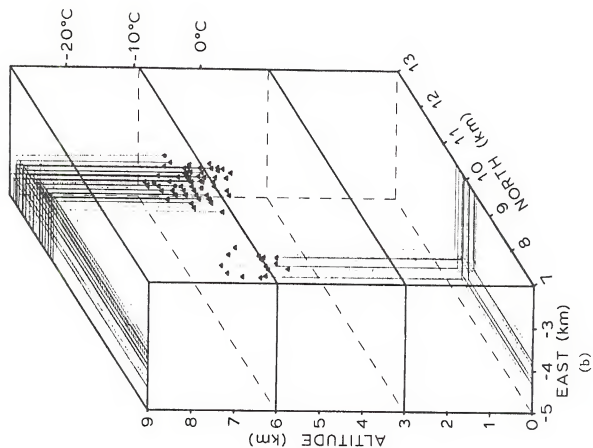
The J1 change lasted 13.2 msec and followed immediately after the FR interval in the VHF record. The J1 change was characterized by a higher pulse rate and shorter pulse width than during the FR interval. Throughout J1 the VHF noise amplitude decreased and the pulse rate increased. During the J1 process the cross-correlated VHF noise sources were located between -3 and -4 km EW, 9 and 12 km NS, and 6 to 7.5 km in altitude.

5.4.6 The Second Stepped Leader

The beginning of the second stepped leader was selected as a point in the transition region when the VHF radiation changed characteristics from the slower pulse rate with higher amplitude pulses from J1 to the shorter pulses with a faster rate during the stepped leader. As soon as stepped leader variation in amplitude was detected in the VHF record, the noise sources showed a vertical propagation. Correlated electric field records for eight ground stations during the interstroke interval showed no significant slope change as would be expected at the occurrence of a stepped leader. However, other characteristics of stepped leaders were observed: decrease in the VHF magnitude of the noise, an increase in the pulse rate, and some downward propagation in the VHF sources. Using these criteria, we suggest that the second stepped leader lasted 14.2 msec.

Figures 5.67(a) and 5.67(b) show three-dimensional views of all the sources and of the cross-correlated sources, respectively, during the second stepped leader. The cross-correlated VHF sources propagated between the heights of 6.5 and 3.4 km. The stepped leader cross-correlated sources in Figure 5.67(b) were located in two separate regions.

Figure 5.67. Three-dimensional view of the noise sources during the second stepped leader.
Figure 5.67(a) shows all the individual noise sources. Figure 5.67(b) shows the cross-correlated sources.



It appears from Figure 5.67 that these two regions merged together and that the stepped leader had a large horizontal component in the NS direction. The stepped leader velocity was about 2.6×10^5 m/sec.

5.4.7 Second Return Stroke

The second return stroke lasted 810 μ sec in the VHF noise record. Four cross-correlated noise sources are shown in Figure 5.67 (circles). All these sources were located in the northern group between the heights of 5 and 6.5 km. Using point P (-3.7, 11.7, 5.9) as the transition point to stepped leader waveform, and the technique described in Section 3.6, we calculated that the second stepped leader-return stroke lowered -8.2 Coul (Table 5.6(b)). This number is comparable to the -9.5 Coul shown for Q2 in Table 5.6(a), however, our source location is about 3.7 km north and 1.7 km lower in altitude than Q1.

5.4.8 The J2 Change

The J2 change lasted 7.2 msec and started after the 5.7 msec quiet period that followed the second return stroke. The noise sources during the J2 change started 0.5 km West and 2.0 km South of J1. During the first 1.5 msec of the J1 period the noise sources propagated upwards between the heights of 5.2 and 8.0 km. This upward propagation appears to be related to additional breakdown caused by extensions of the previous return stroke channel. For the remaining 5.7 msec the VHF noise sources extended between -6.0 and -4.5 km EW, 8.3 and 10.1 km NS, and between the heights of 6.0 and 9.0 km.

5.4.9 Third and Fourth Stepped Leaders and Return Strokes

We studied the electric field change measured at ten different electric field stations but we could not clearly determine any slope

change that indicated the beginning of the leader preceding the third return stroke. However, the VHF noise decreased in amplitude and increased in rate about 35 msec prior to the third return stroke. As discussed in this thesis, this characteristic is typical of stepped leaders. Therefore, we suggest that a stepped leader started 35 msec prior to the third return stroke.

Figures 5.68(a), 5.68(b), and 5.68(c) show two-dimensional graphs of the cross-correlated source locations during the leaders that preceded the third and fourth return strokes. Figure 5.69 shows a three-dimensional view of the same noise sources. The locations A (-5.4, 8.9, 7.9), B (-4.1, 7.8, 6.1), C (-4.6, 12.1, 7.3), and D (-4.4, 12.8, 6.3) shown in these figures are related to the propagation path of the third and fourth stepped leaders.

The sequence of events leading to the third and fourth return strokes is as follows: 1) The fourth stepped leader sources began first and were located in the A region in Figures 5.68 and 5.69. During the beginning of the fourth stepped leader the VHF noise sources were located in the same region of the J2 change. For the first 10.1 msec the noise sources propagated in the A-B region at an average velocity of 2.9×10^5 m/sec. 2) About 10.1 msec after the initiation of the fourth stepped leader, the third stepped leader started in the C region in Figures 5.68 and 5.69. The C location is 3.4 km from A. For the following 5.6 msec the noise sources propagated in the C-D region at an average velocity of 2.3×10^5 m/sec. 3) For the remaining 19.3 msec prior to the third return stroke, the VHF sources propagated mainly downwards from the A-B and C-D regions. 4) About 3.5 msec prior to the third return stroke, the stepped leader that propagated from the C-D region was detected at a height of 1.8 km. This stepped leader appears

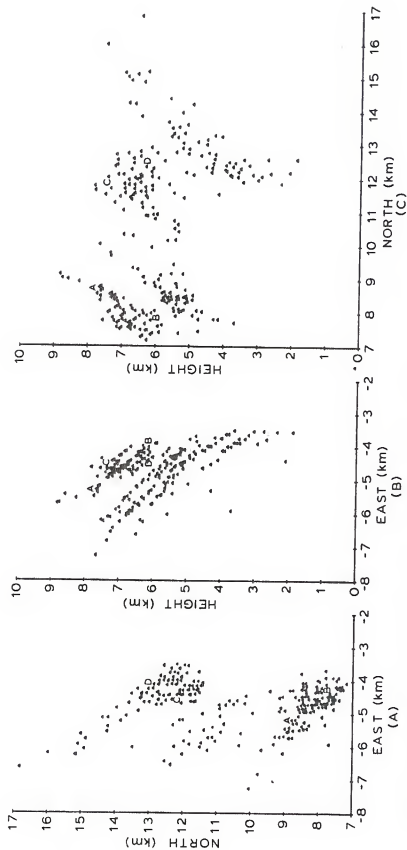


Figure 5.68. Two dimensional views: (A) top view, EW-NS, (B) elevation view, EW-height, and (C) elevation view, NS-height of the cross-correlated sources during the third and fourth stepped leaders. The locations A-B and C-D correspond to the initial propagation of the fourth and third stepped leader, respectively.

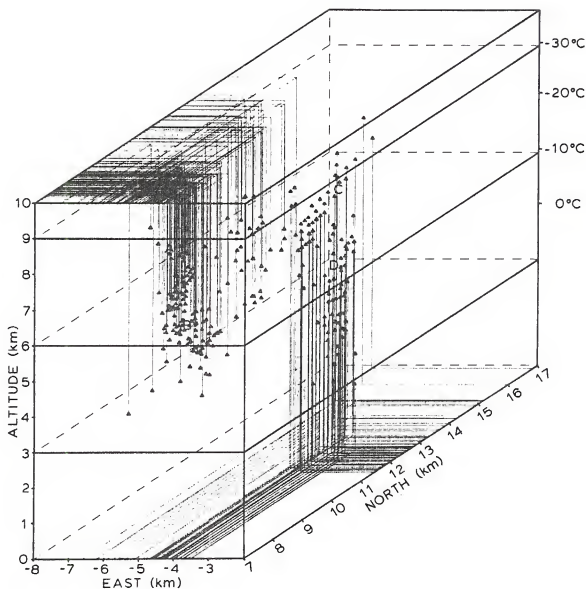


Figure 5.69. Three-dimensional view of the cross-correlated noise sources during the third and fourth stepped leaders. The sources A-B and C-D correspond to the initial propagation of the fourth and third stepped leader, respectively.

to contact the ground first and produce the third return stroke.

5) After the third return stroke, most of the VHF sources were detected below the A-B channel. About 3.9 msec prior to the fourth return stroke, the lowest detectable source from the fourth stepped leader was detected at a height of 3.7 km. It appears that the stepped leader from the A-B region contacted ground 5.4 msec after the third return stroke.

It is worth noting that the sources detected in the neighborhood of C did not propagate from the B region, but there were two different electrified regions. This claim is made from determining the source location in the last pulse of the B region and the first pulse of the C region, and calculating a velocity larger than the speed of light between these sources. The sources that appeared between the A-B and C-D regions in Figures 5.68 and 5.69 appeared in a random sequence during the propagation of the third and fourth stepped leaders.

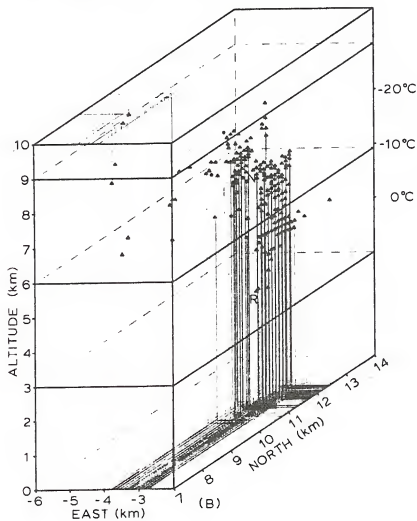
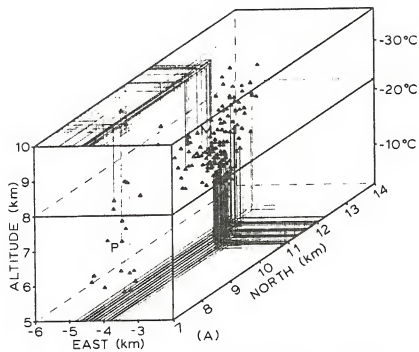
Table 5.6(a) does not show a charge location for the third return stroke because it was not possible to determine the beginning of the stepped leader by analyzing the electric field records. The Q4 charge location for the fourth return stroke is in the region of the A-B path that generated the fourth return stroke. Using the techniques described in Section 3.6, we estimated that the third and fourth stepped leader-return strokes lowered -14.4 and -3.6 Coul, respectively.

5.4.10 The J3 process and the Fifth Stepped Leader

The J3 process lasted 21.1 msec and followed immediately after the fourth return stroke. Figure 5.70(a) shows the location of the cross-correlated VHF sources during the J3 process. Most of the activity was concentrated in a region 1 km east and .6 km south of the source origin

Figure 5.70(A). Three-dimensional view of the cross-correlated noise sources during the J3 process that preceded the fifth stepped leader. The labels M and N represent the beginning and the end of J3 while P indicates a region in the neighborhood of the fourth stepped leader that radiates again or continues to radiate.

Figure 5.70(B). Three-dimensional view of the cross-correlated noise sources during the fifth stepped leader. The sources N and R indicate the region at the end of J3 and the last detectable cross-correlated location, respectively.



of the third stepped leader (M, Figure 5.70(a)). The main M region extended 3 km horizontally and vertically. The fifth stepped leader followed J3 and descended from the center of this concentrated region (N, Figure 5.70(a)). A study of the electric field record and the VHF source locations indicate that negative charges were lowered during the J3 interval. The noise sources in the P region in Figure 5.70(a) correspond to active sources in the previous A-B channel in Figure 5.69.

The fifth stepped leader (Figure 5.70(b)) lasted 30.1 msec and continued the downward propagation of the N region sources in Figure 5.70(a). The fifth stepped leader path to ground remained between one and two km from the previous stepped leader. The lowest detectable cross-correlated noise source was located at a height of 3.1 km (R, Figure 5.70(b)). The average stepped leader velocity was 5.1×10^5 m/sec.

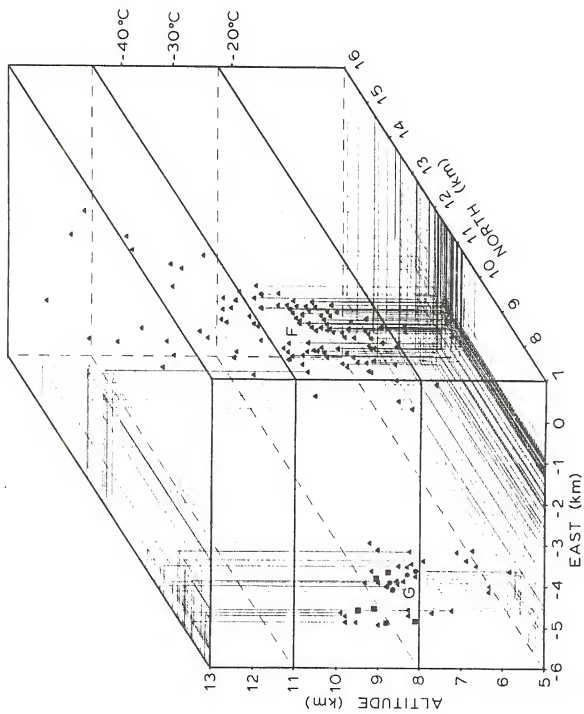
5.4.11 Fifth Return Stroke

The fifth return stroke lasted 450 μ sec in the VHF record. Three cross-correlated noise sources during the fifth return stroke are shown as circles in Figure 5.70(b). Assuming a point charge model and using the technique in Section 3.6, we estimated that -16.2 Coul were lowered by the fifth stepped leader-return stroke.

5.4.12 The J4 Process, the Dart Leader, and the Sixth Return Stroke

The fifth return stroke was followed by a 3.7 msec quiet period and a 26.8 msec J-change (J4, Figure 5.64). The J4 process formed in the neighborhood of the source charge of the third and fifth return stroke. Figure 5.71 shows the cross-correlated noise sources during J4. The two different regions are shown as F and G. The sources in

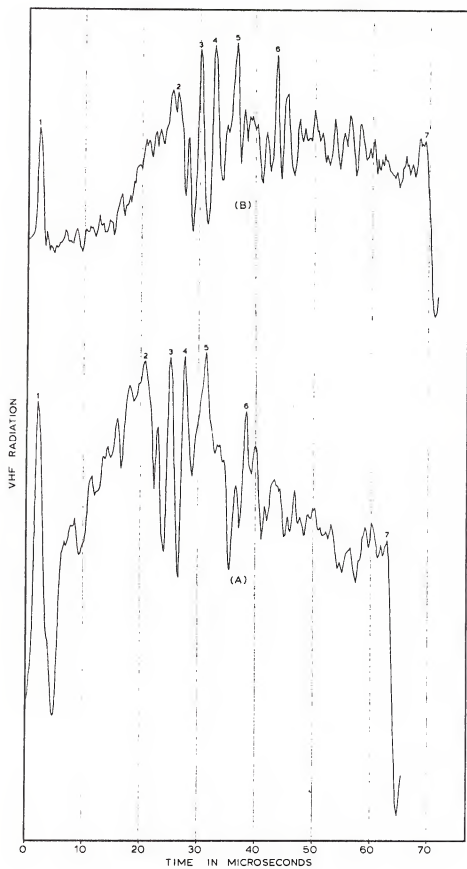
Figure 5.71. Three-dimensional view of the cross-correlated noise sources (triangles) during the J4 process that preceded the dart leader and the sixth return stroke. The rectangles represent the cross-correlated dart leader sources and the circles represent the sixth return stroke cross-correlated sources. F and G show the isolated locations of the two active regions.



the F region extended between a height of 5.6 and 12.8 km while the sources in the G region extended between a height of 5.2 and 9.9 km. The J4 noise sources did not follow a regular progressing sequence. We studied the VHF radiation at the central and the remote stations whenever there was a shift in source locations between the F and G regions. The purpose of this study was to determine whether there was propagation between these regions or whether sources were active simultaneously. Figure 5.72 shows the VHF radiation at the central (a) and one of the remote stations during a transition from F to G. We have displayed the graph such that pulse 1 which corresponded to the F region is lined up in both stations. Some of the subsequent pulses (e.g., 2 through 7) shown in Figure 5.72 were located in the neighborhood of G and the DTOA in these pulses is less than 2 μ sec. When we account for the absolute difference in the time of occurrence of 1 and 2 in stations, it was clear that a source in F producing pulse 1 cannot propagate to G to produce pulse 2 at a speed less than the speed of light. Therefore, the F and G regions are independent. Even though an argument could not be invoked for the source regions of the third and fourth stepped leaders previously described, it provides an example of a process in which two different return strokes could occur almost simultaneously.

A dart leader characteristic was evident from the VLF and VHF record after the J4 process. As shown in this thesis, the dart leader does not radiate in its path to ground along the previous return stroke channel. The noise sources just prior to the dart leader, the dart leader, and the return strokes were located in the G region. Figure 5.71 shows six cross-correlated noise sources during the dart leader

Figure 5.72. VHF noise detected at the central station (A) and one of the remote stations (B). The (B) noise has been shifted such that pulse 1 occurs at the same time. Pulses 2 to 7 show the shift in the VHF noise when the noise is emitted from a different region.



(squares) and four cross-correlated locations for the sixth return stroke (circles).

Figure 5.73 shows the VHF noise during the last 5.8 msec of the J4 process, the 1.7 msec dart leader, the 810 μ sec return stroke, and the first 8 msec of the quiet period following the return stroke. The fact that there is a quiet period after the sixth return stroke is interesting. It appears from our results that the dart leader lowered the negative charge from one of the isolated regions, most likely the G region. Therefore, we would have expected the charges in the remaining region to cause additional breakdown and not be affected by the return stroke of the other region, as occurred in the third and fourth return strokes.

5.4.13 The J5 Process, the Stepped Leader Preceding the Seventh Return Stroke and the Seventh Return Stroke

Active VHF radiation for the next J process (J5) started after the 8.5 msec quiet period that followed the sixth return stroke. The J5 process lasted 55 msec and initiated a new stepped leader. Similar to J4, the cross-correlated VHF noise sources were detected in the neighborhood of the F and G regions in an unorganized sequence. Figure 5.74(a) shows the cross-correlated VHF sources during the J5 process. The cross-correlated sources in the F region extended a horizontal distance of 4 km and between the heights of 5.4 and 10.6 km. Simultaneously, the sources in the G region extended a horizontal distance of 7 km and between the height of 5.3 and 12.8 km. Even though, the cross-correlated noise sources did not follow any regular progressing sequence, most of the sources detected near the beginning of the J5 process were located at the higher altitudes and the sources located near the end of J5 were

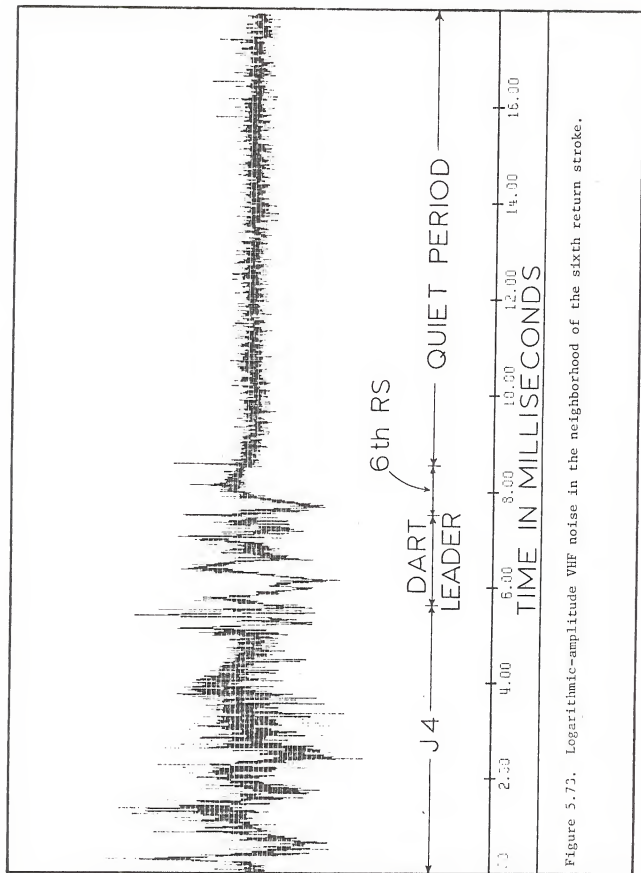
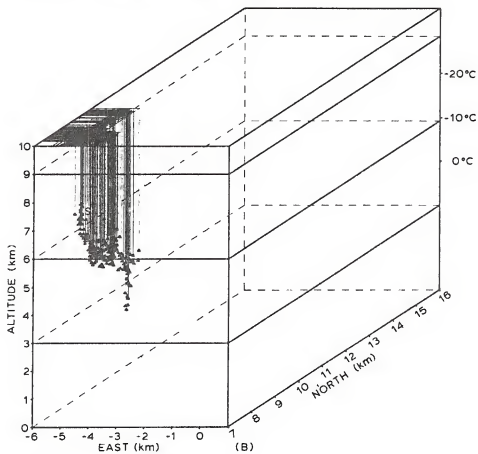
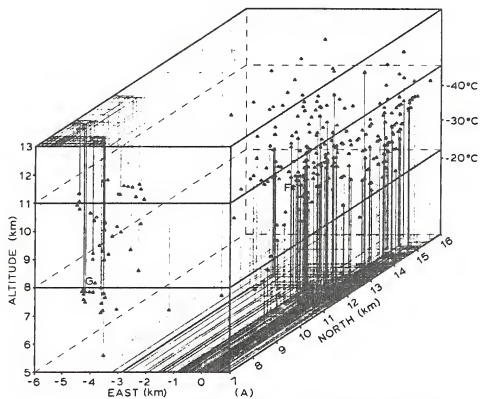


Figure 5.73. Logarithmic-amplitude VHF noise in the neighborhood of the sixth return stroke.

Figure 5.74(A). Three-dimensional view of the cross-correlated noise sources during the J5 process that preceded the sixth and last stepped leader. F and G are the locations of the active regions during J4.

Figure 5.74(B). Three-dimensional view of the cross-correlated noise sources during the sixth stepped leader. The label S represents the first stepped leader cross-correlated source.



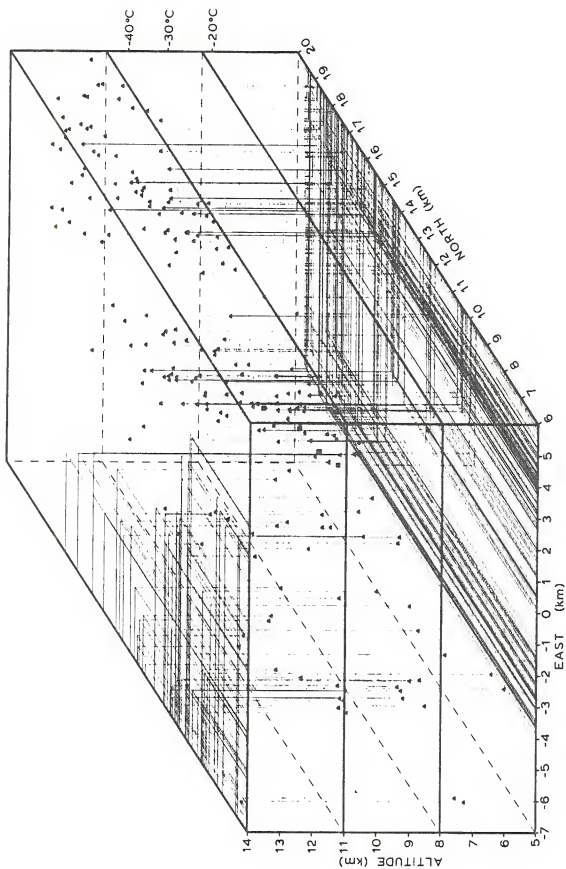
at the lower altitudes. Therefore, it appears that the J5 process lowered a net negative charge in the F-G regions.

A new stepped leader which lasted 30.6 msec immediately followed J5. From the six available electric field records which were not saturated during the stepped leader-seventh return stroke field change, only one of the records (9 km away from the discharge) shows the change of slope corresponding to the beginning of the stepped leader electric field. This electric field change of slope was correlated with the decrease of magnitude of the VHF record, 30.6 msec prior to R7 in the VHF record of Figure 5.63. Figure 5.74(b) shows the cross-correlated noise sources during the stepped leader. For ease of comparison the stepped leader and the previous J-change noise sources are lined up vertically in Figure 5.74. The horizontal projections are the same for both graphs, but the height range of the stepped leader graph is 0 to 10 km while the J5 is 5 to 13 km. The stepped leader progressed from the G region as shown in Figure 5.74(b). The stepped leader velocity ranged between 1.6 and 2.9×10^5 m/sec. Assuming S (-5.3, 8.4, 6.9) to be a point charge representation for the stepped leader-seventh return stroke charge center and the technique described in Section 3.6, we determined that -24.1 Coul were lowered by this process. This is the largest estimate of the charge lowered by any of the return strokes of this flash.

5.4.14 The J6 Process, the Dart Leader, and the Eighth Return Stroke

The J6 process followed immediately after the seventh return stroke and lasted 60.3 msec. Figure 5.75 shows the locations of the cross-correlated VHF noise sources during the J6 process. These sources are spread out over a volume of about 1450 km^3 between the heights of 5.2

Figure 5.75. Three-dimensional view of the cross-correlated noise sources (triangles) during the J6 process. The location of four cross-correlated dart leader sources are shown with squares near the center of the picture.



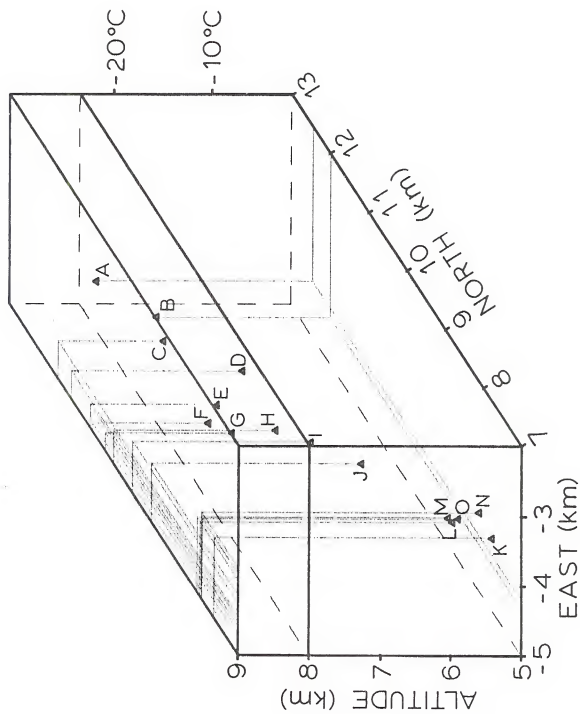
and 13.7 km. The progressing sequence of the noise sources do not follow any specific channel. This J-change is less organized than the previous one. This lack of organization, concentration, and channel formation of the noise sources during this last J-change was previously observed in the last J-change of the 181806 flash. It appears to be an indication that sufficient charge is not available to be lowered to ground in additional subsequent stroke.

During the dart leader that followed the J6 process, the VHF noise sources were located between the heights of 12.5 and 7.7 km. Four cross-correlated dart leader sources are shown as squares in Figure 5.75. No cross-correlation VHF sources were detected during the eighth return stroke.

5.4.15 Discrete Activity Following the Eighth and Last Return Stroke (DAFS)

Solitary pulses were detected in the VHF radiation for 168.7 msec after the eighth return stroke. The pulse repetition rate during DAFS started with a pulse every 800 μ sec and decreased to a pulse every 10 msec toward the end of the flash. This is the same way that all the flashes studied in this thesis have terminated, that is, a decrease in the rate of SP's. We studied the cross-correlated source locations during the SP shown in Figure 5.63. These results are shown in Figure 5.76. This SP started at a height of 8.2 km and propagated downward in a path 50° off vertical. The noise source during this SP, which corresponds to the final VHF pulse of the flash, extended 5 km at a velocity of 2.2×10^6 m/sec.

Figure 5.76. Three-dimensional view of the cross-correlated locations of the VHF noise sources during the SP shown in Figure 5.63. The labels A to N show the regular progressing sequence of the noise sources.



5.4.16 Volume of the Flash

Figure 5.77 shows all the 33,947 individual VHF noise sources (triangles) detected during the 506 msec flash. All the cross-correlated noise sources are also shown as squares. The average rate of pulse location throughout the flash was one every 14.9 μ sec. During the 337 msec period preceding the DAFS the detected rate was a source every 9.5 msec. This rate decreased considerably during the 169 msec DAFS interval. The flash extended about 15 km in the EW direction, 14 km in the NS direction, and up to 14 km in altitude. The volume occupied by the flash was about 1500 km³.

5.4.17 Concluding Remarks About the Flash

Now we provide a summary of what we learned about this flash.

(1) The flash lasted 506 msec and consisted of eight return strokes and, six separate stepped leader channels to ground. (2) The flash started with a PB that lasted 1.8 msec. During the first .6 msec of the PB the VHF sources propagated upwards and there was no detectable electric field change. For the next .6 msec the VHF sources propagated downwards within 500 meters of the previous ascending channel. In the remaining .6 msec of the PB most of the propagation was horizontal at a height of 6.5 km. (3) This flash had stepped leaders preceding return strokes 1 to 5, and 7 and lasting 5.9, 14.2, 35.0, 5.2, 30.1, and 30.6 msec, respectively. The third and fourth stepped leader developed simultaneously about 4 km apart and the 5.2 msec of the fourth stepped leader is only the time of stepped leader propagation that occurred after the third return stroke. Stepped leaders preceding R1, R2, R3, and R5 started within 2 km of each other while stepped leaders preceding R4 and R7 were also 2 km apart but about 4 km from the region of the

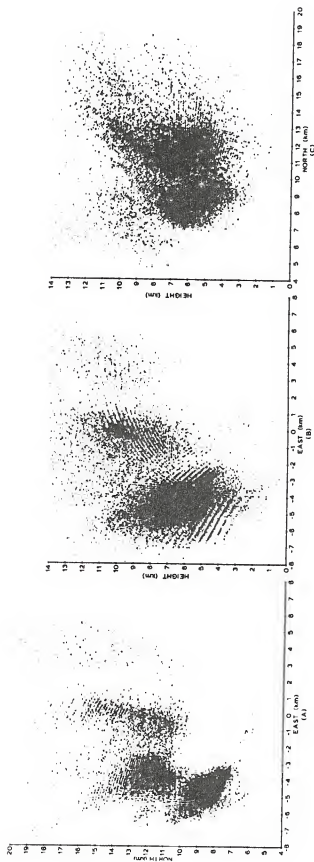


Figure 5.77. Two-dimensional views: (a) top view, EW-NS, (b) elevation view, EW-height, and (c) elevation view, NS-height of all the noise sources during the 182356 Flash.

other stepped leaders. The stepped leader velocities were: 1.9 to 4.3×10^6 ; 2.6×10^5 , 2.3×10^5 , 2.9×10^5 , 5.1×10^5 ; and 1.6 to 2.9×10^5 m/sec, respectively. The first stepped leader in this flash is shorter in duration and propagated an order of magnitude faster than the subsequent stepped leaders. The charge lowered by each one of the stepped leaders was calculated by using a point charge model. We found that -20.5 , -8.2 , -14.2 , -3.6 , -16.2 , and -24.1 Coul were lowered by stepped leader-return stroke processes. That is a total charge of about -86 Coul, considering only six of the eight return strokes. (4) The VHF sources corresponding to the VHF radiation in the first 7.1 msec after the first return stroke were located in a region above the previous stepped leader-return stroke channel. By studying the VHF noise sources of the individual VHF pulses during this interval and the correlated electric field change, we conclude that either -4.5 Coul were lowered into the top of the previous return stroke channel from a region at the higher altitudes, or that 4.5 Coul were raised in the cloud from the top of the previous return stroke. (5) All but one of the subsequent stepped leaders and the dart leaders were preceded by J-change processes. The exception is between the third and fourth return strokes because sources from both the fourth stepped leader and higher location in the cloud are detected. The VHF J-change process durations are: J1, 13.2 msec (preceding the second stepped leader); J2, 7.2 msec (preceding the third stepped leader); J3, 21.1 msec (preceding the fifth stepped leader); J4, 26.8 msec (preceding the first dart leader); J5, 55.0 msec (preceding the sixth stepped leader); and J6, 60.3 msec (preceding the second dart leader). Two active regions about 4 km apart were detected, a northern and a southern region. The J1 noise sources were concentrated

in the northern region and the second stepped leader descended from that region. About 80% of the J2 noise sources were concentrated in the southern region which initiated the fourth stepped leader. The remaining 20% of the J2 sources were located in the northern region and initiated the third stepped leader. Most of the J3 noise sources were located in the northern region and the fifth stepped leader descended from that region. The J4 noise sources were spread in both regions and the dart leader appeared to descend from the southern region. The J5 noise sources were located in both regions and the sixth stepped leader descended from the southern region. Finally the J6 noise sources were spread everywhere and from the dart leader sources it appears to be located in the northern region. All the subsequent J-changes extended higher in altitudes and were less organized. (6) A discrete VHF activity interval was observed for 168 msec after the last return stroke. The pulse repetition rate continuously decreased during this interval. The last solitary pulse in the flash was 21.6 msec from the previous pulse. The noise sources during this SP propagated downwards 50° off vertical in a 5 km path.

5.5 The 180644 Flash

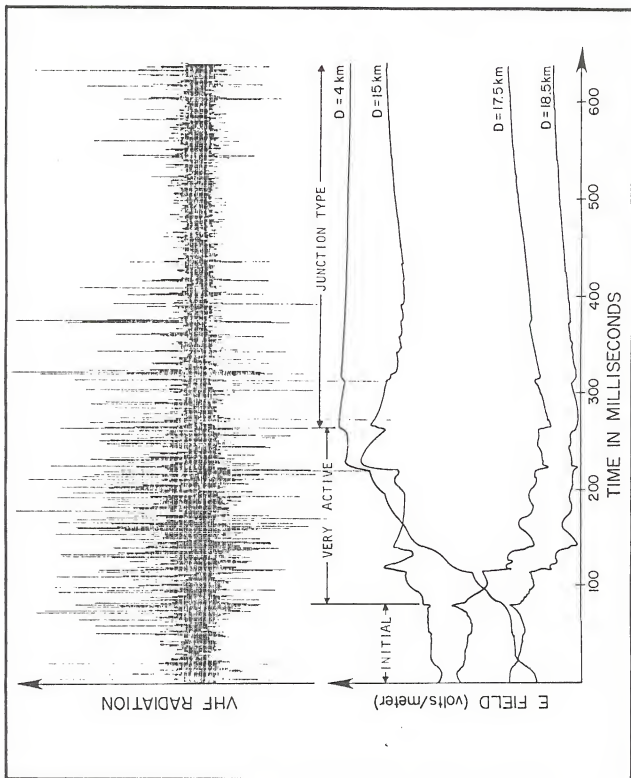
The work reported in this thesis includes three IC flashes. The first of these IC flashes was studied in Section 5.1 because it followed the 165959 flash. The other two IC flashes are discussed in this section and in Section 5.6.

The first lightning discharge during the thunderstorm on the 8th August 1977 happened at 180644 UT. This lightning discharge was an intracloud flash and occurred 56 sec prior to the first cloud-to-ground flash at 180710, previously described in Section 5.2.

Figure 5.78 shows simultaneous records of the logarithmic-amplitude VHF radiation and the electric field reading in four different stations located 4, 15, 17.5, and 18.5 km from the discharge. The fact that the electric field reading at 4 and 15 km showed a positive electric field change while the stations at 17.5 and 18.5 km showed a negative field change indicated that an upper positive and a lower negative polarity charge center were supporting the discharge (equation (3.10)). The electric field reversal with distance, the fact that the field shows no evidence of leader-return stroke sequence, and the locations of the VHF sources in the cloud combine to indicate that the 181416 flash was indeed an intracloud discharge.

The flash lasted 360 msec and can be described as being composed of three different phases on the basis of the relationship between the electric field and the VHF radiation. This pattern is similar to the one described by Kitagawa and Brook (1960) who classified the intracloud discharge into an initial, a very active, and a junction phase, and similar to the 165959 IC flash. These events are shown in Figure 5.78 and lasted 75, 185, and 260 msec, respectively.

Figure 5.76. Simultaneous record of the logarithmic-amplitude VHF radiation observed at 12 km, and the electric field detected at 4, 15, 17.5 and 18.5 km from the discharge. The three active regions of the IC discharge are shown: initial, active and junction phase.



5.5.1 The Initial Phase

The flash started with an initial phase characterized by a smooth variation of the electric field and a VHF pulse rate of one every 20 to 50 μ sec. Figure 5.79 shows the VHF noise during the first 8.5 msec of the intracloud discharge. The flash started with a 100 μ sec wide pulse, similar to the pulse that starts the PB in a cloud-to-ground discharge. However, the lower amplitude, higher frequency VHF radiation following the PB in a CG discharge and characteristic of the stepped leader did not occur.

Figure 5.80 shows the location of the cross-correlated VHF noise sources, 94 μ sec intervals, during the first msec of the intracloud discharge. Most of the VHF source activity is located between the heights of 9.2 and 10.5 km. During the first 13 msec, a channel is formed between the heights of 9.2 and 14.5 km in a path 40° off vertical. As we can see from comparing Figure 5.80 with Figure 5.81, these initial sources become the center of the flash. We also studied the progressing sequence of the VHF noise sources in Figure 5.80. The most active region was at the lower altitude, 9.2 to 10.5 km, but we could not determine the direction of propagation of the VHF sources. We continued this analysis throughout the entire 75 msec of the initial phase, and the only conclusion that we could derive was that at the beginning most of the sources were concentrated at the lower altitude of the slanted channel while at the end of the initial phase there was more activity at the higher altitude. In addition, the original VHF source region became wider throughout the flash.

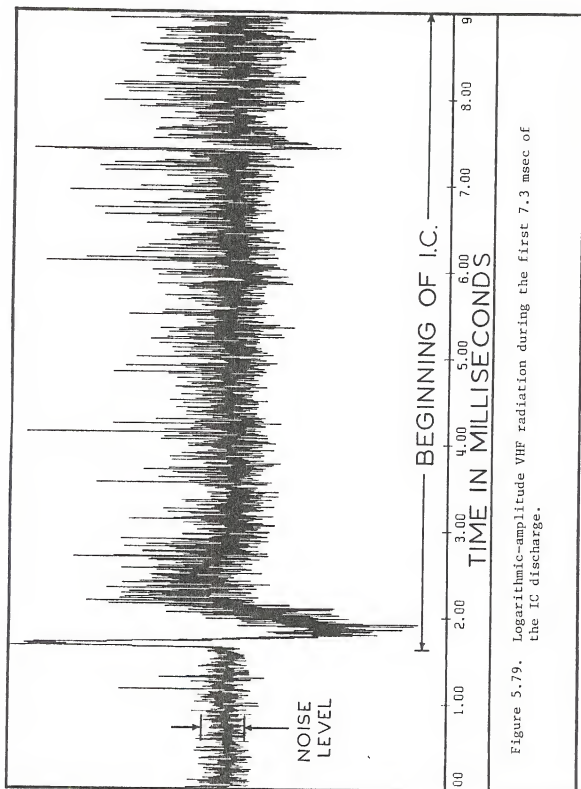


Figure 5.79. Logarithmic-amplitude VHF radiation during the first 7.3 msec of the IC discharge.

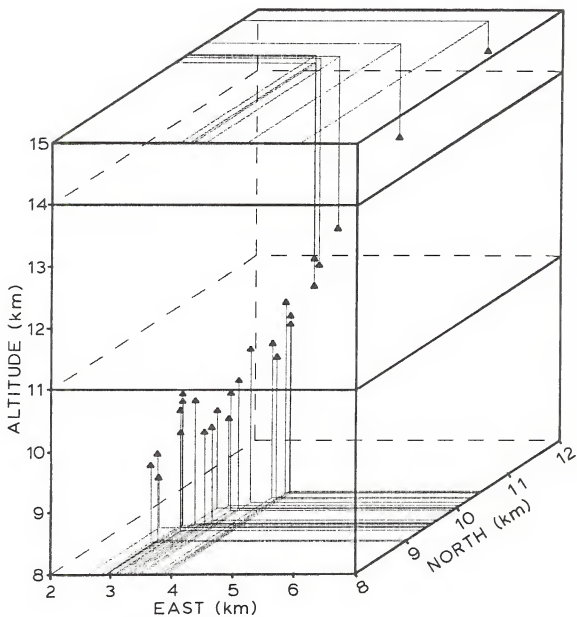


Figure 5.80. Three-dimensional view of the cross-correlated noise sources, 94 μ sec intervals, during the first 13 msec of the intracloud discharge.

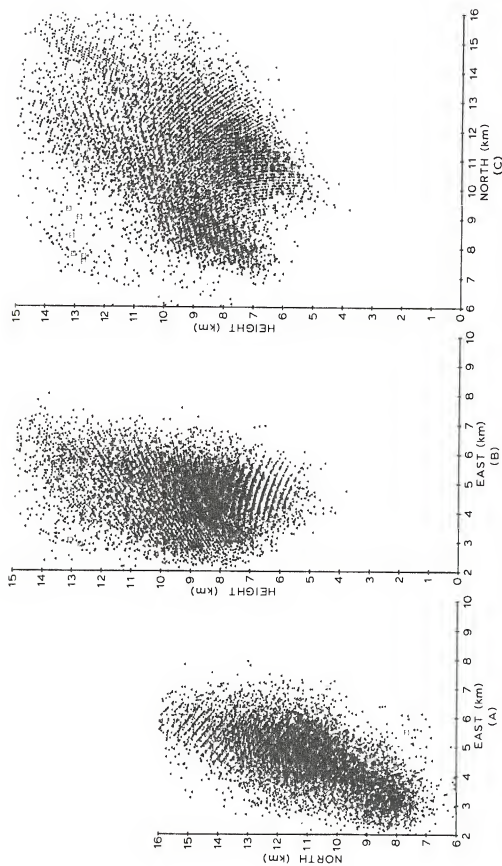


Figure 5.81. Two-dimensional views: (A) top view, EW-NS, (B) elevation view, EW-height, and (C) elevation view, NS-height of all the noise sources during the 180644 intracloud discharge.

5.5.2 The Very Active Phase

The very active portion of the discharge is characterized by a faster rate of change of the electric field than in the initial phase as shown in Figure 5.78. In addition, the VHF noise pulse repetition rate increased from a pulse every 20 to 50 μ sec to a pulse every 5 to 10 μ sec.

A study of the electric field variation with distance in Figure 5.78 suggests that an electric field station about 16 km away from the flash will detect zero field change. Solving the two point charge model in equation (3.10) for zero electric field change, we have

$$\frac{h_1}{\left(h_1^2 + d_1^2\right)^{3/2}} = \frac{h_2}{\left(h_2^2 + d_2^2\right)^{3/2}} \quad (5.1)$$

From a study of the VHF sources during the first 13 msec in Figure 5.80 and all the VHF sources in Figure 5.82, it is reasonable to select the height of the charge centers at 9.5 and 13.5 km along the slanted dipole. For these values of h_1 and h_2 we fitted equation (5.1) and determined that the left and right side agreed within 10%. We also selected other values of heights along the slanted dipole between the heights of 9 and 14 km, but we could not obtain a better fit. Therefore, we conclude that a point charge model of this IC discharge will have charge center at 9.5 and 13.5 km.

5.5.3 The Junction Phase

The junction or final phase of the intracloud discharge has characteristics similar to the discrete activity after return strokes (DAFS), (see, for example, Section 5.2.11.2) in the cloud-to-ground flash and the final part of the IC in the 165959 flash (Section 5.1.13).

This phase is characterized by a pulse every few milliseconds in the VHF record and small variation in the electric field record. Some of the SP's during the junction phase have correlated electric field change as can be observed in Figure 5.78. Therefore, we identify these SP's with K-changes following the work of Brook and Kitagawa (1960), and Ogawa and Brook (1964).

5.5.4 Volume of the Flash

Figure 5.81 shows the 21,752 individual noise sources (triangles) detected during the intracloud flash. The cross-correlated noise sources are also shown with squares. The average rate of pulse location throughout the flash was a pulse every 28.9 μ sec. This low rate of source locations, compared to the typical 7 to 10 μ sec for active VHF periods, is caused by the long duration of the junction phase in which sources were located only during the SP's. The source locations extended from 2.5 to 7 km EW, 8 to 15 km NS, and 6 to 14 km in height, for a total volume of 140 km³.

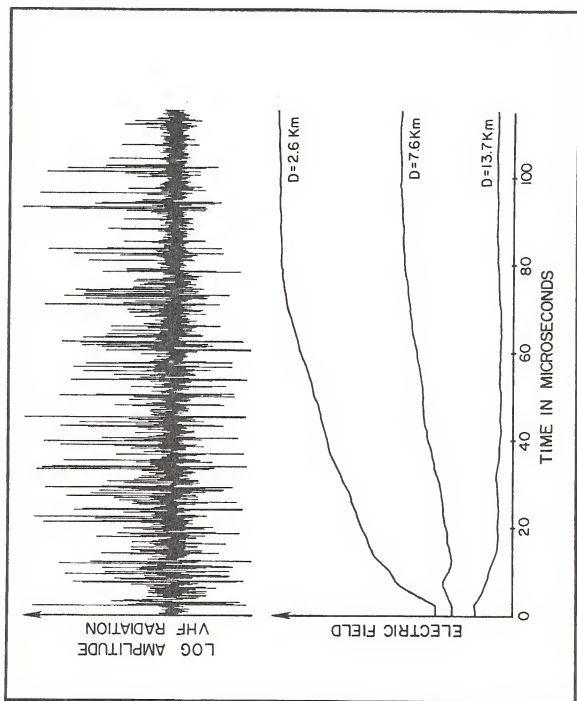
5.6 The 181416 Flash

At 181416 UT during the thunderstorm on 8th August 1977 an intra-cloud discharge occurred. Figure 5.82 shows simultaneous records of the logarithmic-amplitude VHF radiation and the electric field reading at three different stations located 2.6, 7.6, and 13.7 km from the discharge. The fact that the electric field reading at 2.6 km showed a positive field change while the electric field at 13.7 km showed a negative field change indicated that an upper positive and a lower negative polarity charge center were supporting the discharge (equation (3.10)). The electric field reversal with distance, the fact that the field showed no evidence of leader-return stroke sequence, and the locations of the VHF sources in the cloud combine to indicate that the 181416 flash was indeed an intracloud discharge.

5.6.1 Characteristics of the VHF Radiation

The 181416 flash lasted 114 msec and was characterized by pulses one to 5 μ sec wide superimposed on an envelope whose pulse width ranged between 50 and 600 μ sec. Figure 5.83 shows the logarithmic-amplitude VHF radiation during the first 8.4 msec of the intracloud discharge. The VHF radiation pattern at the beginning of the intracloud discharge is markedly different from the VHF radiation for the cloud-to-ground flash studied in this thesis. Since the preliminary breakdown phase in a cloud-to-ground flash studied in this thesis lasted between 2 and 3 msec and was followed by a stepped leader with significantly different VHF characteristics, we can, in the absence of the VHF leader, uniquely identify this present radiation with an

Figure 5.82. Simultaneous record of the logarithmic-amplitude VHF radiation observed at 7 km, and the electric field detected at 2.6, 7.6 and 13.7 km from the discharge.



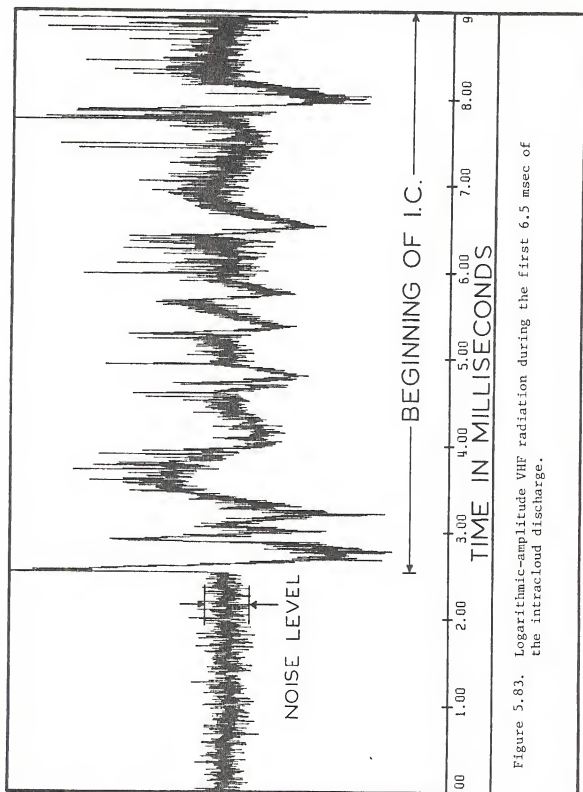


Figure 5.83. Logarithmic-amplitude VHF radiation during the first 6.5 msec of the intracardiac discharge.

intracloud discharge. The initial VHF noise of the intracloud has similar characteristics to that of the cloud-to-ground discharge prior to the stepped leader; that is, both appear to be due to the PB process.

Figure 4.1 shows the first 800 μsec of the VHF radiation detected at the central station, and at the W1, M1, and M3 stations. These stations are identified in Figure 3.1. The ground distance from the discharge to the four stations is 7.6, 4.1, and 12.4 km, respectively. The DTOA between the central and each one of the remote stations is shown in Figure 4.1. This data is taken directly from the digitized tapes and corresponds to the simultaneous recorded VHF radiation. To determine the actual DTOA needed to calculate source locations we have to subtract the retransmission delays for the remote stations (Appendix B).

Similar to the cloud-to-ground discharge after the last return stroke, the VHF noise pulse repetition rate decreases toward the end of the discharge. This decrease of the pulse rate of continuous radiation coupled with the appearance of discrete VHF radiation of SP's mark the end of the intracloud discharge.

The 181416 flash did not have the three previously described phases: initial, very active, and junction phase. The VHF pulse rate of one every 10 to 20 μsec (characteristic of the active phase) decreased toward the end of the flash. Therefore, we could characterize the VHF radiation in two intervals: an active phase and a junction phase as proposed by Brook and Kitagawa (1960) for some of the flashes they studied.

5.6.2 Locations of the VHF Noise Sources

Figure 5.84 shows the cross-correlated VHF noise sources, 94 μsec intervals, during the first 18.8 msec of the IC discharge. The VHF

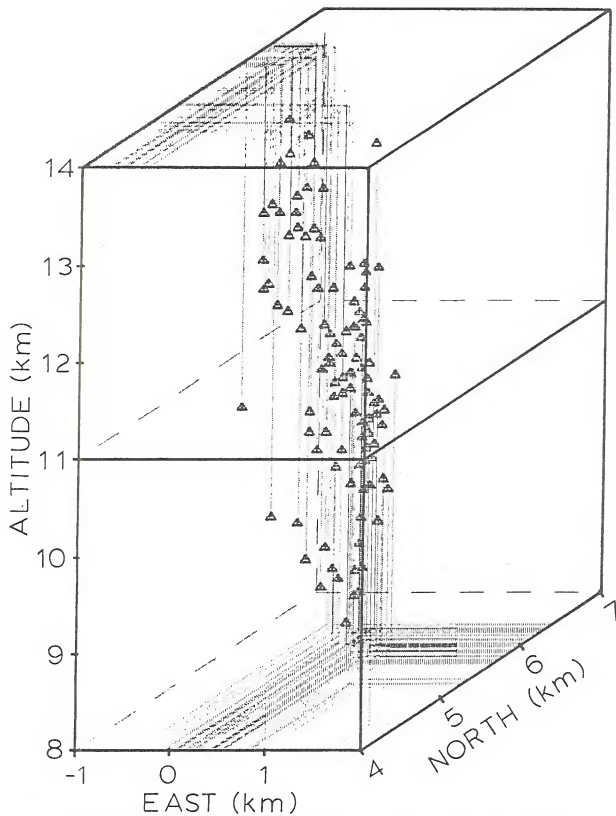


Figure 5.84. Cross-correlated VHF sources, 94 μsec intervals, during the first 18.8 msec of the IC discharge.

noise sources formed a near vertical channel between the heights of 8.5 and 13.5 km. About 90% of the cross-correlated noise sources were located within a cylinder of 0.5 km radius and 5 km length. During the first 18.8 msec the VHF noise sources did not follow a progressing sequence either upwards or downwards. However, in the first 4.5 msec, about 80% of the VHF sources were located in the bottom half of the cylinder.

Figure 5.85 shows a two-dimensional view of all the cross-correlated noise sources, 94 μ sec intervals, during the entire IC discharge. The VHF sources spread radially with increasing height forming an inverted cone about 9 km in height.

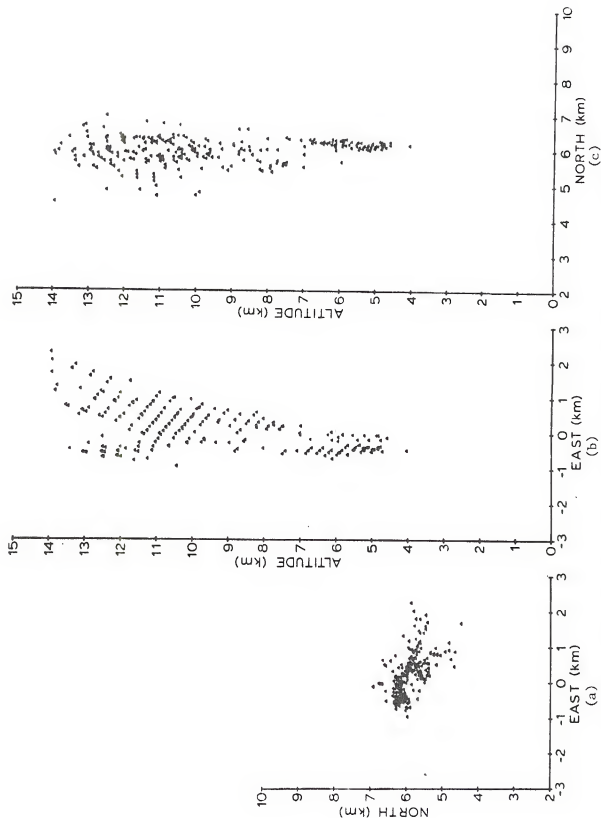


Figure 5.85. Two-dimensional projections: (a) EW-height, (b) EW-height, and (c) NS-height of all the cross-correlated VHF sources, 94 μ sec intervals, for the IC discharge.

CHAPTER VI

DATA MODEL

This chapter is an attempt to use a stochastic model to describe the behavior of some of the different phases of the VHF radiation during lightning discharges. We have attempted data models for the basic noise level, the stepped leader, and the J-change process. The noise level is used for reference and is assumed to be the VHF background noise without a nearby lightning VHF radiation. The stepped leader is characterized by a unique high frequency pulse rate, the properties of which are important to study. The characteristics of the VHF noise during the J-change process accounts for most of the CG radiation.

It is not possible to predict the exact magnitude of the VHF radiation during these phases because the exact physical laws that describe these processes are not known and these processes are not deterministic. Our goal is to derive a stochastic model of the phenomenon, that is, to predict the probability that a future value of the radiation will lie within certain limits. These models in turn can be used to improve the understanding of the physics underlying the activity. To arrive at the models we have identified the parts of the VHF radiation data corresponding to different phases of the lightning on the correlated electric field records. A model can be derived whenever the time series of the VHF radiation $z_1, z_2, \dots, z_{k-1}, z_k$ behaves in such a manner that given $k-1$ samples z_1, z_2, \dots, z_{k-1} , the value of the z_k can be predicted.

For a model to be valid it should fit the specific physical process regardless of the selected flash. Therefore, we selected data from the stepped leader, J-changes, and noise levels for all the flashes, determined their respective models, and then compared the results. If consistent results were obtained, then we can claim that the physical process fits a specific data model.

For a data range larger than 500 microseconds all the analyzed processes present some type of equilibrium because the larger pulses determined in the VHF radiation have a width of the order of 240 microseconds. Each process studied has a constant mean for data records larger than about 2.3 msec (about 10,000 samples) and can be treated as stationary.

Four types of stochastic models are tested. The autoregressive (AR), the moving average models (MA), the autoregressive-moving average (ARMA), and the autoregressive-integrated-moving average models (ARIMA), (Box and Jenkins, 1976). We will identify not only the type of model that reproduces the data, but also the order and properties of such a model. In the AR model a VHF radiation value of the output z_t is defined as

$$z_t = \phi_1 z_{t-1} + \phi_2 z_{t-2} + \dots + \phi_p z_{t-p} + a_t \quad (6.1)$$

where a_t is a white noise representation of the VHF noise input and p is the order of the AR model order. In the MA model z_t is defined as

$$z_t = a_t - \theta_1 a_{t-1} - \theta_2 a_{t-2} - \dots - \theta_q a_{t-q} \quad (6.2)$$

where q is the order of the moving average model. A more general data model, the ARMA, includes both previous values of the output and (z_t 's) and the input (a_t 's):

$$z_t = \phi_1 z_{t-1} + \phi_2 z_{t-2} + \dots + \phi_p z_{t-p} + a_t - \theta_1 a_{t-1} - \theta_2 a_{t-2} - \dots - \theta_q a_{t-q} \quad (6.3)$$

Many test data show nonstationary behavior when models (6.1), (6.2), or (6.3) are tested, but the data are stationary if a new series is found which contains a higher order difference than the original series. Let

$$W_t = \nabla z_t = z_t - z_{t-1} = \nabla^d z_t = \nabla^1 z_t \quad (6.4)$$

where d is the number of differences in the original series. Similarly, the first difference ARIMA model can be defined in a manner similar to equation (6.3). That is

$$W_t = \phi_1 W_{t-1} + \dots + \phi_p W_{t-p} + a_t - \theta_1 a_{t-1} - \dots - \theta_q a_{t-q} \quad (6.5)$$

The procedures used for the model estimate is the Box and Jenkins (1976) approach. We used this approach for model estimates as follows:

(1) Model identification. A total of 12 data records composed of four sets of 5,000 samples each were selected from the noise level, stepped leader, and J-change. For each of the four ground flashes we selected a data record for the three identifiable processes. We determined the autocorrelation and partial correlation of each set of data. We used the Box and Jenkins (1976) selection criteria to determine the stochastic model type (AR, MA, ARMA, or ARIMA) and order based on the properties of the autocorrelation and partial autocorrelation functions. A model was chosen for each data record independent of the physical process.

(2) Parameter estimation. Initial estimates of the coefficients of the original series ($d=0$) or for the first difference ($d=1$) were chosen to ensure convergence of the individual parameters to fit the previously identified model. Next we discuss the results of the data models for the three physical processes.

6.1 Noise Level

For reference purposes we identified the best model for the background noise level of the four flashes. These models were chosen from testing AR, MA, ARMA, and ARIMA for $d=0$ and $d=1$. The results obtained are as follows: (1) Flash 165959, MA, order 3, $d=1$, $\theta_1 = 0.108$, $\theta_2 = -0.431$, $\theta_3 = -0.086$; (2) Flash 180710, AR, order 3, $d=0$, $\phi_1 = -0.1011$, $\phi_2 = 0.5315$, $\phi_3 = -0.1797$; (3) Flash 181806, AR, order 4, $\phi_1 = -0.1332$, $\phi_2 = 0.1009$, $\phi_3 = -0.5598$, $\phi_4 = 0.1687$; (4) Flash 182356, AR, order 3, $d=0$, $\phi_1 = 0.0137$, $\phi_2 = 0.0237$, $\phi_3 = 0.0243$.

The 165959 flash produced a better model for the first difference MA of the 3rd order, however, the original 165959 series ($d=0$) for the noise level also fits an AR 3rd order level. The standard deviation of the above parameters is less than 10%. The fact that this process can be represented as an AR of order 3 or 4 indicates that the VHF radiation dies out quickly as a function of the previous values of the output.

6.2 Stepped Leader

We determined the best model for the initial stepped leader for each of the four CG flashes. These models were chosen from testing AR, MA, ARMA, and ARIMA for $d=0$ and $d=1$. The results obtained are as follows: (1) Flash 165959, AR, order 5, $d=0$, $\phi_1 = -1.084$, $\phi_2 = 0.6686$, $\phi_3 = -0.4453$, $\phi_4 = 0.2141$, $\phi_5 = -0.1105$; (2) Flash 180710, AR, order 3,

$d=0$, $\phi_1 = 1.326$, $\phi_2 = 0.7613$, $\phi_3 = -0.247$; (3) Flash 181806, AR, order 4, $d=0$, $\phi_1 = -1.624$, $\phi_2 = 1.395$, $\phi_3 = -0.8503$, $\phi_4 = 0.3549$; (4) Flash 182356, AR, order 3, $\phi_1 = -0.1875$, $\phi_2 = 0.5632$, $\phi_3 = -0.3164$.

The best model for the stepped leader was AR, order 3 to 5. There were some minor differences between the different stepped leader processes. The standard deviation in the determination of the parameters is about 10%. The characteristics of the stepped leader are similar to those of the basic noise level, that is, an AR process that dies out quickly as a function of the previous values of the output.

6.3 J-Change

During the J-change process and most of the VHF radiation, other than the stepped leader, the magnitude of the VHF radiation is heavily dependent upon the level of the radiation. Pulses 50 to 240 μsec wide contain a low frequency data envelope and a model for $d=0$ was nonstationary. Once we obtained the first difference, we obtained consistent results in all the four flashes' J-changes. The results obtained are as follows: (1) Flash 165959, MA, order 3, $d=1$, $\theta_1 = 0.212$, $\theta_2 = 0.397$, $\theta_3 = 0.108$; (2) Flash 180710, MA, order 3, $d=1$, $\theta_1 = -0.466$, $\theta_2 = 0.361$, $\theta_3 = 0.327$; (3) Flash 181806, MA, order 3, $d=1$, $\theta_1 = -0.452$, $\theta_2 = 0.268$, $\theta_3 = 0.223$; (4) Flash 182356, MA, order 3, $d=1$, $\theta_1 = -0.487$, $\theta_2 = 0.381$, $\theta_3 = 0.358$.

The standard deviation of the above parameters is less than 10%. The model described in this section indicates that the VHF radiation can be described as a model with a pole at the origin which corresponds to the first difference and three separate zeros from the moving average.

6.4 Characteristics of VHF Radiation

The VHF radiation pulse model presented in this chapter provides fairly consistent results for the three selected processes in four different flashes. The basic conclusion of this analysis is that the properties of the sources underlying the physical process are very common from flash to flash. Even though the process is not deterministic, we can predict that any future value of the output will fall between any specified limits. In addition, the consistency of the results allows us to characterize the VHF radiation for the different phases of the lightning discharge without need of other measurements, e.g., electric field. From a study of the variations of the poles and the zeros for the different phases of lightning flashes we can determine properties of the pulse shape emanated by the VHF source.

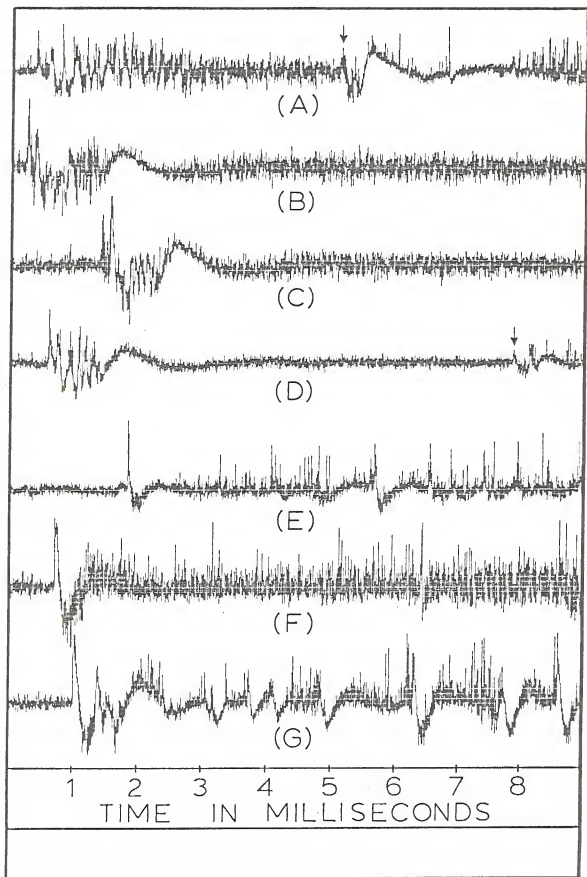
CHAPTER VII

CHARACTERISTICS OF THE VHF RADIATION DURING THE DIFFERENT PHASES OF LIGHTNING

This chapter provides a description of the properties of the individual phases of the cloud-to-ground and intracloud flashes studied in Chapters V and VI. In this description we use the characteristics of the 30-50 MHz VHF radiation, the location of the VHF noise sources, and the correlated electric field measurements (0.1 Hz to 1.5 MHz). Although our study and conclusions are based on a limited sample of four cloud-to-ground and three intracloud flashes, we feel that the results presented are sufficiently consistent that they may be considered valid.

Before we proceed to study the properties of each of the discharge phases, we note that we can tell whether a CG or an IC lightning flash will occur from the first 3 msec of the VHF noise. Figures 7.1(A), 7.1(B), 7.1(C), and 7.1(D) represent the beginning of the VHF radiation in the four CG flashes studied in Sections 5.1 through 5.4, respectively, whereas Figures 7.1(E), 7.1(F), and 7.1(G) represent the three IC flashes studied in Sections 5.1.13, 5.5, and 5.6. The IC discharge that followed 140 msec after the 165959 flash discussed in Section 5.1 is shown separately because its properties are similar to the other two IC discharges. Both CG and IC radiation started with high frequency pulses superimposed on the envelope of a slower varying signal. The CG VHF noise after the first 2 or 3 msec changes to high frequency and uniform low-magnitude pulses, which, in this thesis, are identified with the

Figure 7.1. VHF radiation during the beginning of the four CG and three IC flashes studied in this thesis. (A) 165959 CG flash, the arrow indicates the first return stroke; (B) 180710 CG flash, the first return stroke occurs off the drawing; (C) 181806 CG flash, the first return stroke occurs off the drawing; (D) 182356 CG flash, the arrow indicates the location of the first return stroke; (E) 165959 IC flash; (F) 180644 IC flash; (G) 181416 IC flash.



stepped leader. In the IC flash, however, the VHF noise level remains large and it has additional low frequency pulses. These features can be seen in Figure 7.1. The observation that the two types of flashes can be identified early supports the work of Kitagawa and Brook (1960), who studied the characteristics of the electric field during CG and IC flashes, and claimed that from the initial electric field pulse rate the two types of discharges could be uniquely identified. Proctor (1976) and Hewitt (1962) working at 253 MHz and 600 MHz, respectively, claim that they could not differentiate between CG and IC flashes from their noise records. From observing the electric field record, we know that the presence of a stepped leader-return stroke sequence differentiates CG flashes from IC flashes, but the return strokes do not occur in our records until about 5 to 12 msec. The characteristics of the VHF radiation reported here are evident at the beginning of the discharge, that is, during the formation of the VHF sources for the PB-stepped leader process. Next we look at the characteristics of the different phases of the CG and the IC flashes.

7.1 Cloud-to-Ground Lightning

The VHF noise, the VHF source locations, and the correlated electric field records of eight basically different processes were studied in this thesis. These eight processes are: (1) preliminary breakdown (PB), (2) stepped leader (SL), (3) dart leader (DL), (4) return stroke (RS), (5) activity following the first return stroke (FR), (6) J-change processes, (7) solitary pulses (SP) and K-changes, and (8) continuing current.

7.1.1 Preliminary Breakdown

At the beginning of the CG flashes we detected VHF noise levels about 20 times larger than during the stepped leader. Based on the difference of the VHF noise level we chose to name this time interval "preliminary breakdown" (PB). The VHF noise for the four CG flashes during the PB is shown in Figures 5.5, 5.23, 5.41, and 5.64. The duration of the PB's varied between 1.9 and 2.2 msec. The VHF noise was characterized by high frequency pulses ranging in width from 1 to 150 μ sec superimposed on a lower frequency envelope. Three of the PB's ended with a pulse 300 to 700 μ sec wide (Figures 5.23, 5.41, and 5.64). We suspect that the end portion of these wide pulses are oscillations caused by the tape recorder's sharp low frequency cutoff.

We studied the progressing sequence of the VHF noise source locations during the first few hundred microseconds of the PB, which corresponds to the beginning of the CG discharges. We labeled the progressing sequence of these sources and the time of their occurrence in Figures 5.4, 5.25, 5.42, and 5.65. The initial paths formed by the VHF sources for the four studied flashes were: (1) path length of 4.8 km at 28° off vertical between a height of 9.9 and 6.5 km, (2) path length of 12 km at 55° off vertical between a height of 9.8 and 4.1 km, (3) path length of 7.8 km at 22° off vertical between a height of 11 and 4.9 km, and (4) path length of 7.5 km at 26° off vertical between a height of 9.9 and 4.0 km. The PB sources initially formed a cylinder of about 500 meters. During the period of time that these cylinders were formed there was no correlated electric field change indicating no significant charge transfer. The timing sequence of the beginning of the VHF sources is random in the first two flashes but appears to follow an ascending then

descending sequence in the remaining two PB's. The location of some of the sequential VHF sources were not caused by the propagation of the previous sources, since the time and distance yields a velocity greater than the speed of light. For three of the four CG flashes the initial electric field change occurs within a few hundred microseconds of the final PB pulse, the tail end of which may be due to the recorder response. Proctor (1976) claims that over 90% of the stepped leader radiation began with a sharp burst of noise of higher amplitude. In addition, Proctor (1976) reports that sometime the VHF noise began suddenly before the start of the electric field records. These characteristics observed by Proctor appear to be consistent with our definition of preliminary breakdown.

From a study of the VHF sources during the PB, we determined that the path of the series of pulses riding a slowly varying envelope is generally about 4 km. This path is probably caused by a potential wave that propagates throughout part of the initial PB path. In addition, breakdown regions in different parts of the path are probably the contributors of the high frequency pulses superimposed on the envelope. Most of the individual pulses during the entire PB are detected within about 1 km perpendicular radius from the initial path. Some of the pulses are located in small isolated regions. Pulses during the PB's appear similar to the isolated SP's studied in Chapter V and discussed in Section 7.1.7. That is, both are probably potential waves of about 4 km length with little charge transfer.

7.1.2 Stepped Leader

We studied a total of 20 leader-return stroke sequences in the four randomly selected CG flashes. From these 20 leaders, 12 were

classified as stepped leaders, 1 as a stepped-dart leader, and 7 as dart leaders. Even though we had a limited sample of 20, over 50% of the return strokes were preceded by stepped leaders. The initial stepped leader that followed the preliminary breakdown had slightly different properties from the subsequent stepped leaders. Therefore we chose to divide the stepped leader discussion in two subsections.

7.1.2.1 First Stepped Leader. At the end of the preliminary breakdown the VHF radiation decreased to about twice the noise level, corresponding to the lowest level of VHF radiation for any identified process in either CG or IC flashes. This type of radiation was characterized by high frequency pulses with less than 4 μsec width and a pulse rate of one every 13 to 15 μsec (Figure 5.16). The stepped leader VHF radiation has unique characteristics and has been used throughout this thesis to identify the beginning of CG flashes. The duration of the stepped leader VHF noise ranged between 2.9 and 7.9 msec. In contrast with the low amplitude, high frequency, stepped leader pulses at 30 to 50 MHz shown in this thesis, Proctor (1976), working at 253 MHz, and Brook and Kitagawa (1964), working at 420 and 850 MHz, observed strong radiation during the stepped leader. Work reported by Malan (1958) showed an increase in the stepped leader radiation between 3 KHz and 12 MHz. Therefore, it appears that the stepped leader radiation increases are a function of frequency.

We studied the VHF noise sources during initial stepped leaders and determined that about 70% of the sources followed a regular progressing downward sequence which extended the previous path formed by the PB sources. The remaining 30% of the sources are detected in two other regions as follows: (1) Sources detected in the horizontal direction which widen the main PB-stepped leader path to about 1 or 1.5 km radius,

e.g., stepped leader branches, and (2) Active sources which still radiate at higher altitudes in the neighborhood of the PB-stepped leader junction while the leader propagates to ground.

The fact that the VHF pulses appear to be associated with the stepped leader steps and that correlated electric field change is detected up to about 1 msec prior to the stepped leader pulses suggests the following sequence of events in the formation of a CG flash:

- (1) The path of the PB sources becomes an ionized channel or arc;
- (2) Current starts to flow through the channel providing correlated electric field change from the motion of the electric charges; and
- (3) The steps of the stepped leader formation start and stepped leader propagation continues from the cloud charge.

We found the VHF source locations during the PB-stepped leader transition. A source which corresponds to the locations in the transition between the PB and the stepped leader VHF noise is chosen as the beginning of the stepped leader. The VHF sources are detected throughout the leader path to near-ground. In addition to the poor accuracy of our detection system for altitude locations near-ground, we found two other limitations in trying to obtain stepped leader source locations. First, stepped leader sources, most likely from leader branches or leader path enhancement, are simultaneously active over a large volume. Second, the VHF noise for sources near the ground usually decreases prior to the return stroke. The stepped leader velocity that we calculated from the beginning source of the stepped leader VHF radiation to the last detectable stepped leader source ranged from 9.2×10^5 m/sec to about 4.3×10^6 m/sec. These initial stepped leader velocities are about a factor of 10 larger than those reported from optical measurements by Schonland and his co-workers and by Proctor (1976).

7.1.2.2 Subsequent Stepped Leaders. Subsequent stepped leaders had the following properties that distinguished them from first stepped leaders:

(1) The VHF noise level had the same high frequency, uniform amplitude pulse characteristics but a magnitude twice as large as the initial stepped leaders.

(2) All subsequent stepped leaders were preceded by active VHF radiation from the J-change which lasted for at least 7 msec with a pulse about every 10 μ sec. This high repetition rate of VHF pulses appeared to be a necessary condition before the initiation of subsequent stepped leaders. There is a 5 to 1 ratio between the magnitude of the VHF noise during the J-change and the subsequent stepped leader. This feature in the VHF noise is used to identify subsequent stepped leaders. Some of the J-changes that preceded subsequent stepped leaders were formed in a concentrated region in a slanted path. If the previous J-change was mainly horizontal, the stepped leader descended from a concentrated VHF source region, usually near the center of the VHF source region (SL2 and SL3, Section 5.2). If the previous J-change was mainly vertical, the stepped leader propagated from the lower part of the vertical region (SL2, Section 5.3; SLD, Section 5.1). Clear evidence of the subsequent stepped leader following the vertical propagation path of the J-changes is seen in Figures 5.18 and 5.48.

(3) Subsequent stepped leaders are difficult to identify in the electric field record. Of 12 subsequent stepped leaders identified in the VHF record, only four could be identified at any of ten electric field stations. The beginning of the subsequent stepped leader electric field record often does not show a change in the slope of the

previous J-change. However, we did not have any problem identifying subsequent stepped leaders from a single channel VHF radiation.

(4) Subsequent stepped leaders are considerably longer and propagate at slower velocities than initial stepped leaders. This might be due to the fact that all subsequent stepped leaders that we studied had a much larger horizontal component than the initial stepped leader. A possible explanation of this feature is that negative charges still remaining in the first stepped leader channel to ground will repel the new stepped leader. Therefore, the subsequent stepped leaders had to propagate around the old stepped leader to find a new path to ground. The duration of subsequent stepped leaders ranged from 14.2 to 35.0 msec and we obtained velocities between 1.6×10^5 and 1.1×10^6 msec, close to the range reported by Schonland et al. (1938).

7.1.3 Dart Leader

The properties of the dart leader were quite different from the previously discussed stepped leader properties. We studied seven dart leaders which occurred in the four CG flashes. The magnitude of the VHF noise sources during the dart leader exceeded the stepped leader radiation by a factor of 20 to 1. The VHF noise during the dart leader started with a large pulse, usually between 150 and 200 μ sec wide. The remainder of the dart leader contains mostly high frequency pulses of less than 20 μ sec width superimposed on a slow envelope with a pulse width of about 500 μ sec. The total VHF radiation during dart leaders lasted between 0.35 and 1.70 msec.

The VHF noise sources during the dart leader were either in the neighborhood of the previous J-change (Section 5.3 prior to the fifth and sixth return stroke) or connected the end of the preceding J-change

with the previous return stroke channel (Section 5.1 prior to the second return stroke, and Section 5.3 prior to the third and fourth return strokes). In the former case the dart leader expanded from the bottom of the path formed by the J-change noise sources. However, in the latter case the dart leader radiation path was mainly horizontal between 4 and 6 km. The wide pulse at the beginning of the leader with a magnitude of 20 times that of the stepped leader is probably caused by a potential wave that propagated from the previous J-change. No dart leader VHF sources were detected in the leader path to ground.

Brook and Kitagawa (1964) and Proctor (1976) also reported strong radiation during dart leaders. They also concluded that the dart leader radiating sources were located in the cloud and not along the leader channel to ground. Proctor (1976) did so using the same technique we use; Brook and Kitagawa (1964) used arguments based on the time difference between the electric field and the high frequency radiation.

7.1.4 Return Strokes

The VHF radiation during return strokes lasted between 92 and 859 μsec and was characterized by either one large pulse of duration 92 to 250 μsec or a succession of pulses between 30 and 100 μsec width. VHF radiation was absent during the fourth return stroke in Section 5.3. Otherwise, the maximum magnitude of the VHF radiation during return strokes was about 25 times larger than the stepped leader.

The VHF sources during return strokes preceded by stepped leaders were located in the neighborhood of the previous stepped leader channel and throughout the PB or J-change that preceded the leader. Return strokes VHF sources after stepped leaders were detected between a height of 14.5 and 0.7 km. Similarly, VHF sources during return strokes

preceded by dart leaders were located in the neighborhood of the previous J-change between a height of 12.6 and 6.5 km. It was not possible to detect accurately return stroke velocities because only a few sources were detected and they did not necessarily follow an upward progressing sequence. On the basis of the fact that there was no VHF radiation in one of the return strokes and that the VHF sources in the remaining of the return strokes were located along the channel to ground (for those return strokes preceded by stepped leaders) and in the J-change (for return strokes preceded by dart leaders), it appears that the VHF radiation during return strokes is generated by extensions of the previously existing leader channel. The return stroke wide VHF pulse represents a potential wave that propagates throughout the previous channel toward the higher altitudes.

We presented in our analysis the location of the stepped leader-return stroke source obtained by Krehbiel (private comm.) using the technique of Krehbiel et al. (1979). We determined that the location of Krehbiel's point charge center for the return strokes of the four flashes were in fairly good agreement with the location of the PB-stepped leader path (for initial SL), or J-change-stepped leader path (for subsequent stepped leader). The point charge provided to use for the return strokes of these flashes ranged between -25.7 and -2.9 Coul and a height between 7.9 and 4.4 km.

In addition to finding the return stroke point charge using multiple station electric field measurements, we assumed the location of the stepped leader-return stroke charge was the PB-SL junction and calculated the charge using the technique described in Section 3.6. We obtained results which were comparable to the ones determined by Krehbiel.

The point charges that we determined by using these techniques ranged between -24.1 and -3.6 Coul for heights between 10.5 and 5.9 km.

7.1.5 Activity Following the First Return Stroke (FR)

During the FR interval we obtained the fastest pulse repetition rate and largest amplitude in the CG and IC flashes. We chose to call this process "FR" (following return) because the locations of the VHF noise sources were directly related to the first stepped leader-return stroke sequence. The pulse repetition rate during the FR was a pulse every 3 or 4 μ sec and the magnitude of these pulses were about 25 times larger than that of the stepped leader. At the end of the FR we measured return stroke-like pulses of a magnitude 40 to 50 times larger than the stepped leader. For three of the four FR intervals, the VHF noise started immediately after the return stroke, but for one of the flashes (Section 5.1) there was a 2.4 msec quiet period between the return stroke and the FR interval. The FR interval lasted between 4.3 and 8.8 msec and always ended with a wide pulse of the largest magnitude in the CG, which because of its similarities to the return stroke pulse we associated with the propagation of a potential wave.

The location of the VHF sources for three of the four FR's were in the neighborhood of the previous PB-stepped leader-return stroke channel. In the fourth case (Section 5.4), the VHF sources were located right on the top of the previous PB-leader channel. The height of the VHF sources ranges between 9.5 and 1.8 km. The FR phase of the CG flash may be related to M-components (Malan and Schonland (1947), Kitagawa et al. (1962), and Uman (1969)); that is, the increases in channel luminosity following a return stroke. For two of the four FR's intervals, the VHF sources propagated upwards in a regular progressing

sequence. We correlated the VHF noise with the electric field change at the multiple stations. We determined that during the FR interval either negative charges propagated downward from a region of higher altitudes, or that positive charges (probably from the previous return stroke) propagated upwards or both. We attempted to determine the amount of charge transfer during the FR interval for one of the flashes and found that for electric field ground stations whose distance is greater than the charge height, a charge of 4.5 ± 2.1 Coul was transferred. For close electric field measurements, no consistent charge transfers could be found indicating that the charge distribution could not be approximate as a point charge.

7.1.6 The J-Change Process

Throughout this thesis we have referred to the J-change or the J-change process as the portion of the interstroke process, with continuous active VHF radiation, that preceded dart leaders or subsequent stepped leaders. This J-change process occupied 80, 41, 75, and 59% of the total VHF radiation emitted by the four studied CG flashes (disregarding the VHF radiation after the final return stroke). Other studied characteristics of the interstroke period included the FR interval after the first return stroke, solitary pulses, quiet periods, dart leaders, and subsequent stepped leaders. The quiet periods are discussed in this subsection as they relate to the J-change process.

To study one of the properties of the J-change process, let us first make a comparison to the leader-return stroke sequence and the PB-stepped leader sequence. A return stroke cannot occur without a preceding leader, and an initial stepped leader cannot propagate unless it had a preceding PB. Here we claim that dart leaders or subsequent

stepped leaders cannot propagate unless they are immediately preceded by active VHF radiation from the J-change process. As we shall see in this section, the physical reason for the J-change-leader sequence is that the J-change makes available the charges which are lowered by the dart or subsequent stepped leader.

Two of the studied flashes (Sections 5.1 and 5.3) had VHF radiation emitted during J-changes which originated at a height near 14 km. The path of these two flashes were more vertically inclined and we refer to them as vertical flashes. The other two flashes only extended to a height of about 12 km and we refer to them as horizontal flashes.

The VHF sources for the first J-change in the two vertical flashes followed a regular progressing sequence from a height of 13.7 and 14.2 km, and propagated downwards in paths of 35° and 25° off vertical, respectively. These two J-changes lasted 44.3 and 8.1 msec and the VHF sources propagated at a velocity of 1.5×10^5 m/sec and 5.0×10^5 m/sec, respectively. We fitted a point charge model that lowered negative charge along the regular progressing sequence of the path and found that -2.4 and -1.8 Coul were lowered by these processes. From all the J-change in the four flashes, these two J-changes were the only ones that exhibit a regular progressing sequence of the noise sources. It is interesting to note that these J-changes were the first ones in these two flashes and they were preceded by 16 and 16.5 msec quiet periods. Quiet periods are those time intervals in the flash which have electric field change but no VHF radiation. We do not know if the quiet period had any effect in the sequence of propagation of the noise sources, or if it was a coincidence.

The initial J-change in the other two flashes formed a well defined path. However, the noise sources occurred randomly throughout the path.

The path of the VHF noise sources during subsequent J-changes extended to regions of high altitudes and occupied a larger volume in space. Some of the paths of the noise sources during subsequent J-changes were located in the same location or in the neighborhood of the path of the previous J-change. Other subsequent J-changes developed parallel to the path of the previous one. The fact that some previous VHF sources remain active during subsequent J-changes (Figures 5.53 and 5.55) was previously observed by Proctor (1976). As the stroke number increases, subsequent J-changes became less organized. In the last J-change in the six and the eight stroke flashes the VHF sources did not form an obvious path and were randomly located over a larger volume.

Our interpretation of the given facts about J-change processes is as follows:

- 1) The J-change process makes available the negative charge needed for subsequent strokes to ground.
- 2) As the number of strokes increases, this charge is being drained from higher places in the cloud. Since there is less negative charge available near the end of the flash, the J-changes associated with the last strokes occupied a larger volume.
- 3) As it is clearly shown in this thesis in Figures 5.18, 5.48, 5.70, and 5.74, some of the subsequent stepped leaders propagated from the lower and most concentrated region of the J-change. That is, the negative charge made available by the J-changes is then lowered to ground. In the remaining of the J-changes-leader paths, not shown in the above figures, the dart leaders or the subsequent stepped leaders

VHF sources were detected in the neighborhood of some of the lower regions of the J-change.

7.1.7 SP and K-Changes

Kitagawa et al. (1958) defined a K-change as a small, rapid field change with accompanying pulses of luminosity. We refer to K-changes as those small, rapid field changes with accompanying VHF radiation. In addition, we refer to SP's (solitary pulses) as those isolated VHF pulses with a magnitude 30 to 45 times larger than the stepped leader and with no detectable electric field change. SP's were preceded and followed by quiet periods and were detected during the J-change, after the last return stroke in CG flashes, and in the junction phase of IC discharges. The duration of the SP's is about 1 msec and the VHF noise is characterized by pulses 1 to 30 μ sec wide superimposed in an envelope with a pulse width between 100 and 180 μ sec. Figures 5.13(a), 5.13(b), and 5.13(c) show the VHF noise during three SP's that occurred in a quiet period during the interstroke process. Figure 5.36 shows the VHF noise for a K-change that occurred after the last return stroke of one of the CG flashes.

The VHF noise sources for the SP's in the interstroke process (Figures 5.14(a), 5.14(b), and 5.14(c)) propagated upwards 2 to 5 km at a velocity between 1 and 4×10^7 m/sec. A K-change initiated the J1 change in the flash discussed in Section 5.2. This K-change lasted 1.1 msec and propagated downwards about 4 km from a height of 10.6 km at a velocity of 9.5×10^6 m/sec. No other SP or K-changes were detected during the J-process. Other rapid electric field changes during the

J-process were preceded and followed by continuous VHF radiation and we chose to consider them as an integral part of the J-process.

Solitary pulses and K-changes were observed after the last return stroke of the CG flashes. One SP after the last return stroke in Section 5.1 propagated upwards about 5 km, but most of the SP's and K-changes in the other three CG flashes propagated downwards as shown in Figure 5.76. The VHF noise sources in one of the K-changes shown in Figure 5.37 followed a path similar to that suggested by Kitagawa and Kobayashi (1958). That is, a downward propagation path followed by an upward moving path, except that the velocities of the downward path were much larger than those suggested by Kitagawa.

7.1.8 Continuing Current

We studied only one continuing current interval which occurred after the last return stroke of the flash reported in Section 5.3. Next we summarize our findings about this continuing current.

The continuing current interval lasted 223 msec in the VHF record. On the basis of the VHF radiation and its source locations, we divided the continuing current in two intervals: (a) continuous VHF radiation, and (b) discrete VHF radiation. The continuous and the discrete VHF radiation lasted 85 and 138 msec, respectively. The VHF noise during the continuous portion of the continuing current interval has the same characteristics as the J-change. The discrete portion has similar characteristics to the VHF radiation at the end of two other CG flashes and all other IC flashes. That is, isolated SP's with durations between 1 and 11.5 msec separated by about 10 msec.

During the initial 23 msec the VHF noise sources formed a 14 km channel parallel to the previous J-changes (Figure 5.59). During the

remainder of the continuous radiation, the VHF sources widened the channel. The SP's in the discrete part of the radiation path propagated downward at speeds between 5×10^6 and 4×10^7 m/sec. The paths of these SP's started from regions between 7 and 14 km and joined the main CG channel that lowered negative charge to ground.

7.2 Intracloud Lightning

Three IC lightning flashes were studied in Sections 5.1.13, 5.5, and 5.6. The beginning of the VHF radiation for the IC flashes has been shown in Figures 5.14, 5.79, and 5.83. In addition, we showed the VHF radiation at the beginning of the IC's in Figure 6.1(e), (f), and (g). The intracloud discharge can be divided in three phases: initial, very active, and junction phase, as done by previous investigators (Kitagawa et al., 1960). Next we provide a discussion of these phases.

7.2.1 Initial Phase

Two of the three flashes started with a pulse about 25 times larger than the stepped leader radiation and a pulse width ranging between 20 and 100 μ sec. The pulse repetition rate during this initial phase was a pulse every 25 to 100 μ sec. This phase was not observed in the IC flash described in Section 5.6.

Correlated electric field records during this phase showed an increasing field change at close range and a decreasing change at distances further away. During the initial phase of the IC flashes, the VHF sources formed the IC channel. The IC in Section 5.1.13 formed a 10 km path 35° off vertical between a height of 6 and 15 km. The IC in Section 5.5 formed a path 40° off vertical between the heights of 9.2 and 14.5 km. Our best estimate of the propagation of

the channel was performed by doing histograms of the number of sources along the channel at different heights for selected time intervals. The histograms for one of these flashes are shown in Figure 5.21. Proctor (1976) also observed this type of behavior at the beginning of a cloud flash. That is, the development of the path was composed of small sections which did not join to form a sequential continuous channel. Four of the five flashes studied by Proctor showed a near-horizontal path. Two of the three IC flashes studied in this thesis showed a path of 45° and 30° off vertical and the third flash had a vertical path. On the basis of the electric field reversal with distance and the fact that most of the sources propagated upward during the initial phase as determined from the histograms, we claim that for the IC flashes in Sections 5.1.13 and 5.5, negative charges propagated upward during the initial phase of the discharge.

7.2.2 Very Active Phase

The very active phase was characterized by a faster pulse repetition rate, a pulse every 5 or 10 μsec superimposed on a lower frequency envelope up to 500 μsec width. During the very active phase the VHF source region becomes wider and additional electric field change occurs.

One of the IC, described in Section 5.6, started with the very active phase. For the first 18.8 msec the VHF noise sources for this discharge were nearly vertical between a height of 8.5 and 13.5 km (Figure 5.84). However, by the end of the very active phase, the noise sources had propagated downward to a height of 4.5 km and widened the previous channel. Since most of the propagation of the noise sources were downwards, we claim that the positive charges were lowered during the IC discharge.

For the studied IC flashes, we attempted to determine the location of the estimated point charge centers and the amount of charge lowered or raised by the discharge. By studying the field reversal with distance and using equation (3.10), we determined that the positive and the negative charge centers for the IC flash described in Section 5.5 were located at 13.5 and 9.5 km, respectively. These locations for the charge centers are in agreement with the VHF source locations but are higher than previous estimates of charge centers above mean sea level during IC's. Malan (1956) studied photographs of discharges in intra-cloud and concluded that the negative charge region (lower region) reaches an altitude of 9.8 km. Mackerras (1968) using photographs and time to thunder estimated that high altitude IC flashes ranged between 4 and 12 km. Takagi (1961) using electric field measurements reported altitudes of IC's between 7 and 11 km. We attempted to determine the charge transferred during the IC discussed in Section 5.1.13 using a set of 9 stations. No calibrated electric field measurements were available in the other two IC's. Curve fitting for 6 of the 9 available stations and using equation (3.10), we obtained a charge transfer of 10.5 ± 2.9 Coul. Three of the four stations beyond the field reversal gave us inconsistent results. Even though our result of charge transfer is more consistent than those obtained using one or two electric field readings, these results indicate that the IC discharge in Section 5.1.13 cannot be adequately represented by a two point charge model.

7.2.3 The Junction Phase

Similar to the end of all the CG flashes, the IC flashes ended with a phase in which only solitary pulses or K-changes were detected. These pulses lasted between 0.5 and 2.2 msec and the pulse rate decreases

toward the end of the discharge, starting with a pulse about every 5 msec and ending with a pulse every 30 or 50 msec. The only correlated electric field change, during this phase, was directly related to the detected K-changes.

The VHF sources of these SP's or K-changes were located in the neighborhood of the previous IC path. These pulses extended the previous ends of the paths widening the volume of the discharge.

CHAPTER VIII

CONCLUDING COMMENTS AND SUGGESTIONS FOR FUTURE RESEARCH

Briefly, this chapter provides a review of the sequence of events described in this work and some needed areas of related research.

(1) We recorded VHF radiation simultaneously from multiple stations on analog tapes during thunderstorms. (2) We randomly selected seven lightning flashes, four cloud-to-ground and three intracLOUDS for study. (3) The analog tapes containing these flashes were digitized. (4) From the difference in the time of arrival of the VHF radiation pulses, we determined the three-dimensional space locations. (5) Then, we correlated the source locations with the characteristics of the VHF noise and VLF electric field to determine some important properties of lightning discharges. Even though our sample size was limited, we obtained quite consistent results. Therefore, our findings can be used to improve the understanding of lightning flashes in general.

With the proper VHF recorded data, an algorithm was developed and applied successfully to obtain VHF source locations. Our results indicate that the VHF sources are directly related to the charge motion in the cloud. We differentiated between the the various phases of lightning flashes and determined their properties. Finally we showed a summary of our findings for the different phases of lightning flashes, providing a view of the initiation and development of lightning flashes inside thunderclouds.

Some suggested areas for future research follow:

(1) The results presented in this thesis would be improved if a 5 MHz tape recording system were used. Since we were limited to a 1.5 MHz upper frequency response, we could not properly detect pulses with a risetime faster than $1/1.5 \text{ MHz} = 0.23 \text{ } \mu\text{sec}$. The detection of faster pulses should lead to additional and more accurate source locations.

(2) All the sequential VHF radiation from lightning flashes for a whole thunderstorm or thunderstorms should be studied. The relationship of the VHF source volumes from flash to flash could provide important information about thunderstorm electricity. The statistical results for individual processes (e.g. J-changes) in a large number of flashes could serve to verify those observations of the individual processes presented in this thesis.

(3) Data on cloud winds and precipitation structure obtained from Doppler radar should be correlated with VHF lightning locations in an effort to improve our understanding of cloud charging mechanisms and their relationship to lightning initiation.

APPENDIX A

DERIVATION OF SOURCE LOCATION FROM DIFFERENCE OF TIME OF ARRIVAL MEASUREMENTS

Let r_o and r_i be the distances from the desired space-location $P(X,Y,Z)$ to the central $Q(0,0,0)$ and remote i 's stations $Q_i(X_i,Y_i,Z_i)$ for $i = 1, 2$, and 3 (Figure A.1). Since the relative elevation of the stations is less than 2 m, and the remote stations are about 10 km from the central station (negligible earth curvature), co-planar stations are assumed. Then

$$u_i = r_o - r_i \quad (A.1)$$

represents the measured range difference, and

$$r_o^2 = (PQ)^2 = X^2 + Y^2 + Z^2 \quad (A.2)$$

$$r_i^2 = (PQ_i)^2 = (X-X_i)^2 + (Y-Y_i)^2 + Z^2 \quad (A.3)$$

represent the square of the distances from the space-location to the ground-based stations. From equation (A.1) we have

$$r_i^2 = r_o^2 - 2r_o u_i + u_i^2 \quad (A.4)$$

Substituting equations (A.2) and (A.3) into (A.4), we get

$$X_i^2 + Y_i^2 - 2XX_i - 2YY_i = -2u_i r_o + u_i^2 \quad (A.5)$$

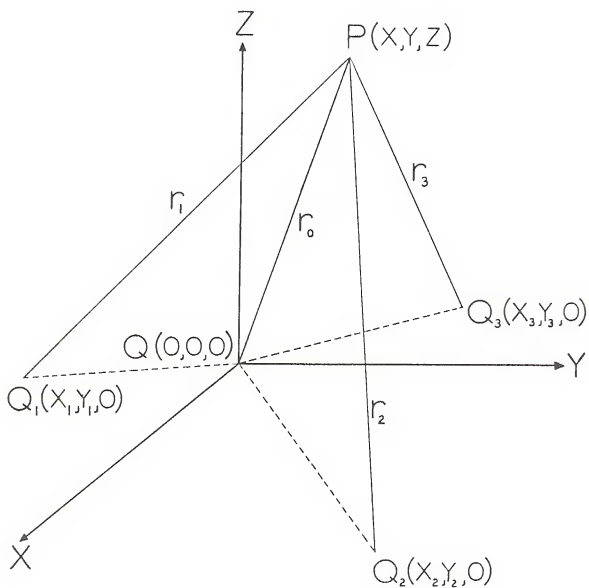


Figure A.1. Three-dimensional hyperbolic system.

Let

$$d_i^2 = X_i^2 + Y_i^2 \quad (\text{A.6})$$

and

$$V_i = \frac{1}{2}(d_i^2 - u_i^2) \quad (\text{A.7})$$

Equation (A.5) becomes

$$XX_i + YY_i - u_i r_o = V_i \quad (\text{A.8})$$

The time difference T_i between a signal arriving at the central and a remote is given by

$$u_i = cT_i \quad (\text{A.9})$$

Since u_i is known from the measurement T_i , equation (A.8) represents three equations with three unknowns (X, Y, r_o) which can be solved for the unknowns. With this solution Z is calculated as

$$Z = \left(r_o^2 - X^2 - Y^2 \right)^{1/2} \quad (\text{A.10})$$

By definition the locus of equation (A.8) represents a hyperbola. The intersection of the three hyperbolas for the three time difference ($i = 1, 2$, and 3) provides a unique source location. Therefore, this method of finding the space-location is called the three dimensional hyperbolic system. Another method of finding space-locations based on a spherical triangulation system is described in Holmes (1951). For the application to our research, the hyperbolic system is used because it provides lower random errors over a wider range of space-locations.

Figure 3.1 indicates the relative location of six remote stations (W1, W2, W3, M1, M2, and M3) and the central station. The position of a calibration signal located on the top of the Kennedy Space Center Vertical Assembly Building is shown as VAB CAL. Analog VHF data are recorded for the central and the six remote stations. Only the central and three of the remote stations are digitized. The factors used in the selection of the three remote stations are: (1) the stations with maximum signal-to-noise ratio , and (2) the stations whose locations provide the maximum accuracy. In our research, the data processed for the summer of 1976 are from the W1, M1, and W3 remote stations which form a T configuration. The 181806 flash on 8th August 1977 was analyzed using the W1, M1, and M3 locations. The remaining flashes studied in this thesis were analyzed using the M1, M2, and M3 stations.

APPENDIX B

ACCURACY OF THE LOCATION OF LIGHTNING SOURCES USING THE HYPERBOLIC EQUATIONS

The errors in source location can be determined from the solution of the hyperbolic equations ((A.7) and (A.8)) previously discussed. Solving equation (A.8) for the source locations, X, Y, and r_o we obtain

$$\begin{aligned} X &= \frac{\begin{vmatrix} V_1 & Y_1 & u_1 \\ V_2 & Y_2 & u_2 \\ V_3 & Y_3 & u_3 \end{vmatrix}}{\begin{vmatrix} X_1 & Y_1 & u_1 \\ X_2 & Y_2 & u_2 \\ X_3 & Y_3 & u_3 \end{vmatrix}} & Y &= \frac{\begin{vmatrix} X_1 & V_1 & u_1 \\ X_2 & V_2 & u_2 \\ X_3 & V_3 & u_3 \end{vmatrix}}{\begin{vmatrix} X_1 & Y_1 & u_1 \\ X_2 & Y_2 & u_2 \\ X_3 & Y_3 & u_3 \end{vmatrix}} & r_o &= \frac{\begin{vmatrix} X_1 & Y_1 & V_1 \\ X_2 & Y_2 & V_2 \\ X_3 & Y_3 & V_3 \end{vmatrix}}{\begin{vmatrix} X_1 & Y_1 & u_1 \\ X_2 & Y_2 & u_2 \\ X_3 & Y_3 & u_3 \end{vmatrix}} \end{aligned} \quad (B.1)$$

or

$$X = \frac{D}{D} \frac{x}{D} \quad Y = \frac{D}{D} \frac{y}{D} \quad r_o = \frac{D}{D} \frac{r}{D} \quad (B.2)$$

Since the coordinates of the three remote stations (X_1, Y_1) , (X_2, Y_2) and (X_3, Y_3) are known to a tenth of a meter, the primary error in X, Y, and Z will be caused by uncertainties in the measurements of u_1 , u_2 , and u_3 . The partial derivatives $\partial X / \partial u_i$, $\partial Y / \partial u_i$, and $\partial r_o / \partial u_i$ can be calculated from equation (B.2). Since $Z = \sqrt{r_o^2 - X^2 - Y^2}$ from equation (A.10) we have that

$$dZ = \frac{1}{Z} \left(r_0 \frac{\partial r_0}{\partial u_1} - X \frac{\partial X}{\partial u_1} - Y \frac{\partial Y}{\partial u_1} \right) \quad (\text{B.3})$$

The X, Y, and Z measurements are a function of the three time delays represented in the u_i 's ($u_i = cT_i$ in equation (A.9)). The u_i 's are independent with RMS error du_i . We define the RMS source location errors as

$$\begin{aligned} dX_{\text{RMS}} &= \sum_{i=1}^3 \left(\frac{\partial X}{\partial u_i} \right)^2 (du_i)^2 \\ dY_{\text{RMS}} &= \sum_{i=1}^3 \left(\frac{\partial Y}{\partial u_i} \right)^2 (du_i)^2 \\ dZ_{\text{RMS}} &= \sum_{i=1}^3 \left(\frac{\partial Z}{\partial u_i} \right)^2 (du_i)^2 \end{aligned} \quad (\text{B.4})$$

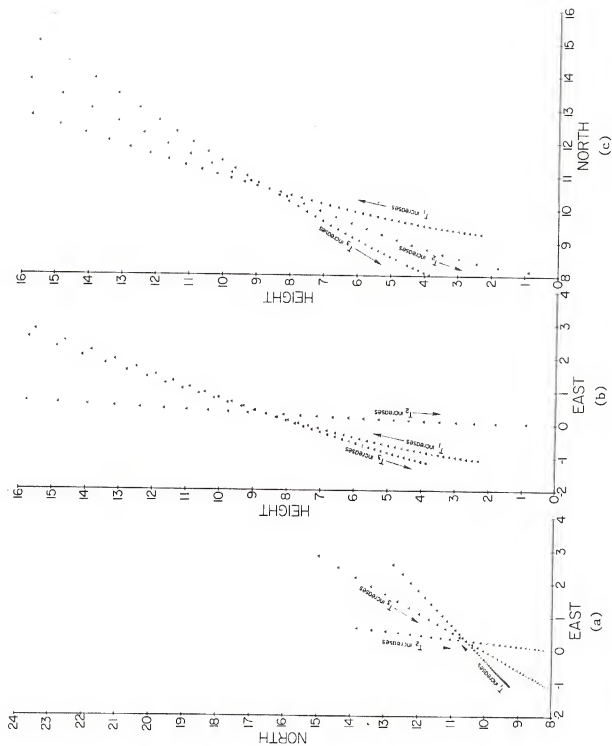
A computer program was developed to determine the error associated with the channel locations. Two classes of errors must be considered: (1) the quantization error, and (2) the calibration error.

The quantization error is due to the discrete sample interval used in digitizing the data. This sample interval limits the measurement of the difference in the time of arrival (DTOA) to 0.23 microseconds ($du_1 = du_2 = du_3$). The raw-data analog tape input had a frequency response between 400 Hz and 1.5 MHz, flat response in the medium range, 3 dB down at the end points, and 20 dB/decade beyond the ends. In order to accurately reproduce this spectrum with sampling, the tapes were digitized at 4.352 MHz, that is, sample intervals of 0.23 microseconds. Hence the original frequency response of the data determines the quantization error.

The RMS quantization error was obtained by using $du_i = cdT_i = 300. * .23 = 68.93$ meters in equation (B.4) and solving for dX_{RMS} , dY_{RMS} , and dZ_{RMS} for any specified DTOA. The relative location of the VHF source with respect to the ground-based station is an important factor in the solution of equation (B.4). The X and Y error increases as we get away from the VHF ground-based network. Since only discrete measurements of time differences are available, we get only discrete locations for X, Y, and Z. These locations are generally within 100 meters for X, and 500 meters for Y and Z for the VHF sources studied in this thesis. The Z error measurement increases for VHF locations near the ground and for Z larger than 10 km. Figure B.1 shows the source locations of every sample, corresponding to variations along T_1 , T_2 , and T_3 . This graph illustrates the effect of the quantization error in any of the three DTOA. Figure D.2 shows a mapping of all the 55,171 three dimensional locations obtained within the range of the graph axis for 50 iterations of T_1 , T_2 , and T_3 every sampling interval (.230 μ sec). The remaining 69,829 locations of the possible 125,000 fell outside the boundaries of the graph. Figure B.2 also shows the discrete pattern of the locations of the hyperbolic equations which is obtained for the discrete sample intervals. Figure B.3 shows a mapping of 49,581 three-dimensional locations obtained within the range of the graph axis for 50 iterations of T_1 , T_2 , and T_3 taken every 0.1 μ sec. Since the quantization error is smaller, the pattern in Figure B.3 is less evident.

In addition to the uncertainties produced by the quantization error, the calibration error must be considered. The calibration error is determined by the uncertainties in the retransmission delay, the

Figure B.1. Two-dimensional views: (a) top view, EW-NS, (b) elevation view, EW-height, and (c) elevation view, NS-height of the noise sources obtained when only one of the time delays (T_1 , T_2 , or T_3) is varied in discrete sample intervals of $0.23 \mu\text{sec}$.



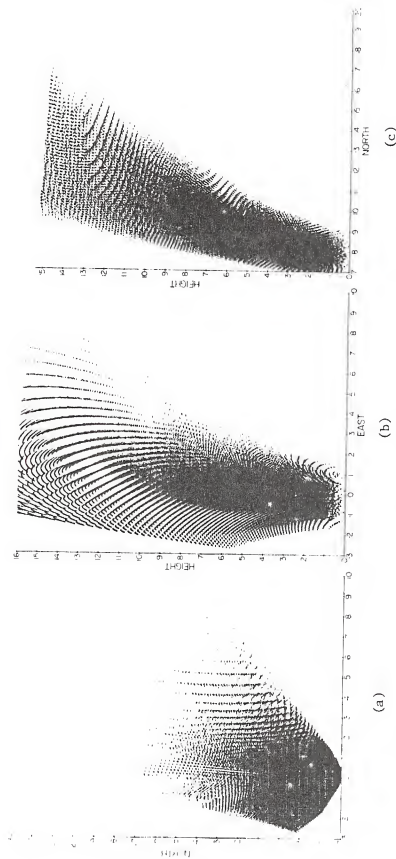
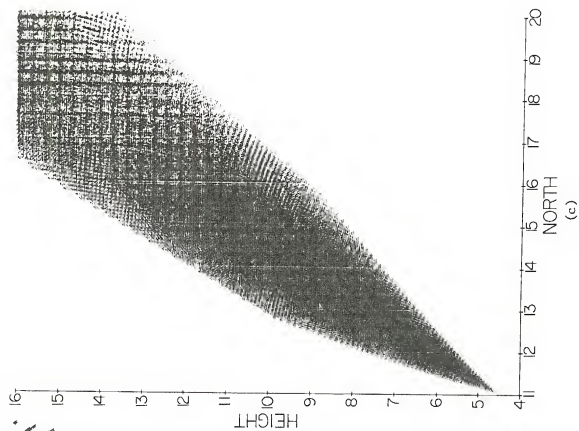
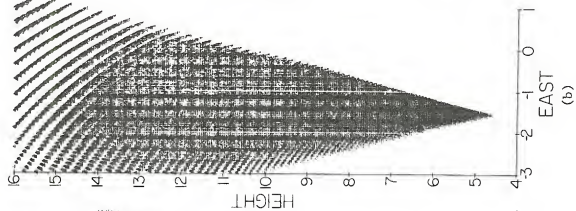
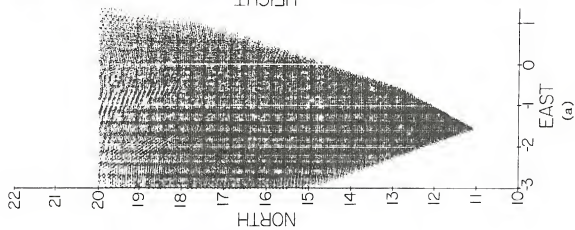


Figure B.2. Two-dimensional views: (a) top view, EW-NS, (b) elevation view, EW-height, and (c) elevation view, NS-height of all noise sources in 50 consecutive iterations of the three time delays for a sample interval of 0.23 μ sec.

Figure B.3. Two-dimensional views: (a) top view, EW-NS, (b) elevation view, EW-height, and (c) elevation view, NS-height for all the noise sources in 50 consecutive iterations of the three time delays for a sample interval of 0.1 μ sec.



electronics, the tape recorder, and reproducer head configurations. Since all the VHF signals were recorded at the central station, we had to subtract the retransmission and other time delays between each one of the remote and the central station. The retransmission and other delays were determined using a calibration signal at a known location (VAB CAL, in Figure 4.1). For each year ten readings of the calibration signal recorded at all the stations were digitized at 8 MHz. Since the location of the calibration signal is known, the average value of these readings is used to determine the average retransmission delays. The RMS error in the measurement of the DTOA for the calibration signal varied between .19 and .62 μsec for the various remote stations. The calibration error can now be determined by using equation (B.4) for the uncertainties in the calibration of the remote stations. Once three of the remote stations in Figure 4.1 are selected, the retransmission delays for these are calculated. The average value of the retransmission delay is fixed for all the calculations relating to any specific flash. However since the error in X, Y, and Z is also a function of the location of the VHF source relative to the location of the ground-based network, the calibration error also varies with the selection of the remote stations and the lightning locations.

The total error related to any calculation of channel location (σ_{tRMS}) is calculated from

$$\sigma_{\text{tRMS}}^2 = \sigma_{\text{QRMS}}^2 + \sigma_{\text{cRMS}}^2 \quad (\text{B.5})$$

The quantized error (σ_{QRMS}) is the random error in the measurement, while the calibration error (σ_{cRMS}) represents any additional time

delay error. Next we present a solution for σ_{QRMS} , σ_{CRMS} , and σ_{TRMS} for the four main flashes studied in this thesis.

B.1. Error Analysis for the Locations of the 165959 Flash on 19th July 1976

The remote stations selected to determine channel locations were W1, M1, and W3 (Figure 4.1). The RMS uncertainties in the calibration error for W1, M1, and W3 were .62, .25, and .41 microseconds. The flash extended between -2 and 6 km EW, 9 and 16 km NS and up to 16 km in altitude. Table B.1 shows the quantization, calibration, and total error for the three-dimensional channel locations over the entire range of the flash.

B.2. Error Analysis for the Locations of the 181806 Flash on 8th August 1977

The remote stations selected to determine channel locations were W1, M1, and M3 (Figure 4.1). The RMS uncertainties in the calibration error for W1, M1, and M3 were .56, .19, and .57 microseconds. The flash extended between -3 and 9 km EW, 7 and 17 km NS and up to 15.5 km of altitude. Table B.2 shows the quantized, calibration, and total error for the three-dimensional VHF sources over the entire range of the flash.

B.3. Error Analysis for the 180710 and 182357 Flashes on 8th August 1977

The remote stations selected to determine channel locations were M1, M2, and M3. The RMS uncertainties in the calibration error for M1, M2, and M3 were .19, .38, and .57 microseconds. The 180710 flash developed in the NE of the central station, 3 to 7 km EW, 8 to 15 km NS, and up to 10 km of altitude. The 182357 flash developed in the NW of the central station, -8 to 1 km EW, 5 to 14 km NS, and up to 13 km of altitude.

Table B.1. Error Analysis for the I65959 Flash. The selected locations cover the entire volume of the flash and they are listed in ascending order in z .

Source Locations (Meters)			Quantization RMS Error (Meters)			Calibration RMS Error (Meters)			Total RMS Error (Meters)		
x	y	z	dx_Q	dy_Q	dz_Q	dx_c	dy_c	dz_c	dx_t	dy_t	dz_t
-307.1	11634.5	1870.9	19.3	260.1	548.9	29.3	419.4	1372.9	35.1	493.5	1478.6
-983.8	10519.8	2761.4	29.7	232.3	304.5	39.4	371.4	750.7	49.3	438.1	810.1
-731.5	10867.9	3771.2	26.1	254.6	274.4	36.9	408.5	676.3	45.2	481.3	729.8
3357.0	15518.8	3713.6	108.4	565.4	778.1	158.5	913.9	1576.7	192.0	1074.6	1758.2
-1332.5	11156.8	3888.6	37.2	264.0	268.0	50.7	423.7	640.8	62.9	499.2	694.5
1506.5	9634.2	5140.2	33.6	301.5	186.4	63.2	485.4	392.8	71.5	571.4	434.8
1126.6	10827.5	5401.8	25.5	327.7	215.3	53.7	528.1	470.8	59.5	621.5	517.7
1724.8	9376.4	5746.8	40.6	310.8	183.0	73.4	501.2	350.6	83.9	589.8	395.4
1468.5	9366.2	6317.3	35.4	313.7	176.9	68.8	506.6	330.2	77.4	595.9	374.6
300.0	11423.7	6739.2	17.0	354.7	213.4	45.0	572.4	447.6	48.1	673.4	495.9
2377.5	13241.3	6887.3	64.2	374.5	239.6	105.1	604.2	392.3	123.1	710.9	459.6
2072.1	10037.2	7577.8	56.2	372.4	228.9	97.2	601.8	336.1	112.3	707.7	431.8
2579.6	10345.1	7876.6	74.3	402.7	265.1	120.6	650.3	397.5	141.7	764.9	477.8
2745.3	10549.0	8653.0	83.3	429.9	293.7	134.3	694.5	420.8	158.0	816.8	513.2
-388.0	13914.4	9718.0	28.7	506.1	303.7	61.7	816.7	559.4	68.1	960.8	636.5
2794.5	11026.8	9895.7	90.4	473.8	337.0	147.3	765.6	470.3	172.8	900.4	578.6
3556.3	11882.5	10888.6	128.3	555.4	434.7	199.4	895.3	583.6	237.1	1053.6	727.7
2747.6	11346.4	11090.6	93.7	510.6	378.0	155.4	825.5	522.5	181.5	970.7	644.9
4307.1	12031.1	11178.4	166.8	599.2	513.4	250.8	984.3	668.3	301.2	1135.4	842.7
3013.8	12092.1	11384.7	107.2	555.6	416.8	173.6	896.5	574.2	204.1	1054.7	709.5
5342.8	13130.3	12431.3	236.7	727.2	694.3	348.3	1165.9	892.8	421.1	1374.1	1131.0
4322.8	13244.3	12549.4	188.9	693.8	604.9	285.4	1114.4	796.0	342.3	1312.7	999.8
6635.1	14013.6	13834.6	342.8	881.8	963.7	496.8	1408.3	1236.5	603.6	1161.6	1567.6
7038.8	15385.6	14319.8	381.3	995.0	1074.6	552.5	1585.3	1383.1	671.3	1871.7	1751.5
5749.6	14127.0	14535.1	278.1	845.7	847.0	413.0	1353.7	1109.3	497.9	1596.1	1395.7
6333.9	14774.4	14947.8	325.1	925.0	962.5	478.7	1477.4	1257.3	578.6	1743.1	1583.4
8061.2	14805.4	15752.0	474.8	1060.7	1315.5	685.6	1639.8	1712.3	834.0	1993.4	2159.3
7787.8	13594.7	15923.4	455.1	1093.4	1281.2	660.5	1677.4	1671.0	802.1	2054.5	2105.6
7474.5	10358.0	15343.6	429.2	1107.7	1215.8	623.4	1761.8	1577.7	756.9	2081.1	1991.8
Average error for locations in this flash.			150	558	535	227	900	813	354	1058	973

Table B.2. Error Analysis for the Locations in the 181806 Flash. The locations are arranged in ascending order in z .

Source Locations (Meters)			Quantization RMS Error (Meters)			Calibration RMS Errors (Meters)			Total RMS Error (Meters)		
x	y	z	dx_Q	dy_Q	dz_Q	dx_c	dy_c	dz_c	dx_t	dy_t	dz_t
-1172	8841	633	50	326	3004	106	710	7302	118	781	7896
-2176	8293	1865	57	276	1887	105	593	3649	120	654	4108
-656	8937	2966	56	432	747	133	936	1804	144	1031	1953
-1093	9191	3287	58	407	648	127	881	1565	140	971	1694
-598	9231	3646	60	473	657	143	1024	1577	155	1128	1708
-458	9295	4510	64	515	526	156	1112	1244	169	1226	1351
-710	9372	4915	65	505	461	153	1089	1085	166	1201	1179
-202	8695	5373	69	530	355	170	1136	801	184	1253	876
-372	9096	5789	70	550	357	171	1181	798	185	1303	875
260	11410	6464	97	846	662	236	1841	1473	256	2026	1615
-50	9320	7033	83	636	309	204	1363	594	221	1504	670
-257	9708	7484	83	657	312	204	1411	591	220	1557	669
819	12050	7763	133	1058	650	311	2298	1292	338	2530	1447
1177	12137	7887	160	1161	702	360	2523	1334	394	2778	1507
48	9704	8237	94	712	302	231	1527	467	250	1685	556
-1235	10545	8682	88	660	285	200	1416	509	218	1562	584
-905	9527	9379	89	665	271	210	1418	391	229	1567	476
1186	10560	9777	162	981	439	370	2106	455	404	2323	633
3959	10526	9953	561	1678	1171	1089	3607	1228	1225	3978	1697
4331	10855	10521	657	1888	1392	1271	4061	1566	1431	4479	2095
1522	11030	10634	195	1107	526	438	2377	537	480	2622	752
4013	10944	10639	570	1757	1221	1117	3779	1347	1254	4167	1819
1313	10634	12385	191	1069	601	443	2285	837	482	2523	1031
5478	11529	12658	923	2280	2069	1805	4895	2989	2029	5600	3636
5547	11793	13152	932	2321	2120	1832	4983	3129	2056	5497	3780
2796	10055	13355	329	1202	914	737	2563	1463	785	2831	1725
2671	12294	13663	341	1530	959	737	3282	1330	812	3621	1640
6318	12710	14364	1152	2717	2719	2281	5830	4326	2555	6432	5110
Average error for loca- tions in this flash.			264	1033	938	547	2222	1632	608	2451	1882

Tables B.3 and B.4 show the quantized, calibration, and total error for the three-dimensional VHF source locations over the entire range of these flashes.

Table B.3. Error Analysis for the Locations in the 181807 Flash. The locations are arranged in ascending order in z .

Source Locations (Meters)			Quantization RMS Error (Meters)			Calibration RMS Errors (Meters)			Total RMS Error (Meters)		
x	y	z	dx _Q	dy _Q	dz _Q	dx _c	dy _c	dz _c	dx _T	dy _T	dz _T
5612	8301	705	101	97	3856	167	200	5387	196	223	6625
5569	8211	1055	98	97	2444	162	198	3455	189	221	4232
7027	14997	1387	225	264	5759	345	328	7888	412	421	9767
5458	8310	2308	92	100	1050	153	195	1537	179	219	1862
6761	14847	2411	208	257	3557	324	320	4924	385	411	6075
5969	9263	3555	103	113	885	173	198	1287	201	228	1563
5633	13719	4048	147	216	1544	240	275	2232	282	350	2714
5982	9486	4369	101	119	737	171	200	1093	199	233	1318
5950	12421	4715	133	178	1127	221	244	1633	258	302	1984
5364	9413	5190	90	123	549	152	203	852	177	237	1014
4038	8864	5226	77	118	393	120	203	661	143	235	769
5358	11929	5865	109	172	754	184	239	1146	214	295	1372
4254	10151	5956	83	139	469	134	216	766	158	257	898
3740	9418	6031	77	130	376	117	211	641	141	247	743
4967	10296	6047	90	141	526	151	216	833	176	258	986
5095	8528	6555	82	119	369	134	198	611	157	231	714
4531	10595	6653	87	150	481	143	223	781	168	269	917
4600	10781	7055	88	155	477	145	227	776	170	275	911
5752	11742	7693	107	178	599	184	246	937	213	303	1112
6333	10613	8390	105	161	515	185	231	817	213	282	966
5074	13639	9003	107	236	629	184	302	1012	213	383	1192
3631	10146	10469	85	165	344	121	238	598	148	290	690
Average error for loca- tions in this flash.			109	156	1247	178	232	1812	209	280	2201

Table B.4. Error Analysis for the Locations in the 182357 Flash. The locations are arranged in ascending order in z.

Source Locations (Meters)			Quantization RMS Error (Meters)			Calibration RMS Errors (Meters)			Total RMS Error (Meters)		
x	y	z	dx _Q	dy _Q	dz _Q	dx _c	dy _c	dz _c	dx _t	dy _t	dz _t
-487	5915	2219	63	99	267	62	192	630	89	216	685
-3655	12638	3332	124	239	821	144	292	1753	191	378	1936
-3940	5458	4421	76	115	243	85	206	525	114	236	579
-2933	13562	4738	123	261	667	137	310	1387	184	406	1339
-3342	12171	5050	120	225	532	133	283	1127	179	362	1247
-2986	11851	5080	112	214	493	122	275	1044	166	348	1155
-5975	9194	5144	135	187	507	180	257	1067	225	318	1182
-4718	7742	5808	106	151	326	127	233	687	166	278	761
-935	10823	6672	90	178	330	86	249	673	124	307	750
-3831	11237	6964	126	212	408	141	275	849	189	348	942
-4560	8509	7199	116	166	323	136	244	667	179	295	741
-4415	11189	7414	136	218	422	159	281	870	210	356	967
-1256	11053	7701	97	189	328	91	257	660	134	320	737
-5393	9276	7862	139	189	387	172	261	785	221	322	876
-2819	12412	8432	125	237	409	130	296	824	181	380	920
-7855	9353	8880	197	221	560	279	288	1097	342	363	1232
-5511	7582	9210	136	165	342	169	247	668	217	297	750
-2262	12857	9546	124	249	410	124	308	807	176	397	906
-137	12522	9764	99	226	379	91	289	719	135	367	813
-3225	13322	10309	146	275	451	155	333	884	213	432	993
-9196	10455	11336	261	271	701	376	336	1332	458	432	1505
582	14293	12192	105	288	467	98	354	850	144	457	970
Average error for loca- tions in this flash.			125	208	444	145	276	905	193	346	1008

APPENDIX C

COMPUTER ALGORITHM TO DETERMINE VHF SOURCE LOCATIONS FROM THE DIFFERENCE IN THE TIME OF ARRIVAL OF VHF RADIATION DATA

In this appendix we give the Fortran computer program code used to determine the three dimensional source locations based on the measured difference in the time of arrival of VHF radiation. The input of the program is a digital tape with four VHF series digitized at 4.352 MHz. There are two types of outputs: (1) a printout of all the three dimensional source locations and their relative time of occurrence, and (2) a digital tape where the same printout information is stored for future access. This appendix also contains on page 355 an example of a computer printout of the output. This output consists of the source location for successive 376 μ sec cross-correlated time intervals and the relative time and location of each one of the individual sources.

DEFINITION OF VARIABLES USED IN THE COMPUTER ALGORITHM DESCRIBED IN THIS APPENDIX:

- LCHAN - Digital tape channel number (0, 1, 2, 3)
- LREC - Six bit byte of data read from seven track digital tape
- LINT - Value of the VHF radiation reconstructed from the bytes
- X6, X7, X8, X9 - Value of the VHF radiation for the central and the three remote stations, respectively
- X1ME, X2ME, X3ME, X4ME - Average value of the VHF radiation in the selected data window for the central and the three remote stations
- TI11, TI21, TI31, TI41 - Value of the VHF radiation for the channels (without a mean value)
- LHOUR, LSEC, LMIN, LMIL - Converting time code value on digital tape to hour, minute, second, and millisecond
- TIL2S, TIL3S, TIL4S - Normalization factor for VHF radiation of remote stations versus central station
- X1, X2, X3, X4 - Subsections of the value of the VHF radiation for the central and the three remote stations
- AVEMO - Moving average of the VHF radiation in the central station
- AVEMO2 - Moving average of the VHF radiation for the remote station
- AVE - Average value of a section of the VHF data
- LAG1, LAG2, LAG3 - Amount of samples needed to maximize the cross-correlation function
- DELTA1, DELTA2, DELTA3 - Time corresponding to the cross-correlation intervals
- X, Y, Z - Three-dimensional locations
- MABLMA - Sample value for local maximum for the central station
- MX2GEN - Estimation of the cross-correlation value for local maximum
- SLPR2 - Slope to the right of local maximum
- SLPL2 - Slope to the left of local maximum
- NDSLRI - Number of reversals on descending slopes to the right of local maximum
- NDSLLE - Number of reversals on descending slopes to the left of local maximum

NGOOD - Degree of acceptance of pattern recognition

DELIUB - Upper bound of the time lag between one remote and the central station

DELLB - Lower bound of the time lag between one remote and the central station

21 JUNE 1979

```

C *****
C * THIS ALGORITHM DETERMINES THE THREE-DIMENSIONAL LOCATIONS *
C * OF VHF NOISE SOURCES DURING A LIGHTNING FLASH. THE PRO- *
C * GRAM IS BASED ON DETERMINING THE DIFFERENCE IN THE TIME *
C * OF ARRIVAL (DOA) OF FOUR TIME SERIES VHF RADIATION DATA. *
C * THE DOA IS DETERMINED BY USING PATTERN RECOGNITION AND *
C * THE CROSS-CORRELATION FUNCTION. *
C *****
C
C DIMENSION LCHAN(1670),LREC(2,1670),X6(8610),X7(8610),
C * X8(8610),AVE(128),ORDLMA(128),MABLMA(128),AVEMQ(2048),
C * AVEMQ2(2048),MX2GEN(128),MABLM2(128),NUMDER(128),
C * NRROWE(128),NRROW2(128)
C DIMENSION SLPR(128),SLPR2(128),SLPL(128),SLPL2(128),
C * NUMDL(128),NUMDL2(128),NGOOD(5),MGOOD(5),DLTA1(128),
C * DLTA2(128),DLTA3(128),X(128),Y(128),Z(128),NOIFBB(5),
C * MABSCI(10),LI(10),NDSLR(10),NDSLLE(10),PENDRI(10),
C * PENDLE(10),X9(8610),NSTDEV(10),MABSCI(128),TIME(128),
C * NIN(128),NUMDR2(128),LINT(1670)
C LOGICAL*1 LCHAN
C INTEGER*2 LREC
C COMMON KK,N,MP,NP,NNN(128),MMM(128),X1(2048),X2(2048)
10 FORMAT(75(75A1))
C ZERO=0.
C WRITE(6,700)
700 FORMAT(1H1)
C WRITE(6,722)
722 FORMAT(33X,32HSTORM ACTIVITY ON 19TH JULY 1976, //21X,
C * 60HSTART TIME = 16 HOURS 59 MINUTES 59 SECONDS
C * 008 MILLISECONDS, //20X, 61HFINISH TIME = 17 HOURS
C * 00 MINUTES 01 SECONDS 009 MILLISECONDS)
C
C ** SKIP THE CALIBRATION BLOCK **
C
C READ(11,10)((LCHAN(I),(LREC(J,I),J=1,2)),I=1,100)
C
C ** SKIP A PRE-DETERMINED TIME CORRESPONDING TO THE NOISE **
C ** LEVEL BEFORE THE SIGNAL IS DETECTED. **
C
C DO 12 LK=1,310
C READ(11,10)
12
C
C ** PROCESS THE NEXT 500 BLOCKS OF DATA. A BLOCK HAS 410 **
C ** DATA POINTS OF EACH OF THE FOUR SERIES. **
C
C DO 520 IIM=1,25
C DO 20 K=1,21
C READ(11,10)((LCHAN(I),(LREC(J,I),J=1,2)),I=1,1670)
C
C ** CONVERT THE DATA ON THE TAPE FROM **
C ** PDP-COMPUTER FORMAT TO IIM FORMAT. **
C
C DO 18 I=1,1670
C DO 16 J=1,2
16 LREC(J,I)=(LREC(J,I)-64)/256
18 LINT(I)=LREC(1,I)*64 + LREC(2,I)
C IF(K.EC.1) GO TO 805
C GO TO 802
C
C ** THE FOLLOWING INFORMATION IS NEEDED TO DETERMINE **
C ** THE ABSOLUTE UNIVERSAL TIME. **
805 LSAVE1=LINT(1641)

```

21 JUNE 1979

```

      LSAVE2=LCHAN(1641)
      MSAVE1=LINT(1642)
      MSAVE2=LCHAN(1642)
802  DO 20 L=1,410
C
C  **  SEPARATING THE FOUR TIME SERIES  **
C
      X6(410*(K-1)+L)=LINT(4*L-3)
      X7(410*(K-1)+L)=LINT(4*L-2)
      X8(410*(K-1)+L)=LINT(4*L-1)
20   X9(410*(K-1)+L)=LINT(4*L)
C
C  **  SUBTRACTING THE MEAN OF THE SERIES  **
C
      XN1=0.0
      XN2=0.0
      XN3=0.0
      XN4=0.0
      TIL1L=BIG(X6,8610)
      TIL2L=BIG(X7,8610)
      TIL3L=BIG(X8,8610)
      TIL4L=BIG(X9,8610)
      DO 22 I=1,8610
      XN1=XN1+X6(I)
      XN2=XN2+X7(I)
      XN3=XN3+X8(I)
22   XN4=XN4+X9(I)
      X1ME=XN1/8610.
      X2ME=XN2/8610.
      X3ME=XN3/8610.
      X4ME=XN4/8610.
      TIL1L=TIL1L-X1ME
      TIL2L=TIL2L-X2ME
      TIL3L=TIL3L-X3ME
      TIL4L=TIL4L-X4ME
C
C  **  DO NOT PROCESS THE DATA IF THE SIGNAL IS WITHIN  **
C  **  THE NOISE LEVEL(100.)  **
C
      IF((TIL1L.LE.100.).OR.(TIL2L.LE.100.).OR.(TIL3L.LE.100.).
* OR.(TIL4L.LE.100.))GO TO 520
      DO 26 J=1,8610
      X6(J)=X6(J)-X1ME
      X7(J)=X7(J)-X2ME
      X8(J)=X8(J)-X3ME
26   X9(J)=X9(J)-X4ME
C
C  **  COMPUTE THE ACTUAL TIME OF DIGITIZATION  **
C
      LSEC=LSAVE1+4096*LSAVE2
      LMIL=MSAVE1+4096*MSAVE2
      LHOURL=LSFC/3600
      LMIN=LSEC/60-LHOURL*60
      LSECR=LSEC-LHOURL*3600-LMIN*60
C
      DO 591 MN=1,14
591  WRITE(6,586)
586  FORMAT(1H0)
      WRITE(6,587) LHOURL,LMIN,LSECR,LMIL
587  FORMAT(1H0,20X,18HDIGITIZATION TIME=,I4,1X,5HHOURS,5X,
* 14,1X,7HMINUTES,5X,14,1X,7HSECONDS,5X,14,1X,
* 12HMILLISECONDS)
      WRITE(6,588) LHOURL,LMIN,LSECR,LMIL
588  FORMAT(11X,18HDIGITIZATION TIME=,I4,1X,5HHOURS,15,
* 1X,7HMINUTES,14,1X,7HSECONDS,14,1X,11HMILLISECONDS)

```

21 JUNE 1979

```

C ** CONVERT TO THE ABSOLUTE TIME **
C
  LHCUR=16
  MINU=59
  LSECD=59
  LMIL=LMIL+1000
  LSEC=LSEC-1
  LSECD1=LSEC-13584
  LMILD1=LMIL-984
  SECD1=LSECD1
  RMILD1=LMILD1
  SECD=SECD1/32.
  RMILD1=RMILD1/32.
  LSECD=SECD
  RMILD=(SECD-FLDGT(LSECD))*1000. + RMILD1
  MILD=RMILD
  RMICRO=(RMILD-FLDGT(MILD))*1000.
  MICROT=RMICRO
  MILST=8+MILD
  IF((MILST.GE.1000).AND.(LSECD.GT.0))GO TO 592
  LSECD=59 +LSECD
  IF(LSECD.GT.59) GO TO 592
  GO TO 593
592 LSECD=C
  MINU=0
  LHCUR=17
  MILST=MILST-1000
593 DO 599 MN=1,6
599 WRITE(6,506) LHCUR,MINU,LSECD,MILST,MICROT
862 FORMAT(12X,'UNIVERSAL TIME =',I3,'HOURS',I3,'MINUTES',
* 2X,I3,1X,'SECONDS',I4,1X,'MILLISECONDS',I4,1X,
* 'MICROSECONDS')
594 FORMAT('UNIVERSAL TIME =',I3,'HOURS',I3,'MINUTES',
* 2X,I3,1X,'SECONDS',I4,1X,'MILLISECONDS',I4,1X,
* 'MICROSECONDS')
  WRITE(8,594) LHCUR,MINU,LSECD,MILST,MICROT
C
C ** NORMALIZING THE FOUR TIME SERIES TO THE CENTRAL **
C ** STATION THRESHOLD LEVEL **
C
  TIL12D=TIL1L-TIL2L
  IF(TIL12D.EQ.0.0)GO TO 521
  TIL2S=TIL1L/TIL2L
  DO 517 J=1,8610
517 X7(J)=TIL2S*X7(J)
521 TIL13D=TIL1L-TIL3L
  IF(TIL13D.EQ.0.0)GO TO 523
  TIL3S=TIL1L/TIL3L
  DO 519 J=1,8610
519 X8(J)=TIL3S*X8(J)
523 TIL14D=TIL1L-TIL4L
  IF(TIL14D.EQ.0.0)GO TO 528
  TIL4S=TIL1L/TIL4L
  DO 526 J=1,8610
526 X9(J)=TIL4S*X9(J)
C
C ** INITIALIZATION **
C
528 KK=512
  N=2048
  MM=16
  TIME1=0.0
  JJ=128
  J1=0

```

21 JUNE 1979

```

500 MKN=0
    WRITE(6,531)
531 FORMAT(1H1,17X,5HDELAY,5X,24HMAXIMUM CROSSCORRELATION,
* 5X,13HTIME INTERVAL)
    DO 501 K=1,2048
501 X1(K)=X6(2048*J1-448*J1+K)
C
C ** CALCULATE ONE AVERAGE POINT PER SUBSET **
C
    DO 1 J=1,JJ
    XS=0.0
    DO 3 JK=1,MM
    XS=XS+X1((J-1)*MM+JK)
    3 AVE(J)=XS/FLCAT(MM)
C
C ** CALCULATE MOVING AVERAGE OF THE SET **
C
    XI=0.0
    DO 5 I=1,MM
    5 XI=XI+X1(I)
    AVEMO(1)=XI/FLOAT(MM)
    KL=MM+1
    DO 9 I=KL,2047
    XI=XI+X1(I)-X1(I-MM)
    9 AVEMO(I-15)=XI/FLOAT(MM)
    113 FCRMAT(3F10.2)
    CALL RMEAN(AVEMO,2032,0.0)
C
C ** CALCULATE THE STANDARD DEVIATION OF THE DATA IN THE SET **
C ** BY USING A FUNCTION SUBPROGRAM STDSET, THE THRESHOLD **
C ** LEVEL BY FUNCTION SUBPROGRAM DIV4SM, AND THE STANDARD **
C ** DEVIATION OF THE SUBSET BY FUNCTION SUBPROGRAM STDSD. **
C
    CALL LCCMAX(MABLMA,MM,JJ,AVE,SLPR,SLPL,NUMBER,
* NUMDEL,NRROWE)
C
C ** LCCMAX IS THE SUBROUTINE THAT CALCULATES LOCAL MAXIMUM **
C ** IN THE DATA **
C
    97 FCRMAT(I10,3F10.2,3I10)
C
C ** THE DATA IS RE-FORMATTED TO BE ABLE TO PROCESS THE DATA **
C ** NEAR THE END OF THE SET **
C
    DO 502 K=1,2048
502 X2(K)=X7(2048*J1-448*J1+K)
C
C ** MKN IS THE COUNTER FOR THE NUMBER OF STATIONS **
C
    17 MKN=MKN+1
C
C ** GETTING THE AVERAGE AND THE MOVING AVERAGE FOR **
C ** THE REMOTE STATIONS **
C
    DO 11 J=1,JJ
    XS=0.0
    DO 13 I=1,MM
    13 XS=XS+X2((J-1)*MM+I)
    11 AVE(J)=XS/FLCAT(MM)
C
    XI=0.0
    DO 15 I=1,MM
    15 XI=XI+X2(I)
    AVEMO2(1)=XI/FLOAT(MM)
    DO 19 I=KL,2047

```

21 JUNE 1979

```

19      XI=XI+X2(I)-X2(I-MM)
        AVEMO2(I-15)=XI/FLOAT(MM)
        CALL RMEAN(AVEMO2,2032,0.0)
C
C **   LAG IS THE SUBPROGRAM THAT CALCULATES THE TIME DELAY **
C **   TO PEAK THE CROSS-CORRELATION FUNCTION. **
C
        LAGL=LAG(AVEMO,AVEMO2,MKN)
        IF(LAGL.LE.5)GO TO 585
        IF(MKN.EQ.1) LAG1=LAGL
        IF(MKN.EQ.2) LAG2=LAGL
        IF(MKN.EQ.3) GO TO 529
        GO TO 530
529     LAG3=LAGL
        DELTA1(1)=.22978*FLOAT(LAG1)
        DELTA2(1)=.22978*FLOAT(LAG2)
        DELTA3(1)=.22978*FLOAT(LAG3)
        NIN(1)=1
C
C **   HYPERM IS THE SUBROUTINE THAT FINDS THE LOCATION **
C **   BASED ON THE DTOA. IN THIS CALL ONLY THE LOCATION **
C **   THAT CORRESPONDS TO THE CROSS-CORRELATION VALUES **
C **   IS FOUND **
C
        WRITE(6,580)
580     FORMAT(1H0,10X,11HX IN METERS,10X,11HY IN METERS,
* 10X,11HZ IN METERS)
        WRITE(6,581) X(1),Y(1),Z(1)
581     FORMAT(3F20.3)
        WRITE(8,724)
724     FORMAT(10X,11HX IN METERS,10X,11HY IN METERS,
* 10X,11HZ IN METERS)
C
C **   IF THE SIGNAL LEVEL IS LOW AND BAD CORRELATION RESULTS, **
C **   THE DATA IS ELIMINATED. **
C
        IF((Z(1).LE.0.).OR.((ABS(X(1))).GE.40000.).OR.
* ((ABS(Y(1))).GE.40000.).OR.(Z(1).GE.16000.))GO TO 585
        IF((LAG1.LE.5).OR.(LAG2.LE.5).OR.
* (LAG3.LE.5)) GO TO 585
C
        WRITE(8,702) X(1),Y(1),Z(1),ZERO
702     FORMAT(4F20.3)
530     CALL LOCMA2(MABLM2,MM,JJ,AVE,SLPR2,SLPL2,NUMDR2,NUMDL2,
* NRROW2)
C
C **   THE PROPERTIES OF THE LARGEST PULSE WITHIN THE **
C **   SUBSET IS STUDIED **
C
        DO 73 K=1,MP
        IF(K.GE.2) MDIFTE=NDIFTE
C
C **   MABLMA IS THE ABSCISSA OF THE LOCAL MAXIMUM IN THE **
C **   CENTRAL, MX2GEN IS THE ABSCISSA OF THE LOCAL MAX- **
C **   IMUM FOR THE REMOTE STATIONS **
C
        MX2GEN(K)=MABLMA(NNN(K))+LAGL
        IF(MX2GEN(K).GT.(N+15)) GO TO 73
        NCOUNT=0
        DO 70 J=1,NP
        IF(ABS(MX2GEN(K)-MABLM2(MMM(J))).LE.(16))GO TO 160
        GO TO 70
160     NCOUNT=NCOUNT+1
        MABSCI(NCOUNT)=MMM(J)
        L1(NCOUNT)=MABLM2(MMM(J))

```

21 JUNE 1979

```

C ** NDSLRI, NOSLLE, PENDRI, PENDLE, AND NSTDEV ARE THE FIVE **
C ** PULSE PROPERTIES BEING USED FOR PATTERN RECOGNITION. **
C ** THEY CORRESPOND TO THE NUMBER OF DESCENDING PATTERN TO **
C ** THE RIGHT AND TO THE LEFT OF THE PULSE, THE SLOPES TO **
C ** THE RIGHT AND TO THE LEFT OF THE LOCAL MAXIMUM, AND **
C ** THE NARROWNESS OF THE PULSE. **
C
  NDSLRI(NCOUNT)=NUMDR2(MMM(J))
  NOSLLE(NCOUNT)=NUMDL2(MMM(J))
  PENDRI(NCOUNT)=SLPR2(MMM(J))
  PENDLE(NCOUNT)=SLPL2(MMM(J))
  NSTDEV(NCOUNT)=NRRW2(MMM(J))
70  CONTINUE
  IF(NCOUNT.EQ.0)GO TO 73
  DO 75 J=1,NCOUNT
    LPASS=0
    JPASS=0
    NPASS=0
    IPASS=0
    KPASS=0
C
C ** MATCHING CHARACTERISTICS FOR THE FIVE GIVEN PROPERTIES **
C
    IF(IABS(NUMDER(NNN(K))-NDSLRI(J)).LE.1) JPASS=JPASS+1
    IF(IABS(NUMDEL(NNN(K))-NOSLLE(J)).LE.1) LPASS=LPASS+1
    IF(ABS(SLPR(NNN(K))).GE.(10.).AND.ABS(PENDRI(J)).GE.(10.))
      * GO TO 79
    IF(ABS(SLPR(NNN(K))-PENDRI(J)).LE.2.5) NPASS=NPASS+1
    IF(ABS(SLPL(NNN(K))-PENDLE(J)).LE.7.5) IPASS=IPASS+1
    GO TO 81
79  IF(ABS(SLPR(NNN(K))-PENDRI(J)).LE.7.5) NPASS=NPASS+1
    IF(ABS(SLPL(NNN(K))-PENDLE(J)).LE.7.5) IPASS=IPASS+1
81  IF(IABS(NRRW(NNN(K))-NSTDEV(J)).LE.(10.)) KPASS=KPASS+1
    NGOOD(NCOUNT)=LPASS+IPASS+KPASS+NPASS+JPASS
75  CONTINUE
  IF(NCOUNT.EQ.1)GO TO 180
  NDIFTE=15
  DO 420 MK=1,NCOUNT
    NDIFBB(MK)=IABS(L1(MK)-MX2GEN(K))
    IF(NDIFBB(MK).LE.NDIFTE)GO TO 435
    GO TO 420
435  NDIFTE=NDIFBB(MK)
    LKNM=MK
420  CONTINUE
C
C ** ALL THE PATTERN RECOGNITION PROPERTIES ARE USED TO **
C ** DETERMINE IF A PROPER MATCH HAS OCCURED. **
C
    IF((NDIFTE.LE.4.AND.NGOOD(LKNM).GE.1).OR.(NDIFTE.LE.8.
      * AND.NGOOD(LKNM).GE.2).OR.(NDIFTE.LE.12.AND.NGOOD(LKNM).
      * GE.3).OR.(NDIFTE.LE.16.AND.NGOOD(LKNM).GE.4))GO TO 430
180  NDIFTE=IABS(L1(1)-MX2GEN(K))
    IF(NDIFTE.LE.4.AND.NGOOD(1).GE.1) GO TO 400
    IF(NDIFTE.LE.8.AND.NGOOD(1).GE.2)GO TO 400
    IF(NDIFTE.LE.12.AND.NGOOD(1).GE.3)GO TO 400
    IF(NDIFTE.LE.16.AND.NGOOD(1).GE.4)GO TO 400
    GO TO 73
400  IF(IABS(L1(1)-LAGL-MABLMA(NNN(K+1))).LE.NDIFTE)GO TO 73
    MBSCI(K)=L1(1)
    IF((K.GE.2).AND.(NDIFTE.GE.MDIFTE).AND.(MBSCI(K).
      * EQ.MBSCI(K-1))) GO TO 73
    GO TO 84
430  IF((IABS(L1(1)-LAGL-MABLMA(NNN(K+1))).GT.NDIFTE).AND.
      * (LKNM.EQ.1)) GO TO 491
    IF((IABS(L1(2)-LAGL-MABLMA(NNN(K+1))).GT.NDIFTE).AND.

```

21 JUNE 1979

```

      * (LKNM,EQ.2)) GO TO 491
      IF((IAES(LI(3)-LAGL-MABLMA(NNN(K+1))))).GT.NDIFTE).AND.
      * (LKNM,EQ.3)) GO TO 491
      GO TO 73
491  MBSCI(K)=LI(LKNM)
      IF((K.GE.2).AND.(NDIFTE.GE.MDIFTE).AND.(MBSCI(K).EQ.
      * MBSCI(K-1))) GO TO 73
84  CONTINUE
      IF(MBSCI(K).GT.(N+15)) GO TO 73
      IF(MKN-2) 87,89,91
C
C ** DELTA1, DELTA2, AND DELTA3 CONTAIN THE TIME DIFFERENCE **
C ** FOR EVERY IDENTIFIED PULSE. **
C
87  DELTA1(K)=(MBSCI(K)-MABLMA(NNN(K)))*.22978
      GO TO 73
89  DELTA2(K)=(MBSCI(K)-MABLMA(NNN(K)))*.22978
      GO TO 73
91  DELTA3(K)=(MBSCI(K)-MABLMA(NNN(K)))*.22978
73  CONTINUE
C
C ** CHECK FOR WHAT STATION SHOULD BE READ NEXT **
C
      IF(MKN,EQ.3) GO TO 93
      IF(MKN,EQ.2) GO TO 95
C
C DO 503 K=1,2048
503  X2(K)=X8(2048*J1-448*J1+K)
      GO TO 17
C
C DO 504 K=1,2048
504  X2(K)=X9(2048*J1-448*J1+K)
      GO TO 17
C
C ** A REASONABLENESS TEST IS USED TO ENSURE THE TIME **
C ** DIFFERENCE IS WITHIN PROPER BOUNDS. **
C
93  DEL1UB=.22978*FLOAT(LAG1)+25.0*.22978
      DEL1LB=.22978*FLOAT(LAG1)-25.0*.22978
      DEL2UB=.22978*FLOAT(LAG2)+25.0*.22978
      DEL2LB=.22978*FLOAT(LAG2)-25.0*.22978
      DEL3UB=.22978*FLOAT(LAG3)+25.0*.22978
      DEL3LB=.22978*FLOAT(LAG3)-25.0*.22978
      NX=0
      DO 452 IK=1,MP
      IF((DELTA1(IK).GE.DEL1LB.AND.
      * DELTA1(IK).LE.DEL1UB).AND.(DELTA2(IK).GE.DEL2LB.
      * AND.DELTA2(IK).LE.DEL2UB).AND.(DELTA3(IK).GE.DEL3LB.
      * AND.DELTA3(IK).LE.DEL3UB)) GO TO 571
      GO TO 452
571  NX=NX+1
      NIN(NX)=IK
452  CONTINUE
C
C ** CALCULATE THE LOCATIONS FOR ALL THE PULSES MATCHED **
C ** FOR ALL THE STATIONS **
C
      CALL HYPERM(DELTA1,DELTA2,DELTA3,X,Y,Z,NIN,NX)
      WRITE(6,535)
535  FORMAT(1H0,10X,11H IN METERS,10X,11H IN METERS,
      * 10X,11H IN METERS,5X,20H TIME IN MICROSECONDS)
      WRITE(8,706)
      DO 172 LK=1,NX
      TIME(LK)=.22978*FLOAT(J1*2048-J1*448)+
      * .22978*FLOAT(MABLMA(NNN(NIN(LK))))

```


21 JUNE 1979

```

      IF((J1.GE.1).AND.(TIME(LK).LE.TIME1))GO TO 172
      WRITE(6,101) X(LK),Y(LK),Z(LK),TIME(LK)
172  WRITE(8,705) X(LK),Y(LK),Z(LK),TIME(LK)
      CONTINUE
      TIME1=TIME(NX)
      GO TO 815
585  IF(J1.EQ.0) TIME1=0.
815  TIME1=TIME1+2.
C
C ** WRITE A ZERO TO INDICATE THAT THE THREE-DIMENSIONAL **
C ** LOCATIONS, FOR ALL THE MATCHED PULSES, HAVE BEEN READ. **
C
      WRITE(8,705)ZERO,ZERO,ZERO,ZERO
      J1=J1+1
      IF(J1.LE.4) GO TO 500
      WRITE(6,537)
537  FORMAT('1','1')
C
C ** BACKSPACE THE TAPE TO ENSURE THE DATA AT THE END OF **
C ** THE LAG INTERVAL IS NOT MISSED. **
C
      BACKSPACE 11
520  CONTINUE
      REWIND 11
101  FORMAT(4F20.3)
109  FORMAT(3F10.3)
170  FORMAT(5I10)
162  FORMAT(F10.2)
164  FORMAT(2I10,F10.2,I10)
107  FORMAT(15)
705  FORMAT(3F18.3,F26.3)
706  FORMAT(8X,11HX IN METERS, 8X, 11HY IN METERS,
* 8X, 11HZ IN METERS, 3X, 20HTIME IN MICROSECONDS)
      STOP
C
C ** THIS IS THE END OF THE MAIN PROGRAM TO CALCULATE **
C ** LIGHTNING LOCATIONS FROM TIME SERIES MEASUREMENTS. **
C ** NEXT A DESCRIPTION OF ALL THE SUBROUTINES AND **
C ** SUBPROGRAMS USED IN THIS ALGORITHM IS GIVEN. **
C
      END

```

21 JUNE 1979

```

      FUNCTION STDSET(X1,N)
C
C  **  FUNCTION SUBROUTINE TO CALCULATE THE STANDARD  **
C  **  DEVIATION OF SET                               **
C
      DIMENSION X1(1)
      TSUMS=0.0
      DO 536 I=1,N
536   TSUMS=TSUMS+X1(I)
      AVSET=TSUMS/FLCAT(N)
      TSUMS=0.0
      DO 538 I=1,N
538   SUMS=(X1(I)-AVSET)**2
      TSUMS=TSUMS+SUMS
      STDSET=SQRT(TSUMS/FLCAT(N-1))
      RETURN
      END

```

21 JUNE 1979

```

      SUBROUTINE RMEAN(DATA,NDATA,XMEAN)
C
C  ** THIS SUBROUTINE SUBTRACTS THE MEAN OF THE DATA **
C
      DIMENSION DATA(1)
      DOUBLE PRECISION DDATA,DSUM,DNDATA
      DSUM=0.0
      DNDATA=NDATA
      DO 10 I=1,NDATA
      DDATA=DATA(I)
10    DSUM=DSUM+DDATA
      DSUM=DSUM/DNDATA
      AVG=DSUM
      DO 20 I=1,NDATA
20    DATA(I)=DATA(I)-AVG*XMEAN
      RETURN
      END

```

21 JUNE 1979

```
      FUNCTION BIG(X,N)
C    ** THIS SUBROUTINE FINDS THE LARGEST NUMBER IN THE SET **
C
      DIMENSION X(1)
      T=X(1)
      DO 570 I=1,N
      IF (T-X(I)) 565,570,570
565  T=X(I)
570  CONTINUE
      BIG=T
      RETURN
      END
```

21 JUNE 1979

```
      FUNCTION SMALL(X,N)
C    ** THIS SUBROUTINE FINDS THE SMALLEST NUMBER IN THE SET **
C
      DIMENSION X(1)
      T=X(1)
      DO 575 I=1,N
      IF (T-X(I))575,575,580
580   T=X(I)
575   CONTINUE
      SMALL=T
      RETURN
      END
```

21 JUNE 1979

```

C      FUNCTION DIV4SM(X1,N)
C C **  FUNCTION SUBPROGRAM TO CALCULATE THRESHOLD, DIV4SM **
C
  DIMENSION X1DIM(4),X1DIV4(512),X1(2048)
  KK=512
  DO 2 MK=1,4
  DO 4 I=1, KK
4    X1DIV4(I)=X1((MK-1)*KK+I)
2    X1DIM(MK)=BIG(X1DIV4,512)
  DIV4SM=SMALL(X1DIM,4)
  RETURN
  END

```

21 JUNE 1979

```

C      FUNCTION STDSUB(X1LM,AVESET,MM)
C  **  SUBPROGRAM TO CALCULATE THE STANDARD DEV.  **
C  **  OF THE SUBSET (STDSUB)  **
C
      DIMENSION X1LM(16)
      TSUMS=0.0
      DO 14 I=1,MM
      SUMS=(X1LM(I)-AVESET)**2
14     TSUMS=TSUMS+SUMS
      STDSUB=SQRT(TSUMS/FLOAT(MM-1))
      RETURN
      END

```

21 JUNE 1979

```

C      FUNCTION LAG(AVEMO,AVEMO2,MKN)
C **   SUBPROGRAM TO CALCULATE THE CROSS-CORRELATION **
C **   OF THE ENVELOPE **
C
C      DIMENSION RHC(2048),PRO(2048),AVEMO(2048),AVEMO2(2048)
C      RHOFTE=-1.0
C
C **   LK1 AND LK2 ARE THE BEGINNING AND THE END OF **
C **   THE CORRELATION LAG. **
C
C      LK1=1
C      LK2=300
C      NK=2032
C      IF(MKN.EQ.3) GO TO 891
C      IF(MKN.EQ.1) LK2=150
C      GO TO 892
891    LK1=300
C      LK2=600
892    DO 37 K=LK1,LK2
C      XI1=0.0
C      XI2=0.0
C      NK1=NK-K+1
C      PRD=0.0
C      DO 35 I=1,NK1
C      PRC(I)=AVEMO(I)*AVEMO2(I+K-1)
C      XI1=XI1+AVEMO(I)**2
C      XI2=XI2+AVEMO2(I+K-1)**2
35    PRD=PRD+PRC(I)
C      SNORM=SQRT(XI1*XI2)
C      RHO(K)=PRD/SNORM
37    CONTINUE
49    FORMAT(10F10.3)
C      LK1=LK1+4
C
C **   DETERMINING THE LARGEST CROSS-CORRELATION **
C
C      DO 41 K=LK1,LK2
C      IF(RHO(K).GT.RHOFTE)GO TO 53
C      GO TO 41
53    LAG=K
C      RHOFTE=RHO(K)
41    CONTINUE
C      TIMEX=.22978*FLOAT(LAG)
C      WRITE(6,389) LAG,RHOFTE,TIMEX
389    FORMAT(I22.2F22.3)
C      RETURN
C      END

```


21 JUNE 1979

```

      SUBROUTINE LOCNAX(MABLMA,MM,JJ,AVE,SLPR,SLPL,NUMBER,
      * NUMDEL,NRRQWE)
C
C ** SUBROUTINE TO CALCULATE THE LOCAL MAXIMUM OF CENTRAL **
C ** STATION **
C
      DIMENSION MAELMA(128),XILM(16),SLPR(128),SLPL(128),
      * NUMBER(128),NUMDEL(128),NRRQWE(128),AVE(128)
      COMMON KK,N,MP,NP,NNN(128),MMM(128),X1(2048),X2(2048)
C
C ** THIS SUBROUTINE COMPUTES THE COORDINATES OF A LOCAL **
C ** MAXIMUM PER SUBSET. FOR A POINT TO BE A LOCAL MAXIMUM **
C ** ONE OF THESE THREE CONDITIONS MUST BE MET. A) ORDINATE **
C ** LARGER THAN 1/2 OF THE SMALLEST VALUE OF THE SECTION, **
C ** B) STANDARD DEVIATION OF SUBSET LARGER THAN STANDARD **
C ** DEVIATION OF SET, AND/OR C) ORDINATE LARGER THAN THE **
C ** AVERAGE PLUS TWO TIMES THE STD DEV. OF THE SUBSET. **
C
      MP=0
      RT=2.0
      DO 6 K=1,JJ
      AVESET=AVE(K)
      DO 8 J=1,MM
8      XILM(J)=X1((K-1)*MM+J)
      XISM=BIG(XILM,MM)
      XITEST=(DIV4SM(X1,N))/RT
      XIPEQ=SMALL(XILM,MM)
      XI0IFE=XISM-XIPEQ
      DO 22 J=1,MM
      IF(XILM(J).NE.XISM)GO TO 22
      MAELMA(K)=J+(K-1)*MM
      GO TO 200
22      CONTINUE
200      NABCIS=MAELMA(K)
      IF(NABCIS.LE.5)GO TO 6
      IF(NABCIS.GE.2043) GO TO 6
      IF(XISM.GE.XITEST)GO TO 24
      IF(STDSDUB(XILM,AVESET,MM).GE.STDSET(X1,N)) GO TO 24
      TEST=AVESET+RT*STDSDUB(XILM,AVESET,MM)
      IF(XISM.GE.TEST)GO TO 24
      MRR=0
      MLL=0
      DO 202 MN1=1,5
      IF(X1(NABCIS+MN1-1).GE.X1(NABCIS+MN1)) MRR=MRR+1
      IF(X1(NABCIS-MN1+1).GE.X1(NABCIS-MN1)) MLL=MLL+1
202      CONTINUE
      IF((MRR+MLL).GE.8)GO TO 24
      IF(XI0IFE.GE.(100.).AND.(MRR+MLL).GE.7)GO TO 24
      GO TO 6
24      CALL PULSE(X1,NABCIS,SLOPR,SLOPL,MR,ML,NRRQWE)
      SLPR(K)=SLOPR
      SLPL(K)=SLOPL
      NUMBER(K)=MR
      NUMDEL(K)=ML
      NRRQWE(K)=NRRQWE
      IF(SLPL(K).LL.0.)GO TO 6
      IF(SLPR(K).GE.0.)GO TO 6
      MP=MP+1
      NNN(MP)=K
      IF(MP.EQ.1) GO TO 6
      IF((MAELMA(NNN(MP))-MAELMA(NNN(MP-1))).LE.3) MP=MP-1
6      CONTINUE
121      FORMAT(2F10.2,5I10)
      RETURN
      END

```

21 JUNE 1979

```

SUBROUTINE PULSE(X1,NABCIS,SLOPR,SLOPL,MR,ML,NARROW)
C
C ** THIS PULSE SUBROUTINE DETERMINES THE CHARACTERISTICS **
C ** OF THE PULSE **
C
  DIMENSION X1(2048)
  HIGHL=X1(NABCIS)-X1(NABCIS-5)
  HIGHR=X1(NABCIS)-X1(NABCIS+5)
  SLOPR=-HIGHR/5.0
  SLOPL=HIGHL/5.0
  MR=0
  DO 30 MN=1,5
    IF(X1(NABCIS+MN-1).GE.X1(NABCIS+MN)) MR=MR+1
  30 CONTINUE
  ML=0
  DO 32 MN=1,5
    IF(X1(NABCIS-MN+1).GE.X1(NABCIS-MN)) ML=ML+1
  32 CONTINUE
  CALL NARRO(X1,NABCIS,NARROW)
  RETURN
END

```

21 JUNE 1979

```

      SUBROUTINE NARRO(X1,NABCIS,NARROW)
C
C ** THIS SUBROUTINE FINDS THE STANDARD DEVIATION OR **
C ** NARROWNESS OF THE PULSE AROUND THE LOCAL MAXIMUM **
C
      DIMENSION X1(2048)
      NARR=0
      NARL=0
      DO 34 ML=1,5
      IF(X1(NABCIS+ML-1).GE.X1(NABCIS+ML)) GO TO 38
      NARR=ML
      GO TO 36
38  NARR=NARR+1
34  CCNTINUE
36  DO 40 KJ=1,5
      IF(X1(NABCIS-KJ+1).GE.X1(NABCIS-KJ)) GO TO 42
      NARL=KJ
      GO TO 44
42  NARL=NARL+1
40  CCNTINUE
44  TSUMS=0.0
      DO 46 JK=1,NARR
      DIF=(X1(NABCIS)-X1(NABCIS+KJ))*2
46  TSUMS=TSUMS+DIF
      DO 48 JK=1,NARL
      DIF=(X1(NABCIS)-X1(NABCIS-KJ))*2
48  TSUMS=TSUMS+DIF
      NARROW=SQRT(TSUMS/FLD(1/(NARR+NARL+1)))
      RETURN
      END

```

21 JUNE 1979

```

SUBROUTINE LCCMA2(MABL2,MM,JJ,AVE,SLPR2,SLPL2,NUMDR2,
* NUMDL2,NRRW2)
C
C ** THIS SUBROUTINE COMPUTES THE LOCAL MAXIMUM FOR **
C ** THE REMOTE STATIONS **
C
DIMENSION MABL2(128),X2LM(16),SLPR2(128),SLPL2(128),
* NUMDR2(128),NUMDL2(128),NRRW2(128),AVE(128)
COMMON KK,N,MP,NP,NNN(128),MMM(128),X1(2048),X2(2048)
C
C ** THIS SUBROUTINE IS SIMILAR TO THE CENTRAL STATION LOCAL **
C ** MAXIMUM. DOING THIS ANALYSIS SEPARATELY WE CAN ESTABLISH **
C ** STRICTER TOLERANCES FOR PULSE SELECTION IN THIS STATION. **
C
NP=0
RT=2.0
MT=1.75
DO 50 K=1,JJ
MABL2(K)=0
AVESET=AVE(K)
DO 52 J=1,MM
52 X2LM(J)=X2((K-1)*MM+J)
X2SM=BIG(X2LM,MM)
IX2SM=X2SM
X1TEST=(DIV4SM(X2,N))/RT
X2PEQ=SMALL(X2LM,MM)
X2DIF=X2SM-X2PEQ
DO 56 J=1,MM
IX2LM=X2LM(J)
IF(IX2LM.NE.(X2SM)GO TO 56
MABL2(K)=J+(K-1)*MM
GO TO 300
56 CCNTINUE
300 MABCIS=MABL2(K)
IF(MABCIS.LE.5) GO TO 50
IF(MABCIS.GE.2043)GO TO 50
IF(X2SM.GE.X1TEST)GO TO 60
IF(STDOSUB(X2LM,AVESET,MM).GE.STDSET(X2,N))GO TO 60
TEST=AVESET+MT*STDOSUB(X2LM,AVESET,MM)
IF(X2SM.GE.TEST)GO TO 60
MRR=0
MLL=0
DO 302 MN1=1,5
IF(X2(MABCIS-MN1+1).GE.X2(MABCIS-MN1)) MLL=MLL+1
IF(X2(MABCIS+MN1-1).GE.X2(MABCIS+MN1)) MRR=MRR+1
302 CONTINUE
IF((MRR+MLL).GE.8)GO TO 60
IF(X2DIF.GE.100.AND.(MRR+MLL).GE.7) GO TO 60
GO TO 50
60 CALL PULSE(X2,MABCIS,SLOPR2,SLOPL2,MR2,ML2,NARRW2)
SLPR2(K)=SLOPR2
SLPL2(K)=SLOPL2
NUMDR2(K)=MR2
NUMDL2(K)=ML2
NRRW2(K)=NARRW2
IF(SLPL2(K).LE.0.)GO TO 50
IF(SLPR2(K).GE.0.)GO TO 50
NP=NP+1
MMM(NP)=K
IF(NP.EQ.1) GO TO 50
IF(MABL2(MMM(NP))-MABL2(MMM(NP-1))).LE.3)NP=NP-1
50 CONTINUE
125 FORMAT(2F10.2,5I10)
RETURN
END

```

21 JUNE 1979

```

C      SUBROUTINE HYPERM(DELTA1,DELTA2,DELTA3,X,Y,Z,NIN,NX)
C  **  THIS SUBROUTINE USES THE HYPERBOLIC EQUATIONS TO  **
C  **  DETERMINE THE THREE-DIMENSIONAL LOCATIONS.  **
C
C      DIMENSION DELTA1(128),DELTA2(128),DELTA3(128),M(9),
C      * V(3),X(128),Y(128),Z(128),NIN(128)
C      REAL M
C      DO 62 K=1,NX
C      M(7)=(DELTA1(NIN(K))-33.55)*(-300.)
C      M(8)=(DELTA2(NIN(K))-29.520)*(-300.)
C      M(9)=(DELTA3(NIN(K))-113.43)*(-300.)
C      V(1)=(10312.28**2-M(7)**2)/2.0
C      V(2)=(8222.076**2-M(8)**2)/2.0
C      V(3)=(8089.20**2-M(9)**2)/2.0
C
C  **  THE NEXT PARAMETERS ARE THE COORDINATES OF THE  **
C  **  REMOTE STATIONS IN METERS.  **
C
C      M(1)=-3677.05
C      M(2)=-8160.79
C      M(3)=7432.93
C      M(4)=9634.44
C      M(5)=-1002.01
C      M(6)=3191.68
C      CALL SIMQ(M,V,3,0)
C      ZSQ=V(3)**2-(V(1)**2+V(2)**2)
C      X(K)=V(1)
C      Y(K)=V(2)
C      IF(ZSQ)63,64,64
64      Z1=SQRT(ZSQ)
C      Z(K)=Z1
C      GO TO 62
68      ZSQ=-ZSQ
C      Z(K)=-SQRT(ZSQ)
62      CONTINUE
C      RETURN
C      END

```

21 JUNE 1979

```

      SUBROUTINE SIMQ(A,B,N,KS)
C
C
C ** THIS SUBROUTINE SOLVES SIMULTANEOUS EQUATIONS BY **
C ** USING GAUSSIAN ELIMINATION. **
C
      DIMENSION A(1),E(1)
C
C ** FORWARD SOLUTION **
C
      TOL=0.0
      KS=0
      JJ=-N
      DO 65 J=1,N
      JY=J+1
      JJ=JJ+N+1
      BIGA=0
      IT=JJ-J
      DO 30 I=J,N
C
C ** SEARCH FOR MAXIMUM COEFFICIENT IN COLUMN **
C
      IJ=IT+I
      IF(ABS(BIGA)-ABS(A(IJ))) 20,30,30
20    BIGA=A(IJ)
      IMAX=I
30    CONTINUE
C
C ** TEST FOR PIVOT LESS THAN TOLERANCE (SINGULAR MATRIX) **
C
      IF(ABS(DIGA)-TOL) 35,35,40
35    KS=1
      RETURN
C
C ** INTERCHANGE ROWS IF NECESSARY **
C
40    II=J+N*(J-2)
      IT=IMAX-J
      DO 50 K=J,N
      II=II+N
      I2=II+IT
      SAVE=A(II)
      A(II)=A(I2)
      A(I2)=SAVE
C
C ** DIVIDE EQUATION BY LEADING COEFFICIENT **
C
50    A(II)=A(II)/BIGA
      SAVE=B(IMAX)
      B(IMAX)=B(J)
      B(J)=SAVE/BIGA
C
C ** ELIMINATE NEXT VARIABLE **
C
      IF(J-N) 55,70,55
55    IQS=N*(J-1)
      DO 65 IX=JY,N
      IXJ=IQS+IX
      IT=J-IX
      DO 60 JX=JY,N
      IXJX=N*(JX-1)+IX
      JJX=IXJX+IT
60    A(IXJX)=A(IXJX)-(A(IXJ)*A(JJX))
      B(IX)=B(IX)-(B(J)*A(IXJ))
      65

```

21 JUNE 1979

```
C ** BACK SOLUTION **
C
70  NY=N-1
    IT=N*N
    DO 80 J=1,NY
      IA=IT-J
      IB=N-J
      IC=N
      DO 80 K=1,J
        B(IB)=B(IB)-A(IA)*B(IC)
      IA=IA-N
80  IC=IC-1
    RETURN
    END
```

21 JUNE 1979

STORM ACTIVITY ON 19TH JULY 1976

START TIME = 16 HOURS 59 MIN 59 SEC 008 MIL

FINISH TIME = 17 HOURS 00 MIN 01 SEC 009 MIL

DIGITIZATION TIME = 3 HOURS 46 MIN 25 SEC 59 MIL

UNIVERSAL TIME = 16 HOURS 59 MIN 59 SEC 10 MIL 343 MICROSEC

X IN METERS	Y IN METERS	Z IN METERS	
370.292	11573.102	6925.770	
X IN METERS	Y IN METERS	Z IN METERS	TIME IN MICROSEC
337.332	11503.008	6838.449	2.068
222.583	11542.492	7512.641	8.961
328.820	11510.613	6670.266	18.382
370.759	11610.777	8816.242	22.289
294.204	10929.129	5781.823	28.033
828.517	13032.410	9908.430	36.075
332.326	11934.977	7672.242	40.441
268.880	12131.840	7899.738	53.998
170.478	11650.094	7151.047	57.675
502.776	11264.688	5723.504	63.419
358.633	10492.359	5967.738	76.057
229.142	10562.195	6537.320	88.006
-56.677	14875.063	11791.336	98.116
487.560	11295.305	5602.984	100.873
644.544	10253.074	5113.477	103.401
488.974	10967.379	5344.094	109.146
588.818	12416.773	8445.395	114.660
27.458	12505.129	8631.641	124.081
147.415	12125.922	8042.113	129.826
231.690	12206.934	7644.430	134.881
-46.448	11944.910	7964.465	142.693
249.756	13016.941	8542.285	147.289
-207.222	11049.027	5787.840	159.238
241.063	11808.273	7346.617	173.254
424.066	12409.723	8332.617	181.986
285.637	11657.086	7006.504	187.500
1341.814	12474.340	8217.180	213.006
444.904	10839.117	5971.152	230.010
356.226	11513.692	7491.148	236.673
17.986	10783.199	5903.059	241.039
307.271	12058.375	8154.840	246.784
466.636	12313.809	7962.027	259.422
120.853	11752.563	6788.270	275.506
302.856	11622.184	7127.852	279.872
223.584	11843.574	7223.500	286.535
216.027	11504.516	6817.984	292.280
378.720	10712.215	5801.590	298.484
195.021	11964.461	7691.543	306.986
289.562	11774.191	6315.930	312.730
195.683	12277.715	7388.688	316.407
423.099	12877.262	8012.141	324.219
674.408	11266.602	4388.184	327.896
1124.674	14503.461	12378.633	347.198

APPENDIX D

COMPUTER ALGORITHM TO DISPLAY A THREE-DIMENSIONAL DRAWING OF VHF NOISE SOUNDS

This appendix contains the computer algorithm we wrote to display the VHF noise sources in three-dimensions. The input of the algorithm is the three-dimensional sources stored in digital tape which are produced by the algorithm given in Appendix C. The output of the algorithm is an isometric view of either the cross-correlated (94 or 376 μ sec intervals) or the individual VHF noise sources. Examples of the output of this program are shown several times in Chapter V.

21 JUNE 1979

```

C *****
C * THIS PROGRAM PLOTS THE THREE-DIMENSIONAL LOCATIONS OF THE *
C * VHF NOISE SOURCES. THE INPUT IS A 9-TRACK 1600 BPI TAPE *
C * WITH VHF SOURCE LOCATIONS. THE OUTPUT IS AN ISOMETRIC VIEW *
C * OF THE COORDINATES OF THE NOISE SOURCES. *
C *****
C
C      REAL MUZ,MUY,MUZ
C      DIMENSION XM(100),YM(100),ZM(100),TIME(128),A(15),B(15),
C      * C(15),D(15),E(15),F(15),XPM(100),ZPM(100),YPM(100),
C      * XXM(100),YXM(100),XYM(100),YYM(100),XNP(100),YMP(100),
C      * ZMP(100),YPPM(100),XPB(100),YPB(100),XPT(100),YPT(100),
C      * XXT(100),YXT(100),YYT(100),XYT(100),XXB(100),XVB(100),
C      * YVB(100),XVB(100),YPPB(100),YPPB(100)
10  READ(13,10)((A(I),I=1,8),(B(I),I=1,15),(C(I),I=1,15))
10  FORMAT(33X,8A4, //21X,14A4,A3, //20X,15A4)
      PI=3.141593
      KRS=1.0
      N=0
      M=1
      NM=0
      NN=8
      XSHIFT=1.0
      YSHIFT=2.0
      RX=2.0
      RY=2.0
      RZ=2.0
      DEGX=0.0
      DEGY=33.0
C
C ** ANGX AND ANGY ARE THE PLANAR PROJECTION ANGLES. **
C
C      ANGX=DEGX*PI/180.0
C      ANGY=DEGY*PI/180.0
C      DO 29 I=M+1,NN
C
C ** READING TAPE HEADINGS **
C
C      READ(13,12)((A(I),I=1,5),LHOUR,(B(I),I=1,2),LMIN,(C(I),
C      * I=1,2),LSECR,(D(I),I=1,2),LMIL,(E(I),I=1,2))
12  FORMAT(11X,4A4,A2,I4,1X,A4,A1,I5,1X,A4,A3,
C      * I4,1X,A4,A3,I4,1X,2A4,A3)
C      READ(13,14)((A(I),I=1,4),LHOUR,(B(I),I=1,2),LMIN,(C(I),
C      * I=1,2),LSECR,(D(I),I=1,2),MILST,(E(I),I=1,3),MICROT,(F(I),
C      * I=1,3))
14  FORMAT(4A4,I3,A4,A1,I3,A4,A3,2X,I3,1X,A4,A3,
C      * I4,1X,2A4,A3,I4,1X,3A4)
C      DO 28 J=1,5
16  READ(13,16)((A(I),I=1,3),(B(I),I=1,3),(C(I),I=1,3))
16  FORMAT(10X,2A4,A3,10X,2A4,A3,10X,2A4,A3)
C
C ** READING THE CROSS-CORRELATED LOCATION **
C
C      READ(13,18) X1,Y1,Z1,ZERO
18  FORMAT(4F20.3)
C      IF(X1.EQ.0.0) GO TO 28
C      IF((Z1.LE.0.).OR.(X1.GE.40000.).OR.(Y1.GE.40000.))
C      * GO TO 28
C      NM=NM+1
C      XM(NM)=X1/1000.0
C      YM(NM)=Y1/1000.0
C      ZM(NM)=Z1/1000.0

```

21 JUNE 1979

```

      WRITE(6,18) XM(NM),YM(NM),ZM(NM)
      READ(13,20)((A(I),I=1,3),(B(I),I=1,3),(C(I),I=1,3),
20    * (D(I),I=1,5))
      FORMAT(8X,2A4,A3,8X,2A4,A3,8X,2A4,A3,3X,5A4)
      DO 22 I=1,128
C
C    ** READING ALL THE LOCATIONS **
C
      READ(13,42) X1,Y1,Z1,TIME(I)
      MX=X1
      IF(MX.EQ.0) GO TO 28
      IF(Z1.LE.0.0) GO TO 22
      N=N+1
22    CONTINUE
      GO TO 28
69    READ(13,42) ZERO,ZERO,ZERO,ZERO
28    CONTINUE
29    CONTINUE
42    FORMAT(3F18.3,F26.3)
      WRITE(6,50)
50    FORMAT(////////)
      NF=0
      DO 3 I=1,NM
      NF=NF+1
      XMP(NF)=XM(I)
      YMP(NF)=YM(I)
      ZMP(NF)=ZM(I)
      WRITE(6,18) XMP(NF),YMP(NF),ZMP(NF)
3    CONTINUE
      NL=NF
C
C    ** DETERMINATION OF THE SCALES **
C
      SX=SMALL(XMP,NF)
      SY=SMALL(YMP,NF)
      SZ=SMALL(ZMP,NF)
      BX=0IG(XMP,NF)
      BY=0IG(YMP,NF)
      BZ=0IG(ZMP,NF)
      IF(SX-0.0) 4,6,5
4     SX=AINT(SX-1.0)
      GO TO 6
5     SX=AINT(SX)
6     IF(SY-0.0) 7,9,8
7     SY=AINT(SY-1.0)
      GO TO 9
8     SY=AINT(SY)
9     SZ=AINT(SZ-1.0)
      IF(BX-0.0) 11,15,13
11    BX=AINT(BX)
      GO TO 15
13    BX=AINT(BX+1.0)
15    IF(BY-0.0) 17,21,19
17    BY=AINT(BY)
      GO TO 21
19    BY=AINT(BY+1.0)
21    BZ=AINT(BZ+1.0)
      IF(KRS.EQ.1) SZ=0.0
      XDS=BX-SX
      YBS=BY-SY
      ZBS=BZ-SZ
      WRITE(6,26) BX,SX,BY,SY,BZ,SZ
26    FORMAT(10X,6(E10.3,5X))
      DO 23 I=1,NL

```

21 JUNE 1979

```

C ** SETTING THE VALUES INSIDE THE SCALES **
C
  XMP(I)=XMP(I)-SX
  YMP(I)=YMP(I)-SY
23 ZMP(I)=ZMP(I)-SZ
  DO 45 I=1,NL
45 WRITE(6,18) XMP(I),YMP(I),ZMP(I)
  WRITE(6,50)
  PX1=0.0

C
C ** PROJECTION OF THE SCALE ON THE BASE EARTH'S AXES. SETTING **
C ** UP THE OUTER PERIMETER. **
C
  PX2=XB*S*COS(ANGX)
  PX3=YB*S*COS(ANGY)
  PX4=PX2+PX3
  PY1=0.0
  PY2=XB*S*SIN(ANGX)
  PY3=YB*S*SIN(ANGY)
  PY4=PY2+PY3
  PY5=ZB*S
  PY6=PY5+PY2
  PY7=PY5+PY4
  PY8=PY3+PY5
  X1=PX3
  Y1=PY3
  X2=PX2
  Y2=PY2

C
C ** SETTING UP THE GOULD PLOTTER **
C
  CALL PLOTS(-15.0,20.0,0.0,1,XSHIFT,YSHIFT)
  CALL LINEWT(-2)

C
C ** DRAWING THE THREE-DIMENSIONAL BOX AND DOING ALL **
C ** THE PROJECTIONS. **
C
  CALL PLOT(PX1,PY1,3)
  CALL PLOT(PX1,PY5,2)
  CALL PLOT(PX2,PY6,2)
  CALL PLOT(PX2,PY2,2)
  CALL PLOT(PX1,PY1,2)
  CALL PLOT(PX2,PY2,3)
  CALL PLOT(PX4,PY4,2)
  CALL PLOT(PX4,PY7,2)
  CALL PLOT(PX2,PY6,2)
  CALL PLOT(PX1,PY5,3)
  CALL PLOT(PX3,PY8,2)
  CALL PLOT(PX4,PY7,2)
  CALL PLOT(0.0,0.0,3)
  CALL LINEWT(0)
  SPACE=0.25
  L=YB5/SPACE
  L=L/2
  DO 25 I=1,L
  CALL WHERE(XW,YW,XF,YF)
  XW=XW+SPACE*COS(ANGY)
  YW=YW+SPACE*SIN(ANGY)
  CALL PLOT(XW,YW,2)
  XW=XW+SPACE*COS(ANGY)
  YW=YW+SPACE*SIN(ANGY)
25 CALL PLOT(XW,YW,3)
  CALL WHERE(XW,YW,XF,YF)
  XSS=XW
  YSS=YW

```

21 JUNE 1979

```

L=ZBS/SPACE
L=L/2
DO 27 I=1,L
CALL WHERE(XW,YW,XF,YF)
YW=YW+SPACE
CALL PLOT(XW,YW,2)
YW=YW+SPACE
27 CALL PLOT(XW,YW,3)
CALL PLOT(XSS,YSS,3)
L=XBS/SPACE
L=L/2
DO 31 I=1,L
CALL WHERE(XW,YW,XF,YF)
XW=XW+SPACE*COS(ANGX)
YW=YW+SPACE*SIN(ANGX)
CALL PLOT(XW,YW,2)
XW=XW+SPACE*COS(ANGX)
YW=YW+SPACE*SIN(ANGX)
31 CALL PLOT(XW,YW,3)
CALL PLOT(0.0,0.0,3)
SKIP=3.0
LP=ZBS/SKIP
DO 43 J=1,LP
CALL LINEWT(-2)
CALL PLOT(0.0,SKIP,-3)
CALL PLOT(PX1,PY1,3)
CALL PLOT(PX2,PY2,2)
CALL PLOT(PX4,PY4,2)
CALL LINEWT(0)
DO 44 I=1,L
CALL WHERE(XW,YW,XF,YF)
XW=XW-SPACE*COS(ANGX)
YW=YW-SPACE*SIN(ANGX)
CALL PLOT(XW,YW,2)
XW=XW-SPACE*COS(ANGX)
YW=YW-SPACE*SIN(ANGX)
44 CALL PLOT(XW,YW,3)
LL=YBS/SPACE
LL=LL/2
DO 43 I=1,LL
CALL WHERE(XW,YW,XF,YF)
XW=XW-SPACE*COS(ANGY)
YW=YW-SPACE*SIN(ANGY)
CALL PLOT(XW,YW,2)
XW=XW-SPACE*COS(ANGY)
YW=YW-SPACE*SIN(ANGY)
43 CALL PLOT(XW,YW,3)
CALL PLOT(0.0,0.0,3)
POS=FLOAT(LP)*SKIP
CALL PLOT(0.0,POS,-3)
CALL LINEWT(-2)
ZB=ZBS/2.0
CALL SYMBOL(-0.25,ZB,0.15,'ALTITUDE (KM)',90.0,13.0,15.1)
NTICK=ZB*1
DO 38 I=1,NTICK
XN=-0.1
YN=FLOAT(I-1)
VAL=SZ+YN
CALL NUMBER(XN,YN,0.1,VAL,0.0,-1.0,1,1)
CALL SYMBOL(0.0,YN,0.1,15.0,0.0,-1.0,1,1)
38 CONTINUE
XBX=XBS*COS(ANGX)/2.0+0.4*SIN(ANGX)
XBY=XBS*SIN(ANGX)/2.0-0.4*COS(ANGX)
CALL SYMBOL(XBX,XBY,0.15,'EAST (KM)',DEGX,9.0,15.1)
NTICK=XBS*1

```

21 JUNE 1979

```

DO 39 I=1,NTICK
  XN=FLOAT(I-1)*COS(ANGX)+0.2*SIN(ANGX)
  YN=FLOAT(I-1)*SIN(ANGX)-0.2*COS(ANGX)
  VAL=SX+FLOAT(I-1)
  CALL NUMBER(XN,YN,0.1,VAL,DEGX,-1.0,1,1)
  XN=FLOAT(I-1)*COS(ANGX)
  YN=FLOAT(I-1)*SIN(ANGX)
  THETA=90.0+DEGX
  CALL SYMBOL(XN,YN,0.1,15,THETA,-1.0,1,1)
39 CONTINUE
  CALL PLOT(0.0,0.0,3)
  CALL PLOT(X2,Y2,-3)
  YBX=YBS*COS(ANGY)/2.0+0.4*SIN(ANGY)
  YBY=YBS*SIN(ANGY)/2.0-0.4*COS(ANGY)
  CALL SYMBOL(YBX,YBY,0.15,'NORTH (KM)',DEGY,10.0,15,1)
  NTICK=YBS+1
DO 41 I=1,NTICK
  XN=FLOAT(I-1)*COS(ANGY)+0.2*SIN(ANGY)
  YN=FLOAT(I-1)*SIN(ANGY)-0.2*COS(ANGY)
  VAL=SY+FLOAT(I-1)
  CALL NUMBER(XN,YN,0.1,VAL,DEGY,-1.0,1,1)
  XN=FLOAT(I-1)*COS(ANGY)
  YN=FLOAT(I-1)*SIN(ANGY)
  THETA=90.0+DEGY
  CALL SYMBOL(XN,YN,0.1,15,THETA,-1.0,1,1)
41 CONTINUE
  CALL PLOT(0.0,0.0,3)
  CALL PLOT(-X2,-Y2,-3)
  CALL TRANSFM(XMP,YMP,ZMP,NL,XXM,YXM,XYM,YYM,XPM,YPM,
  *YPPH,ANGX,ANGY)
  DS=(Y2-Y1)/(X2-X1)
  WRITE(6,50)
  N1=0
  N2=0
DO 35 I=1,NL
  DSS=YPM(I)/XPM(I)
  XINT=(DS*X1-Y1)/(DS-DSS)
  IF(XINT.LT.XPM(I)) GO TO 36
  N1=N1+1
  XPB(N1)=XPM(I)
  YPB(N1)=YPM(I)
  YYB(N1)=YYM(I)
  XYB(N1)=XYM(I)+XBS
  XXB(N1)=XXM(I)
  YXB(N1)=YXM(I)
  YPPB(N1)=YPPH(I)
GO TO 35
36 N2=N2+1
  XPT(N2)=XPM(I)
  YPT(N2)=YPM(I)+ZBS
  YYT(N2)=YYM(I)+ZBS
  XYT(N2)=XYM(I)
  XXT(N2)=XXM(I)
  YXT(N2)=YXM(I)+ZBS
  YPPT(N2)=YPPH(I)
35 CCNTINUL
DO 33 I=1,N1
  WRITE(6,47) XPB(I),YPB(I),YYB(I),XYB(I),XXB(I),YXB(I)
33 CONTINUE
  WRITE(6,50)
DO 37 I=1,N2
  WRITE(6,47) XPT(I),YPT(I),YYT(I),XYT(I),XXT(I),YXT(I)
37 CCNTINUE
  WRITE(6,50)
DO 46 I=1,NL

```

21 JUNE 1979

```

46 WRITE(6,47) XXM(I),YXM(I),XYM(I),YYM(I),XPM(I),YPM(I),
  * YPPM(I)
C
C ** GETTING THE SCALES LOWER BOUND **
C
47 FORMAT(7F15.7)
  XPB(N1+1)=0.0
  XPB(N1+2)=1.0
  YPPB(N1+1)=0.0
  YPPB(N1+2)=1.0
  XPT(N2+1)=0.0
  XPT(N2+2)=1.0
  YPPT(N2+1)=0.0
  YPPT(N2+2)=1.0
  XPB(N1+1)=0.0
  XPB(N1+2)=1.0
  YPB(N1+1)=0.0
  YPB(N1+2)=1.0
  XPT(N2+1)=0.0
  XPT(N2+2)=1.0
  YPT(N2+1)=0.0
  YPT(N2+2)=1.0
  CALL LINEWT(-2)
C
C ** PROJECTING THE SOURCE LOCATIONS EITHER ON THE TOP **
C ** PLANE(N1) OR ON THE BOTTOM PLANE(N2). **
C
  CALL LINE(XPB,YPPB,N1,1,-1,2,0.1)
  CALL LINE(XPT,YPPT,N2,1,-1,2,0.1)
  CALL LINEWT(-1)
  CALL LINE(XPB,YPB,N1,1,-1,10,0.1)
  CALL LINE(XPT,YPT,N2,1,-1,10,0.1)
  CALL LINEWT(1)
  DO 24 I=1,N1
    CALL PLOT(XPB(I),YPB(I),3)
    CALL PLOT(XPB(I),YPPB(I),2)
24  CONTINUE
  DO 32 I=1,N2
    CALL PLOT(XPT(I),YPT(I),3)
    CALL PLOT(XPT(I),YPPT(I),2)
32  CONTINUE
  DO 30 I=1,N1
    CALL PLOT(XXB(I),YXB(I),3)
    CALL PLOT(XPB(I),YPB(I),2)
    CALL PLOT(XYB(I),YYB(I),2)
30  CONTINUE
  DO 34 I=1,N2
    CALL PLOT(XXT(I),YXT(I),3)
    CALL PLOT(XPT(I),YPT(I),2)
    CALL PLOT(XYT(I),YYT(I),2)
34  CONTINUE
  CALL PLOT(0.0,0.0,999)
  STOP
  END

```

21 JUNE 1979

```

      SUBROUTINE TRNSFM(X,Y,Z,N,XX,YX,XY,YY,XP,YP,YPP,AX,AY)
C
C  ** THIS SUBROUTINE IS USED FOR COORDINATE TRANSFORMATION. **
C
      DIMENSION X(100),Y(100),Z(100),XX(100),YX(100),XY(100),
      *YY(100),XP(100),YP(100),YPP(100)
      DO 1 I=1,N
      XX(I)=X(I)*COS(AX)
      YX(I)=X(I)*SIN(AX)
      XY(I)=Y(I)*COS(AY)
      YY(I)=Y(I)*SIN(AY)
      XP(I)=XX(I)+XY(I)
      YP(I)=YY(I)+YX(I)
      YPP(I)=YP(I)+Z(I)
1  CONTINUE
      RETURN
      END

```


APPENDIX E

FREQUENCY DOMAIN APPROACH TO
DETERMINE DIFFERENCE IN THE TIME OF ARRIVAL

There are several techniques to measure time delays in either the frequency or the time domain. Chapter IV describes the theoretical basics of our time domain technique. This technique is implemented using the algorithm in Appendix C. For the work in this thesis we did not select a frequency domain technique for reasons discussed in this appendix. We investigated some of the frequency domain techniques using Fast Fourier Transforms (FFT). The two most effective frequency domain techniques consist of measuring time delays by determining either the properties of the magnitude of the phase of the transfer function between the input and the output (can be interpreted as central and remote stations). However, for the data under study neither of these techniques was appropriate because every pulse within a selected interval in the time series had a different time delay with respect to each consecutive pulse. To yield good results in a frequency domain we had to isolate the frequency content of identifiable VHF pulses which normally have a pulse width between one and five microseconds. After some preliminary test results we decided that the use of any frequency domain algorithm to systematically determine time delays required more computations and made it more difficult to understand the results than the use of any time domain technique. We will briefly summarize those frequency domain techniques that we investigated. Both

of these techniques make use of the two point measurement problem (see Figure E.1).

Let x_n and y_n represent the discrete time series at the central (x_n) and either of the three remote stations (y_n).

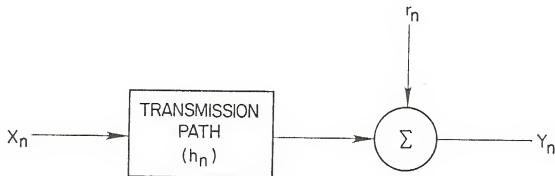


Figure E.1. The two point measurement problem.

$$y_n = x_n * h_n + r_n \quad (E.1)$$

where $*$ is the convolution operator, h_n is the transmission path, and r_n is random noise. The transmission path in this case does not represent a physical transmission path but a conceptual one which is introduced with the purpose of illustrating a number of digital techniques. Now we can proceed to determine the time difference between identifiable pulses in x_n and y_n . Once this time has been determined, the procedure is repeated for the remaining two remote stations.

E.1. Measurement of Time Delay by Determining the Peak of the Impulse Function

This method has been explored by Roth (1970), and consists of finding the time pulse response of the transfer function between x_n and y_n based on

$$G_{xy} = S_x S_y^* \quad (E.2)$$

$$G_{xx} = S_x S_x^* \quad (E.3)$$

$$S_y = H S_x + R_n \quad (E.4)$$

$$G_{xy} = (H S_x + R_n) (S_x^*) = H S_x S_x^* + R_n S_x^* \quad (E.5)$$

where S_x is the Fourier Transform of x_n , S_y is the Fourier Transform of y_n , G_{xy} is the cross-spectrum density between x_n and y_n , G_{xx} is the auto-spectrum of x_n , the upper index $*$ is the complex conjugate operator, and equations (E.2) through (E.5) represent the two point measuring problem illustrated in Figure E.1. Assuming that the system is linear and averaging the cross and auto-spectrum obtained from different ensembles in the same series, we can express the impulse transfer function as

$$h_n = F^{-1} \overline{(G_{xy}(w)/G_{xx}(w))} \quad (E.6)$$

where F^{-1} is the inverse Fourier transform operator.

The averaging process eliminates the contributions of NS_x , and it improves the estimate of h_n . Therefore h_n should be an impulse function at $n = a$ or $h_n = \delta(n-a)$. Several investigators, Roth (1970), Enochson (1973), French (1971), Dummermuth (1967) have implemented this procedure

obtaining satisfactory results. Also looking at the number of computations involved, there are fewer computations in this technique than in other frequency techniques such as the phase measurement which will be described in the next section.

E.2. Measurement of Time Delay by Measuring the Phase of the Frequency Response Function

We can estimate the time difference by measuring the phase of the frequency response function. Since x_n and y_n can be approximated by a linear system, we have

$$y_n = \sum_{k=-\infty}^{\infty} h_k x_{n-k} \quad (E.7)$$

where h_k is the impulse response between x_n and y_n . Using the two point measuring problem, we get

$$y_n = x_{n-\lambda} + r_n \quad (E.8)$$

$$Y(f) = \exp(-j2\pi f\lambda)X(f) + R(f) \quad (E.9)$$

averaging different ensembles, dividing, and calculating the phase, we obtain

$$\overline{Y(f)/X(f)} = \overline{H_{xy}(f)} = \text{Phase}(2\pi f\lambda) \quad (E.10)$$

Therefore the time delay λ is determined as

$$\lambda = 2\pi f\lambda/2\pi f \quad (E.11)$$

The question still remains as to what frequency to use in the computation of (E.11). This can be solved by using the frequency that

maximizes the coherence function between x_n and y_n . The coherence function is defined as

$$\gamma_{xy} = |G_{xy}|^2 / G_{xx} G_{yy} \quad \text{where} \quad 0 < \gamma_{xy} < 1 \quad (E.12)$$

Either by determining the time lag at which the peak of the impulse function occurs or by determining the time delay of the phase in the frequency response, we are limited to the data sample size. In the impulse function, a time delay is determined between two selected intervals in x_n and y_n , whereas in the phase frequency response, we can select different intervals of y_n to maximize the coherence function. In either case we need to determine the proper sample size to use to obtain correct results. If a sample size in the neighborhood of 5 μsec width is used, then we have to ensure that at least one entire pulse is within the selected interval for all the stations. On the other hand, if a sample size of several hundred microseconds is used, then we only get one cross-correlated location.

REFERENCES

- Baudry, M. and B. Dupeyrat, "Speech pattern recognition," Proceedings of the Second Joint International Conference on Pattern Recognition, Copenhagen, 356-357, 1974.
- Box, G. E. and G. M. Jenkins, Time Series Analysis: Forecasting and Control, Holden-Day, San Francisco, 1976.
- Brook, M. and N. Kitagawa, "Radiation from lightning discharges in the frequency range 400 to 1000 Mc/s," J. Geophys. Res., 69, 2431-2434, 1964.
- Brook, M., N. Kitagawa and E. J. Workman, "Quantitative study of strokes and continuing currents in lightning discharges to ground," J. Geophys. Res., 67, 649-659, 1962.
- Cianos, N., G. N. Oetzel and E. T. Pierce, "A technique for accurately locating lightning at close ranges," J. Appl. Meteorol., 11, 1120-1127, 1972.
- Clegg, R. J. and E. M. Thomson, "Some properties of em radiation from lightning," J. Geophys. Res., 84, 719-724, 1979.
- Davenport, W. B. and W. L. Root, An Introduction to the Theory of Random Signals and Noise, McGraw-Hill, New York, 1958.
- Dennis, A. S. and E. T. Pierce, "The return stroke of the lightning flash to earth as a source of VHF atmospheric," Radio Sci., 68D, 777-794, 1964.
- Dummermuth, G. and H. Fluhler, "Some modern aspects in numerical spectrum analysis of multichannel electroencephalographic data," Med. Biol. Engng., 5, 319-331, 1967.
- Enochson, L., "The application of digital time series analysis to the determination of time delays," U. S. Government Doc. Report #9024, 3199, Nov. 1973.
- Erich, R. W. and J. P. Foith, "Peak detection on picture rasters," IEEE Trans., C-25, 725, 1976.
- Fisher, R. J. and M. A. Uman, "Measured electric field risetimes for first and subsequent lightning return strokes," J. Geophys. Res., 77, 399-405, 1972.
- Fitzgerald, D. R., "Some theoretical aspects of the relation of surface electric field observations to cloud charge distributions," J. Meteorol., 14, 505-512, 1957.

French, A. S. and A. V. Holden, "Frequency domain analysis of neurophysiological data," Computer Programs in Biomedicine, 1, 219-234, 1971.

Gish, O. H. and G. R. Wait, "Thunderstorms and the earth's general electrification," J. Geophys. Res., 55, 473-484, 1950.

Gottman, J. and P. Gloor, "Automatic recognition and quantification of interictal epileptic activity in the human scalp EEC," Electroenceph. Clin. Neurophysiol., 41, 513-529, 1976.

Harth, W., "The propagation of atmospherics," in H. Dolezalek and R. Reiter (eds.), Electrical Processes in Atmospheres, 663-682, Dr. Dietrich Steinkopff Verlag, Darmstadt, 1974.

Hewitt, F. J., "The study of lightning streamers with 50cm. radar," Proc. Phys. Soc. London, Sec. B., 66, 895-897, 1953.

Hewitt, F. J., "Radar echoes from inter-stroke processes in lightning," Proc. Phys. Soc. London, Sect. B., 70, 961-979, 1957.

Hewitt, F. J., "Radar studies of noise in lightning, in monograph on radio noise of terrestrial origin," edited by F. Horner, Elsevier Pub. Co., Amsterdam, 72-84, 1962.

Holmes, C. R., M. Brook, P. Krehbiel and R. McCrory, "Reply," J. Geophys. Res., 76, 7443, 1971.

Holmes, T. G. and P. H. Reedy, "Geometrical dilution of precision," Report 21, Patrick AFB, Fla., 1951.

Horner, F., "Radio Noise from thunderstorms," in J. A. Saxton (ed.), Advances in Radio Research, vol. 2, 121-204, Academic Press, Inc., New York, 1964.

Horner, F. and P. Bradley, "The spectra of atmospherics from near lightning discharges," J. Atm. and Terr. Phys., 26, 1155-1166, 1964.

Ishikawa, H., "Nature of lightning discharges as origin of atmospherics," Proc. Res. Inst. Atmos. Nagoya Univ., 8A, 1, 1960.

Jacobson, E. A. and E. P. Krider, "Electrostatic field changes produced by Florida lightning," J. Atm. Sci., 33, 103-117, 1976.

Jerri, A., "The Shannon sampling theorem," Proc. IEEE, 65, Nov. 1977.

Jones, D. L., "Electromagnetic radiation from multiple return strokes of lightning," J. Atmos. Ter. Phys., 32, 1077-1093, 1970.

Khastgir, S. R. and S. K. Saha, "On intra-cloud discharges and their accompanying electric field changes," J. Atmos. Ter. Phys., 34, 775-786, 1972.

Kimpara, A., "Electromagnetic energy radiated from lightning," in S. C. Coroniti (ed.), Problems of Atmospheric and Space Electricity, 352-365, American Elsevier Pub. Co., New York, 1965.

- Kitagawa, N. and M. Brook, "A comparison of intracloud and cloud-to-ground lightning discharges," J. Geophys. Res., 65, 1189-1201, 1960.
- Kitagawa, N. M. Brook and E. J. Workman, "Continuing currents in cloud-to-ground lightning discharges," J. Geophys. Res., 67, 637-647, 1962.
- Kitagawa, N. and M. Kobayashi, "Distribution of negative charge in the cloud taking part in a flash to ground," Papers Meteorol. Geophys. (Tokyo), 9, 99-105, 1958.
- Krehbiel, P. R., Private Communication, 1979.
- Krehbiel, P. R., M. Brook and R. A. McCrory, "An analysis of the charge structure of lightning discharges to ground," J. Geophys. Res., 84, 2432-2456, 1979.
- Krehbiel, P. R., R. McCrory and M. Brook, "The determination of lightning charge location from multi-station electrostatic field change measurements," Conf. on Cloud Phys., 21-24, Tucson, Arizona, Oct. 1974.
- Krider, E. P., R. C. Noggle and M. A. Uman, "A gated, wideband magnetic direction finder for lightning return strokes," J. Appl. Meteorol., 15, 301-306, 1976.
- Krider, E. P., G. J. Radda and R. C. Noggle, "Regular radiation field pulses produced by intracloud lightning discharges," J. Geophys. Res., 80, 3801-3804, 1975.
- Krider, E. P., C. D. Weidman and D. M. LeVine, "The temporal structure of the HF and VHF radiation produced by intracloud lightning discharges," Submitted for publication in J. Geophys. Res., Spring 1979.
- Krider, E. P., C. D. Weidman and R. C. Noggle, "The electric fields produced by lightning stepped leaders," J. Geophys. Res., 82, 951-960, 1977.
- Lee, Y. W., Statistical Theory of Communication, Wiley and Sons, Pub., New York, 1960.
- Lennon, C. L., "LDAR - A new lightning detection and ranging system," Trans. Amer. Geophys. Union, 56, 991, 1975.
- Lennon, C. L., "The performance of a real-time, time of arrival lightning location system (LDAR)," EOS Trans., AGU, 57, #12, 1976.
- LeVine, D. M. and E. P. Krider, "The temporal structure of HF and BHF radiations during Florida lightning return strokes," Geophys. Res. Lett., 4, 13-16, 1977.
- Lewis, E. A., R. B. Harvey and J. E. Rasmussen, "Hyperbolic direction finding with sferics of transatlantic origin," J. Geophys. Res., 65, 1879-1905, 1960.

- Livingston, J. M. and E. P. Krider, "Electric fields produced by Florida thunderstorms," J. Geophys. Res., 83, 385-401, 1978.
- MacClement and R. C. Murty, "VHF direction finder studies of lightning," J. Appl. Meteorol., 17, 786-795, 1978.
- Mackerras, D., "A comparison of discharge processes in cloud and ground lightning flashes," J. Geophys. Res., 73, 1175-1183, 1968.
- Malan, D. J., "Les décharges dans l'air et la charge enférieure positive d'un nuage orageux," Ann. Geophys., 8, 385-401, 1952.
- Malan, D. J., "Visible electrical discharges inside thunderclouds," Geofis. pura Appl., 34, 221-236, 1956.
- Malan, D. J., "Les décharges orageuses intermittentes et continues de la colonne de charge négative," Ann. Geophys., 10, 271-281, 1954.
- Malan, D. J., "Radiation from lightning discharges and its relation to the discharge process," in L. G. Smith (ed.), Recent Advances in Atmospheric Electricity, 557-563, Pergamon Press, New York, 1958.
- Malan, D. J., Physics of Lightning, The English Universities Press, London, 1963.
- Malan, D. J. and B. F. Schonland, "Progressive lightning, pt. 7, directly correlated photographic and electrical studies of lightning from nine thunderstorms," Proc. Roy. Soc., A191, 485-503, 1947.
- Malan, D. J. and B. F. Schonland, "The electrical processes in the intervals between the strokes of a lightning discharge," Proc. Roy. Soc. London, A206, 145-163, 1951.
- McLain, D. K. and M. A. Uman, "Exact expression and moment approximation for the electric field intensity of the lightning return stroke," J. Geophys. Res., 76, 2101-2105- 1971.
- Murty, R. C. and W. D. MacClement, "VHF direction finder for lightning location," J. Appl. Meteorol., 12, 1401-1405, 1973.
- Nakano, M., "Lightning channel determined by thunder," Proc. Res. Inst. Atmos. Nagoya Univ., 20, 1-7, 1973.
- Nakano, M., "Characteristics of lightning channel in thunderclouds determined by thunder," J. Meteorol. Soc. Japan, 54, 441-447, 1976.
- Nishino, M., A. Iwai and M. Kashiwagi, "Location of the sources of atmospheres in and around Japan," Proc. Res. Inst. Atmos. Nagoya Univ., 20, 9-18, 1973.
- Oetzel, G. N. and E. T. Pierce, "Radio emissions from close lightning," in S. C. Coroniti and J. Hughes (eds.), Planetary Electrodynamics, Vol. 1, 543-569, Gordon and Breach, New York, 1969.

- Ogawa, T. and M. Brook, "The mechanism of the intracloud lightning discharge," J. Geophys. Res., 69, 5141-5150, 1964.
- Pierce, E. T., "Electrostatic field changes due to lightning discharges," Quart. J. Roy. Meteorol. Soc., 81, 211-228, 1955.
- Pierce, E. T., "Atmospherics from lightning flashes with multiple strokes," J. Geophys. Res., 65, 1867-1871, 1960.
- Pierce, E. T., "Atmospherics: Their characteristics at the source and propagation," in Progress in Radio Science 1963-1966, pt. 1, 987-1039, International Scientific Radio Union, Berkley, Calif., 1967.
- Pierce, E. T., "Source characteristics of atmospherics generated by lightning," Proceedings of Waldorf Conference on Long-Range Geographic Estimation of Lightning Sources, NRL Report 7763, Washington, D. C., 64-79, 1974.
- Pierce, E. T., "The thunderstorm research international program (TRIP) - 1976," Bull. Amer. Meteorol. Soc., 57, 1214-1216, 1976.
- Pierce, E. T., "Atmospherics and radio noise," in R. H. Golde (ed.), Lightning Volume 1: Physics of Lightning, 351-384, Academic Press, London, 1977.
- Pitman, G. R., Inertial Guidance, Wiley and Sons, Pub., New York, 1962.
- Proctor, D. E., "A hyperbolic system for obtaining VHF radio pictures of lightning," J. Geophys. Res., 76, 1478-1489, 1971.
- Proctor, D. E., "VHF radio pictures of lightning," in H. Dolezalek and R. Reiter (eds.), Electrical Processes in Atmospheres, 694-699, Dr. Dietrich Steinkopff Verlag, Darmstadt, 1974a.
- Proctor, D. E., "VHF radio pictures of lightning," CSIR Special Report, TEL 118, Pretoria, South Africa, 1974b.
- Proctor, D. E., "VHF radio pictures of lightning," CSIR Special Report, TEL 119, Pretoria, South Africa, 1974c.
- Proctor, D. E., "VHF radio pictures of lightning," CSIR Special Report, TEL 120, Pretoria, South Africa, 1974d.
- Proctor, D. E., "A radio study of lightning," Ph.D. Thesis, 574 pp., University of Witwatersrand, Johannesburg, South Africa, 1976.
- Rogers, J. G., "Structured programming for virtual storage systems," IBM Systems Journal, Vol. 14, 4, 385-406, 1975.
- Roth, P. R., "Effective measurements using digital signal analysis," IEEE Spectrum, 62-70, 1971.
- Rustan, P. L., M. A. Uman, D. G. Childers, W. H. Beasley and C. L. Lennon, "Lightning properties for a flash at Kennedy Space Center via multiple time series analysis," Submitted to Science, Summer, 1979.

- Schonland, B. F. J., D. B. Hodges and H. Collens, "Progressive Lightning - V: A comparison of photographic and electrical studies of the discharge process," Proc. Roy. Soc. London, A168, 455-469, 1938.
- Serhan, G. I., M. A. Uman, D. G. Childers and Y. T. Lin, "The RF spectra of first and subsequent lightning return strokes in the 1-200 km range," To be published in J. Geophys. Res., Spring 1979.
- Simpson, G. C. and G. D. Robinson, "The distribution of electricity in thunderclouds," Proc. Roy. Soc. London, A177, 281-329, 1941.
- Skolnik, M. I., Introduction to Radar Systems, McGraw-Hill, New York, 1962.
- Smith, L. G., "Intracloud lightning discharges," Quart. J. Roy. Meteorol. Soc., 83, 103-111, 1957.
- Takagi, M., "The mechanism of discharges in a thundercloud," Proc. Res. Inst. Atmos. Nagoya Univ., 8B, 1-106, 1961.
- Takagi, M., "Polarization of VHF radiation from lightning discharges," J. Geophys. Res., 80, 5011-5014, 1975.
- Takagi, M. and T. Takeuti, "Atmospheric radiation from lightning discharge," Proc. Res. Inst. Atmos. Nagoya Univ., 10, 1, 1963.
- Taylor, W. L., "Radiation field characteristic of lightning discharges in the band 1 kc/s to 100 kc/s," J. Res. NBS-D Radio Propagation, 67D, 539-550, 1963.
- Taylor, W. L., "Lightning characteristics as derived from sferics," in S. C. Coroniti (ed.), Problems of Atmospheric and Space Electricity, 388-404, American Elsevier Pub. Co., New York, 1965.
- Taylor, W. L., "Detecting tornadic storms by the burst rate nature of electromagnetic signals they produce," Ninth Conf. on Severe Local Storms, 311-315, 1975.
- Taylor, W. L., "Space-time mapping of lightning discharge processes in thunderstorms at the NASA Kennedy Space Center," Trans. Amer. Geophys. Union, 57, 922, 1976.
- Taylor, W. L., "A VHF technique for space-mapping of lightning discharge processes," J. Geophys. Res., 83, 3575-3584, 1978.
- Taylor, W. F., "A VHF technique for space-time mapping of lightning discharge processes," To be published in J. Geophys. Res., Spring 1979.
- Teer, T. L. and A. A. Few, "New York, Horizontal lightning," J. Geophys. Res., 79, 3436-3441, 1974.
- Thomas, J., Statistical Communication Theory, Wiley and Sons, Pub., New York, 1969.

Uman, M. A., Lightning, McGraw-Hill, New York, 1969.

Uman, M. A., W. H. Beasley, J. A. Tiller, Yung-Tao Lin, E. P. Krider, C. D. Weidman, P. R. Krehbiel, M. Brook, A. A. Few, Jr., J. L. Bohannon, C. L. Lennon, H. A. Poehler, W. Jafferis, J. R. Bulick and J. R. Nicholson, "An unusual lightning flash at the NASA Kennedy Space Center," Science, 201, 9-16, 1978.

Uman, M. A., R. D. Brantley, Y. T. Lin, J. A. Tiller, E. P. Krider, and D. K. McLain, "Correlated electric and magnetic fields from lightning return strokes," J. Geophys. Res., 80, 373-376, 1975.

Uman, M. A. and D. K. McLain, "Lightning return stroke current from magnetic and radiation field measurements," J. Geophys. Res., 75, 5143-5147, 1970.

Watson-Watt, R. A. and J. F. Herd, "An instantaneous direct - reading radiogoniometer," J. Inst. Elec. Engrs., 64, 611-622, 1926.

Weinberg, H. and R. Cooper, "The recognition index: A pattern recognition technique for noisy signals," Electroenceph. Clin. Neurophysiol., 33, 608-613, 1972.

Widrow, B., "The 'Rubber Mask' technique - 1 pattern measurement and analysis," Report - Stanford Univ., 1974.

Wilson, C. T. R., "On some determinations of the sign and magnitude of electric discharges in lightning flashes," Proc. Roy. Soc. London, A92, 555-574, 1916.

Wood, L. C. and S. Treitel, "Seismic signal processing," Proc. IEEE, 63, 649-661, 1975.

BIOGRAPHICAL SKETCH

Pedro Luis Rustan, Jr., was born in Guantanamo, Cuba, in 1947. He graduated first in his class from the Guantanamo High School in 1964. He received the degree of Bachelor of Science in Electrical Engineering in December 1969, and the degree of Master of Science in Electrical Engineering in December 1970, both from the Illinois Institute of Technology. In 1971 he became a United States citizen and entered active service with the United States Air Force. From 1971 to 1976 he worked in the areas of electromagnetic radiation, and guidance and control. In June 1976, he was selected to attend the University of Florida and work toward a degree of Doctor of Philosophy. He is presently a captain in the Air Force, working as an instructor at the Air Force Institute of Technology.

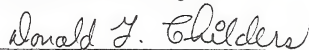
He is a member of Tau Beta Pi, Eta Kappa Nu, the Institute of Electrical and Electronics Engineers and the American Geophysical Union. He is married to the former Alexandra Cary, from Lake Bluff, Illinois, and has a son, Peter Cary.

I certify that I have read this study and that in my opinion it conforms to acceptable standards of scholarly presentation and is fully adequate, in scope and quality, as a dissertation for the degree of Doctor of Philosophy.



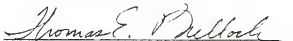
Martin A. Uman, Chairman
Professor of
Electrical Engineering

I certify that I have read this study and that in my opinion it conforms to acceptable standards of scholarly presentation and is fully adequate, in scope and quality, as a dissertation for the degree of Doctor of Philosophy.



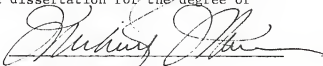
Donald G. Childers, Co-Chairman
Professor of
Electrical Engineering

I certify that I have read this study and that in my opinion it conforms to acceptable standards of scholarly presentation and is fully adequate, in scope and quality, as a dissertation for the degree of Doctor of Philosophy.



Thomas E. Bullock
Professor of
Electrical Engineering

I certify that I have read this study and that in my opinion it conforms to acceptable standards of scholarly presentation and is fully adequate, in scope and quality, as a dissertation for the degree of Doctor of Philosophy.



Michael E. Warren
Assistant Professor of
Electrical Engineering

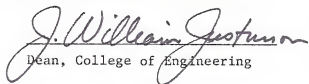
I certify that I have read this study and that in my opinion it conforms to acceptable standards of scholarly presentation and is fully adequate, in scope and quality, as a dissertation for the degree of Doctor of Philosophy.



James T. McClave
Associate Professor of Statistics

This dissertation was submitted to the Graduate Faculty of the College of Engineering and to the Graduate Council, and was accepted as partial fulfillment of the requirements for the degree of Doctor of Philosophy.

December 1979


Dean, College of Engineering

Dean, Graduate School

Date Due

Due

JUL 08 1966 JUL 09 1966

OCT 13 1986 OCT 10 1986

MAY 10 1968 APR 26 1968

FEB 28 2013

Engineering and Physics Library